Synthesis and Characterization of Polyhedral Oligomeric Silsesquioxane (POSS) Based Amphiphiles

Yang Liu

Thesis submitted to the Faculty of the Virginia Polytechnic Institute and State University in partial fulfillment of the requirements for the degree of

Doctor of Philosophy

in

Chemistry

Alan R. Esker, Chair
Richard D. Gandour
John R. Morris
Hervé Marand

August 23, 2011

Blacksburg, VA

Keywords: POSS, air/water (A/W) interface, Π–*A* isotherms, Brewster angle microscopy (BAM), Langmuir films

Synthesis and Characterization of Polyhedral Oligomeric Silsesquioxane (POSS) Based Amphiphiles

Yang Liu

Department of Chemistry

Virginia Polytechnic Institute and State University

ABSTRACT

Polyhedral oligomeric silsesquioxanes (POSS) have attracted substantial academic interest for many years as hybrid materials and nanofillers for controlling thermal and mechanical properties, and providing thermal and chemical resistance while retaining ease of processing. A natural extension of these studies has been POSS-based amphiphiles and thin film coatings. Studies at the air/water (A/W) interface have shown that trisilanol-POSS derivatives are amphiphilic and form uniform Langmuir films, whereas closed-cage POSS derivatives are hydrophobic and aggregate.

In previous work, a triester (POSS-triester) and a triacid (POSS-triacid) were synthesized from PSS-(3-hydroxypropyl)-heptaisobutyl (POSS-OH) and Weisocyanate and fully characterized by surface pressure – area per molecule (Π-*A*) isotherm and Brewster angle microscopy (BAM) studies at the A/W interface. The results indicated that POSS-triester is surface active forming a liquid expanded (LE) monolayer, whereas POSS-triacid forms a liquid condensed (LC) monolayer that is only weakly affected by pH. A face-on conformation was proposed and examined to understand the packing of POSS-based amphiphilic molecules at the A/W interface. The face-on/vertex-on comparison is rarely discussed for Langmuir monolayers at the A/W interface.

In this thesis, three other POSS-based esters were synthesized from POSS-OH and aminopropylisobutyl-POSS (POSS-NH_2) using Weisocyanate and a similar isocyanate containing two *tert*-butyl protected carboxylic acids. The synthesized materials are characterized by Π-*A* isotherm and BAM. For POSS-OH based diester (P*Al*DE) and POSS-NH_2 based diester (P*Am*DE), LE/LC phase transitions were observed in Π-*A* isotherms over part of the experimentally accessible temperature range and were attributed to a change from a vertex-on to face-on conformation. Apparent BAM images confirmed LC islands coexisted with the LE phase. The experimentally observed dynamic estimates of the critical temperatures (T_c) were estimated from a two-dimensional Clausius-Clapeyron analysis and were consistent with the temperature dependence of the Π-*A* isotherms. These LE/LC phase transitions are the first observed for POSS amphiphiles.

To my country I would like to serve forever

and my wife, Changqin Chen, who has always been supportive even in my hardest times.

ACKNOWLEDGEMENTS

I would like to extend heartfelt thanks to my advisor, Dr. Alan R. Esker for accepting me into his group and giving me opportunities to work in my area of interest with precious counsel. I would like to thank Dr. Richard D. Gandour, Dr. John R. Morris, and Dr. Herve Marand for serving on my research committee. I would like to thank Dr. Gandour's research group for generous support and materials. I appreciate the generous guidance of Dr. Louis P. Madsen, Dr. Harry C. Dorn, Dr. Harry, W. Gibson, Dr. Sungsool Wi, and Dr. Gordon, T. Yee. I would also like to thank Dr. Patricia G. Amateis and Mike Johnson for their guidance and support in my TA sections.

I would like to thank my colleagues in Dr. Esker's group who made my research joyful and successful: Dr. Soulong Ni, Dr. Bingbing Li, Dr. Rituparna Paul, Dr. Ufuk Karabiyik, Dr. Wojin Lee, Dr. Wen Yin, Dr. Adulaziz Kaya, Dr. Qiongdan Xie, Jae-Hyun Sim, Dr. Zelin Liu, Chuanzi Ou-Yang, Xiaosong Du, Joshua Kittle, Xijing Yuan, Chao Wang, Xiao Zhang, Chen Qian, Ying Ni, Chistopher Estes, Emma Edgar, Heejun Choi, and Liz Huh. I would like to thank Dr. Guangbin Wang, Dr. Min Mao, Dr. Yanpeng Hou, Dr. Ting Cai, Dr. Nan Dai, Dr. Liangming Hu, Dr. Jun Qi, Zhenbin Niu, Ronald Chen, Grace Xu, Bin Zhang, Anderson Sun, and Yi Li for their help without reservation when I had questions. I would also extend special thanks to Dr. Jielu Zhao, Dr. Ende Pan, Dr. Jianfei Zhang, Liaosa Xu, Dr. Wujun Fu, Dr. Chao Yang, Zhu Wang, Yixuan Lin, Dr. Bin Xu, Yan Hu, Dr. Yang Pu, and Jing Wang, for their friendship which made my spare time in Blacksburg colorful.

I would like to thank my parents and brother for their love and support. At last, I would like to thank my wife, Changqin Chen, who sacrificed her career for me. Thanks for her trust and sharing, especially during hard times. I cannot imagine my journey through life without her.

TABLE OF CONTENTS

ABSTRACT **ii**
ACKNOWLEDGMENTS **v**
TABLE OF CONTENTS **vii**
LIST OF FIGURES **x**
LIST OF SCHEMES **xvi**
LIST OF TABLES **xvii**
CHAPTER 1: Overview 1
CHAPTER 2: Introduction and Literature Review 5
2.1 Introduction to Colloids and Interfaces 5
2.2 Introduction to Molecular Films 6
2.3 Terminology and Historical Background of Langmuir Films 8
2.4 Formation of Langmuir Monolayers 9
2.5 Experimental Techniques 11
2.5.1 Surface Pressure-Area per Molecule (Π-*A*) Isotherms 11
2.5.1.1 Surface Pressure (Π) and Surface Tension (γ) 11
2.5.1.2 Π-*A* Isotherms and Phase Transitions in Langmuir Films 19
2.5.2 Langmuir-Blodgett (LB) Technique 23
2.5.3 Brewster Angle Microscopy (BAM) 26
2.6 Phase Diagrams of Langmuir Monolayers 32
2.6.1 Monolayer Phases 32
2.6.2 Chain-length Dependence of Monolayer Phase Diagrams 34
2.7 Introduction to Polyhedral Oligomeric Silsesquioxanes (POSS) 35
2.7.1 POSS Cage Synthesis 36
2.7.2 Synthesis of POSS-based Polymers 39
2.7.3 Physical Properties and Applications of POSS 40
2.7.4 Conformational Analysis of Closed-Cage POSS Derivatives 42
CHAPTER 3: Experimental Materials and Method 51
3.1 Materials and Sample Preparations 51
3.1.1 Obtained Materials 51
3.1.2 Purified and Synthesized Materials 52
3.1.2.1 Purification and Characterization of POSS-OH 52
3.1.2.2 Synthesis and Characterization of POSS-OH Based Diester (P*Al*DE) 53
3.1.2.3 Synthesis and Characterization of POSS-NH_2 Based Triester (P*Am*TE) 54
3.1.2.4 Synthesis and Characterization of POSS-NH_2 Based Diester (P*Am*DE) 55
3.2 Sample Characterization 56
3.2.1 Nuclear Magnetic Resonance (NMR) Spectroscopy 56
3.2.2 Melting Point Determinations 57
3.2.3 High Resolution Mass Spectrometry (HRMS) 57

3.3 Experimental Methods 58
3.3.1 Langmuir Trough Configuration 58
3.3.2 Constant Compression Rate Experiments 61
3.3.3 Stepwise Compression Experiments 61
3.3.4 Brewster Angle Microscopy (BAM) 61
CHAPTER 4: Synthesis and Characterization of POSS-NH_2 Based Triester at the Air/Water Interface 62
4.1 Abstract 62
4.2 Introduction 62
4.3 Experimental 67
4.4 Results and Discussion 67
4.4.1 Synthesis and Characterization of POSS-NH_2 Based Triester (P*Am*TE) 67
4.4.2 POSS Molecules that Exhibit Face-on Conformations 70
4.4.3 Possible Conformations for POSS-NH_2 Based Triester at the A/W Interface 73
4.4.4 Comparison of POSS-Based Triesters 77
4.5 Conclusions 79
CHAPTER 5: Synthesis and Characterization of POSS-OH Based Diester at the Air/Water Interface 81
5.1 Abstract 81
5.2 Introduction 82
5.3 Experimental 85
5.4 Results and Discussion 85
5.4.1 Synthesis and Characterization of POSS-OH Based Diester (P*Al*DE) 85
5.4.2 Observation of a LE/LC Phase Transition 90
5.4.3 Different Compressibility between the LE and LC Phases 93
5.4.4 Temperature Dependence of the LE/LC Phase Transition 94
5.4.5 Possible Conformations for POSS-OH Based Diester at the A/W Interface 104
5.4.6 Comparison of POSS-OH Based Esters 107
5.5 Conclusions 109
CHAPTER 6: Synthesis and Characterization of POSS-NH_2 Based Diester at the Air/Water Interface 111
6.1 Abstract 111
6.2 Introduction 112
6.3 Experimental 113
6.4 Results and Discussion 114
6.4.1 Synthesis and Characterization of POSS-NH_2 Based Diester (P*Am*DE) 114
6.4.2 Observation of a LE/LC Phase Transition 116
6.4.3 Different Compressibility between the LE and LC Phases 119
6.4.4 Temperature Dependence of the LE/LC Phase Transition 120
6.4.5 Possible Conformations for POSS-NH_2 Based Diester at the A/W Interface 128

6.4.6 Comparison of POSS-Based Diesters 129
6.5 Conclusions 133
CHAPTER 7: Overall Conclusions and Future Work 134
7.1 Overall Conclusions 134
7.2 Suggestions for Future Work 135
7.2.1 Synthesis and Characterization of POSS-Based Monoesters 135
7.2.2 Synthesis and Characterization of POSS-Based Monoesters with Different 140
7.2.3 Synthesis and Characterization of POSS-Based Non-*tert*-butyl Esters 143
7.2.4 Synthesis and Characterization of POSS-Based Esters with Different Substituents on the POSS Cage 151
7.2.5 Blends of Amphiphilic POSS Derivatives at the A/W Interface 153
References 157

LIST OF FIGURES

Chapter 2

Figure 2.1 Schematic depictions of thin film types from crystalline, liquid crystalline, assembled films, amorphous, and partially oriented polymeric films**.** The Langmuir – Blodgett and self-assembled films represent side views, whereas the other films are top views. 7

Figure 2.2 Examples of amphiphilic molecules that form Langmuir monolayers: (A) *n*-octadecanoic acid, (B) *n*-hexadecanoic methyl ester, (C) diacylphosphatidylethanolamine (DPPE), (D) diacylphosphatidylcholine (DPPC), and (E) POSS-OH based triester (P*Al*TE). 10

Figure 2.3 Example of polymers that form Langmuir monolayers: (A) poly(*tert*-butyl acrylate) (PtBA), (B) poly(dimethylsiloxane) (PDMS), (C) poly(tetrahydrofuran) (PTHF), and (D) poly(vinyl acetate) (PVAc). 11

Figure 2.4 Diagram of the forces on two liquid molecules, one in the bulk versus one at the surface. Red arrows highlight attractive forces acting on a given molecule. 13

Figure 2.5 Schematic depiction of a Langmuir trough. 14

Figure 2.6 Measurement of surface pressure with a Wilhelmy plate. 17

Figure 2.7 Contact angles of water on hydrophilic and hydrophobic surfaces. 18

Figure 2.8 A schematic depiction of a Π-*A* isotherm for amphiphilic molecules at the A/W interface. The area scale on the plot roughly corresponds to room temperature values for fatty acids, where A_0 for the condensed phase is in the vicinity of 20 $Å^2 \cdot molecule^{-1}$. 20

Figure 2.9 A schematic depiction of a Langmuir film undergoing collapse from a monolayer into multilayer domains. 22

Figure 2.10 Y-type deposition of LB-multilayers onto a hydrophobic substrate: (A) formation of a stable Langmuir monolayer at the A/W interface by compression, (B) first immersion of a hydrophobic substrate, (C) first withdrawal, and (D) LB-multilayers with head-to-head and tail-to-tail configurations. 25

Figure 2.11 Structures of LB-multilayers: (A) X-, (B) Y-, and (C) Z-type. The structural difference between Figure 2.10 D and (B) reflects the fact that (B) depicts a hydrophilic substrate. X- and Z-type depositions do not normally guarantee that the multilayers will have the corresponding structure as rearrangement with time after deposition is possible. 26

Figure 2.12 Schematic depiction of the reflection of unpolarized light at Brewster's angle. 27

Figure 2.13 Reflectivity at different incident angles for *s* (solid line) and *p* (dotted line) polarized light. 30

Figure 2.14 Schematic depiction of a BAM. A *p*-polarized laser beam is incident on the water surface at Brewster's angle for water ($\theta_B = 53.1^o$). Light reflected by the interface is detected by a CCD camera. A *p*-polarizer is placed in the path of the reflected beam to

remove residual s-polarized light. 31
Figure 2.15 Experimental Π -*T* phase diagram for an eicosanoic acid Langmuir film, which was modified from the original source. 33
Figure 2.16 The chain-length dependence of the monolayer phase diagram for fatty acids (C_{14} – C_{24}). Solid lines exhibit first-order transitions and dashed lines indicate second-order transitions. 35
Figure 2.17 Two most common types of POSS. R = alkyl group. 36
Figure 2.18 ∏-*A* isotherms of TiBP, POSS-OH, and P*Al*TE at 22.5°C at the A/W interface. 44
Figure 2.19 (A) The T_8 POSS cage was treated as an ideal cube with the substituents evenly distributed at the vertices of the cage. In this model, *Si* atoms are located at the eight corners of the cube while omitted *O* atoms are in the middle of the 12 edges. (**B**) The Atomium for Brussels World's Fair. The labeling of the cube in (**A**) and Atomium in (**B**) are consistent with balancing the cube on vertex A for a vertex-on conformation. 47
Figure 2.20 (**A**) Π-*A* isotherm for PtBA on water at T= 22.5 °C. The red dashed line indicates A_0 for PtBA. (**B**) Structure of P*Al*TE highlighting the POSS-OH piece and the three PtBA "repeating units". 49
Figure 2.21 Schematic depictions of P*Al*TE (top view) in Langmuir films at various *A*: (**A**) $A = A_{lift\text{-}off}$, (**B**) $A_c < A < A_{lift\text{-}off}$, and (**C**) $A = A_c$. 50

Chapter 3

Figure 3.1 Structure of POSS-OH. 52
Figure 3.2 (**A**) Schematic depiction of positions on the trough and (**B**) calibration curves for the temperatures of the subphase. 60

Chapter 4

Figure 4.1 Circumcircle O_1 of equilateral triagle A_1BD. A_1E, BG, and DF are perpendicular bisectors of BD, A_1D, and A_1B and intersect at E_1, G_1, and F_1, respectively. $r_1 = A_1O_1$ represents the radius of the circumcircle centered at O_1. 65
Figure 4.2 Circumcircle O_2 of the square *ABCD*. Two diagonals *AC* and *BD* intersect at O_2, the center of the circumcircle. $r_2 = DO_2$ represents the radius of circumcircle centered at O_2. 66
Figure 4.3 ^{1}H NMR of P*Am*TE. 68
Figure 4.4 ^{13}C NMR of P*Am*TE. 69
Figure 4.5 Expanded ^{13}C NMR of P*Am*TE. 70
Figure 4.6 Chemical structures of POSS-MA and P*Al*TA. Substituent R represents an isobutyl group. 71
Figure 4.7 ∏-*A* isotherms for isobutyl substituted POSS derivatives: P*Al*TA, POSS-NH_2, POSS-OH, and POSS-MA at the A/W interface (T = 22.5 ^{o}C). 72
Figure 4.8 (A) ∏-*A* isotherms for trisilanolisobutyl-POSS (TiBP) and P*Am*TE at the A/W interface (T = 22.5 ^{o}C) and **(B)** the chemical structure of TiBP. 74
Figure 4.9 (**A**) Π-*A* isotherm for PtBA at A/W interface at T= 22.5 °C. The red dashed line

indicates A_0 for PtBA. (**B**) Structure of P*Am*TE highlighting the POSS-NH_2 piece and the three PtBA "repeating units". 76
Figure 4.10 Schematic depictions of P*Am*TE (top view) in Langmuir films at various *A*: (**A**) $A = A_{lift\text{-}off}$, (**B**) $A_c < A < A_{lift\text{-}off}$, and (**C**) $A = A_c$. 77
Figure 4.11 Π-*A* isotherms for POSS-NH_2, POSS-OH, P*Am*TE and P*Al*TE at the A/W interface at 22.5 °C. 79

Chapter 5

Figure 5.1 Experimentally accessible windows of Π-*A* isotherms for fatty acids and barrel-like POSS model. 84
Figure 5.2 ^{1}H NMR and T_m of purified POSS-OH. 86
Figure 5.3 ^{13}C NMR of purified POSS-OH. 87
Figure 5.4 ^{1}H NMR and T_m of P*Al*DE. 88
Figure 5.5 ^{13}C NMR of P*Al*DE. 89
Figure 5.6 Expanded ^{13}C NMR of P*Al*DE. 90
Figure 5.7 Π-*A* isotherms of P*Al*DE at the A/W interface at 5 °C. Four regions are depicted: (a) G or G/LE; (b) a LE phase; (c) LE/LC coexistence; and (d) a LC phase. BAM images at different *A* are provided: (i) 141.0 Å^2•molecule^{-1}, LE monolayer prior to phase transition; (ii) 136.8 Å^2•molecule^{-1}, circular domains of coexistent LE and LC domains; (iii) 133.8 Å^2•molecule^{-1}, approaching the end of the plateau; and (iv) 133.8 Å^2•molecule^{-1}, a LC monolayer. All BAM images are 2.0 × 2.4 mm^2, cut from the original BAM images. Each BAM image has an independent gray scale. 92
Figure 5.8 Comparison of the ∏-*A* isotherm (red dotted lines ----) and ε_s-*A* plot (black crosses +) for P*Al*DE at 5.0 °C. The dashed vertical lines break the isotherms into the same regions defined in Figure 5.7. 94
Figure 5.9 Temperature dependence of the LE/LC phase transition of P*Al*DE at the A/W interface. Isotherms at different temperatures are labeled by different colors and different line styles. LE/LC phase coexistence is observed for isotherms below 37.5 °C, and is not observed at 40 °C, indicating the critical temperature (T_c) lies between 37.5 °C and 40 °C. 96
Figure 5.10 Temperature dependence of $\prod_{collapse}$ (red squares) and A_{collapse} (black triangles) for P*Al*DE Langmuir films at the A/W interface. Each point is the average value from three experiments. The standard deviation error bars are provided to indicate uncertainties. 97
Figure 5.11 Schematic depiction of the procedure to determine A_{LC} at the end of LE/LC phase transition for an isotherm of P*Al*DE at 5 °C. A_{LE} is obtained from the kink in the ∏-*A* isotherm and a horizontal line represents $\prod_{tr}$ = 9.1 mN•m^{-1} at the onset of the LE/LC phase transition. A_{LC} is obtained from the intersection of the line used for obtaining the limiting area of the LC monolayer and the horizontal line. 99
Figure 5.12 Temperature dependence of the LE/LC phase transition surface pressure, $\prod_{tr}$, for P*Al*DE Langmuir films at the A/W interface. The best linear fit line is provided a slope of 0.15 ± 0.01 mN•m^{-1}•K^{-1}. 101
Figure 5.13 Temperature dependence of ΔH_{tr} (red crosses) and ΔS_{tr} (black filled squares)

for P*Al*DE Langmuir films at the A/W interface. Both ΔS_{tr} and ΔH_{tr} were calculated using the linear fit from Figure 5.12. 102
Figure 5.14 Π-*A* isotherms comparison for P*Al*DE at the A/W interface at (A) 5 °C and (B) 22.5 °C. The stepwise experiment is set up with a constant rate of 10 $cm^2 \cdot min^{-1}$, a trough area decrement of 20 cm^2, and a time interval between compressions of 300 seconds. 104
Figure 5.15 Π-*A* isotherms at the A/W interface (T= 22.5 °C) for (**A**) POSS-OH (red dotted line) and P*Al*DE (blue solid line) and (**B**) PtBA along with the chemical structure of PtBA. (**C**) The structure of P*Al*DE highlighting the POSS-OH piece and the two PtBA "repeating units" connected by a short linker. 106
Figure 5.16 Schematic depictions of P*Al*DE (top view) in Langmuir films at various *A*: (**A**) $A = A_{lift\text{-}off}$, the size of P*Al*DE is determined by $A_{0,POSS\text{-}OH}$ (~125 $Å^2 \cdot molecule^{-1}$) with a face-on conformation plus 2 PtBA repeating units (~30 $Å^2 \cdot molecule^{-1}$ each); (**B**) $A = A_{0,LE}$, the size of POSS cage is determined by the circumcircle of the equilateral triangle of a vertex-on conformation; and (**C**) $A = A_c$, the size of POSS cage is determined by the circumcircle of the square in a face-on conformation. 107
Figure 5.17 Π-*A* isotherms for POSS-OH, P*Al*TE, and P*Al*DE at the A/W interface at T = 22.5 °C. 109

Chapter 6

Figure 6.1 ^{1}H NMR of P*Am*DE. 114
Figure 6.2 ^{13}C NMR of P*Am*DE. 115
Figure 6.3 Expanded ^{13}C NMR of P*Am*DE. 116
Figure 6.4 Π-*A* isotherm of P*Am*DE at the A/W interface at 5 °C. Four regions are depicted: (a) a G or G/LE phase; (b) a LE phase; (c) LE/LC coexistence; and (d) a LC phase. BAM images at different *A* are provided: (i) 125.2 $Å^2 \cdot molecule^{-1}$, monolayer prior to the LE/LC phase transition; (ii) 120.5 $Å^2 \cdot molecule^{-1}$, circular LC domains growing in the LE film; (iii) 117.6 $Å^2 \cdot molecule^{-1}$, approaching the end of the plateau; and (iv) 110.3 $Å^2 \cdot molecule^{-1}$, formation of a LC monolayer. BAM image i is 4.8 × 6.4 mm^2 while images ii-iv are 2.0 × 2.4 mm^2, cut from the original BAM images. Each BAM image has an independent gray scale. 118
Figure 6.5 Comparison of the ∏-*A* isotherm (red dotted lines ----) and ε_s-*A* plot (black crosses +) for P*Am*DE at 5.0 °C. 120
Figure 6.6 Temperature dependence of the LE/LC phase transition of P*Am*DE at the A/W interface. LE/LC phase coexistence is observed for isotherms below 27.5 °C, and is not observed at 30 °C, indicating the critical temperature (T_c) lies between 27.5 °C and 30 °C. 121
Figure 6.7 Temperature dependence of $\prod_{collapse}$ (red triangles) and $A_{collapse}$ (black squares) for P*Am*DE Langmuir films at the A/W interface. Each point is the average of three measurements with one standard deviation error bars. 122
Figure 6.8 Temperature dependence of $\prod_{tr}$ for the LE/LC phase transition of P*Am*DE Langmuir films at the A/W interface. The best fit yields a slope of 0.15 ± 0.01 $mN \cdot m^{-1} \cdot K^{-1}$. 123

Figure 6.9 Temperature dependence of ΔH_{tr} (red crosses) and ΔS_{tr} (black filled squares) for P*Am*DE Langmuir films at the A/W interface. Both ΔS_{tr} and ΔH_{tr} are calculated using the linear fit from Equations 5.3, 5.4, and Figure 6.8. 125
Figure 6.10 Π-*A* isotherms comparison for P*Am*DE at the A/W interface. Red and blue curves represent experiments at 22.5 °C and 5 °C, respectively. The stepwise experiments are set up with a constant compression rate of 10 $cm^2 \cdot min^{-1}$, a trough area decrement of 20 cm^2, and a time interval of 300 seconds between compressions. 127
Figure 6.11 Schematic depictions of P*Am*DE (top view) in Langmuir films at various *A*: (**A**) $A = A_{lift\text{-}off}$, the size of P*Am*DE is determined by $A_{0,POSS\text{-}NH2}$ (~130 $Å^2 \cdot molecule^{-1}$) with a face-on conformation plus 2 PtBA repeating units (~30 $Å^2 \cdot molecule^{-1}$ each). (**B**) $A = A_{0,LE}$, the size of POSS cage is determined by the circumcircle of the equilateral triangle in a vertex-on conformation. (**C**) $A = A_{0,\ LC}$, the size of POSS cage is determined by the circumcircle of the square in a face-on conformation. 129
Figure 6.12 Π-*A* isotherms for P*Al*DE, and P*Am*DE at the A/W interface at T= 5.0 °C. Green dotted line and solid line are $A_{0,LE}$ and $A_{0,LC}$ for P*Al*DE, respectively. Blue dotted line and solid line are $A_{0,LE}$ and $A_{0,LC}$ for P*Am*DE, respectively. 130
Figure 6.13 Schematic depictions for packing of (**A**) triesters and (**B**) diesters at the A/W interface. 132

Chapter 7

Figure 7.1 Structures of POSS-NH_2 and POSS-OH based monoester. 136
Figure 7.2 Examples of POSS-based carbamate esters with different linker lengths. 140
Figure 7.3 Π-*A* isotherms of POSS-OH and P*Al*TE at the A/W interface at 22.5 °C. The shaded peach region represents a region of interest for controlling POSS packing through the synthesis of new POSS amphiphiles. 144
Figure 7.4 Examples of POSS-OH and POSS-NH_2 based non-^{t}butyl esters. 145
Figure 7.5 ^{1}H NMR of POSS-NH_2 based triacid (P*Am*TA). 147
Figure 7.6 ^{1}H NMR of POSS-OH based diacid (P*Al*DA). 148
Figure 7.7 ^{13}C NMR of POSS-OH based diacid (P*Al*DA). 149
Figure 7.8 Expanded ^{13}C NMR of POSS-OH based diacid (P*Al*DA). 150
Figure 7.9 ^{1}H NMR of POSS-NH_2 based diacid (P*Am*DA). 151
Figure 7.10 Π-*A* isotherms of TiOP, TPP, and a 50 : 50 blend by mass at the A/W interface at T = 22.5 °C. The 4.8 mm × 6.4 mm BAM images for 50% TiOP were captured at *A* = 85 and 45 $Å^2 \cdot molecule^{-1}$. 154
Figure 7.11 A demonstration of "interdigitating" or "interlocking" phenyl groups for TPP at the A/W interface. Gray atoms are carbon, red atoms are oxygen, purple atoms are silicon, and green atoms are hydrogen. The model represents the configuration where the three silanol groups of POSS are exposed to water (out of the page). With the "interdigitating" phenyl groups, the recalculated cross-sectional area (*AMM2* = 158 $Å^2 \bullet molecule^{-1}$) of TPP is smaller than the one without interdigitation (*AMM2* ≈ 210 $Å^2 \bullet molecule^{-1}$) and close to the experimental limiting area (A_o = 152 ± 8 $Å^2 \bullet molecule^{-1}$)

obtained from Π-*A* isotherms. 155

LIST OF SCHEMES

Chapter 2

Scheme 2.1 Scheme for synthesizing closed-cage POSS derivatives. 37
Scheme 2.2 Scheme for synthesizing open-cage POSS derivatives. 38
Scheme 2.3 Synthesis of incompletely condensed POSS cages from the cleavage of completely condensed POSS in the presence of an acid or base catalyst. 39
Scheme 2.4 Synthesis of P*Al*TE. 43

Chapter 3

Scheme 3.1 Synthesis of P*Al*DE. 54
Scheme 3.2 Synthesis of P*Am*TE. 55
Scheme 3.3 Synthesis of P*Am*DE. 56

Chapter 7

Scheme 7.1 Synthetic scheme for *tert*-butyl 4-methyl-4-nitropentanoate (**3**). 137
Scheme 7.2 Synthetic scheme for *tert*-butyl 4-amino-4-methylpentanoate (**4**). 138
Scheme 7.3 Synthetic scheme for *tert*-butyl 4-isocyanato-4-methylpentanoate, isocyanatemonoester (**7**). 139
Scheme 7.4 Synthetic scheme for obtaining POSS-OH based monoester (P*Al*ME, **10**) and POSS-NH_2 based monoester (P*Am*ME, **11**). 139
Scheme 7.5 Synthetic scheme for methoxylisobutyl-POSS (**13**) from methacrylate isobutyl-POSS (**12**). 141
Scheme 7.6 Synthetic scheme for POSS-based carbamate monoester (**15**) and monoacid (**16**) with a single linking methylene unit between the POSS cage and the carbamate. 142
Scheme 7.7 Synthetic scheme for POSS-OH derivatives (**15**) with different length of methylene spacers. 143
Scheme 7.8 Synthetic scheme for POSS-OH based triacid (**20**). 146
Scheme 7.9 Synthetic scheme for POSS-OH based trimethylester (**21**). 146
Scheme 7.10 Synthetic scheme for obtaining closed-cage POSS derivatives with a single primary amine from trisilanol-POSS with different R. 152

LIST OF TABLES

Chapter 2

Table 2.1 A summary of condensed phases of Langmuir monolayer. 34

Chapter 5

Table 5.1 A_{LC}, A_{LE}, ΔA, ΔS_{tr}, and ΔH_{tr}, at different temperatures for the LE/LC phase transition of P*Al*DE. 103

Chapter 6

Table 6.1 A_{LC}, A_{LE}, ΔA, ΔS_{tr}, and ΔH_{tr}, at different temperatures for the LE/LC phase transition of P*Am*DE. 126

Table 6.2 Comparison of $\varepsilon_{s,\,max}$, T_c, and T_0, for P*Al*DE and P*Am*DE. 133

Chapter 1

Overview

Studies on monolayers of amphiphilic molecules at the air/water (A/W) interface provide a unique way to investigate two-dimensional (2D) materials at asymmetric interfaces.[1] For over more than a century, a rich variety of physical phenomena and applications have been reported.[2] In past decades, the importance of Langmuir trough technique increased with the evolution of optical techniques, such as laser light scattering,[3] fluorescence,[4] and Brewster angle microscopy (BAM).[5] This development allowed visualization of monolayer morphology associated with collapsed structures and phase transitions.[6]

Polyhedral oligomeric silsesquioxanes (POSSs) are a new generation of lighter weight, higher performance materials.[7] As a hybrid material, POSS is composed of a rigid inorganic core and a flexible organic corona. The nanoscopic sizes of POSS provide opportunities to behave as nanofillers in a variety of polymers. Although POSS has received considerable attention, extra efforts are still strongly desired. From previous work, trisilanol-POSS derivatives seem more interesting for surface studies because of their amphiphilic character in contrast to closed-cage POSS molecules which tend to aggregate at the A/W interface. In this dissertation, a series of closed-cage POSS-based amphiphilies have been synthesized and characterized by ^{1}H NMR, ^{13}C NMR, melting point tests, high resolution mass spectrometry (HRMS), surface pressure-area per molecule (Π-*A*) isotherm, and Brewster angle microscopy (BAM). The possible conformations of molecules at the A/W interface and phase behavior are also discussed.

Chapter 2, Introduction and Literature Review, provides a general introduction to interfaces, thin films, and Langmuir monolayers. Experimental instruments and techniques, such as the Langmuir-Blodgett (LB) trough and BAM are discussed in detail. In order to understand the LB-technique, the 2-dimensional (2D) Π-*A* isotherms of fatty acids with phase transitions are explained as an analog to 3-dimensional (3D) bulk *P*-*V* isotherms. Different phases, such as gas (G), liquid expanded (LE), liquid condensed (LC), and solid (S) are used to describe phase transitions that arise from differences in packing and tilt angle of amphiphiles at the A/W interface. In addition, POSS is reviewed as a core material in this dissertation. The POSS cage synthesis, POSS-based polymers, physical properties, and applications are discussed. Based upon previous work, the conformation of POSS derivatives as well as phase behavior of amphiphiles with different length/diameter ratios are introduced. In general, trisilanol-POSS molecules exhibit a vertex-on conformation through the entire monolayer region. On the other hand, a closed-cage amphiphile based upon PSS-(3-hydroxypropyl)-heptaisobuyl (POSS-OH), a triester (P*Al*TE) has a Π-*A* isotherm that is consistent with a conformational change from a vertex-on to face-on upon collapse.

Chapter 3, Experimental Materials and Methods, contains a detailed description of the material synthesized for this dissertation. Preparations of materials, experimental techniques, methods of characterization, and procedures used in subsequent chapters are summarized. This information will not be repeated in detail in the subsequent research chapters.

Chapter 4, Synthesis and Characterization of POSS-NH_2 Based Triester at the Air/Water Interface, discusses the surface behavior of a POSS derivative (P*Am*TE) synthesized from aminopropylisobutyl-POSS (POSS-NH_2) and Weisocyanate. Π-*A* isotherm studies confirm POSS-NH_2 and P*Am*TE are both amphiphilic at the A/W interface. Analysis of the Π-*A*

isotherms reveals packing of these amphiphiles at the A/W interface is similar to that of P*Al*TE. Unlike the vertex-on conformation for trisilanol-POSS derivatives, POSS-NH_2 exhibits a face-on conformation at the A/W interface. P*Am*TE starts with the POSS-cage and three *tert*-butyl esters adsorbed to the plane of the interface. As the film is compressed, P*Am*TE initially exhibits a vertex-on conformation and ultimately a face-on conformation when the film collapses. Isotherms of four closed-cage POSS derivatives (POSS-OH, POSS-NH_2, P*Al*TE, and P*Am*TE) are compared.

Chapter 5, Synthesis and Characterization of POSS-OH Based Diester at the Air/Water Interface, describes the phase transition and conformational analysis of a newly synthesized POSS-OH derivative (P*Al*DE). P*Al*DE is obtianed from POSS-OH and an isocyanate diester. Π-*A* isotherm studies and BAM confirm POSS-OH and P*Al*DE are both amphiphilic at the A/W interface. Whereas trisilanol-POSS derivatives pack in a vertex-on conformation, POSS-OH packs in a face-on conformation. For P*Al*DE, a transition from vertex-on to face-on packing is observed during dynamic compression of the molecules at the A/W interface. Π-*A* isotherms indicate that P*Al*DE Langmuir monolayers exhibit a liquid expanded-to-condensed (LE/LC) phase transition. BAM images reveal large islands of the LC phase are dispersed in the LE phase during phase coexistence. The apparent critical temperature (T_c) of the phase transition is obtained from a 2D Clausius-Clapeyron analysis. The result agrees well with experimental observations of T_c, however, the transition is obtained under non-equilibrium conditions and "T_c" is probably influenced by the close proximity of the collapse transition. This result is the first example of a POSS material that exhibits a LE/LC phase transition at the A/W interface.

Chapter 6, Synthesis and Characterization of POSS-NH_2 Based Diester at the Air/Water Interface, examines Π-*A* isotherms of another POSS-NH_2 derivative (P*Am*DE). P*Am*DE is

synthesized from POSS-NH_2 and an isocyanate diester. Π-*A* isotherm studies and BAM are used to characterize P*Am*DE at the A/W interface. Analysis of the Π-*A* isotherms revealed packing of these amphiphiles at the A/W interface was similar to that of P*Al*DE discussed in Chapter 5. Similar to P*Al*DE, P*Am*DE also exhibits a LE/LC phase transition that is consistent with a change from a vertex-on to a face-on conformation during compression. BAM images show large islands of the LC phase dispersed in the LE phase in the phase coexistence region. The critical temperature of the phase transition is predicted from a 2D Clausius-Clapeyron analysis. The result agrees well with the temperature dependence of the Π-*A* isotherms. However, the results for P*Am*DE are even more strongly affected by a completion between collapse and phase separation that is more pronounced than for P*Al*DE.

Chapter 7, Overall Conclusions and Future Work, provides a summary of this dissertation and suggests several natural extensions of this study. A series of close-cage POSS derivatives are designed and synthesized to examine their surface behaviors by Π-*A* isotherm and BAM. Conformational analysis agrees with the conclusion drawn from P*Al*TE. A first-order LE/LC phase transition is firstly observed for POSS derivatives. These studies provide new insights into design and interfacial properties of silicon based surfactants and surface modifying agents. In addition, some suggestion for future work are given as follows: (1) synthesis and characterization of POSS-based monoesters; (2) synthesis and characterization of POSS-based monoesters with different linkers; (3) synthesis and characterization of POSS-based non-*tert*-butyl esters; (4) synthesis and characterization of POSS-based esters with different substituents on the POSS cage; and (5) blends of amphiphilic POSS derivatives at the A/W interface.

Chapter 2

Introduction and Literature Review

2.1 Introduction to Colloids and Interfaces

Interfaces, the dividing region which separates two phases from each other, generally include the solid/liquid, solid/gas, and liquid/gas interfaces. Since the boundary between water and oil can be distinguished as two immiscible liquids, liquid/liquid interfaces are also studied as well as solid/solid interfaces. However, gas/gas interfaces are not considered because all gases are miscible. Colloids, usually discussed with interfaces, are disperse systems, with dispersed phase lateral dimensions on the order of nm to μm.[8] Colloids and interfaces are intimately related since the interface-to-volume ratio is so large that their behavior is critically dependent upon the interfacial properties. For this reason, some properties of nanoscience and nanotechnology are intimately related to interfacial behavior as properties deviate from their bulk values.

Interest in interfaces and colloids has developed in a variety of areas including lipid membranes in biology,[9] swelling of clay or soil in geology,[10] butter manufacturing in food science,[11] detergency,[12] thin films,[13] coatings,[14] paints,[15] etc. However, a surface is seldom an infinitesimally sharp boundary in the direction of its surface normal; rather it is rough, and this roughness affects properties and applications. In this thesis, the air/water (A/W) interface is the main interface. The density of a liquid surface decreases from its bulk value to its vapor value over a few molecular diameters.[16]

2.2 Introduction to Molecular Films

Molecular films by definition are ordered monolayers of molecules with a thickness ranging from the scale of nanometers to hundreds of nanometers. Due to their attractive properties, molecular films offer many challenging scientific and technological opportunities, such as sensors,[17] displays,[18] solar cells,[19] electroluminescent devices,[20] field-effect transistors,[21] etc. As molecular thin films exhibit promise for molecular engineering with desired structure and functionality, researchers developed interests in adhesion and biomedical applications.[22] Along with the development of techniques and materials, dimensions of devices are continually being reduced to the monolayer level and various methods have been reported to achieve thin films, such as spin coating,[23] direct deposition,[24] thermal deposition,[25] electrodeposition,[26] micro-imprinting,[27] brush tethering,[28] laser micro-patterning,[27] self-assembly (SAM),[29] the Langmuir-Blodgett (LB) technique,[1e, 30] etc.

In order to study the ordering of molecules as films, the LB-technique is one of the best on the basis of a few advantages: (1) the ability to precisely control the films from monolayer to multilayer, (2) controllable compression rates allowing for the transfer of molecules in different relaxation states (i.e. different orientations), and (3) the possibility to deposit films onto a variety of solid and liquid substrates.

Although a preponderance of the work has been performed on organic thin films, studies of inorganic films, such as silanes and siloxanes, cannot be disregarded. Based upon intermolecular interactions between the film and the substrate and the intramolecular interaction of the film, molecular films can be divided into thin crystalline and amorphous films of individual molecules, thin films of liquid crystals, LB-films, self-assembled films, and polymeric films (Figure 2.1).

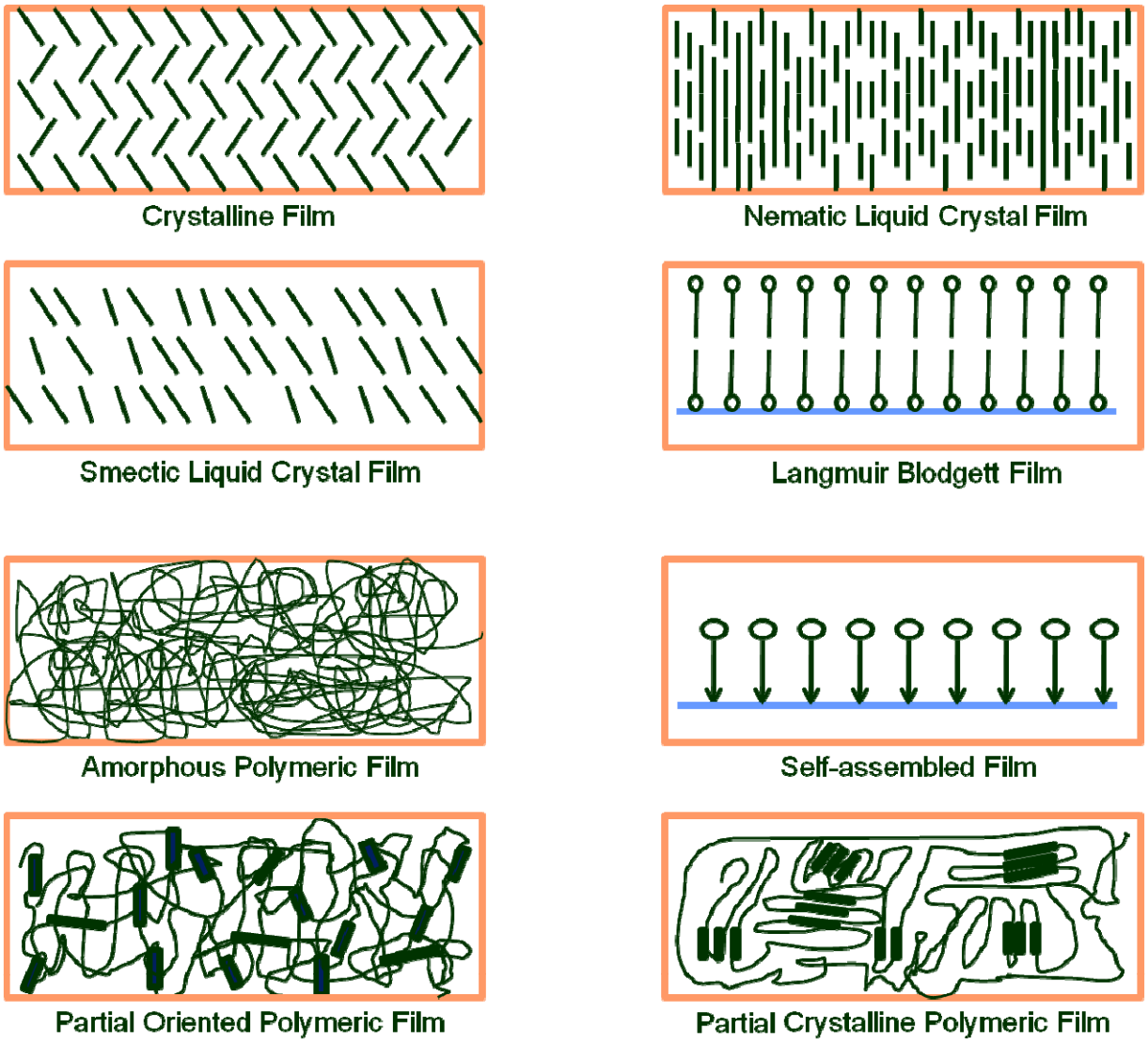

Figure 2.1 Schematic depictions of thin film types from crystalline, liquid crystalline, assembled films, amorphous, and partially oriented polymeric films.[31] The Langmuir –Blodgett and self-assembled films represent side views whereas the other films are top views.

2.3 Terminology and Historical Background of Langmuir Films

In this dissertation, some terms have to be clarified because they represent different information although they seem similar, such as *Langmuir films* and *Langmuir-Blodgett (LB) films*. To be specific, when amphiphilic molecules are spread at the A/W interface and monolayers are generated, they are Langmuir films. Amphiphiles form *Gibbs monolayer* if they are soluble in water and adsorb at the A/W interface from solution, whereas a *Langmuir monolayer* is generally insoluble in water. A Langmuir film is an excellent model for studying ordering in a two-dimensional (2D) system.[1a, 1c, d] First, similar to traditional solid substrates, such as silica or gold, water has a very smooth surface with a roughness 3~5 Å,[32] which minimizes the boundary and fluctuation effects on the organic films. Second, thermodynamic variables, such as temperature (*T*), surface area occupied per molecule or monomer (*A*) and surface pressure (Π) are controllable. Third, interactions between the polar head groups and the water subphase can mimic biomedical surroundings because phospholipids bilayers comprising the cell membranes can be considered as two weakly coupled monolayers.[33] Moreover, only a minimal amount of sample is required for a single experiment. For example, 0.5 μg of a material with a molecular weight of 1000 $g \cdot mol^{-1}$ is enough to cover a 600 cm^2 surface to the point where each molecule occupies 200 $Å^2$ (relevant parameters for a polyhedral oligomeric silsesquioxane (POSS) molecule).

On the other hand, a *Langmuir-Blodgett film* is not necessarily identical to a *Langmuir monolayer* since it could also be a multilayer rather than a single monolayer. In experiments, *LB-films* are generated on solid substrates by Langmuir-Blodgett or Langmuir-Scheaffer deposition.[1f, 34] In this dissertation, *Langmuir monolayers* are mainly discussed.

It is interesting to note that thin film, or even a monolayer, has been made and applied by ancient people. Babylonians predicted success, marriage, birth, death and luck by spreading an oil layer on

water and observing the shape of the film around the 18th century BC.[35] Two thousand years ago, Chinese applied *suminagashi*, which involves early 'ink-stream', on marble sculptures.[35] People did not regard monolayers as a scientific field until Benjamin Franklin designed his famous Clapham pond experiment in 1774.[36] During the later 100 years, scientist discussed monolayers more systematically. In the early 1900's, Irving Langmuir developed techniques and exhibited evidence for the monomolecular nature of the film as well as the orientation of the molecules at the A/W interface.[37] Seventeen years after Langmuir successfully transferred a monolayer onto a solid substrate,[38] Katharine Blodgett transferred multiple layers of long aliphatic carboxylic acids onto a solid substrate.[39] Their work in surface chemistry led to a Nobel Prize for Langmuir in 1932. Nowadays, these films are known as Langmuir-Blodgett films.

However, isotherm studies alone are often ambiguous and led to dispute and controversy, such as the order of phase transitions in Langmuir films.[40] During past few decades, *in situ* techniques have been developed to assist the study of Langmuir films with respect to thermodynamic, kinetic, and mechanical properties. Such techniques include Brewster angle microscopy (BAM),[41] X-ray diffraction techniques (XRD),[42] fluorescence microscopy (FM),[43] surface light scattering (SLS),[6f, 44] interfacial stress rheometer (ISR),[28, 45] and ellipsometry.[42j, 46]

2.4 Formation of Langmuir Monolayers

Langmuir monolayers are composed of amphiphiles with polar head groups anchoring the molecules to the interface and hydrophobic tail oriented towards air that prevent dissolution. Such amphiphilic molecules include long chain fatty acids, alcohols, esters, and phospholipids (Figure 2.2)[47] and polymers such as polyethers,[48] polyesters,[49] polysiloxanes,[50] polyacrylates and polymethacrylates,[30e, 51] etc. (Figure 2.3).

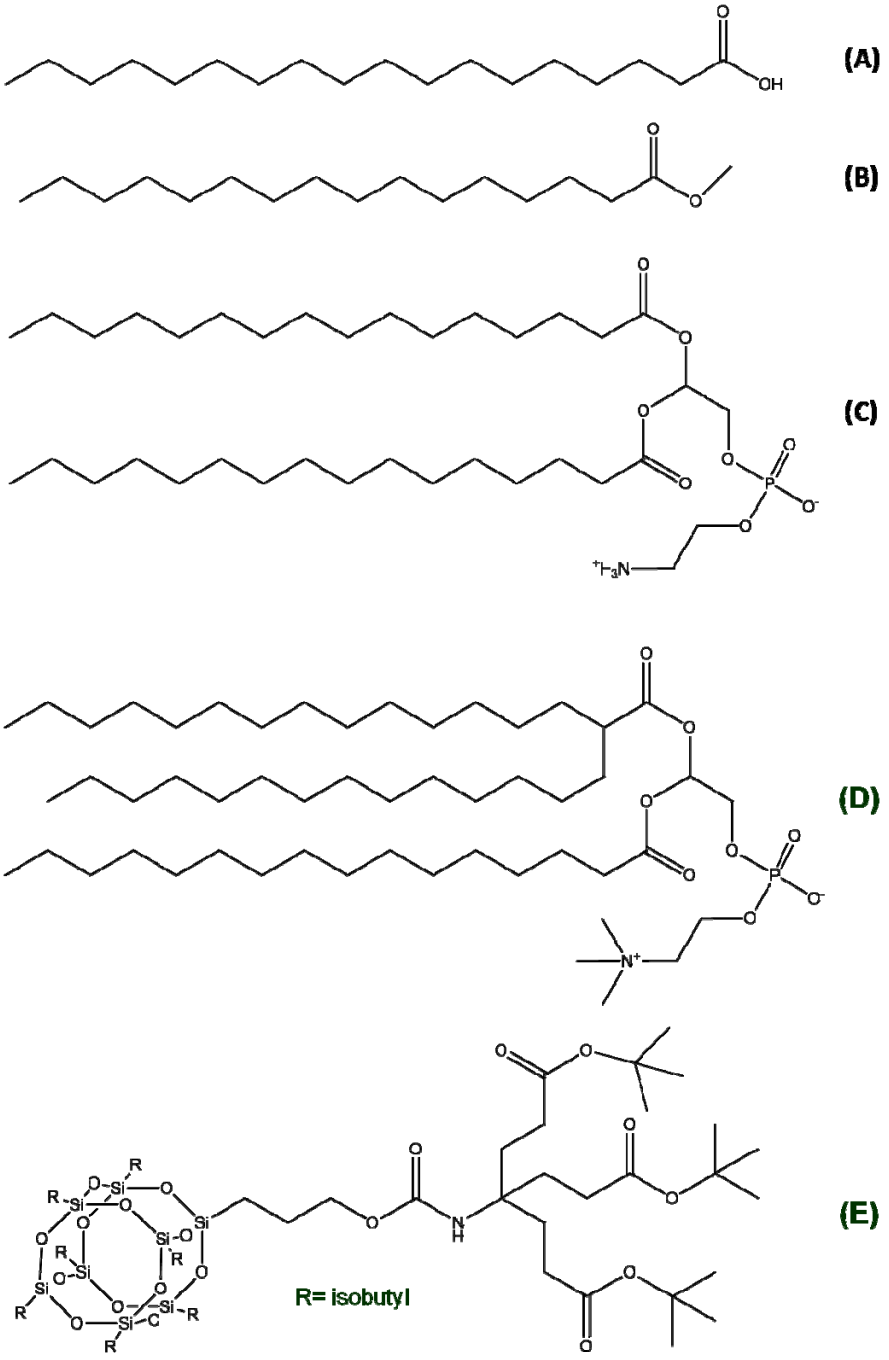

Figure 2.2 Examples of amphiphilic molecules that form Langmuir monolayers: (A) *n*-octadecanoic acid,[52] (B) *n*-hexadecanoic methyl ester,[53] (C) diacylphosphatidylethanolamine (DPPE),[54] (D) diacylphosphatidylcholine (DPPC),[55] and (E) POSS-OH based triester (P*AI*TE).[47d]

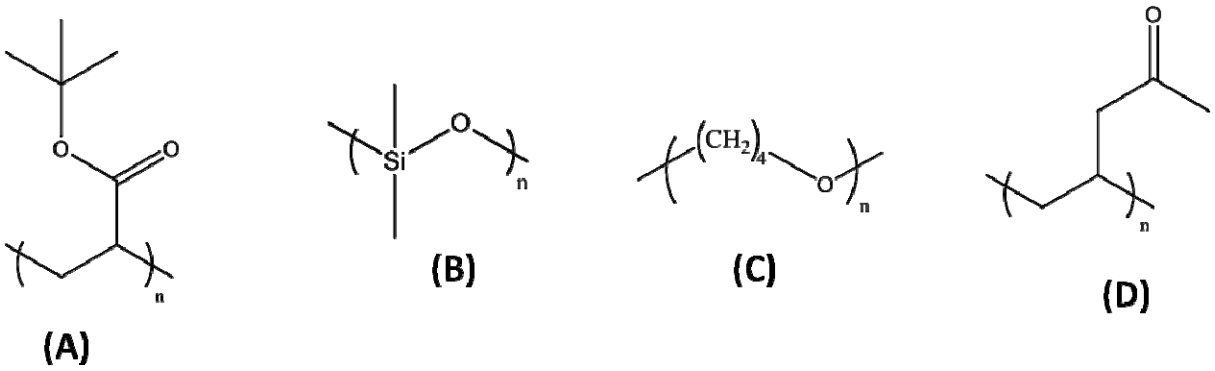

Figure 2.3 Example of polymers that form Langmuir monolayers: (A) poly(*tert*-butyl acrylate) (PtBA),[56] (B) poly(dimethylsiloxane) (PDMS),[57] (C) poly(tetrahydrofuran) (PTHF),[58] and (D) poly(vinyl acetate) (PVAc).[59]

2.5 Experimental Techniques

The objective of my research is to synthesize and characterize closed-cage POSS-based triesters at the A/W interface. The Langmuir-Blodgett (LB) and associated techniques will be used to study the phase behavior of POSS derivatives at the A/W interface. In order to study the morphology of amphiphilic molecules, Brewster angle microscopy (BAM) is coupled with a Langmuir trough.

2.5.1 Surface Pressure-Area per Molecule (Π-*A*) Isotherms

2.5.1.1 Surface Pressure (Π) and Surface Tension (γ)

Surface tension (γ) is a critical property of a liquid caused by cohesive forces between molecules. This effect is depicted in Fiugre 2.4. For molecules within the bulk liquid, forces

experienced on the molecules are symmetrical resulting in a net force of zero. These forces include van der Waals forces, hydrogen bonding, dipolar interactions, etc. Without these attractions there would not be a condensed phase. However, for molecules located at the interface, forces are not balanced and result in a net attractive force that pulls molecules at the surface of a liquid towards the bulk. In order to bring a molecule from the bulk to the surface, a "surface free energy" penalty represented by the surface tension or surface energy is required. This surface tension with a unit of force per unit length can also be considered as surface energy density (energy per unit area), reflecting the tendency of liquids to reduce their surface area. At thermodynamic equilibrium, the surface tension of a planar interface can be expressed as:[1b]

$$\gamma = \left(\frac{\partial F}{\partial A}\right)_{T,V,n} \; or \; \gamma = \left(\frac{\partial G}{\partial A}\right)_{T,P,n} \tag{2.1}$$

where T, P, and V are temperature, pressure, and volume, respectively, *A* is the surface area, and *F* and *G* are the Helmholtz and Gibbs free energies, respectively. In this thesis, only water is discussed because it is not only the most frequently used liquid, but it also has a higher surface tension (about 73 $mN \cdot m^{-1}$ at 20 ^{o}C) than traditional organic liquids. The larger γ arises from strong hydrogen bonding between H_2O molecules.

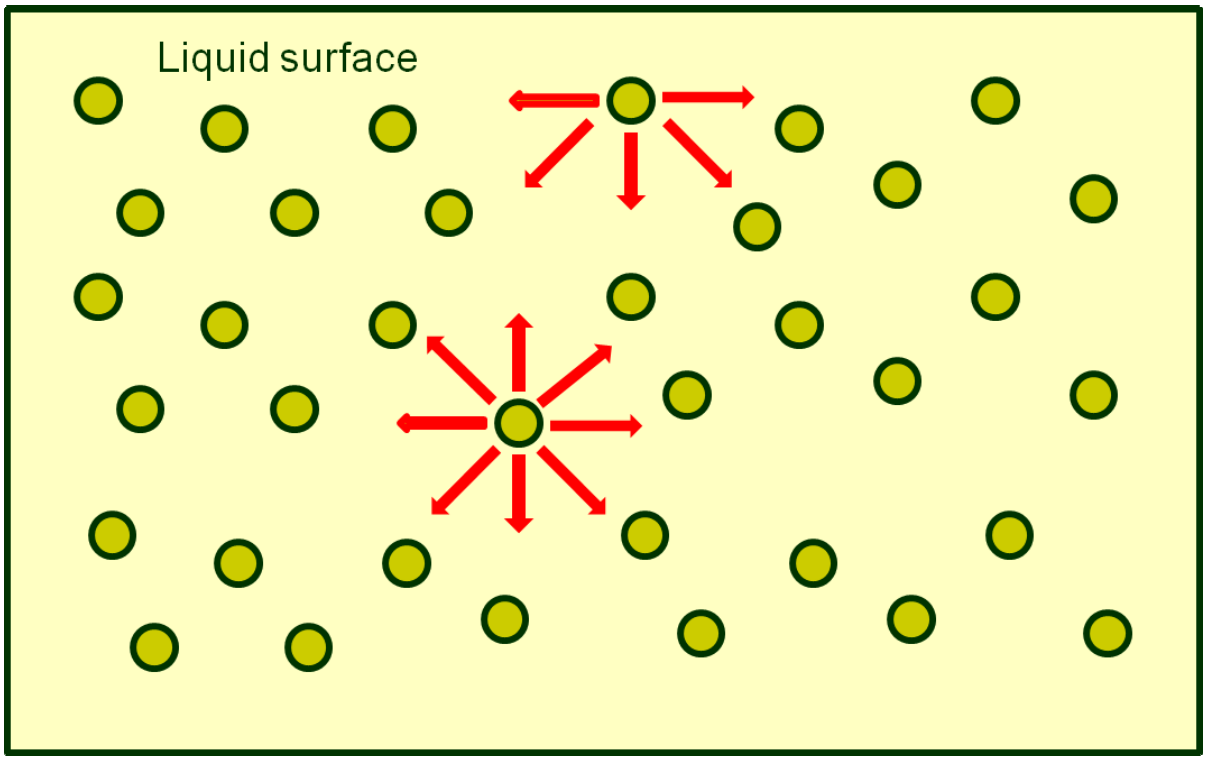

Figure 2.4 Diagram of the forces on two liquid molecules, one in the bulk versus one at the surface. Red arrows highlight attractive forces acting on a given molecule. [60]

A Langmuir-trough (Figure 2.5) is a laboratory instrument used to study the properties of amphiphilic molecules. The instrument can be used to compress the monolayer to create a surface pressure-area per molecule (Π–A) isotherm. With the addition of a dipper and dipping well, a Langmuir trough becomes a Langmuir-Blodgett (LB) trough that allows the deposition of LB-films onto solid substrates. The instrument is named after Irving Langmuir and Katharine Blodgett, who demonstrated it was possible to create monomolecular coatings on surfaces of

water, metal, and glass.[61] Films on water have become known as Langmuir films while films transferred to solid substrates by vertical deposition are known as LB-films.

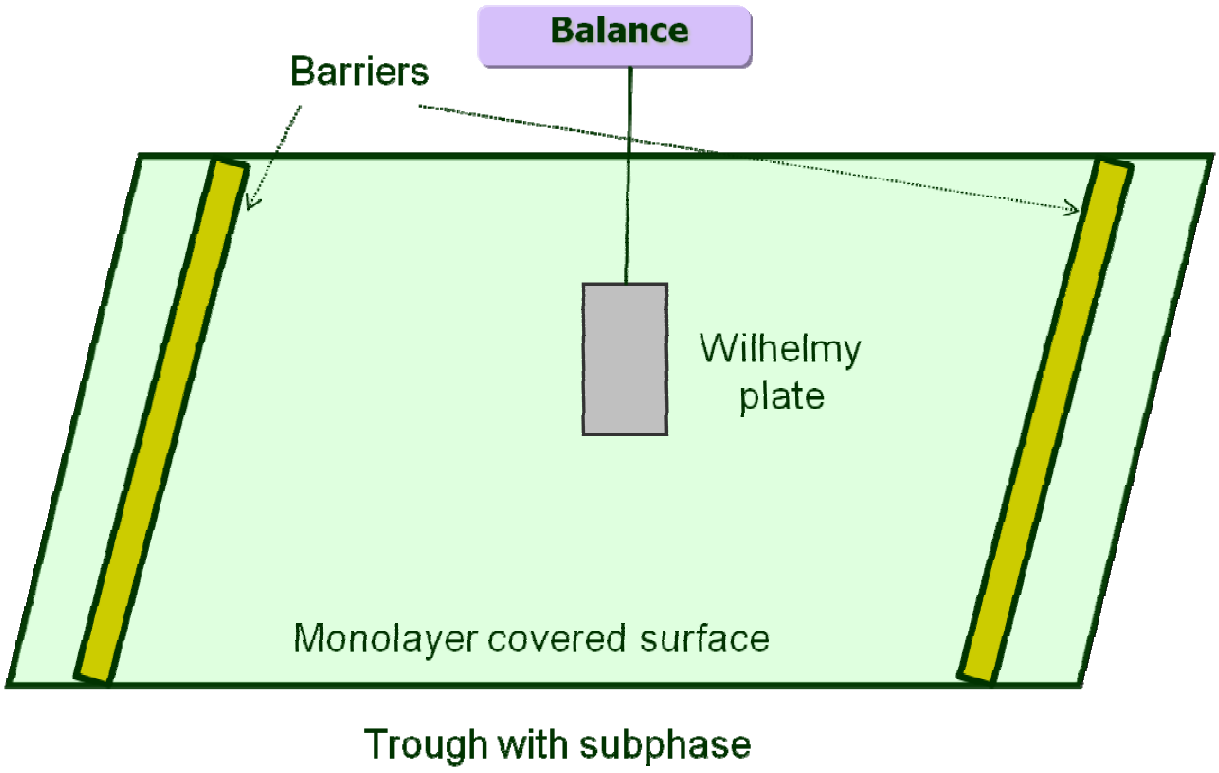

Figure 2.5 Schematic depiction of a Langmuir trough.

Monolayers on water are usually composed of amphiphilic molecules with hydrophilic heads and hydrophobic tails.[62] Most of the early work involving Langmuir monolayers was conducted with long-chain carboxylic acids (such as stearic acid), which contain a polar headgroup anchoring the molecules to the surface of water and a hydrophobic tail preventing dissolution of the molecule. These amphiphilic molecules are also known as surfactants, since they lower the

surface tension of water and allow easier spreading of the liquid on another liquid or solid. As the monolayer molecules are compressed, their steric or repulsive interactions generate a force that counteracts the contracting tendency of the liquid, thereby further lowering the surface tension. This change in the surface tension is usually called the surface pressure, $\Pi = \gamma_{liquid} - \gamma_{film}$, where γ_{liquid} is the surface tension of the neat liquid and γ_{film} is the surface tension of the liquid with a surface film. Π can be considered as the two-dimensional (2D) analog of a three-dimensional (3D) bulk pressure (P). Semi-quantitatively, Π is analogous to a pressure distributed over the thickness of the thin film:

$$P(mN \cdot m^{-2}) = \frac{\Pi(mN \cdot m^{-1})}{thickness(m)} \tag{2.2}$$

Likewise, a 2D lateral modulus, ε_s (to be discussed later):

$$\varepsilon_s = -A\left(\frac{\partial \Pi}{\partial A}\right)_T \tag{2.3}$$

can be considered as an analog of the 3D bulk modulus, K:

$$K = -V\left(\frac{\partial P}{\partial V}\right)_T \tag{2.4}$$

In these studies, the amphiphilic molecules are normally dissolved in a spreading solvent (chloroform, dichloromethane, hexane, etc.). The solvent chosen must have a positive spreading coefficient:

$$S = \gamma_{air/water} - \gamma_{air/solvent} - \gamma_{solvent/water} \tag{2.5}$$

where $\gamma_{air/water}$, $\gamma_{air/solvent}$ and $\gamma_{solvent/water}$ correspond to the interfacial tensions between air and water, air and solvent, and the spreading solvent and water, respectively.[63] Ideally, the spreading solution is deposited onto the surface of the trough to disperse the material in a monomolecular state.

The aqueous subphase is normally placed in a trough made of a hydrophobic material, like Teflon. Π can be monitored by the Wilhelmy plate method (Figure 2.6). In the Wilhelmy plate method, absolute forces acting on the plate, usually made of roughened platinum or filter paper, and partially immersed in the subphase, are measured. Downward forces working on the plate, such as gravity and surface tension, are balanced by upward forces, such as buoyancy, resulting from the displacement of water by the plate, and the pressure sensor itself. These forces are usually measured with a sensitive electrobalance.[64] γ and Π can be calculated from:

$$\Pi = \gamma_0 - \gamma_{film} = \frac{F_{obs,0} - F_{obs,film}}{2(L+t)\cos\theta} \tag{2.6}$$

where γ_0 is the surface tension of the pure liquid and γ_{film} is the surface tension of the film covered surface. $F_{obs,0}$ is the force measured by the Wilhelmy plate when there is no Langmuir film on the surface, $F_{obs,film}$ is the force measured by the Wilhelmy plate when there is a Langmuir film on the surface, L is the length of the plate, t is the thickness of the plate, which is usually small relative to L and is frequently ignored, and θ is the contact angle between the water and the Wilhelmy plate.

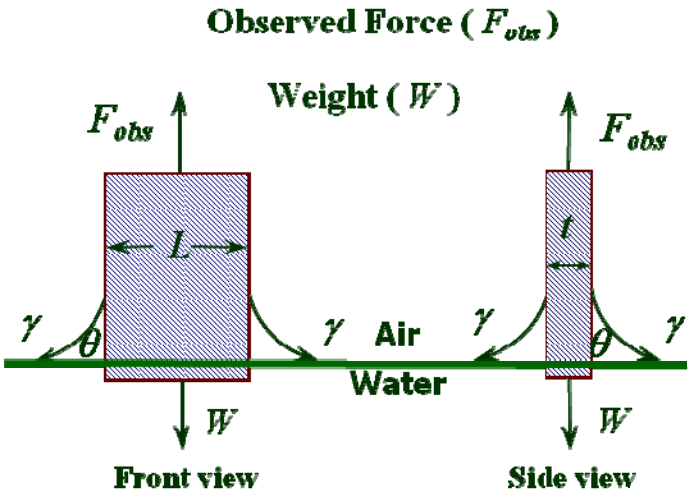

Figure 2.6 Measurement of surface pressure with a Wilhelmy plate.

The contact angle is the angle at which a liquid-gas interface touches a solid surface. When a droplet of liquid is at rest on a solid surface, the contact angle only depends on the material properties of the liquid and the solid. In this thesis, the liquid phase discussed is water unless otherwise mentioned. As shown in Figure 2.7, if a water droplet is on a hydrophilic solid surface, water molecules spread and $\theta < 90^{o}$ is observed. On the other hand, if water droplet is on a hydrophobic solid surface, the contact angle will be in the range of 90^{o} to 180^{o}. Young's equation provides a quantitative description of wetting phenomena:[65]

$$\gamma_{air/solid} - \gamma_{liquid/solid} - \gamma_{air/liquid} \cos\theta = 0 \qquad (2.7)$$

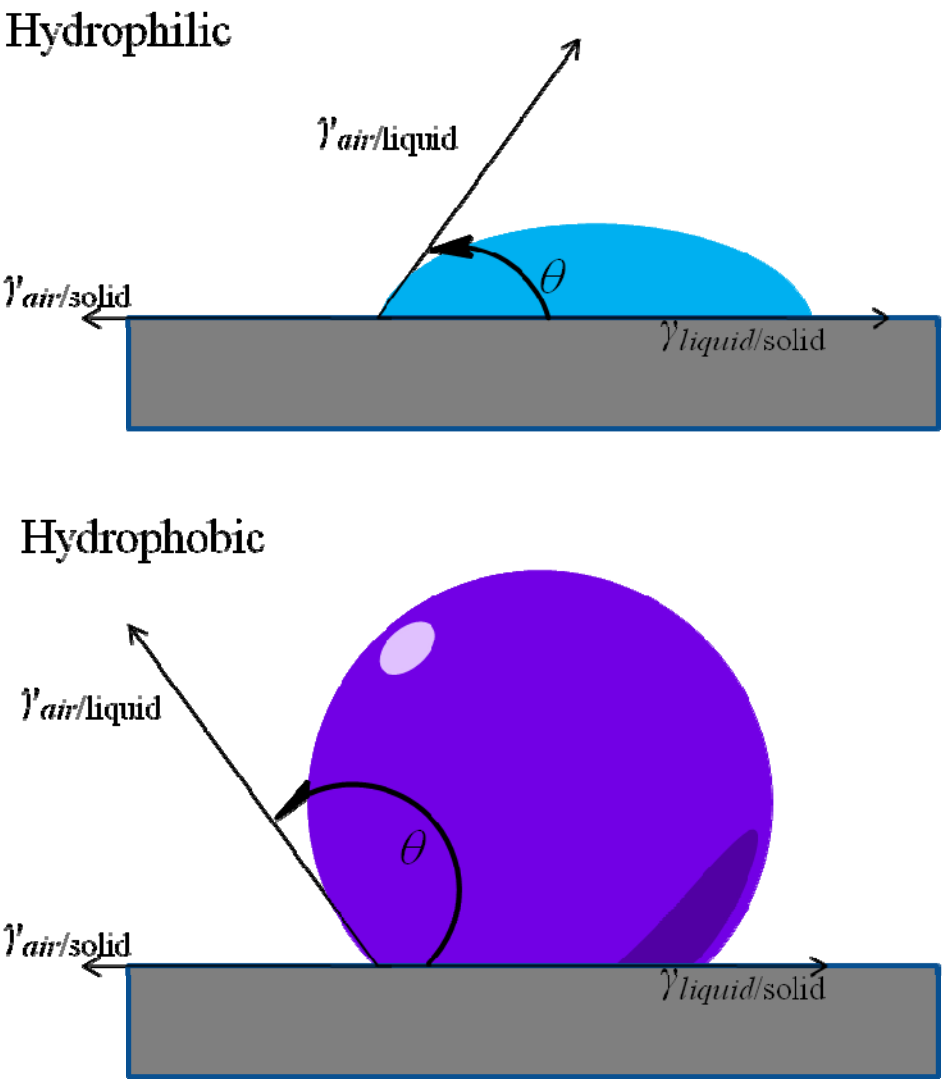

Figure 2.7 Contact angles of water on hydrophilic and hydrophobic surfaces.[66]

Paper or roughened plates often lead to perfect wetting ($\theta = 0^{o}$). Therefore, Equation 2.6 is sometimes written as:

$$\Pi = \gamma_0 - \gamma_{film} = \frac{F_{obs,0} - F_{obs,film}}{2L} \quad (2.8)$$

when t << L.

As seen in Equation 2.8, the surface pressure is the difference in surface tension between a clean or pure liquid (water) surface and a film covered surface. Π as a function of molecular (or monomer) area (*A*) at constant temperature is called a Π–*A* isotherm. Π-*A* isotherms are two-dimensional analogs of three dimensional pressure versus molar volume isotherms. Conceptually, A is nothing more than

$$A = \frac{A_{trough}}{N} \quad (2.9)$$

where A_{trough} is the area of the trough and *N* is the number of molecules on the surface. *A* and *N* are easily calculated by knowing A_{trough}, the concentration of the spreading solvent and the amount of spreading solution spread. Phase changes may be identified by monitoring Π as a function of *A*.

2.5.1.2 Π-*A* Isotherms and Phase Transitions in Langmuir Films

Figure 2.8 is a classic depiction of a Π-*A* isotherm.[67] When *A* is very large, molecules are far apart from each other; therefore the interactions between adjacent molecules are very weak. At this point, the amphiphilic molecules exist in a phase similar to a gas (G). As the molecules are compressed, the molecules will start to interact with each other and repulsive interactions will cause the molecules to start rising off the surface. As a consequence of the compression, liquid-expanded (LE) and condensed (LC) phases can form. A key difference between liquid phases is

their densities. While condensed phases have densities that are similar to bulk liquids and solids, LE phases have densities that are ~ 50% smaller than 3D liquids. The other major difference is long-range order. For the LE phase, the orientation of molecules is random. In contrast, traditional LC phases for molecules structurally similar to fatty acids are a collection of ordered phases with different tilt angles and unique packing which can be differentiated in grazing incidence X-ray diffraction (GIXRD) studies.[47a, 67-68] Prior to monolayer formation, LE and the LC phases can coexist with G to form G/LE or G/LC coexistent phases at $\Pi \sim 0$.[40a]

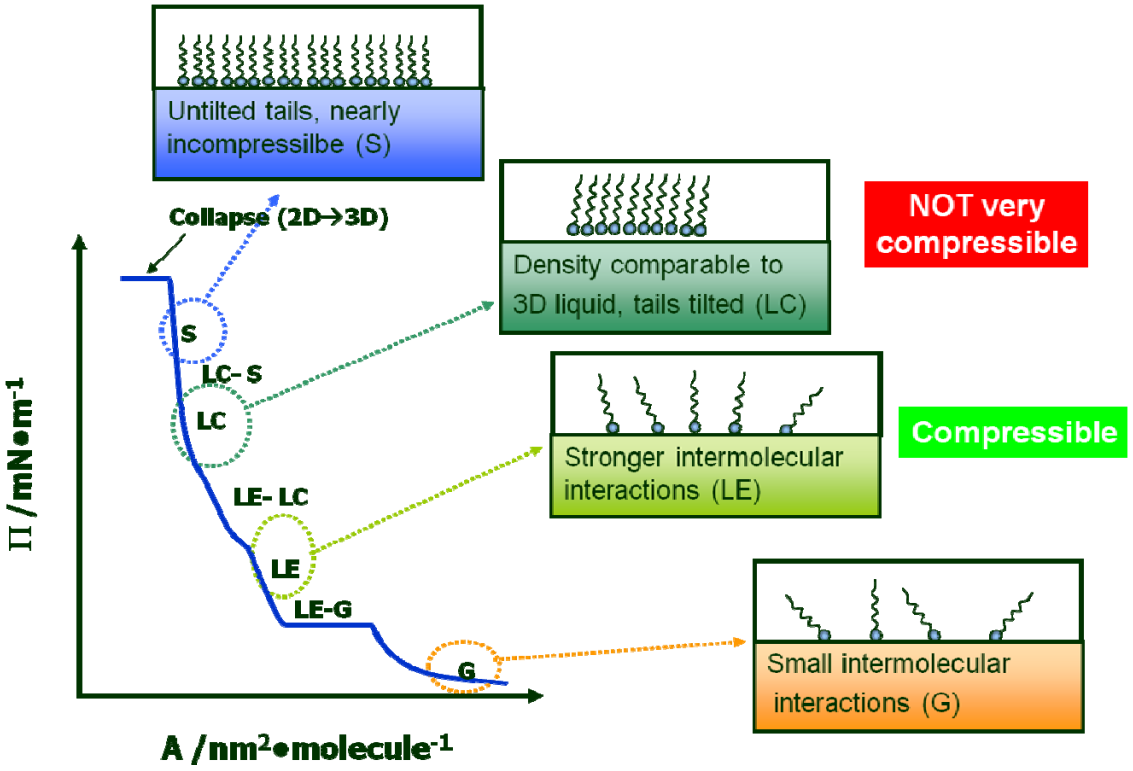

Figure 2.8 A schematic depiction of a Π-*A* isotherm for amphiphilic molecules at the A/W interface. The area scale on the plot roughly corresponds to room temperature values for fatty acids, where A_0 for the condensed phase is in the vicinity of 20 $Å^2 \cdot molecule^{-1}$.[67]

Figure 2.8 is idealized. A film need not exhibit both LE and LC nor solid (S) phases. Special molecules like stearylamine (deposited on water acidified to pH=2.5 with HCl),[69] 4-(((10,12-pentacosadiynoyl)oxy)methyl)pyridine in the presence of Cu^{+2},[70] amino-acid-derivatized diacetylene lipid,[71] *n*-octadecyltrichlorosilane (OTS),[72] phospholipid,[73] poly(L-lactic acid) (PLLA),[30m, 74] exhibit both LE and LC phases. For these systems there is a first order phase transition between the LE and LC phases leading to phase coexistence.[75] As already noted, GIXRD studies showed the traditional LC phase was actually a collection of different phases that could be distinguished on the basis of their long-range order and average tilt angles. For example, fatty acids are known to form up to 9 condensed phases.[76] One of these is the solid phase (S), where the tilt angle is zero. Transitions between other LC phases and S are manifested as kinks rather than plateaus and tend to be second-order transitions.[40c] At sufficiently high Π, all monolayers undergo collapse transitions.[40a] Whether this transition entails the formation of multilayer structures (Figure 2.9) or dissolution into the bulk subphase is dependent upon the molecular structure.

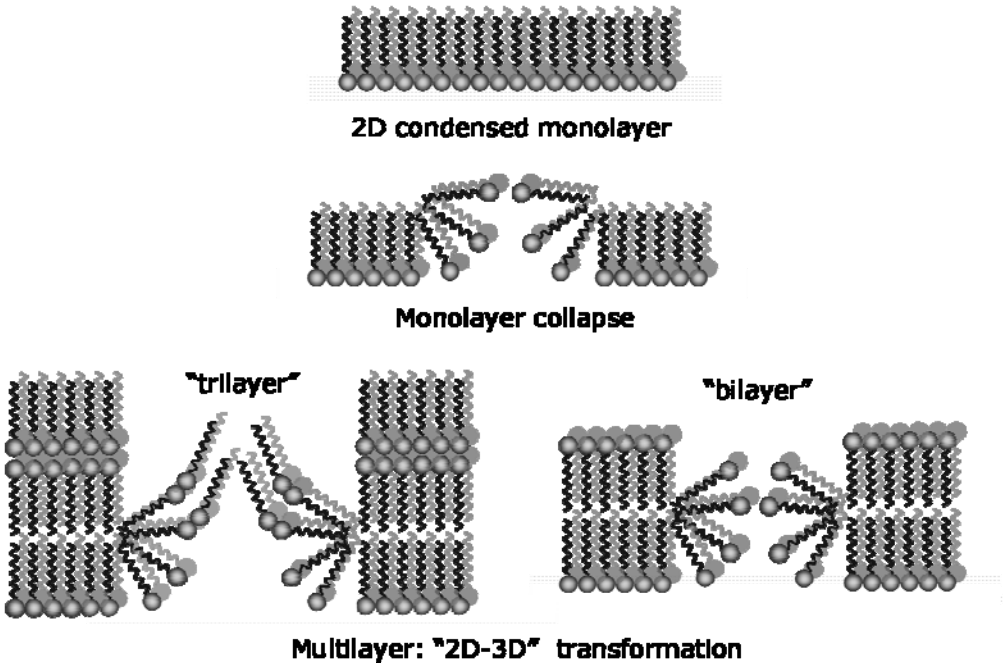

Figure 2.9 A schematic depiction of a Langmuir film undergoing collapse from a monolayer into multilayer domains.

As noted in the previous paragraph, monolayer phase transitions can be either first-order (common phase transition from undergraduate thermodynamics) or second-order (much rarer).[40c] In general, a transition for which the first derivative of the chemical potential with respect to temperature is discontinuous is classified as a first-order transition. As a result, the densities of the two phases are discontinuous and a plateau in the Π-*A* isotherm is observed. In contrast, for second-order transitions, the first derivative of the chemical potential with respect of temperature is continuous but the second derivative is discontinuous. As noted, G-LE, G-LC, and LE-LC phase transitions are first-order. However, Π-*A* isotherm studies may be ambiguous because of

kinetic effects and the influence of line tension.[77] For example, the nature of the LE-LC transition of *n*-pentadecanoic acid was argued for years and scientists only reached agreement after BAM and fluorescence microscopy showed the nucleation and growth of the LC phase.[40c]

As one may notice in Figure 2.8, at the end of solid phase, molecules are no longer compressible and after a so-called "collapse" transition 3D structures are formed as depicted in Figure 2.9 or dissolution of parts of the Langmuir film occurs. The surface pressure corresponding to collapse is defined as the "collapse pressure" ($\Pi_{collapse}$), which indicates the limit of the stability of a 2D monolayer. Normally, the value of $\Pi_{collapse}$ is related to the barrier speed (compression rate) and the history of the film. A schematic diagram (Figure 2.9) demonstrates the process of collapse. As seen in Figure 2.9, compression of amphiphilic molecules with a constant force after the formation of a stable 2D monolayer ultimately pushes some molecules out of the monolayer away from the water subphase. During the transition, the hydrophobic tails of the upper molecules will interact with hydrophobic tails of the molecules in the bottom layer. However, the exact multilayer structure depends upon specific materials with most molecules tending to form different multilayer structures.[57d]

2.5.2 Langmuir-Blodgett (LB) Technique

A LB-film contains one or more monolayers of a material deposited onto a solid substrate from a Langmuir film. A LB-film is formed by passing a solid substrate through the A/W interface of a Langmuir film. For special materials a monolayer is added with each immersion or emersion step, resulting in films with precisely controlled thicknesses. The procedures for preparing LB-films and measuring Π–*A* isotherms are similar.

Several transfer modes for the deposition of molecules onto a substrate are depicted in Figures 2.10 and 2.11. For Y-type deposition onto a hydrophobic substrate (Figure 2.10), the substrate is lowered into the subphase and the molecules are oriented with their hydrophobic tail towards the substrate for the first layer. On the upstroke, the polar hydrophilic headgroups of the molecules on the surface are attracted to the outward facing headgroups that have already been deposited on the substrate. Continuous upstrokes and downstrokes can yield a multilayer LB-film. With an even number of layers, the hydrophobic tails face the air in the final layer. For the less common types of transfer, X-type (Figure 2.11b) and Z-type (Figure 2.11c) deposition, molecules are only deposited on the downstroke or upstroke, respectively. In contrast to Y-type deposition where molecules are deposited into an alternating superstructure, X- and Z-type transfer yield mutilayer films where each molecule in every layer theoretically has the same orientation. X-ray diffraction studies of multilayers prepared via X-type deposition usually show that a bilayer structure exists. As such, molecules rearrange during or after transfer to form a more energetically favorable conformation.[1b, 78] Normally, these conformations have hydrophobic tails of the final layer oriented toward air.

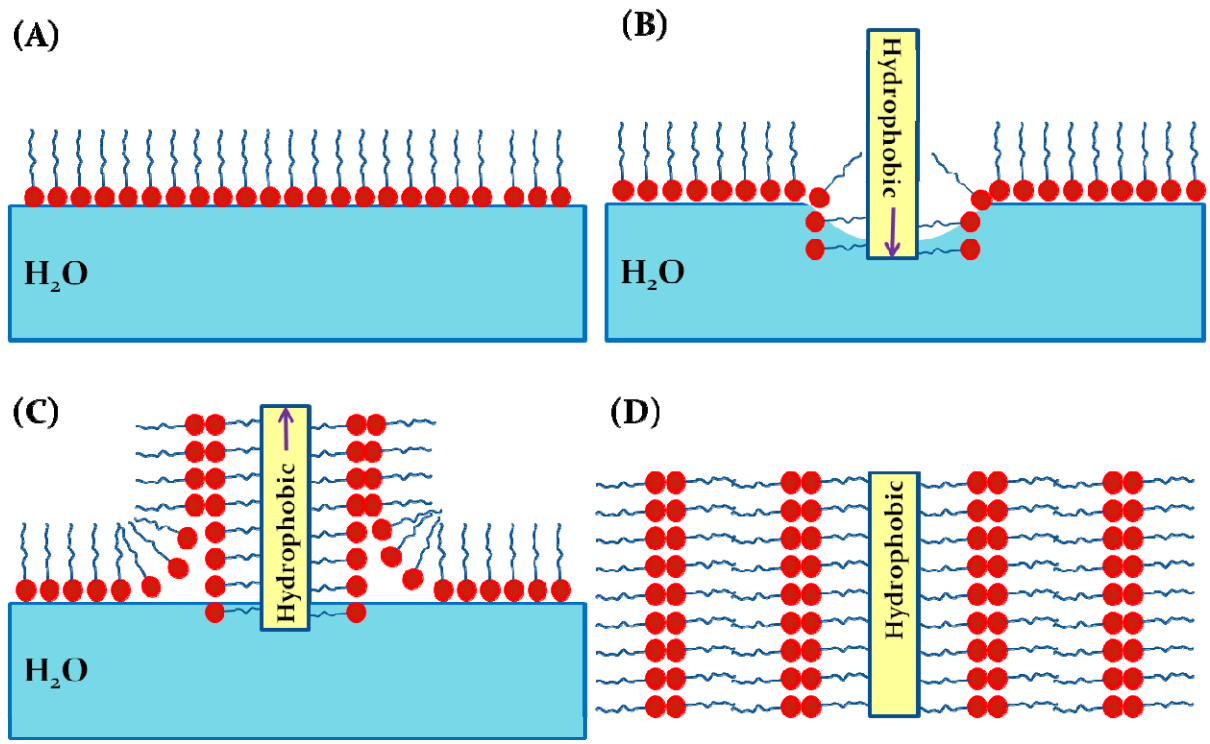

Figure 2.10 Y-type deposition of LB-multilayers onto a hydrophobic substrate: (A) formation of a stable Langmuir monolayer at the A/W interface by compression, (B) first immersion of a hydrophobic substrate, (C) first withdrawal, and (D) LB-multilayers with head-to-head and tail-to-tail configurations.[79]

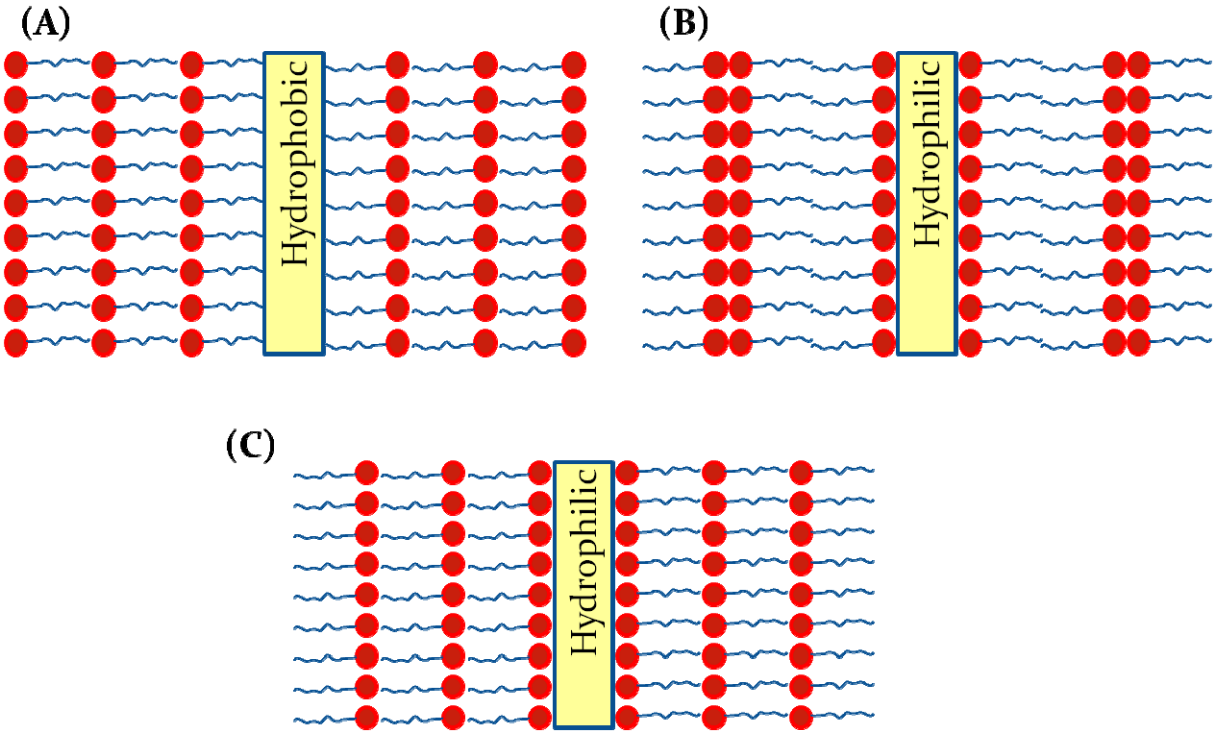

Figure 2.11 Structures of LB-multilayers: (A) X-, (B) Y-, and (C) Z-type. The structural difference between Figure 2.10 D and (B) reflects the fact that (B) depicts a hydrophilic substrate. X- and Z-type depositions do not normally guarantee that the multilayers will have the corresponding structure as rearrangement with time after deposition is possible.[80]

2.5.3 Brewster Angle Microscopy (BAM)

Π–*A* isotherms have limitations with respect to determining phases and phase transitions in Langmuir monolayers.[1b] Therefore, BAM and fluorescence microscopy are usually used to visualize the domain formation and growth during phase transitions in Langmuir films. A fundamental difference between the two techniques is that BAM is label-free, whereas a fluorescent probe must be added to most systems to do fluorescence microscopy. As the Esker

group primarily uses BAM, I will discuss this technique further. In addition to the ability of BAM to study phase transitions, BAM can even reveal *in situ* morphological information about the texture and homogeneity of Langmuir films.[81]

When light passes through an interface between two media, some of the light will be reflected at the boundary while the remainder will be refracted. However, at a specific angle (Figure 2.12), *p*-polarized light is not reflected. This special incident angle is called Brewster's angle, θ_B, which is named after the Scottish physicist, David Brewster.

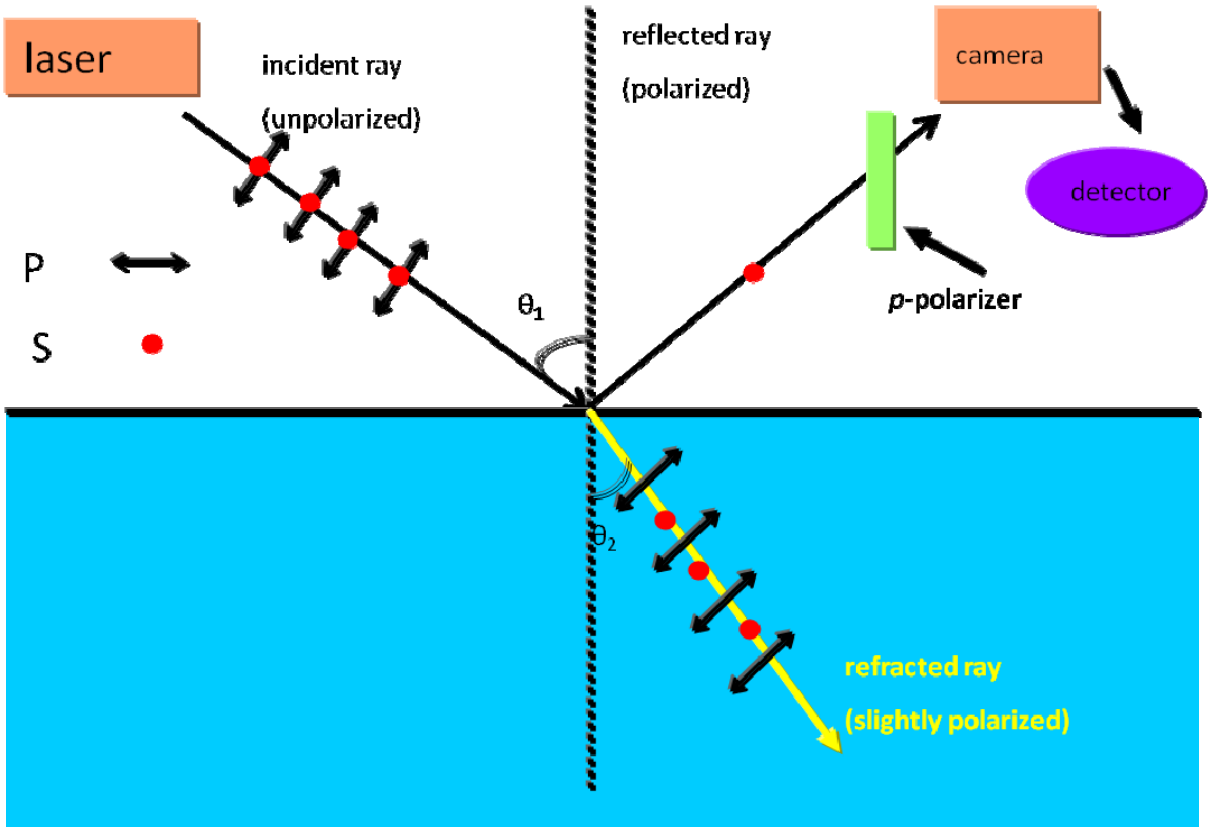

Figure 2.12 Schematic depiction of the reflection of unpolarized light at Brewster's angle.

Different components of linearly polarized light are defined according to their orientation relative to the plane of incidence (the surface of the paper in Figure 2.12). By convention, the electric field vector of *p*-polarized light is parallel to the plane of incidence, while the electric field vector of *s*-polarized light is perpendicular to the plane of incidence.[82] In Figure 2.12, *p* stands for *p*-polarized light and *s* represents *s*-polarized light. θ_1 is the angle of incidence and the angle of reflection, and θ_2 is the angle of refraction. Brewster's angle (θ_B) can be deduced from Snell's law:

$$n_1 \sin(\theta_1) = n_2 \sin(\theta_2) \tag{2.10}$$

where n_1 and n_2 are the refractive indices of medium *1* and *2*, respectively, and θ_1 and θ_2 are the angle of incidence and angle of refraction, respectively. At Brewster's angle, $\theta_1 + \theta_2 = 90°$. For the A/W interface, Brewster's angle corresponds to $\theta_1 = \theta_B = 53.1°$.

Brewster's angle can also be deduced from Fresnel's laws, which describe the reflectivity (R) of light as a function of incident angle and polarization. The reflectivity of *s*-polarized light (R_s) and *p*-polarized light (R_p) can be calculated from Equations 2.11 and 2.12, respectively:

$$R_s = \left(\frac{n_i \cos\theta_i - n_r \cos\theta_r}{n_i \cos\theta_r + n_r \cos\theta_i} \right)^2 = \frac{\sin^2(\theta_r - \theta_i)}{\sin^2(\theta_r + \theta_i)} \tag{2.11}$$

$$R_p = \left(\frac{n_r \cos\theta_i - n_i \cos\theta_r}{n_i \cos\theta_r + n_r \cos\theta_i} \right)^2 = \frac{\tan^2(\theta_i - \theta_r)}{\tan^2(\theta_r + \theta_i)} \tag{2.12}$$

where subscripts *i* and *r* represent incidence and refraction, respectively.

For an ideal isotropic interface (Figure 2.13), R_s increases continuously with increasing incident angle while R_p exhibits a minimum, where the sum of θ_i and θ_r approach 90° causing $\tan(\theta_r + \theta_i) \rightarrow \infty$. For the case of Langmuir films where a sample is spread onto the surface of water, the thickness of the film and refractive index of the sample will cause some light to reflect at θ_B for the A/W interface. Under these conditions:[81a]

$$R_p(\theta_B) = R_s(\theta_B)\overline{\rho_B}^2 \tag{2.13}$$

where $R_p(\theta_B)$ and $R_s(\theta_B)$ represent the reflectivity of a Frensnel interface at Brewster's angle for *p*- and *s*-polarized light, respectively, and $\overline{\rho_B}$ is the average ellipticity at Brewster's angle which is defined as:

$$\overline{\rho_B} = \frac{\pi}{\lambda}\frac{\sqrt{n_2^2 + n_1^2}}{n_2^2 - n_1^2}\int_{-\infty}^{+\infty}\frac{[n(z)^2 - n_1^2][n(z)^2 - n_2^2]}{n(z)^2}dz \tag{2.14}$$

where λ is the wavelength of the incident light, and *z* within the integral indicates the distance from the average interfacial position, $z = 0$. If we can make the approximation that the thin film has a refractive index profile *n(z)* that is uniform, the reflected intensity (I_r), at Brewster's angle will be proportional to the square of film thickness, h^2:

$$I_r = I_i R_p(\theta_B) \propto \overline{\rho_B}^2 \approx \left[\pi\frac{h}{\lambda}\frac{\sqrt{n_2^2 + n_1^2}}{n_2^2 - n_1^2}\frac{[n^2 - n_1^2][n^2 - n_2^2]}{n^2}\right]^2 \tag{2.15}$$

For any particular system, like the A/W interface, n_1 and n_2 are constants. Therefore, the thickness of the film can be obtained.

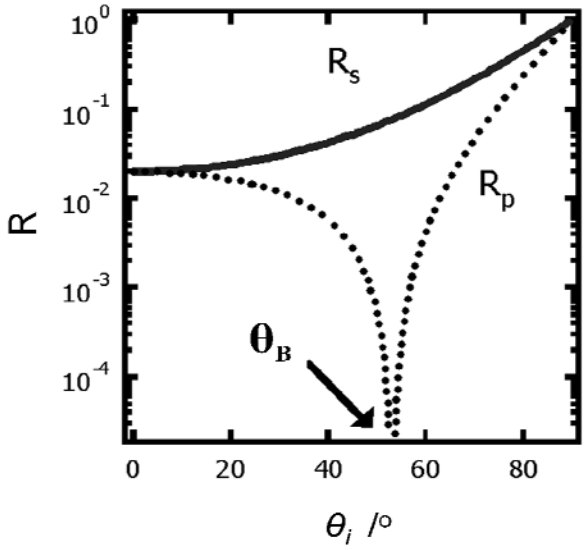

Figure 2.13 Reflectivity at different incident angles for *s* (solid line) and *p* (dotted line) polarized light.

Figure 2.14 is a schematic depiction of a BAM with a laser source, a Glan-Thompson polarizer with the electric field vector parallel to the plane of incidence, and a light detector (such as a charge coupled device (CCD) camera). Since the light source is required to have a high intensity and a well defined polarization (*p*) for uniform illumination, a laser is the only reasonable choice. A polarizer is a device that converts a beam of light of undefined or mixed polarization into a beam with well-defined polarization. Depending on various applications, there are basically two types of polarizers: linear polarizers and circular polarizers. Linear polarizers can be further divided into two categories: absorptive polarizers, where the filtered polarization states are absorbed and beam-splitting polarizers, where the unpolarized beam is split into two beams with opposite polarization states. Beam splitting polarizers are used for BAM. In traditional BAM, the polarizer is placed in the path of the incident beam to polarize the radiation

in the *p* direction before it meets the surface. As the technique developed, the polarizer was moved to the path of the reflected beam to remove residual *s*-component before any reflected *p*-radiation reaches the CCD detector. This approach was found to enhance resolution.

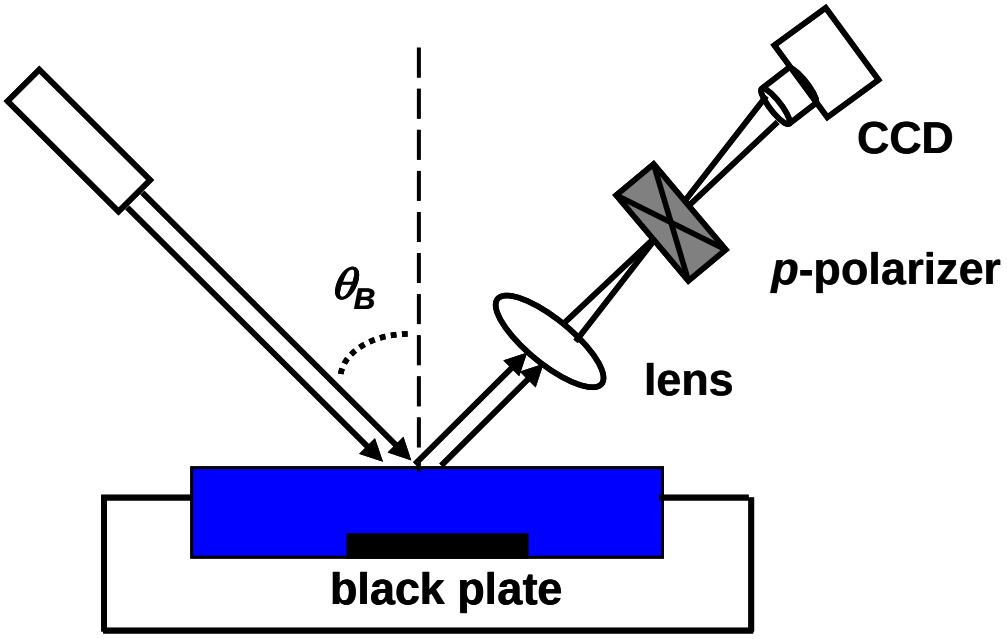

Figure 2.14 Schematic depiction of a BAM. A *p*-polarized laser beam is incident on the water surface at Brewster's angle for water (θ_B = 53.1°). Light reflected by the interface is detected by a CCD camera. A *p*-polarizer is placed in the path of the reflected beam to remove residual s-polarized light.

In the experiment, a tilted black glass plate is used underneath the water surface to prevent the light from randomly scattering from the subphase and trough. A set of lenses is used to direct the reflected beam to a CCD camera for imaging. Theoretically, nothing can be observed on the

monitor when no film is present at the interface because *p*-polarized light is not reflected at Brewster's angle, while *s*-polarized light is blocked by the *p*-polarizer. However, once a sample is spread onto the A/W interface, Brewster's angle changes as the refractive index of the sample differs from water. Thus, even a trivial alteration results in some reflected *p*-polarized light reaching the CCD camera. Therefore, BAM is widely considered as a sensitive instrument for detecting and studying phase transitions, phase separation, crystallization, aggregation, etc, when it is coupled with Π-*A* isotherms.[30b, c, 30i, j, 83]

2.6 Phase Diagrams of Langmuir Monolayers

2.6.1 Monolayer Phases

Figure 2.8 describes the packing stages of amphiphilic molecules at the A/W interface. However, scientists studied fatty acids, classic and traditional amphiphiles, from a different perspective prior to the 1980s. For example, both gas (G) and liquid-expanded (LE or L_1) phases can be considered as expanded phases while both liquid condensed (LC) and solid (S) phases can be considered as condensed phases. Accordingly, some argued that liquid-condensed (LC or L_2) is actually a 2D solid rather than liquid phase. Stallberg-Stenhagen and Stenhagen obtained a surface pressure-temperature phase diagram by the study of behenic acid. Solid phase was even divided into S and LS while L_2 was divided into L_2 and L_2'.[84] The completion of the phase diagrams for fatty acids was not possible until FM and BAM were invented. With the help of optical instruments, the nature of the different condensed phases was explored with respect to the conformation of molecules. An example is shown in Figure 2.15. Experiments with XRD drew the same conclusion and introduced more condensed phases. According to the tilt angles, their

azimuths could be differentiated into toward nearest neighbor (NN), toward next-nearest neighbor (NNN), and untilted hexagonal (U) (Table 2.1).

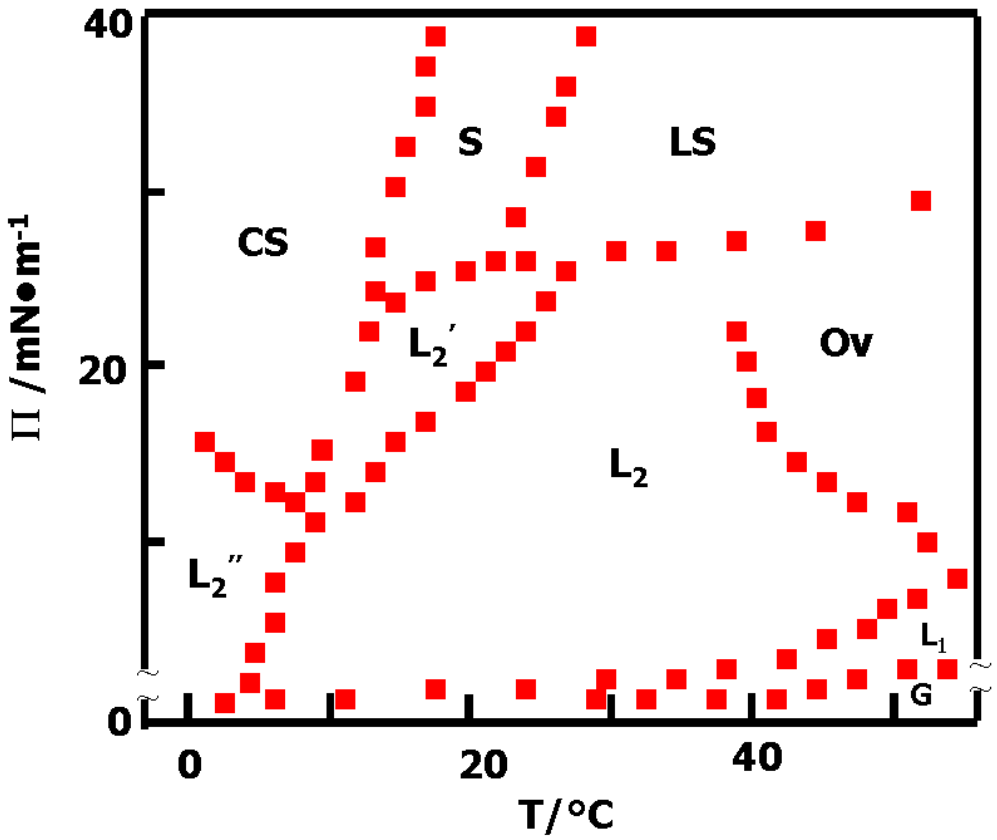

Figure 2.15 Experimental Π -*T* phase diagram for an eicosanoic acid Langmuir film, which was modified from the original source.[85]

Table 2.1 A summary of condensed phases of Langmuir monolayer.

	Liquid Condensed				Superliquid		Solid	
Notation	L_2	L_2'	L_2''	O_v	LS_I	LS_{II}	S	CS
Tilt azimuth	NN	NNN	NN	NNN	U	U	U	U

NN = tilt to the nearest-neighbor molecule, NNN = tilt to the next-nearest neighbor, U = untilted hexagonal.[76]

2.6.2 Chain-length Dependence of Monolayer Phase Diagrams

Amphiliphilic molecules, such as fatty acids, have been thoroughly studied at the A/W interface through Langmuir film studies. In the experiments, the temperature is controlled. Therefore, the accessible temperature window is narrow since water freezes below 0 ^oC and evaporation interferes with the stability of the film above 45 ^oC. In this window, fatty acids with shorter chains (less than C_{13}) are soluble and lead to Gibbs monolayer formation. Alcohols, esters, and acetates may behave similarly if they are structurally close to fatty acids.[86] A chain-length dependent phase diagram is depicted in Figure 2.16.

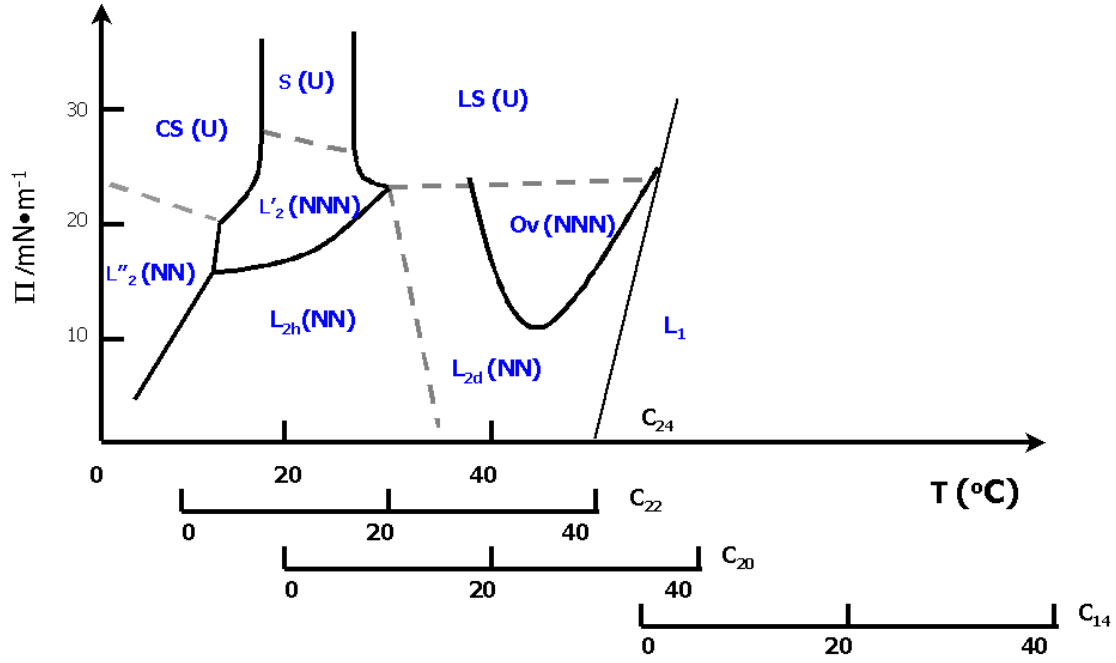

Figure 2.16 The chain-length dependence of the monolayer phase diagram for fatty acids ($C_{14}-C_{24}$). Solid lines exhibit first-order transitions and dashed lines indicate second-order transitions.[40c, 87]

2.7 Introduction to Polyhedral Oligomeric Silsesquioxanes (POSS)

Polyhedral oligomeric silsesquioxanes are more commonly known as POSS. These compounds have attracted substantial academic interest for many years as hybrid materials.[7b-d, 88] The most common POSS derivatives are the closed-cage comprised of eight silsesquioxane units (T_8) and the seven-unit (T_7) open cage trisilanol POSS (Figure 2.17). T_8 and T_7 POSS are composed of a relatively hard 0.5 nm diameter inorganic core and that makes the overall

diameter of the molecules 1 to 3 nm. While octaalkyl-POSS derivatives are normally hydrophobic, many open cage trisilanol-POSS derivatives are amphiphilic. Since the octaalkyl-POSS can be synthesized from a trisilanol-POSS, opportunities to build molecules with different rigidities and amphiphilic properties in nanoscale dimensions exist.[88a] POSS has attracted considerable interest for high-temperature nanocomposites, space-survivable coatings,[7d] low-*k* dielectric materials,[88b] liquid crystalline polymers,[88c] and catalysts.[7c] Varieties of POSS-based polymers have been made and have shown interesting properties.[7b, 88d-f] Such hybrid materials have properties between inorganic and organic compounds with respect to glass transition temperature, mechanical strength, thermal and chemical resistance, and ease of processing.[88g]

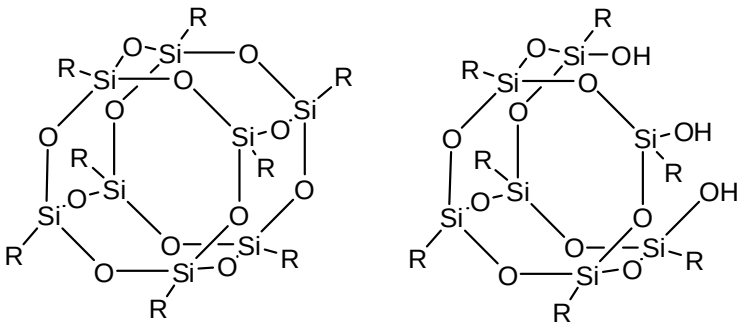

Figure 2.17 Two most common types of POSS. R = alkyl group.

2.7.1 POSS Cage Synthesis

A silsesquioxane has a general empirical chemical formula $RSiO_{1.5}$, in which R is hydrogen or an alkyl, alkene, aryl, or arylene group. However, substituents are not necessarily the same on every Si atom. Frequently, one substituent on closed-cage POSS derivatives has a more branched arm that ends with a functional group, such as an alcohol, amine, alkene, etc.

Synthesis of the POSS cages requires hydrolytic condensation. POSS derivatives have been formed from trialkoxysilanes and trichlorosilanes ($RSiX_3$) (Scheme 2.1 and 2.2).[89] In order to obtain different POSS derivatives, the reaction rate is controlled with a catalyst or by the choice of solvent.

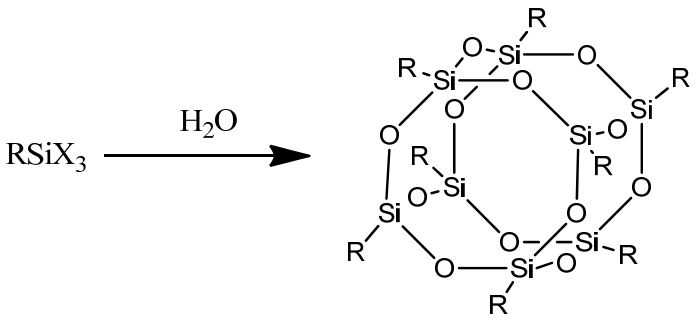

Scheme 2.1 Scheme for synthesizing closed-cage POSS derivatives.[89]

Problems with Scheme 2.1, where R is usually a chemically stable organic substituent or H, include the need to carefully control the initial concentration of the monomer and catalyst, the temperature, the rate of addition of water, etc.[89-90] The character of the substituent X and solubility of polyhedral oligomers can also influence the rate and distribution of products for the reaction in Scheme 2.1.[88a] For example, higher temperature tends to favor polymer formation; hence room temperature reactions under mild conditions are normally preferred. Furthermore, dropwise addition of H_2O is suggested to control the concentration of silanol groups to avoid extensive side reactions (such as branched oligomers and linear polymers). Different solvents (such as cyclohexane, benzene, methanol, and acetone) and catalyst (either HCl or KOH) have been used depending on the organic substituents.[91]

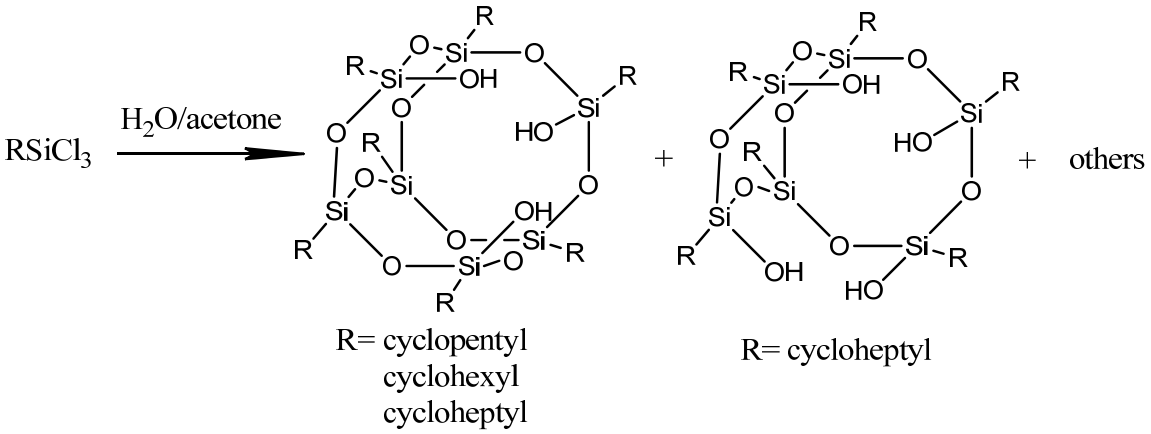

Scheme 2.2 Scheme for synthesizing open-cage POSS derivatives.[89]

Open cage trisilanol POSS derivatives are one example of a series of incompletely condensed POSS cages. Here, an open cage POSS means that at least one hydroxyl group exists with at least one missing vertex. Feher and his coworkers[92] have designed a method to control the reactivity of the monomer $RSiX_3$ to synthesize open-cage POSS (Scheme 2.2). By introducing acetone, it was possible to slow the hydrolytic condensation when R was a cyclopentyl or cyclohexyl group. However, these reactions usually took a few days and the yields were relatively low (< 30%). Later, strong acids proved to be effective for the selective cleavage of completely condensed octameric polyhedral silsesquioxane ($R_8Si_8O_{12}$) cubes (Scheme 2.3).[93]

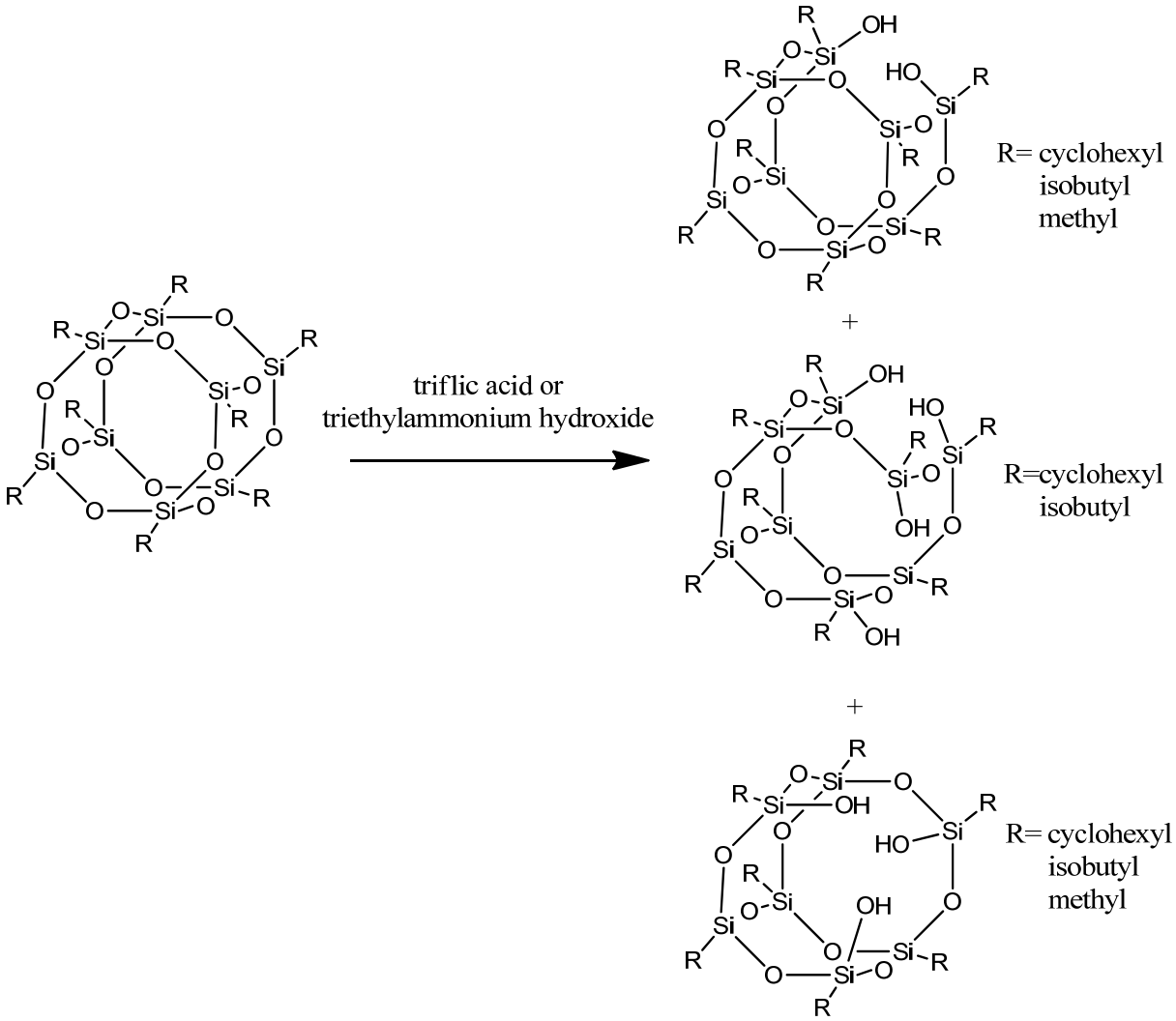

Scheme 2.3 Synthesis of incompletely condensed POSS cages from the cleavage of completely condensed POSS in the presence of an acid or base catalyst.

2.7.2 Synthesis of POSS-based Polymers

As an organic/inorganic hybrid material, POSS is of interest for blends with polymers or dendrimers. These blends tend to exhibit increases in use temperature, reductions in flammability, better oxidation resistance, and surface hardening.[94] One major advantage for POSS in these

potential applications is the ability to tailor the POSS cage in order to control blending with polymers.[95] The physical properties of these hybrid materials depend on the miscibility of the host polymer and the POSS derivative.[96]

Polyaddition and polycondensation are common methods for the synthesis of POSS-based polymers.[97] One interesting study used epoxy-functionalized cubes, octaaminophenylsilsesquioxane (OAPS), polyaminophenylsilsesquioxane (PAPS), octa(dimethylsiloxypropylglycidyl ether) silsesquioxane (OG), diaminodiphenylmethane (DDM), and diglycidyl ether of Bisphenol A (DGEBA) to create nanocomposites.[98] For the resulting nanocomposite, it was believed that the rigidity, processability and thermomechanical properties could be improved by adjusting the architecture of the organic tethers between vertices.[99] Many examples of asymmetric POSS derivatives derived from an octafunctional-POSS have been studied.[88c, 100]

2.7.3 Physical Properties and Applications of POSS

As a hybrid material, POSS is a bridge between ceramics and polymers. Compared to conventional organic and inorganic materials, it has intermediate properties with respect to oxidation resistance, toughness, density and ease of processing. POSS has tremendous potential as a space survival material based on its low density, reduced heat evolution and good oxidation resistance, and as case insulation for solid rocket engines and ducting for liquid rocket engines.[101] In order to achieve these properties, control of molecular weight and composition led to the modification of open-caged POSS derivatives to create polymerizable and crosslinkable

units for the development of model silica surfaces,[102] building blocks for network solids,[103] and ligands.[104]

The morphology of POSS-based polymers has attracted greater attention. Crystalline polymers, such as polynorbornene[105] and poly(lactide-co-glycolide) (PLGA)[106] were introduced into POSS segments. Compared to the earlier work done on block copolymers with amorphous POSS segments,[107] the nanoconfinement effect within microphase-separated domains highly depended upon the state of the POSS. The POSS-rich domains mainly acted as crosslinks, however, "pseudo-network" systems were sometimes observed during physical aging experiments.[108] Many techniques have been used to examine the morphology of POSS-containing copolymers. For example, wide-angle X-ray scattering (WAXS) was used to investigate POSS-based ABA triblock microstructures[109] and the intermediate ordering of POSS homopolymer.[110] Transmission electron microscopy (TEM) and dynamic mechanical analysis (DMA) were also used to study phase-separated microstructures with different POSS components.[109]

Open cage POSS derivatives are surface active and closed-cage POSS derivatives can also be coupled with hydrophilic polymers to create amphiphilic materials. These new materials usually exhibit an affinity for interfaces, which makes them potential compatibilizers and dispersion aides. POSS is also an excellent model nanofiller with well-defined size. The Esker group has demonstrated an increase in the T_g of polymeric thin films with small amounts of trisilanolphenyl-POSS (TPP).[111] Meanwhile, different filling behaviors based on different POSS derivatives were also examined at the A/W interface. For example, when trisilanolisobutyl-POSS (TiBP) is benlded with polydimethylsiloxane (PDMS), TiBP was believed to platicize the blend films at low surface pressure, thereby reducing mechanical strength.[112] TPP could also form thin

film bilayers and thin film blends with polymers leading to interesting morphological behavior.[30o, 113] For example, thin film bilayers of polystyrene (PS) and TPP were studied with respect to morphological evolution during annealing at elevated temperatures. The dewetting mechanism in work by Paul *et al.* was different from similar studies with polymer/polymer bilayers.[114] These results indicate that dewetting of both the upper TPP and the lower PS layers led to the exposure of the silicon substrate.[113a]

Topological constraints in POSS-based polymers also affect physical properties. For example, molecular motion associated with network junctions slowed when the weight percentage of epoxy-POSS increased in the blend with diglycidyl ether of bisphenol A (DGEBA) and 1,4-butanediol diglycidyl ether (BDGE).[115] Fu *et al*. increased the rubbery plateau modulus by introducing trisilanolphenyl-POSS into the tetraglycidyl diamino diphenyl methane / 2-methyl-1,5-pentadiamine (TGDDM) / (MPDA) system.[116]

2.7.4 Conformational Analysis of Closed-Cage POSS Derivatives

In a previous study, (3-hydroxypropyl)heptaisobutyl-POSS (POSS-OH) was added to an isocyanate in the presence of triethylamine[117] to give a triester (P*Al*TE) (Scheme 2.4). As POSS-OH and P*Al*TE are amphiphilic, surface pressure–area per molecule (Π-A) isotherms were used to probe the quasi–two-dimensional thermodynamic properties of these materials at the A/W interface.

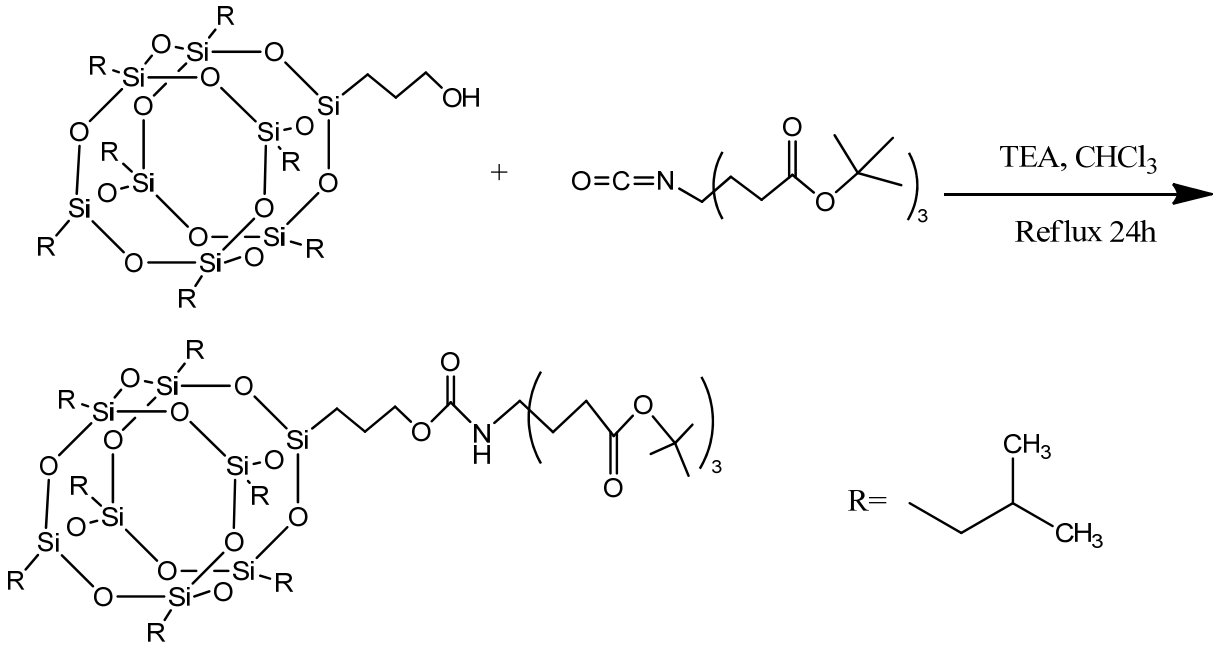

Scheme 2.4 Synthesis of P*AI*TE

Figure 2.18 has Π-*A* isotherms for POSS-OH and P*AI*TE at the A/W interface at 22.5 ^{o}C. A Π-*A* isotherm for trisilanolisobutyl-POSS (TiBP)[83b] is also provided on Figure 2.18 as a reference. The Π-*A* isotherm for POSS-OH reveals a lift-off surface concentration ($A_{lift\text{-}off,}$ where Π increases from zero) around $A_{lift\text{-}off}$ ~185 Å^2•molecule^{-1}, followed by a long plateau until lower *A* (~ 125 Å^2•molecule^{-1}) at low Π (~ 1 mN•m^{-1}). This smaller *A* value corresponds to the limiting area (A_0), which was obtained by extrapolating the steepest portion of the Π-*A* isotherm back to Π = 0. At a relatively low collapse pressure (Π_c ~ 5 mN•m^{-1}), the POSS-OH film collapses into multilayer domains.

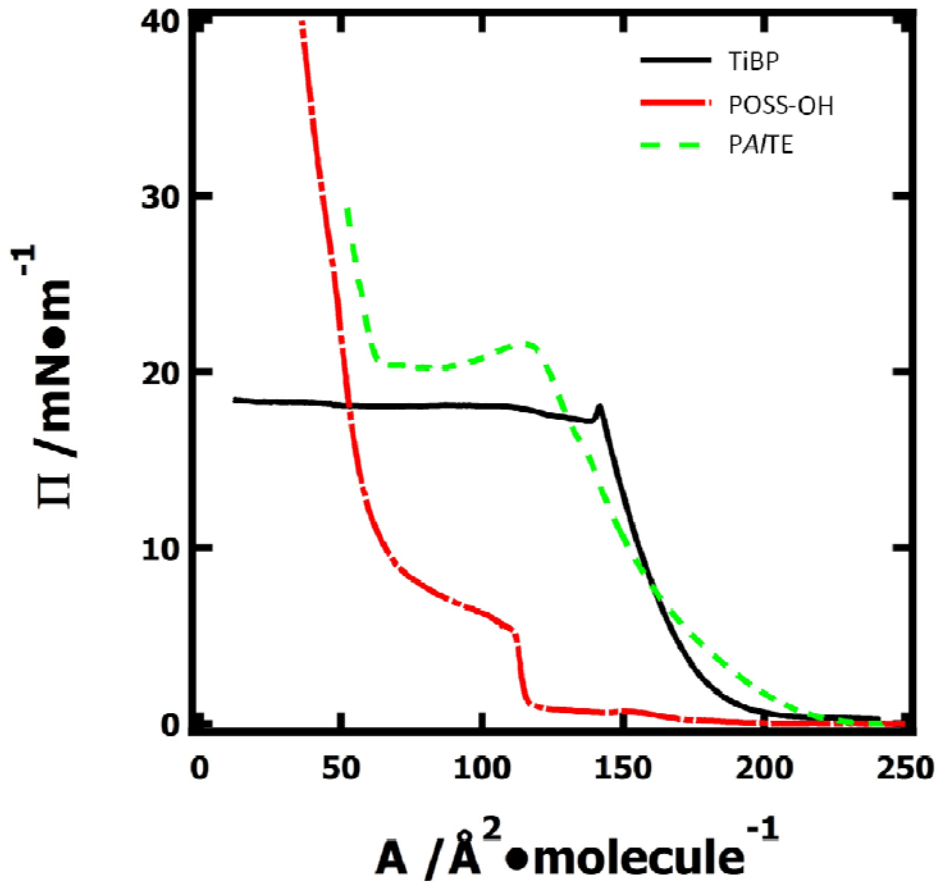

Figure 2.18 ∏-*A* isotherms of TiBP, POSS-OH, and P*AI*TE at 22.5°C at the A/W interface.

The second plateau (65 Å^2•molecule^{-1} < *A* < 110 Å^2•molecule^{-1}) corresponds to multilayer formation. The factor of two changes in area may be consistent with bilayer formation. The long plateau at intermediate Π has also been observed for other weakly amphiphilic POSS derivatives, trisilanolcyclohexyl-POSS[30c] and trisilanolcyclopentyl-POSS.[85] At even smaller *A*, Π increases further as the multilayer structures are rigid.

For P*AI*TE, the isotherm is consistent with a more compressible monolayer. $A_{lift\text{-}off}$ ~215 Å^2•molecule^{-1} and A_0 ~175 Å^2•molecule^{-1} are much larger than POSS-OH. Moreover, the rise in

---

Π in the monolayer regime (125 $Å^2$•$molecule^{-1}$ < A < 215 $Å^2$•$molecule^{-1}$) is more gentle, like a LE monolayer. Collapse of the film at $A_c \approx$ 125 $Å^2$•$molecule^{-1}$ and $\Pi_c \approx$ 22 mN•m^{-1} is followed by a plateau (65 $Å^2$•$molecule^{-1}$ < A < 125 $Å^2$•$molecule^{-1}$) that is similar to POSS-OH. Further compression of the film (A < 65 $Å^2$•$molecule^{-1}$) also causes Π to increase like POSS-OH.

The other isotherm in Figure 2.18 is for trisilanolisobutyl-POSS (TiBP). Deng *et al.*[30b] interpreted this isotherm as follows:

$A > A_{lift\text{-}off}$ = 230 $Å^2$•$molecule^{-1}$: coexisting G/LE monolayer.

A_0 = 177 $Å^2$•$molecule^{-1}$ < A < $A_{lift\text{-}off}$ = 230 $Å^2$•$molecule^{-1}$: LE monolayer.

A_c = 140 $Å^2$•$molecule^{-1}$ < A < A_0 = 177 $Å^2$•$molecule^{-1}$: more condensed liquid-like monolayer.

$A < A_c$ = 140 $Å^2$•$molecule^{-1}$: collapse into multilayer structures.

It is interesting to note similarities and differences among the isotherms in Figure 2.18. The P*Al*TE seems similar to TiBP with respect to $A_{lift\text{-}off}$ and A_0, however, A_c is similar to A_0 for POSS-OH. As both A_0 and A_c serve as estimates of molecular cross-sections, and the cage portion of the molecules are the same (isobutyl substituents on seven silicon atoms), a natural question arises, "How are the POSS cages packing?" Before addressing this question, it is necessary to explore how electrostatic interactions associated with deprotonation of POSS-triacid influence isotherm.

Traditional modeling of the structure of fatty acids in Langmuir films has treated the molecules as rod-like objects due to their large length/diameter ratio. In contrast, the silsesquioxane core of POSS molecules is essentially a cube, while the flexible organic coronae have led to treatments of POSS as nanometer sized spheres. Hence the overall shape is

essentially the same whether the POSS is a closed T_8 cage or an open T_7 cage. One key difference is that the T_7 trisilanols exist as hydrogen bonded dimers in the crystalline state.[102c] Previous studies with POSS have focused on trisilanol-POSS derivatives.[30b, c, 30o, 83c, 113a, 118] In order to understand the liquid-like state, TiBP was modeled with known crystal structure of TCyP[102c] and CS Chem Draw Pro to substitute isobutyl groups for cyclohexyl groups on the cage. In Chem Draw 3D, MM2 and MOPAC calculations in vacuum were run to minimize the energy state of the structures. Finally, a barrel-like model and a cross-sectional area around 177 $Å^2$•molecule^{-1} were suggested for TiBP.[30b] In this model, the silsesquioxane core had a vertex-on conformation at the A/W interface.

The T_8 POSS cage is considered as an ideal cube, *ABCD-$A_1B_1C_1D_1$*, where the substituents R are distributed evenly at each vertex of the cube and fill out the pink sphere (in Figure 2.19A). In this model, silicon atoms are located on the eight corners while omitted oxygen atoms are in the middle of the 12 edges. Therefore, the sizes (limiting area) of the POSS derivatives are effectively spherical areas determined by the largest cross-sectional areas. If the molecule is tilted on one corner, *A*, as proposed for TiBP,[30b] a vertex-on conformation would be observed that would look like the labeled "Atomium" built for the World's Fair in Brussels (Figure 2.19B). As shown in Figure 2.19B, its largest cross-sectional area would be the circumcircle of the triangle *A_1BD* or *B_1CD_1*.

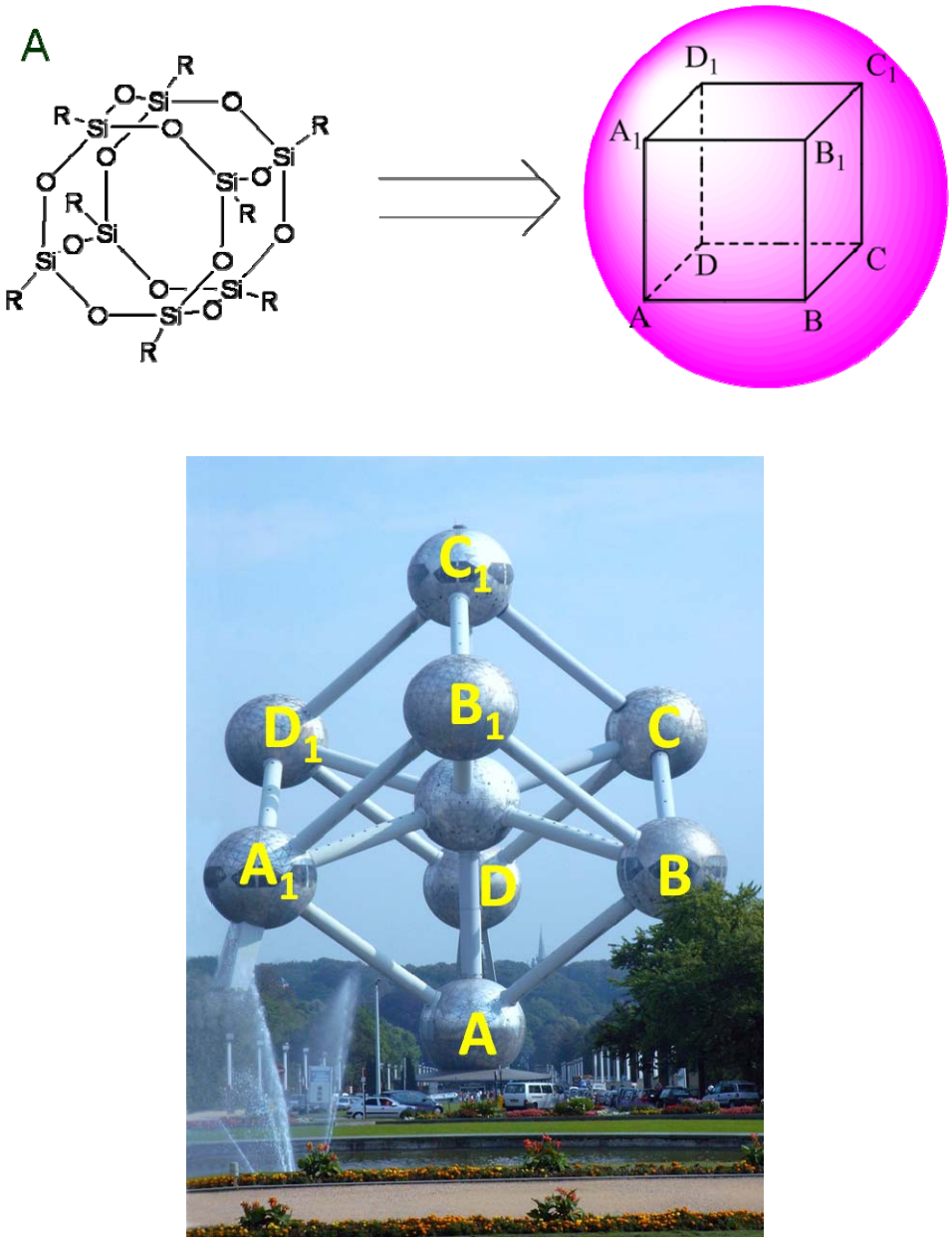

Figure 2.19 (A) The T_8 POSS cage was treated as an ideal cube with the substituents evenly distributed at the vertices of the cage. In this model, *Si* atoms are located at the eight corners of the cube while omitted *O* atoms are in the middle of the 12 edges. (**B**) The Atomium for Brussels World's Fair.[119] The labeling of the cube in (**A**) and Atomium in (**B**) are consistent with balancing the cube on vertex A for a vertex-on conformation.

On the other hand, if the POSS cage is packed on one of its faces, the biggest cross-sectional area is the circumcircle of the square *ABCD* or $A_1B_1C_1D_1$ and turns out to be the face-on conformation. Therefore, the ratio of largest spherical areas between a vertex-on conformation (S_1) and a face-on conformation (S_2) is 4:3. Since the limiting area of TiBP is $A_0 \sim 177$ Å^2·molecule^{-1}, the limiting area of a POSS molecule on its face should be ~ 130 Å^2·molecule^{-1}. This value is in accord with the observed limiting area for POSS-OH. On the basis of these experiments, POSS cages with longer tethering chains or fewer hydrophilic end groups tend to lie on one of the six faces of the molecule at the A/W interface.[47d]

Poly(*tert*-butyl acrylate) (PtBA) was used to understand the packing of P*Al*TE. Figure 2.20A shows a Π-*A* isotherm for PtBA where A is expressed as a function of the area per repeating unit (monomer for short). As seen in Figure 2.20A, Π for the PtBA film initially shows a slow rise in the region $35 < A < 55$ Å^2·molecule^{-1} = $A_{lift\text{-}off,\ PtBA}$. Further compression of the film causes Π to rise rapidly for $A < 35$ Å^2·molecule^{-1} before the film collapses at $A_c \sim 21$ Å^2·molecule^{-1} and $\Pi_c \sim$ 23 mN·m^{-1}. The rapid rise in Π for $A < 35$ Å^2·molecule^{-1} is consistent with the formation of a condensed (LC) film. Extrapolation of the Π-*A* isotherm for the LC monolayer back to Π = 0 yields $A_0 \approx 30$ Å^2·molecule^{-1}. As seen in Figure 2.20B if one neglects the short linker, POSS-triester is essentially POSS-OH plus three PtBA repeating units. Interestingly, $A_{0,\ POSS\text{-}OH} + 3A_{0,PtBA}$ yields 215 Å^2·molecule^{-1} ($\approx A_{lift\text{-}off,\ PAlTE}$). As such, we speculate that P*Al*TE starts with the POSS-cage and three *tert*-butyl esters adsorbed to the plane of the interface (Figure 2.21A). Throughout the monolayer regime, the POSS cage is likely riding on top of the *tert*-butyl esters (Figure 2.21B). Recalling that TiBP and P*Al*TE Π-*A* isotherms essentially coincided throughout the monolayer regime (Figure 2.18), a somewhat more speculative conclusion is that the POSS cage tilts during the transformation from a cage on the A/W interface to a cage on the *tert*-butyl

esters as depicted in Figure 2.21B. However, there is a difference in A_c between P*Al*TE and TiBP. TiBP collapsed at A_c = 140 Å^2·molecule^{-1}, whereas P*Al*TE collapsed at a smaller A_c = 125 Å^2·molecule^{-1}. This value is consistent with a face-on conformation for POSS-triester at collapse (Figure 2.21C).

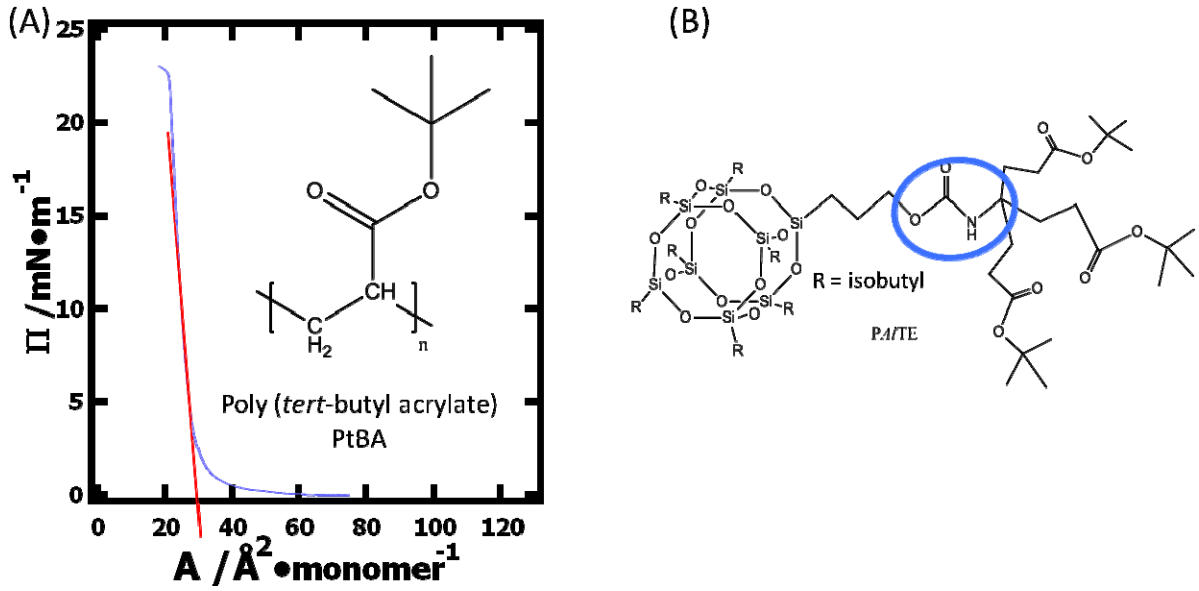

Figure 2.20 (**A**) Π-*A* isotherm for PtBA on water at T= 22.5 °C. The red dashed line indicates A_0 for PtBA. (**B**) Structure of P*Al*TE highlighting the POSS-OH piece and the three PtBA "repeating units".

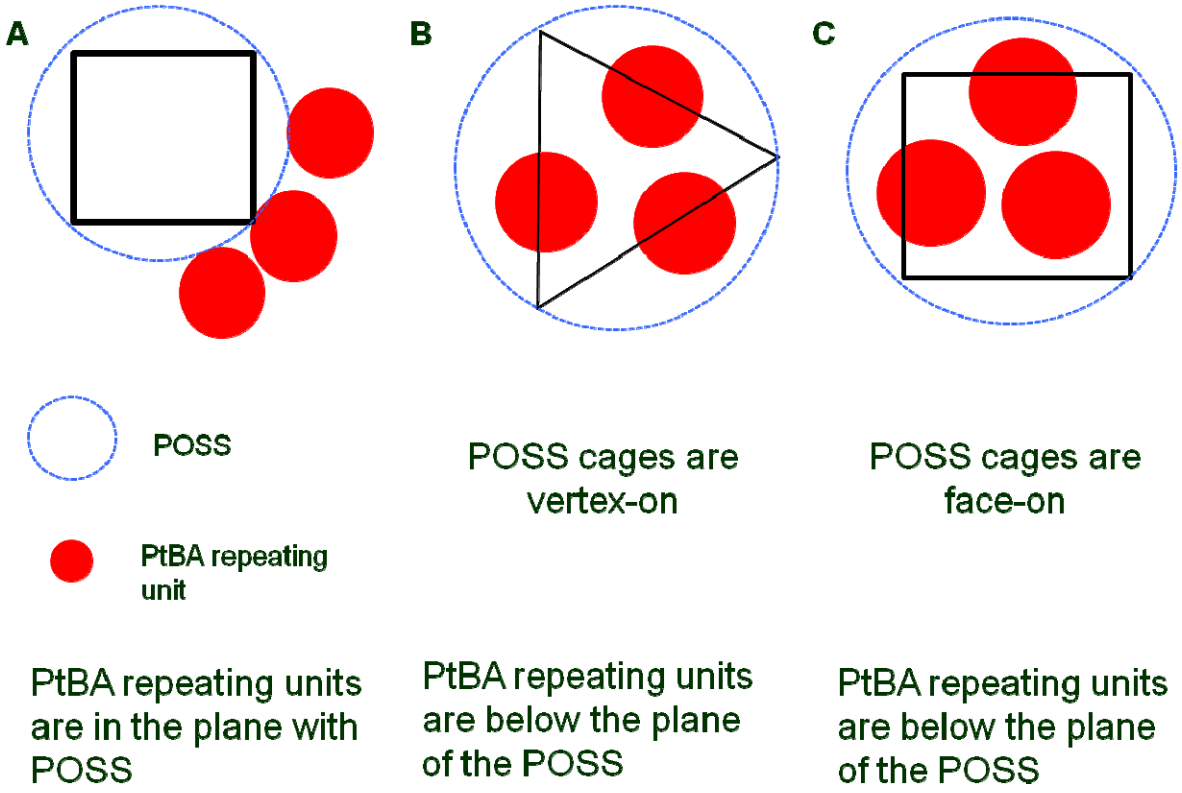

Figure 2.21 Schematic depictions of P*AI*TE (top view) in Langmuir films at various A: (**A**) $A = A_{lift\text{-}off}$, (**B**) $A_c < A < A_{lift\text{-}off}$, and (**C**) $A = A_c$.

Chapter 3

Experimental Materials and Methods

3.1 Materials and Sample Preparation

3.1.1 Obtained Materials

The reagents and solvents noted in this section were used for the synthesis and characterization of the polyhedral oligomeric silsesquioxane (POSS) derivatives from PSS-(3-hydroxypropyl)-heptaisobuyl (POSS-OH) and aminopropylisobutyl-POSS (POSS-NH_2) described in this thesis. POSS-OH (FW 875.30 g•mol^{-1}, mp 233.0-234.1 ºC) from the Sigma-Aldrich Corporation was purified by flash chromatography. POSS-NH_2 (FW 874.58 g•mol^{-1}, mp 227.6-228.8 ºC) was purchased from Hybrid Plastics Incorporated. All other reagents were used without further purification. Weisocyanate (FW 441.56 g•mol^{-1}) was purchased from Frontier Scientific, Incorporated. Isocyanatediester (FW 327.42 g•mol^{-1}) was provided by Bhadreshkumar Maisuria from Dr. Richard Gandour's research group in the Chemistry Department at Virginia Tech. Triethylamine (TEA, reagent, ACS grade, FW 101.12 g•mol^{-1}) was purchased from Sigma-Aldrich Corporation as a catalyst. Chloroform ($CHCl_3$, reagent, 99%, ACS grade, FW 119.38 g•mol^{-1}), hexanes (reagent, 99%, ACS grade, FW 86.18 g•mol^{-1}), ethyl acetate (EtOAc, reagent, 99%, ACS grade, FW 88.11 g•mol^{-1}), methanol (MeOH, reagent, 99%, ACS grade, FW 32.04 g•mol^{-1}) were purchased from Sigma-Aldrich Corporation as solvents. Spreading solutions were prepared with nominal concentrations of around 0.5 mg·mL^{-1} in chloroform. All aqueous

---

subphases were prepared from ultrapure water (Milli-Q Gradient A-10, 18.2 MΩ·cm, < 10 ppb organic impurities).

3.1.2 Purified and Synthesized Materials

3.1.2.1 Purification and Characterization of POSS-OH

From 206 mg of commercial POSS-OH (**1**, in Figure 3.1) was isolated as a crystalline white solid (195 mg, 94.7%) from a silica gel (60 Å) column using methanol/ethyl acetate/ and hexane (10/10/80) as the eluant, and characterized: mp 233.0-234.1 °C; ^{1}H NMR (500 MHz, $CDCl_3$) δ 3.61 (q, J = 6.5 Hz, 2H), 1.88-1.80 (m, 7H), 1.69-1.63 (m, 2H), 1.33 (t, J = 5.5 Hz, 1H), 0.94 (d, J = 6.5 Hz, 42H), 0.64-0.58 (m, 16H); ^{13}C NMR (125 MHz, $CDCl_3$) δ 65.1, 26.1, 25.8, 24.0, 22.5; ^{29}Si NMR (82 MHz, $CDCl_3$) δ -66.8, -67.1, -67.4; HRMS calcd for $C_{31}H_{71}O_{13}Si_8$ $(M+H)^+$ 875.3043, found 875.3065; IR υ (cm^{-1}) 3405, 1081; Anal. Calcd for $C_{31}H_{70}O_{13}Si_8$: C, 42.52; H, 8.06. Found: C, 42.49; H, 8.16.

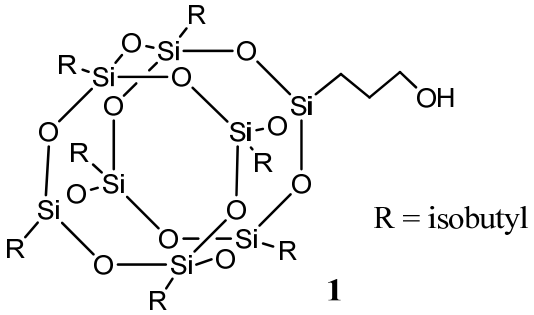

Figure 3.1 Structure of POSS-OH

3.1.2.2 Synthesis and Characterization of POSS-OH Based Diester (P*Al*DE)

As shown in Scheme 3.1, compound **1** (0.350 g, 0.40 mmol) and isocyantatediester[120] (**2**, 0.137 g, 0.42 mmol) were dissolved with 7.0 mL $CHCl_3$ in a 50 mL round bottom flask. 0.5 mL triethylamine (TEA) were added dropwise to the mixture. The solution was allowed to stir and reflux overnight. Then the solvent was removed under reduced pressure and a white gel was obtained. The white gel was dissolved with 4 mL hexanes at 65 °C and 10 drops of MeOH were added into the solution until it was cloudy. 2 mL hexanes were added to make the solution clear. The flask was capped with parafilm and stored in the freezer (-15 °C) overnight. After filtration, a white crude product P*Al*DE (**3** in Scheme 3.1) was collected. Finally, **3** was purified by a silica gel (60 Å) column with EtOAc : hexanes = 10 : 90 (0.407 g, 84.6%): mp 101.8-103.5 °C; ^{1}H NMR (500 Hz, $CDCl_3$) δ 4.69 (s, 1H), 3.92 (t, *J* = 5.5 Hz, 2H), 2.33 (t, *J* = 8.0 Hz, 4H), 2.03-1.97 (m, 2H), 1.89-1.79 (m, 9H), 1.66 (quintet, *J* = 7.5 Hz, 2H), 1.43 (s, 18H), 1.23 (s, 3H), 0.95 (d, *J* = 6.5 Hz, 21H), 0.94 (d, *J* = 6.5 Hz, 21H), 0.61-0.58 (m, 16H). ^{13}C NMR (125 MHz, $CDCl_3$) δ 173.0, 154.9, 80.5, 66.4, 54.4, 33.8, 30.3, 28.1, 25.7, 23.9, 23.0, 22.5, 22.1, 8.3; HRMS calcd for $C_{48}H_{99}NO_{18}Si_8$ 1201.4974, found 1201.5016.

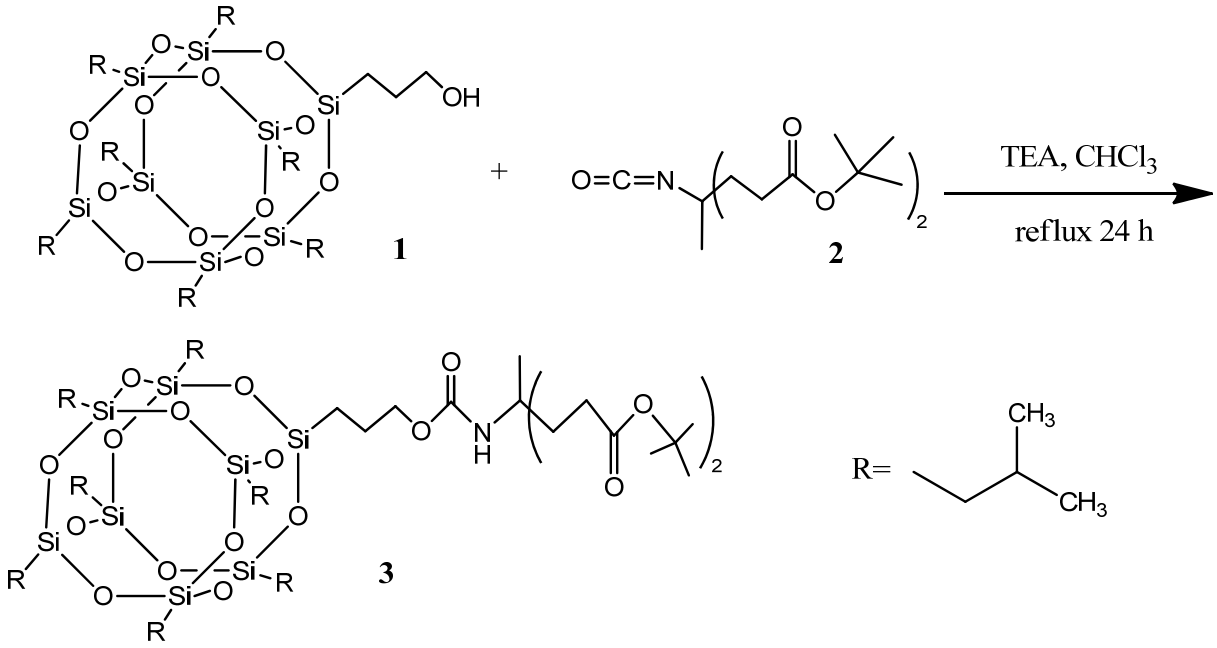

Scheme 3.1 Synthesis of P*Al*DE

3.1.2.3 Synthesis and Characterization of POSS-NH_2 Based Triester (P*Am*TE)

As shown in Scheme 3.2, compound **4** (0.262g, 0.30 mmol) and **5** (0.146g, 0.33 mol) were dissolved in 1.0 mL of chloroform. Triethylamine (TEA) 1.0 mL was added to the solution dropwise. The reaction was stirred and refluxed for 24 hours. The solution was then removed under reduced pressure and the residue was separated by a silica gel (60 Å) column with ethyl acetate : hexane (10 : 90) yielding compound **6** (in Scheme 3.2) as a white solid (0.246 g, 62.3%): mp 145.6-146.9 °C; ^{1}H NMR (500 MHz, $CDCl_3$) δ 4.57 (s, 1H), 4.03 (t, *J* = 5.0 Hz, 1H), 3.06 (q, *J* = 6.5 Hz, 2H), 2.23 (t, *J* = 8.0 Hz, 6H), 1.94 (t, *J* = 8.0 Hz, 6H), 1.89-1.81 (m, 7H), 1.60-1.56 (m, 2H), 1.43 (s, 27H), 0.95 (d, *J* = 6.5 Hz, 21H), 0.94 (d, *J* = 6.5 Hz, 21H), 0.61-0.58 (m, 16H);

---

^{13}C NMR (125 MHz, $CDCl_3$) δ 173.2, 156.7, 80.6, 56.6, 43.1, 30.7, 30.0, 28.2, 25.8, 23.5, 22.6, 9.5; HRMS calcd for $C_{54}H_{110}N_2O_{19}Si_8$ 1314.5897, found 1314.5857.

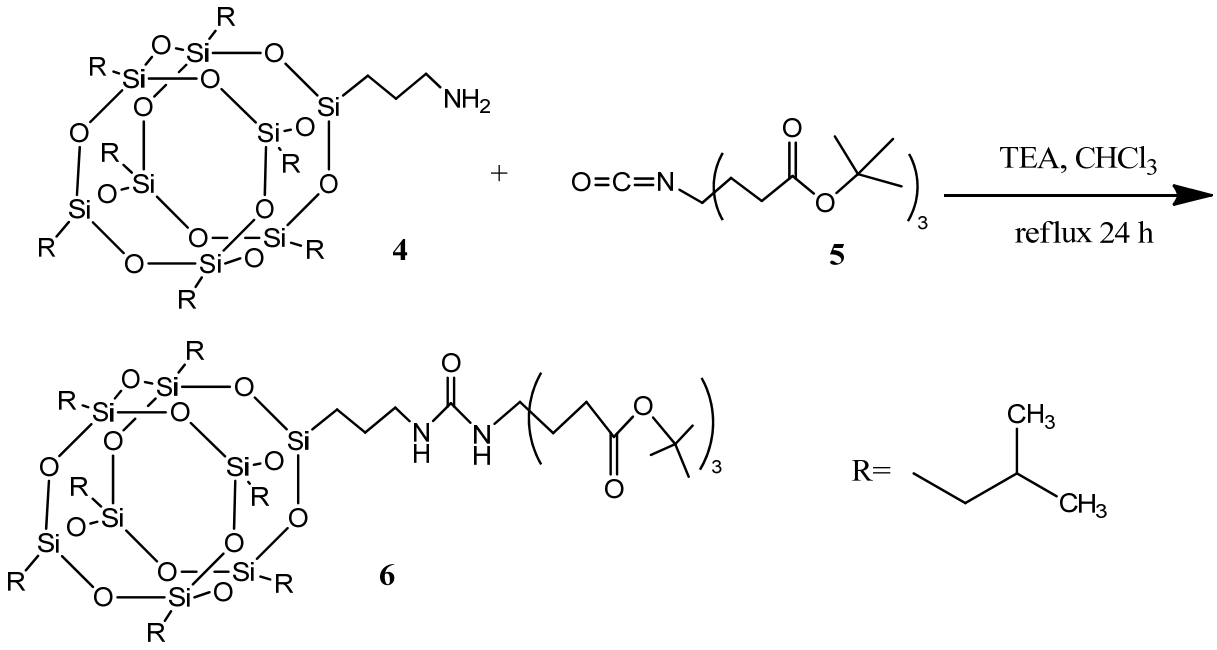

Scheme 3.2 Synthesis of P*Am*TE

3.1.2.4 Synthesis and Characterization of POSS-NH_2 Based Diester (P*Am*DE)

As shown in Scheme 3.3, compound **4** (0.262g, 0.30 mmol) and **2** (0.108g, 0.33 mol) were dissolved in 1.0 mL of chloroform. Triethylamine (TEA) 1.0 mL was added to the solution dropwise. The reaction was stirred and refluxed for 24 hours. The solution was then removed under reduced pressure and the residue was separated by a silica gel (60 Å) column with ethyl acetate : hexane (25 : 75) yielding compound **7** (in Scheme 3.3) as a white solid (0.217 g, 60.2%): mp 137.3-138.8°C; ^{1}H NMR (500 MHz, $CDCl_3$) δ 3.06 (t, J = 7.0 Hz, 2H), 2.26 (t, J = 8.0 Hz,

---

4H), 2.05-1.97 (m, 2H), 1.90-1.78 (m, 9H), 1.58-150 (m, 2H), 1.43 (s, 27H), 1.27 (s, 3H), 0.95 (d, J = 6.5 Hz, 21H), 0.93 (d, J = 6.5 Hz, 21H), 0.61-0.56 (m, 16H); ^{13}C NMR (125 MHz, $CDCl_3$) δ 173.7, 157.8, 80.9, 55.5, 43.4, 34.1, 30.4, 28.2, 25.8, 24.4, 23.9, 23.2, 22.6, 9.5; HRMS calcd for $C_{48}H_{100}N_2O_{17}Si_8$ 1200.5165, found 1200.5176.

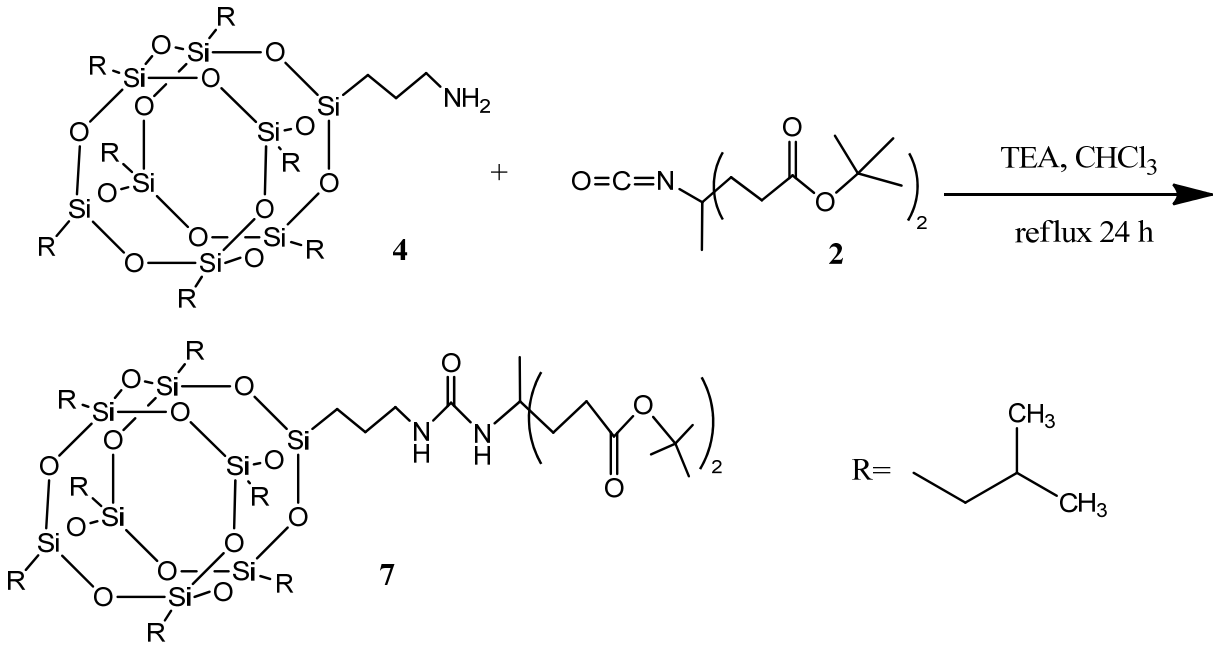

Scheme 3.3 Synthesis of P*Am*DE

3.2 Sample Characterization

3.2.1 Nuclear Magnetic Resonance (NMR) Spectroscopy

^{1}H NMR spectra were obtained with a JOEL Eclipse+ spectrometer operating at 500 MHz with a 45° pulse angle, acquisition time of 3.6 s and a 1 s relaxation delay with 32 scans.

Samples were dissolved in $CDCl_3$ at a typical concentration of 0.2 mg/mL. ^{13}C NMR spectra were obtained in $CDCl_3$ at a typical concentration of 0.1 g/mL on a JOEL Eclipse+ spectrometer operating at 125 MHz with a 45° pulse angle, acquisition time of 1.0 s and a 1 s relaxation delay with 25000 scans. Abbreviations used in the splitting pattern were as follows: s = singlet, d = doublet, t = triplet, q = quartet, and m = multiplet.

3.2.2 Melting Point Determinations

Melting points were determined in open capillary tubes and were uncorrected. Melting point data are reported as a range: the temperature at onset of melting and the temperature at which the sample was completely liquid and a meniscus was evident. Rough measurements were made at a rate of 5 ^{o}C/minute. Final measurements were made at a heating rate of 1 ^{o}C/minute. Three experiments with differences less than 0.5 ^{o}C were considered acceptable.

3.2.3 High Resolution Mass Spectrometry (HRMS)

In this thesis, all HRMS spectra were obtained with an Agilent 6220 Accurate-Mass TOF LC/MS in the Analytical Services Laboratory of the Chemistry Department at Virginia Tech.

3.3 Experimental Methods

3.3.1 Langmuir Trough Configuration

The experimental results presented in this thesis were conducted with a standard Langmuir trough (700 cm^2, Nima Technology, Ltd., 702 BAM) equipped with a BAM (MicroBAM3, NanoFilm Technologie, Ltd., lateral resolution of 8 μm). The instruments were housed in a Plexiglas™ box at 70 to 75% relative humidity and a dust free environment. The instruments (Langmuir trough, BAM, and Plexiglas box) rested on a floating optical table to minimize mechanical vibrations (Newport RS-2000 & I-2000). The Langmuir trough was made of hydrophobic Teflon® and was cleaned by dichloromethane or chloroform. The Langmuir trough was filled with ultrapure water. Two movable barriers, made of hydrophilic acetal resin polymer (Delrin®) were cleaned with 2-propanol. In the experiments, barriers were used to sweep the water surface during the compression of the monolayer to vary the surface area symmetrically from both sides of the film (in Figure 2.5). The hydrophobic trough supported an approximately 1 mm brim of water above the top of the trough edge.

After the trough was cleaned, it was filled with ultrapure water; the barriers were allowed to move toward each other thereby collecting dust and surface-active contaminations into the center of the trough. Next, the dust and surface-active contaminants were suctioned off by a clean pipette connected to a vacuum pump. The cleaning procedure was repeated several times until the surface tension in the opened and closed barrier positions matched the reported value for water and remained constant for at least 30 minutes. After spreading the organic solution (usually chloroform), 25 to 30 minutes was allowed before measurements to allow evaporation

---

of the spreading solvent. Surface pressure, Π, was recorded by the Wilhelmy plate technique to ± 0.1 $mN \bullet m^{-1}$ during all isotherm measurements.

As depicted in Figure 2.6, a piece of completely wetted filter paper was used as the Wilhelmy plate to detect the surface pressure. In this thesis, the aqueous subphase is ultrapure water unless otherwise mentioned. The temperature of the subphase was usually maintained at 22.5 ^{o}C by circulating water from a water bath (Neslab RTE-111) through the base of the trough. Surface pressure-area (Π-*A*) isotherms were obtained automatically by a computer, which controlled the barrier positions and provided a read-out of Π.

The relationship between the temperature of the circulating water and the actual temperatures of the water subphase at various positions for the 702 BAM trough indicated that the actual temperature of the subphase at different positions differed from the temperature of the circulating water; however, the values at different trough positions were quite similar for a given temperature.[121] Calibration curves for the temperatures of the subphase are provided in Figure 3.2. At position 1, 2, 4, and 5, three points were measured as depicted in Figure 3.2(A) and the average value was used. Position 3 was at the center of the dipping well and only one point was measured. For Π-*A* isotherms reported in this thesis, the temperatures correspond to the measured temperatures rather than the setting on the circulating bath.

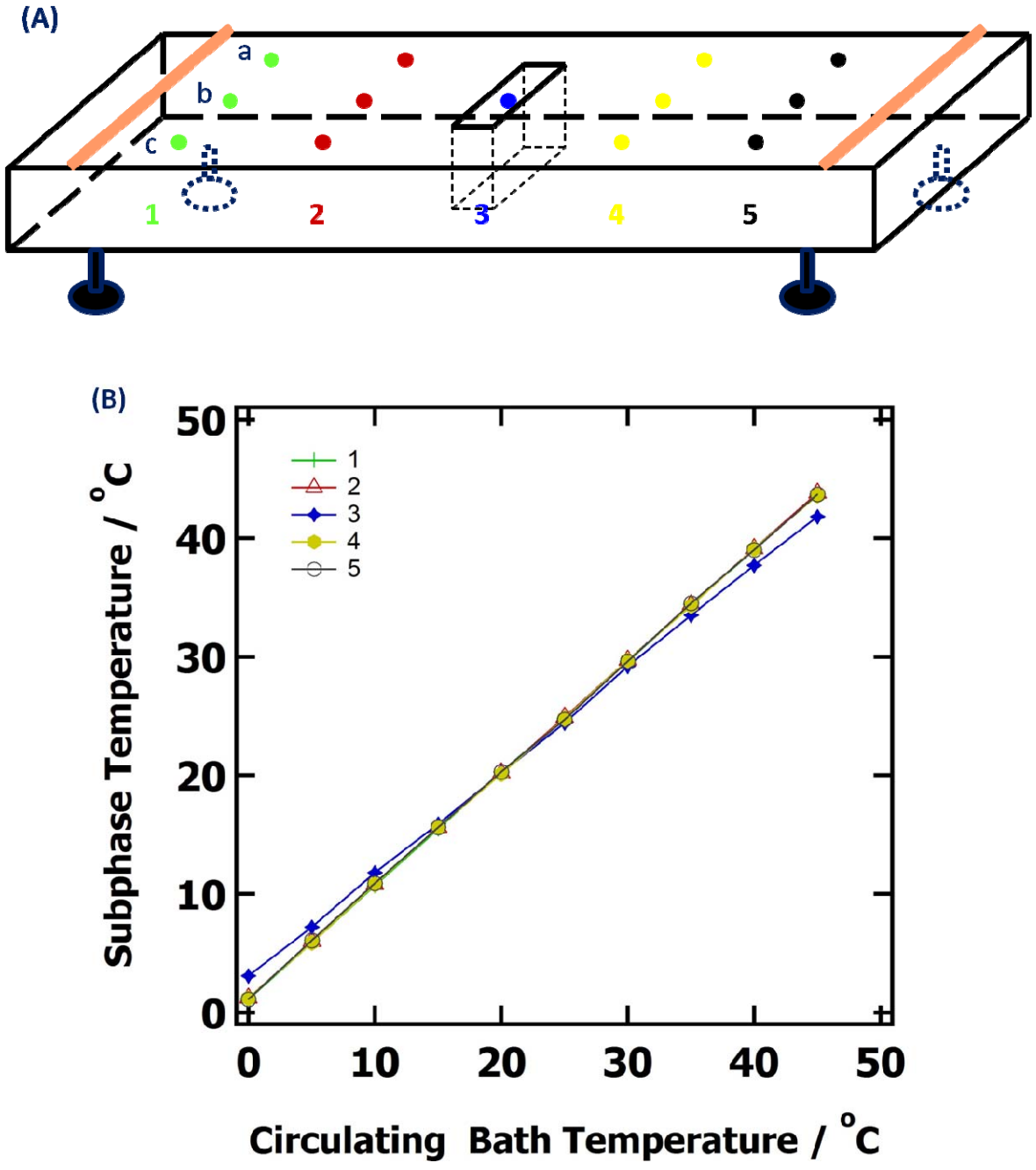

Figure 3.2 (**A**) Schematic depiction of positions on the trough and (**B**) calibration curves for the temperatures of the subphase.

3.3.2 Constant Compression Rate Experiments

Π-*A* isotherms were obtained at a constant compression rate of 10 $cm^2 \cdot min^{-1}$. This rate meant the compression rates varied from 3 to 5 $Å^2 \cdot molecule^{-1} \cdot min^{-1}$. The static elastic moduli, $\varepsilon_s = -A(\partial\Pi/\partial A)_T$, of the films were deduced from the recorded Π-*A* isotherms.

3.3.3 Stepwise Compression Experiments

Π-*A* isotherms were obtained at a constant compression rate of 10 $cm^2 \cdot min^{-1}$ in 10 cm^2 steps. After 10 cm^2 steps, the barriers were stopped and Π was allowed to relax for 5 min. After waiting 5 min, the process is repeated leading to saw-tooth Π-*A* isotherms.

3.3.4 Brewster Angle Microscopy (BAM)

BAM studies (MicroBAM3, NanoFilm Technologie, Ltd., lateral resolution of 8 μm) were carried out simultaneously during isotherm measurements, and BAM images were taken by a charge-coupled device (CCD) camera under the "automatic gain control" mode to obtain an optimal average brightness rather than absolute intensity values. The original size of all BAM images taken during the measurements was 3.6 × 4.8 mm^2. Some BAM images presented in this thesis were cut from the original images utilizing imaging software and their sizes are noted in the figure legends.

Chapter 4

Synthesis and Characterization of POSS-NH_2 Based Triester at the Air/Water Interface

4.1Abstract

A triester, polyhedral oligomeric silsesquioxane (POSS) derivative was successfully synthesized from aminopropylisobutyl-POSS (POSS-NH_2) and Weisocyanate. Surface pressure-area per molecule (Π-*A*) isotherm studies confirmed POSS-NH_2 and POSS-NH_2 based triester (P*Am*TE) were amphiphilic at the air/water (A/W) interface. The Π-*A* isotherms of POSS-NH_2 and P*Am*TE were compared to two other POSS-derivatives, (3-hydroxypropyl)-heptaisobutyl-POSS (POSS-OH) and a POSS triester (P*Al*TE) synthesized from Weisocyanate and purified POSS-OH. Unlike the vertex-on conformation for trisilanol-POSS derivatives, both POSS-NH_2 and POSS-OH exhibit face-on conformations at the A/W interface. Analysis of the Π-*A* isotherms revealed P*Am*TE and P*Al*TE behaved similarly. P*Am*TE starts with the POSS-cage and three *tert*-butyl esters adsorbed to the plane of the interface, and as the film is compressed P*Am*TE may exhibit a vertex-on conformation in the liquid-expanded monolayer before taking up a face-on conformation near the collapse transition.

4.2 Introduction

Polyhedral oligomeric silsesquioxanes (POSSs) have attracted substantial academic interest for many years as hybrid materials and nanofillers for controlling thermal and mechanical properties, and for providing thermal and chemical resistance while retaining ease of processing.

Trisilanol-POSS derivatives have been studied and reported as a class of amphiphilic molecules that form stable Langmuir monolayers at the air/water (A/W) interface. As a material firstly reported by Scott in 1946,[122] POSS molecules have attracted considerable interest as shape memory materials,[123] coatings,[7d, e, 30b, 41h, 113a, 124] low-*k* dielectric materials,[125] and catalysts for the preparation of nanostructured materials[7c, 126] and dendrimers.[7g, 88a, 127] Due to the core-shell structure and intermediate properties between ceramics and polymers, POSS cages have been incorporated into polymers for enhancement of the glass transition temperature[123h, 128] and thermal stability[127c, 128a, b, 128d, 128l, 129] and the development of superoleophobic surfaces[130] at the A/W interface. Since POSS derivatives also manifested interesting phase transitions and aggregation behavior and were considered to be excellent model nanofillers with well defined sizes, the Esker group has systematically investigated these compounds.[30b, 83c, 111-112, 118e, 131] For example, trisilanolphenyl-POSS (TPP) has been blended with poly(t-butyl acrylate) (PtBA) as a nanofiller. Although both the bulk and surface glass transition temperatures (T_g) increased as TPP was added to PtBA, the surface T_g increased more significantly with limited incorporation of the POSS component.[111] In another study, an open-cage POSS, trisilanolisobutyl-POSS (TiBP), and a closed-cage POSS, octaisobutyl-POSS, were blended with polydimethylsiloxane (PDMS) to compare their effects on PDMS films at the A/W interface.[118e] The amphiphilic trisilanol-POSS exhibited more interesting phase behavior than hydrophobic closed-cage POSS molecules at the A/W interface because the closed-cage POSS was hydrophobic and aggregated.

Although trisilanol-POSS has been more thoroughly studied at the A/W interface, the Esker group achieved progress on the modification and characterization of closed-cage POSS.[47d] Purified (3-hydroxypropyl)-heptaisobutyl-POSS (POSS-OH) was modified to a POSS-OH based triester (P*Al*TE). Surface pressure-area per molecule (Π-*A*) isotherms and Brewster angle

microscopy (BAM) were used to probe the quasi-two-dimensional thermodynamic and morphological properties of these materials, respectively, at the A/W interface. The results indicate that P*AI*TE is surface active with different packing orientations at the A/W interface. The studies were inspired by the ideal cube representation of the eight silsesquioxane unit (T_8) POSS closed-cage (Figure 2.18A) and the "Atomium" built for the World's Fair in Brussels (Figure 2.18B) which was hypothesized to correspond to a vertex-on conformation.[47d]

According to this hypothesis, the largest cross-sectional area for the vertex-on conformation would be the circumcircle of the triangle A_1BD or B_1CD_1 (shown in Figure 4.1). Since the side length of the cube $ABCD\text{-}A_1B_1C_1D_1$, is assumed as a, $A_1B = BD = A_1D = \sqrt{2}a$ indicating an equilateral triangle A_1BD as shown in Figure 4.1. Their perpendicular bisectors A_1E, BG, and DF pass through vertices and intersect at O_1, the center of the circle. As the areas of triangles AO_1B, A_1O_1D, and BO_1D are equal, the area of triangle BO_1D is equivalent to 1/3 of the area of triangle A_1BD. Hence,

$$\frac{1}{2}(BD \times O_1E_1) = \frac{1}{3} \times \frac{1}{2}(BD \times A_1E_1) \tag{4.1}$$

$$3\ O_1E_1 = A_1E_1 = A_1O_1 + O_1E_1 \tag{4.2}$$

$$r_1 = A_1O_1 = 2\ O_1E_1 = \frac{2}{3}A_1E_1 = \frac{2}{3}\left(\frac{\sqrt{3}}{2}BD\right) = \frac{2}{3}\left(\frac{\sqrt{3}}{2} \times \sqrt{2}a\right) = \frac{\sqrt{6}}{3}a \tag{4.3}$$

Therefore, the area of circumcircle O_1 (S_1):

$$S_1 = \pi {r_1}^2 = \pi\left(\frac{\sqrt{6}}{3}a\right)^2 = \frac{2}{3}\pi a^2 \tag{4.4}$$

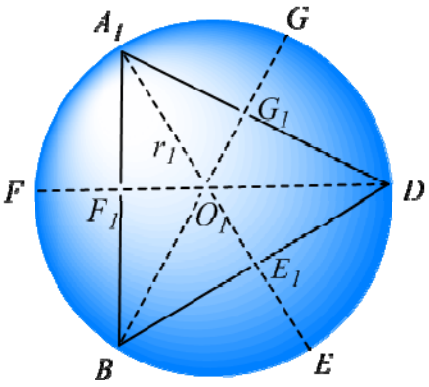

Figure 4.1 Circumcircle O_1 of equilateral triagle A_1BD. A_1E, BG, and DF are perpendicular bisectors of BD, A_1D, and A_1B and intersect at E_1, G_1, and F_1, respectively. $r_1 = A_1O_1$ represents the radius of the circumcircle centered at O_1.

On the other hand, the face-on conformation is determined by the biggest cross-sectional area of the square $ABCD$ or $A_1B_1C_1D_1$. As shown in Figure 4.2, the side length of the cube $ABCD$-$A_1B_1C_1D_1$ is still considered as a, the effective radius of the circumcircle, and the area of circumcircle O_2 (S_2) are:

$$r_2 = DO_2 = \frac{\sqrt{2}}{2} AB = \frac{\sqrt{2}}{2} a \tag{4.5}$$

$$S_2 = \pi r_2^2 = \pi \left(\frac{\sqrt{2}}{2} a\right)^2 = \frac{1}{2} \pi a^2 \tag{4.6}$$

Therefore, the ratio of largest spherical areas between a vertex-on conformation (S_1) and a face-on conformation (S_2) is 4:3. Since the limiting area (the area obtained by extrapolating the

Π-*A* isotherm in the monolayer regime back to the *A* axis) of TiBP is $A_0 \sim 177$ Å^2·molecule^{-1}, the limiting area of a POSS molecule on its face should be ~ 130 Å^2·molecule^{-1}.

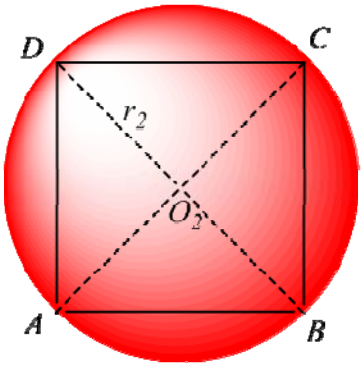

Figure 4.2 Circumcircle O_2 of the square *ABCD*. Two diagonals *AC* and *BD* intersect at O_2, the center of the circumcircle. $r_2 = DO_2$ represents the radius of circumcircle centered at O_2.

In order to examine the vertex-on conformation hypothesis, P*Am*TE was synthesized and characterized by ^{1}H NMR, ^{13}C NMR, high resolution mass spectrometry (HRMS), and melting point measurement. P*Am*TE Langmuir monolayers were examined at the A/W interface. The conformation of the P*Am*TE at the A/W interface is explained relative to a previous study of P*Al*TE.

4.3 Experimental

Experimental details regarding the synthesis of P*Am*TE (**6** in Scheme 3.4) are provided in Chapter 3.1.2.4. Experimental methods for Π-*A* isotherms (Chapter 3.3.1) are covered in Chapter 3.3.

4.4 Results and Discussion

4.4.1 Synthesis and Characterization of POSS-NH_2 Based Triester (P*Am*TE)

The starting materials POSS-NH_2 and Weisocyanate were used without purification. Chemical compositions and purity were confirmed via ^{1}H NMR, ^{13}C NMR, melting point, and HRMS. Figure 4.3 contains the ^{1}H NMR spectrum for P*Am*TE in $CDCl_3$. Figures 4.4 and 4.5 contain the ^{13}C NMR and expanded ^{13}C NMR spectra for P*Am*TE in $CDCl_3$, respectively. The spectra reveal sharp, well-resolved peaks. The characteristic differences in the splitting pattern of the protons of the linker and essentially quantitative integrations were consistent with the labeled structures on each spectrum.

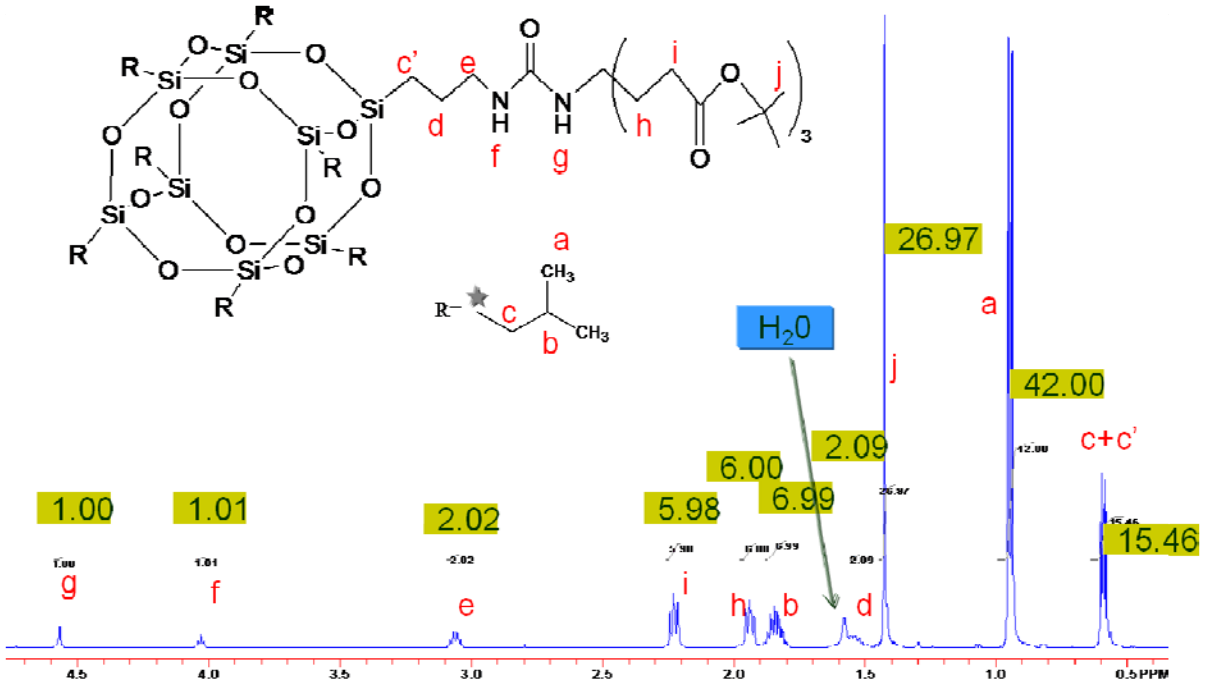

Figure 4.3 ^{1}H NMR of P*Am*TE.

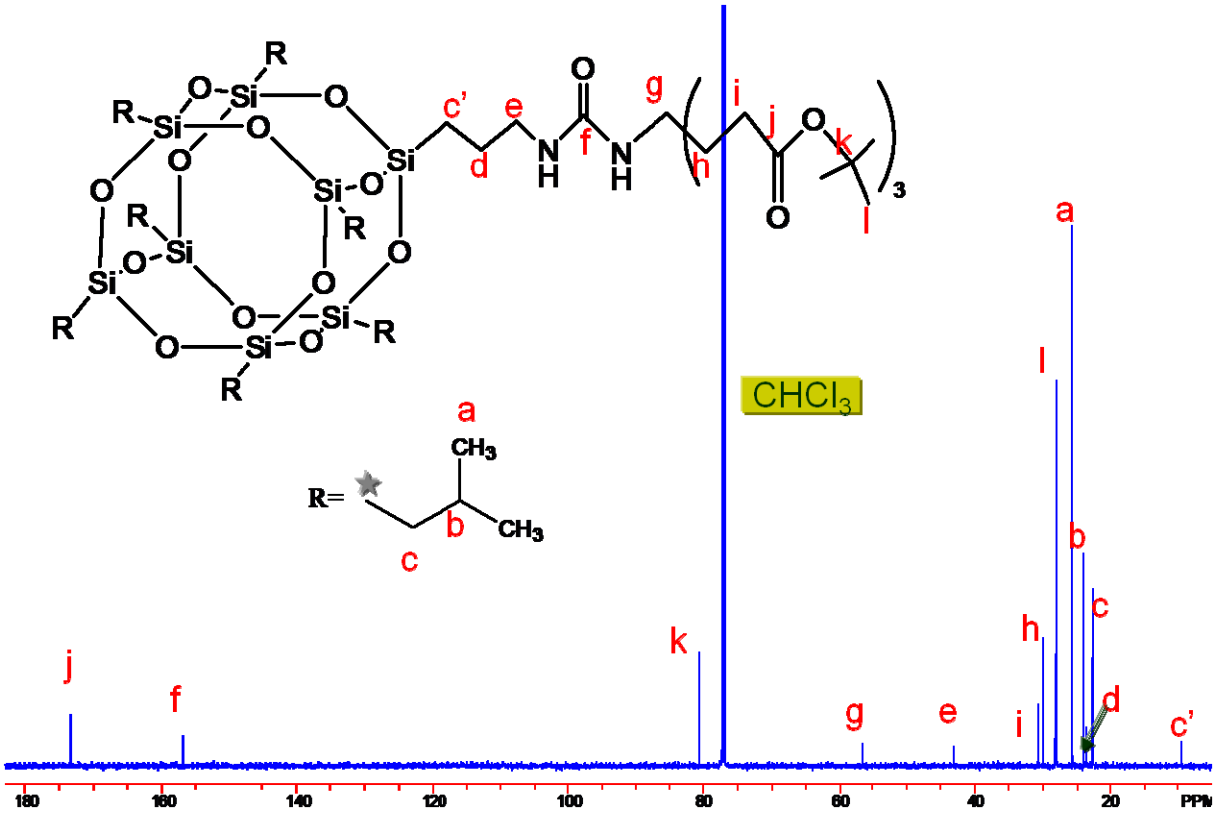

Figure 4.4 ^{13}C NMR of P*Am*TE.

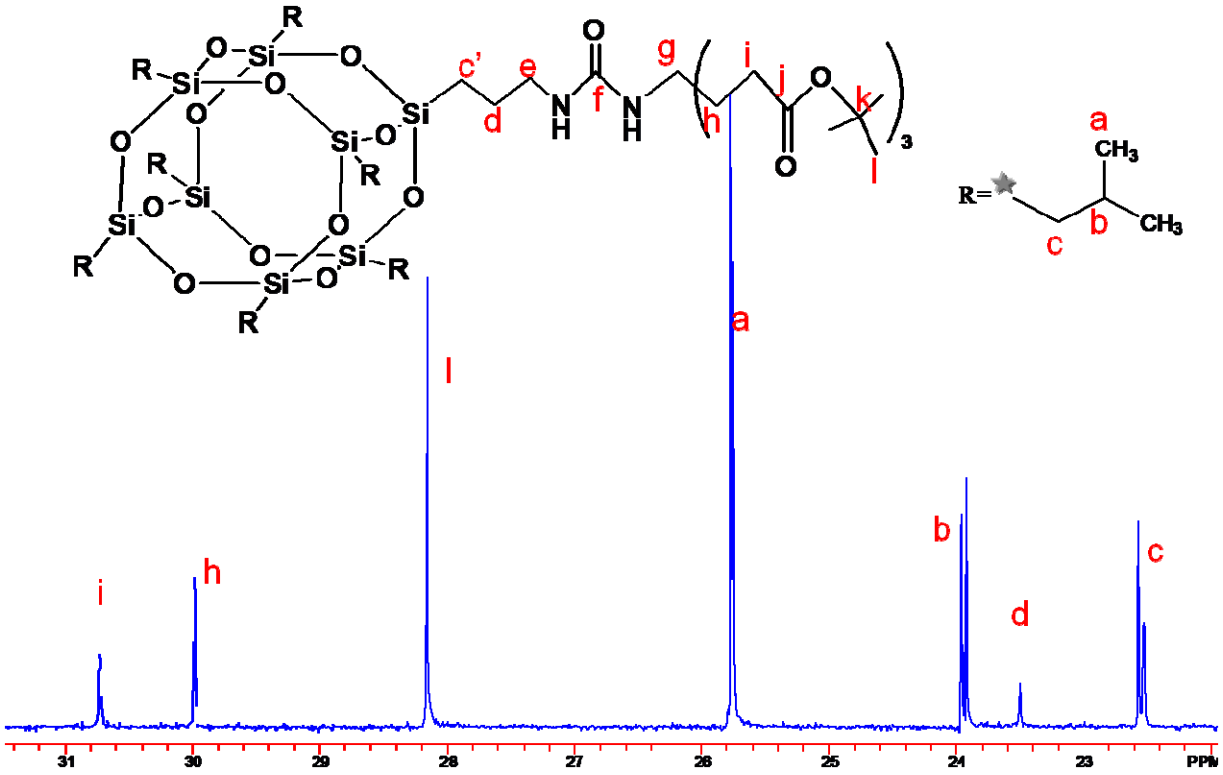

Figure 4.5 Expanded ^{13}C NMR of P*Am*TE.

4.4.2 POSS Molecules that Exhibit Face-on Conformations

In order to explore the hypothesis for conformations of P*Al*TE at the A/W interface, experiments on other compounds were performed at 22.5 ^{o}C. The structure of POSS-OH based triacid (P*Al*TA) and propylmethyacrylate-POSS (POSS-MA) are provided in Figure 4.6. ∏-*A* isotherms of POSS materials with seven isobutyl substituents and a different eighth hydrophilic substituent are compared in Figure 4.7.

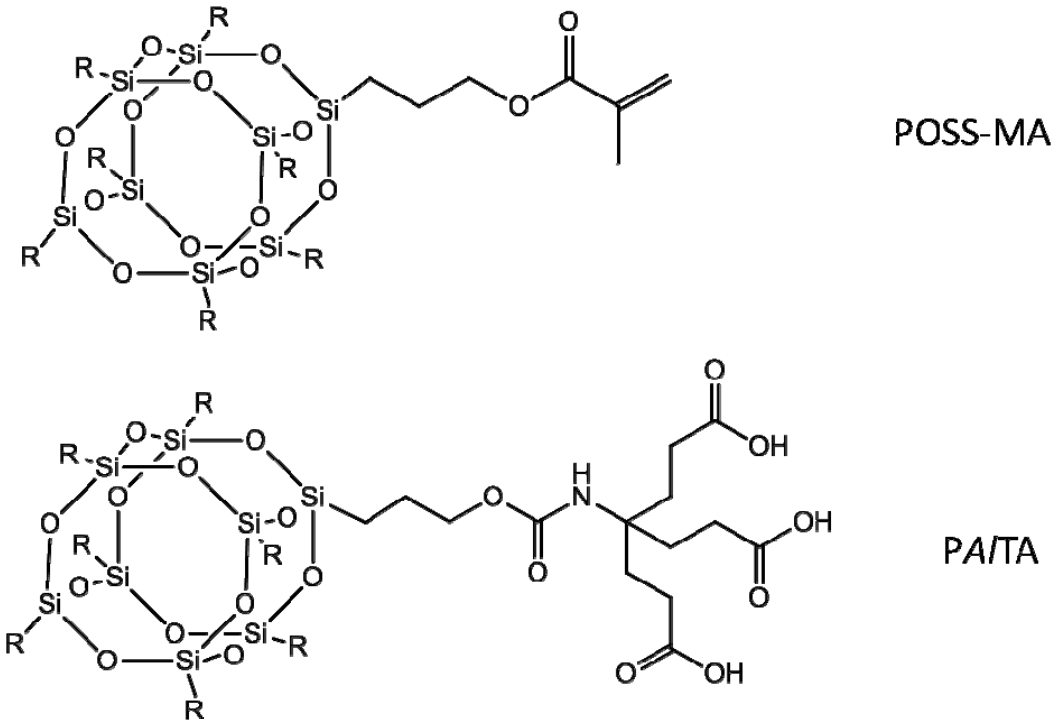

Figure 4.6 Chemical structures of POSS-MA and P*AI*TA. Substituent R represents an isobutyl group.

As seen in Figure 4.7, the lift-off areas ($A_{lift\text{-}off}$) where $\prod$ increases from zero are $A_{lift\text{-}off} \approx A_0$ = 130 Å^2·molecule^{-1} for POSS-NH$_2$ and $A_{lift\text{-}off} \approx A_0$ = 120 Å^2·molecule^{-1} for POSS-MA. The A_0 of P*AI*TA [47d] is reported as 125 Å^2·molecule^{-1}. These values are consistent with the results observed for POSS-OH. Furthermore, the shapes of the POSS-NH$_2$ and POSS-MA isotherms are similar to POSS-OH. All three isotherms exhibit plateaus after collapse of the films. For POSS-MA, collapse occurs at an area of A_c = 110 Å^2·molecule^{-1} and a surface pressure of $\prod_c$ = 3 mN·m^{-1} with a plateau from 75 Å^2•molecule^{-1} < A < 110 Å^2•molecule^{-1}, whereas collapse for POSS-NH$_2$ starts at A_c = 120 Å^2·molecule^{-1} and $\prod_c$ = 17 mN·m^{-1} with a plateau from 80 Å^2•molecule^{-1} < A <

120 $Å^2$•molecule^{-1}. The Π_c follow the trend $\Pi_{c,\ POSS\text{-}MA} < \Pi_{c,\ POSS\text{-}OH} < \Pi_{c,\ POSS\text{-}NH2}$ and reflect stronger interactions between the hydrophilic moiety and the subphase. As seen in Figure 4.7, Π_c for POSS-triacid is in excess of 35 mN·m^{-1}. Furthermore, POSS-NH_2 and POSS-MA exhibit increases in Π at small *A* that are similar to POSS-OH. On the basis of these observations, it appears that POSS-MA and POSS-NH_2 also pack in face-on conformations. Although P*AI*TA has a longer side chain, the interactions between three carboxylic groups and water surface is strong enough for all three carboxylic acid groups to reside under the cube. Therefore, P*AI*TA also appears to pack with a face-on conformation and form a rigid liquid-condensed (LC) film.

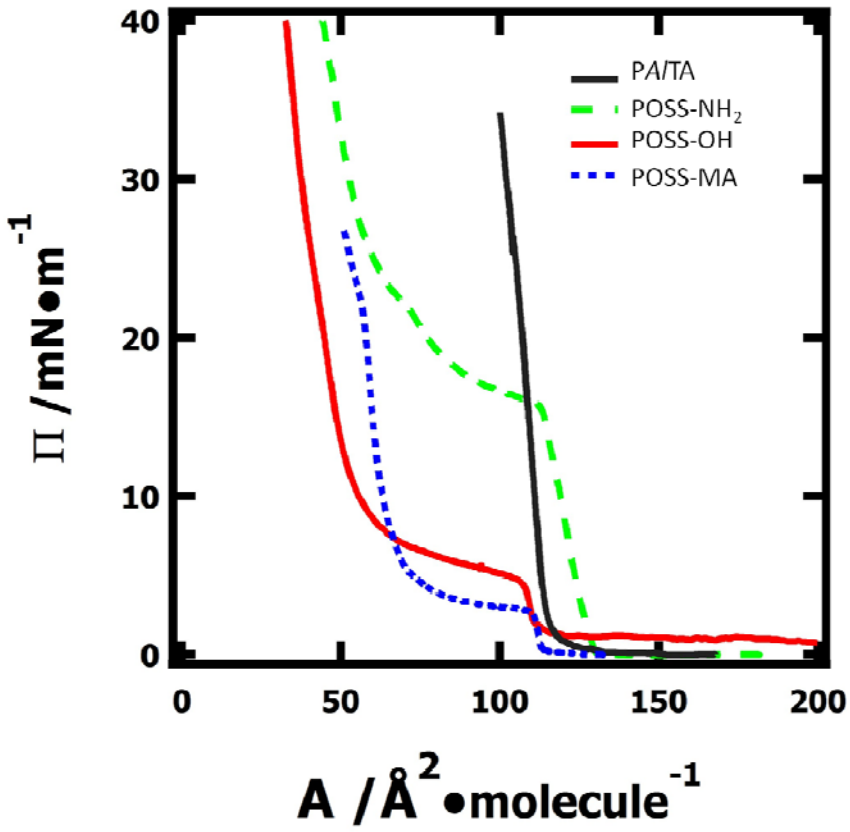

Figure 4.7 Π-*A* isotherms for isobutyl substituted POSS derivatives: P*AI*TA, POSS-NH_2, POSS-OH, and POSS-MA at the A/W interface (T = 22.5 ^oC).

4.4.3 Possible Conformations for POSS-NH_2 Based Triester at the A/W Interface

Compared to the isotherms for POSS derivatives with face-on conformations (in Figure 4.7), the isotherm for P*Am*TE (Figure 4.8A) is consistent with a more compressible monolayer. An isotherm of trisilanolisobutyl-POSS (TiBP) is also provided as a reference. $A_{lift\text{-}off,\ PAmTE}$ ~220 $Å^2$•molecule^{-1} and $A_{0,PAmTE}$ ~175 $Å^2$•molecule^{-1} are much larger than those of POSS-OH and POSS-NH_2. Moreover, the rise in Π in the monolayer regime (100 $Å^2$•molecule^{-1} < A < 220 $Å^2$•molecule^{-1}) is more gentle, like a LE monolayer. Collapse of the film at $A_{c,\ PAmTE}$ ≈ 100 $Å^2$•molecule^{-1} and $\Pi_{c,\ PAmTE}$ ≈ 23 mN•m^{-1} is followed by a plateau (70 $Å^2$•molecule^{-1} < A < 100 $Å^2$•molecule^{-1}) that is similar to POSS-OH. Further compression of the film (A < 70 $Å^2$•molecule^{-1}) also cause Π to increase like POSS-OH. The isotherm for P*Am*TE is similar to that of P*Al*TE since they are similar in chemical structure. A further comparison of the two esters and their starting materials will be discussed later. Therefore, the conformation of P*Am*TE is discussed according to the analysis of P*Al*TE.

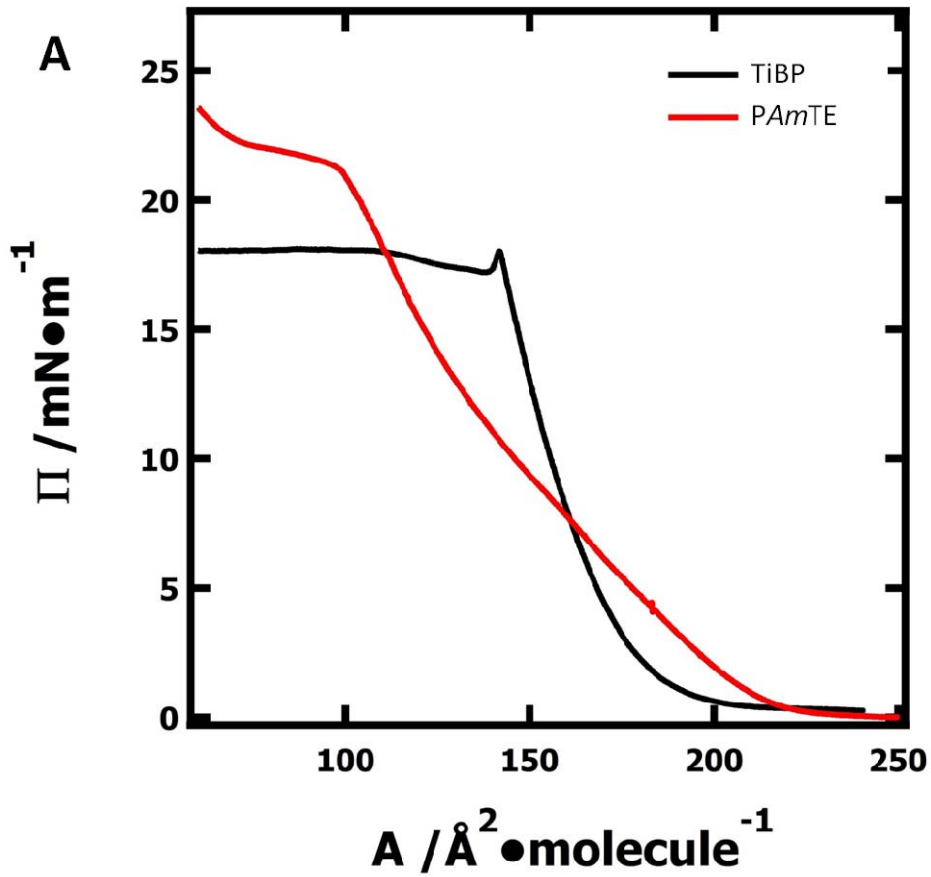

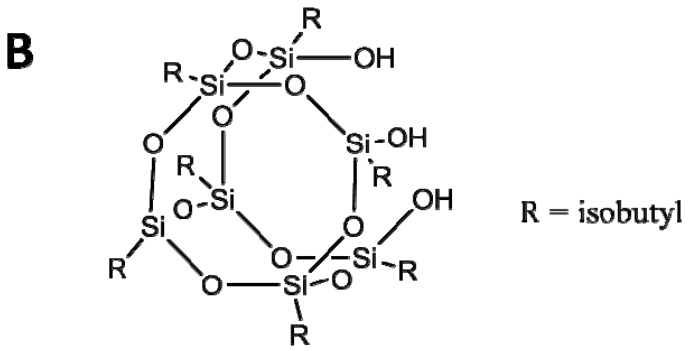

Figure 4.8 (A) Π-*A* isotherms for trisilanolisobutyl-POSS (TiBP) and P*Am*TE at the A/W interface (T = 22.5 ^{o}C) and **(B)** the chemical structure of TiBP.

In order to understand why the film of P*Am*TE forms a LE monolayer, it is useful to consider the Π-*A* isotherm for poly(*tert*-butyl acrylate) (PtBA). Figure 4.9A shows a Π-*A* isotherm for PtBA where *A* is expressed as a function of the area per repeating unit (monomer for short). As seen in Figure 4.9A, Π for the PtBA film initially shows a slow rise in the region $35 < A < 55$ Å^2·molecule^{-1} = $A_{lift\text{-}off,\ PtBA}$. Further compression of the film causes Π to rise rapidly for $A < 35$ Å^2·molecule^{-1} before the film collapses at $A_c \sim 21$ Å^2·molecule^{-1} and $\Pi_c \sim 23$ mN·m^{-1}. The rapid rise in Π for $A < 35$ Å^2·molecule^{-1} is consistent with the formation of a condensed (LC) film. Extrapolation of the Π-*A* isotherm for the LC monolayer back to Π = 0 yields $A_0 \approx 30$ Å^2·molecule^{-1}. As seen in Figure 4.9B if one neglects the short linker, P*Am*TE is essentially POSS-NH_2 plus three PtBA repeating units. Interestingly, $A_{0,\ POSS\text{-}NH2} + 3A_{0,PtBA}$ yields 220 Å^2·molecule^{-1} ($\approx A_{lift\text{-}off,\ PAmTE}$). As such, we speculate that P*Am*TE starts with the POSS-cage and three *tert*-butyl esters adsorbed to the plane of the interface (Figure 4.10A). Throughout the monolayer regime, the POSS cage is likely riding on top of the *tert*-butyl esters (Figure 4.10B). However, a somewhat more speculative conclusion is that the POSS cage tilts during the transformation from a cage at the A/W interface to a cage on the *tert*-butyl esters as depicted in Figure 4.10B. There is a difference in A_c between P*Am*TE and TiBP. TiBP collapsed at $A_c = 140$ Å^2·molecule^{-1}, whereas P*Am*TE collapsed at a smaller $A_c \sim 100$ Å^2·molecule^{-1}. This value is consistent with a face-on conformation for P*Am*TE at collapse (Figure 4.10C).

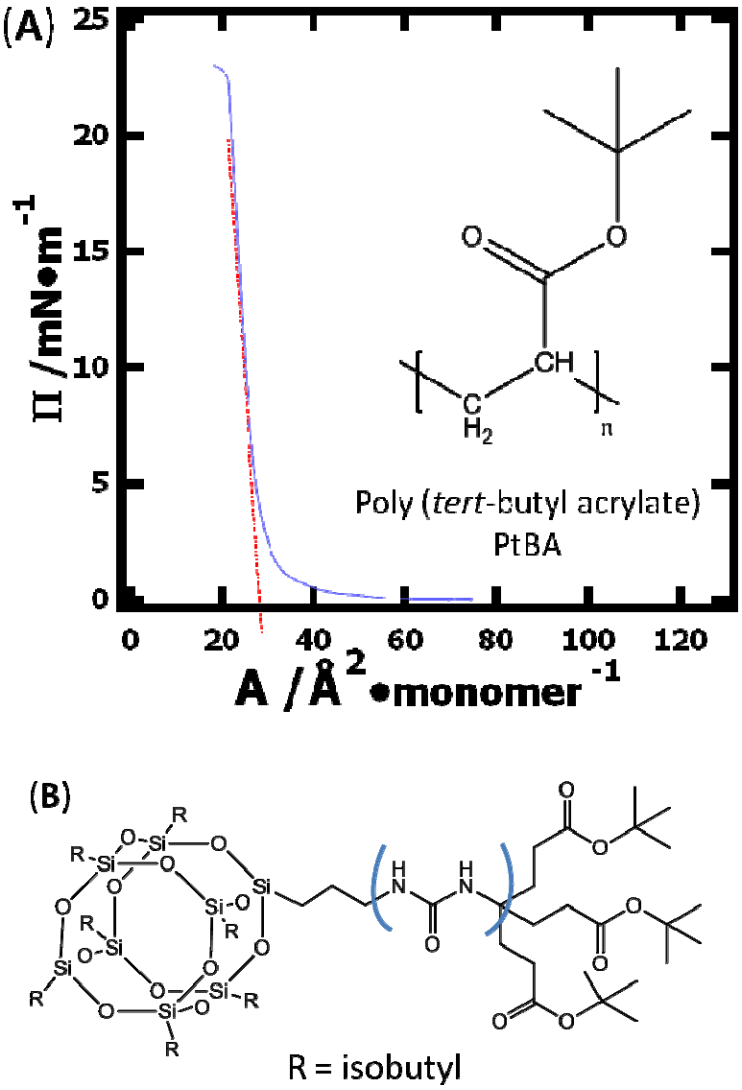

Figure 4.9 (**A**) Π-*A* isotherm for PtBA at the A/W interface at T= 22.5 °C. The red dashed line indicates A_0 for PtBA. (**B**) Structure of P*Am*TE highlighting the POSS-NH_2 piece and the three PtBA "repeating units" (outside the linker, circled in blue).

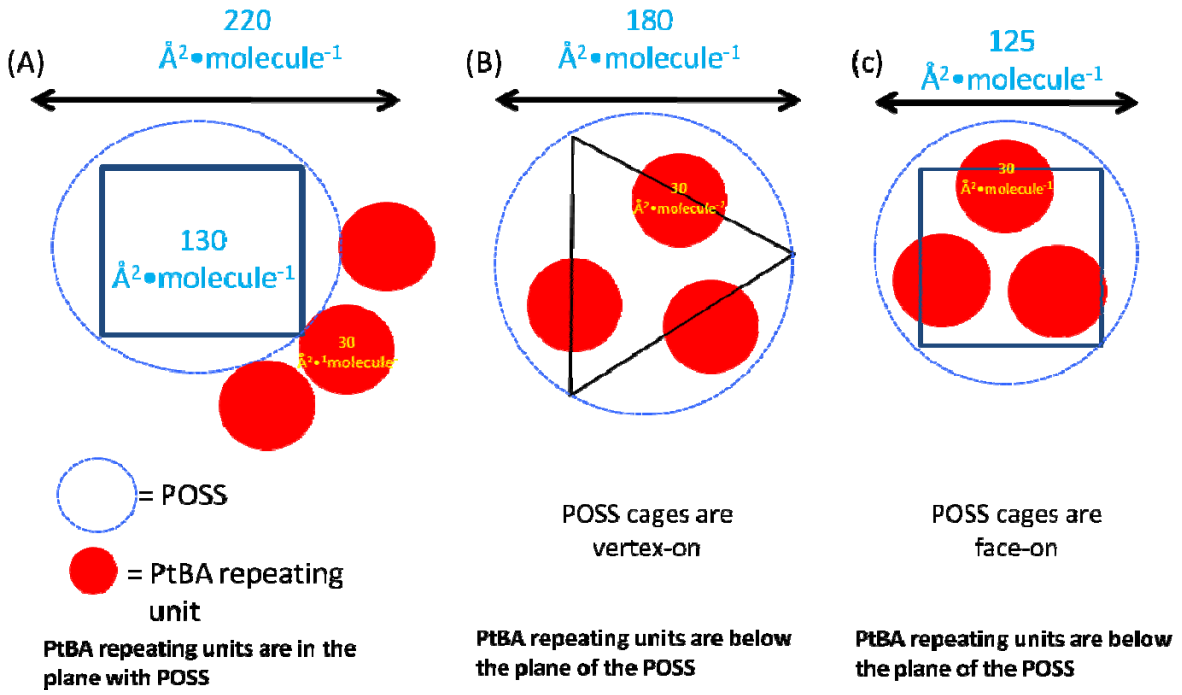

Figure 4.10 Schematic depictions of P*Am*TE (top view) in Langmuir films at various *A*: (**A**) $A = A_{lift\text{-}off}$, (**B**) $A_c < A < A_{lift\text{-}off}$, and (**C**) $A = A_c$.

4.4.4 Comparison of POSS-Based Triesters

Since POSS-NH_2 is very similar to POSS-OH in structure, the A_0 of POSS-NH_2 is similar to that of POSS-OH (Figure 4.11). These A_0 values are consistent with a face-on conformation. Furthermore, similar collapse areas suggest that they both tend to aggregate to form multilayers at the same molecular area. However, it is interesting to note that Π_c of POSS-NH_2 (~ 16 $mN \cdot m^{-1}$) is obviously larger than that of POSS-OH (~ 6 $mN \cdot m^{-1}$) due to the stronger solvation effect of the amino group.[132]

Moving onto POSS-based triesters (Figure 4.11), their difference in lift-off areas (~ 10 $Å^2 \cdot molecule^{-1}$) is consistent with the difference in A_0 between POSS-OH and POSS-NH_2. More importantly, the A_0 for both triesters is consistent with the PtBA repeating units and POSS cages both residing at the A/W interface as the monolayer forms. At the other end of the monolayer regime, P*Am*TE and P*Al*TE show a similar collapse area (~ 100 $Å^2 \cdot molecule^{-1}$) with a difference less than 2 $Å^2 \cdot molecule^{-1}$ (within experimental error) and nearly identical collapse pressures (Π_c ~ 23 $mN \cdot m^{-1}$). Therefore, P*Am*TE forms a softer LE film in monolayer regime than P*Al*TE even if they both exhibit a limiting area of ~ 175 $Å^2 \cdot molecule^{-1}$. This result is consistent with a vertex-on conformation around A_0 in the LE monolayer region. It is also interesting to note that the Π_c ~ 23 $mN \cdot m^{-1}$ are identical even though the collapse pressure of POSS-OH is ~ 1/3 that of POSS-NH_2. This coincidence indicates that ureido (-NH-CO-NH-) and carbamate (-O-CO-NH-) interactions with the water surface are similar and likely insignificant compared to the ester linkages as $\Pi_{c,\ PtBA}$ ~ 23 $mN \cdot m^{-1}$ as well. This behavior would be consistent with POSS cages and the ureido or carbamate linker residing on top of the three ester groups forming a tripodal face-on conformation. Therefore, the POSS-based triesters are essentially PtBA repeating units in contact with water with POSS cages on top.

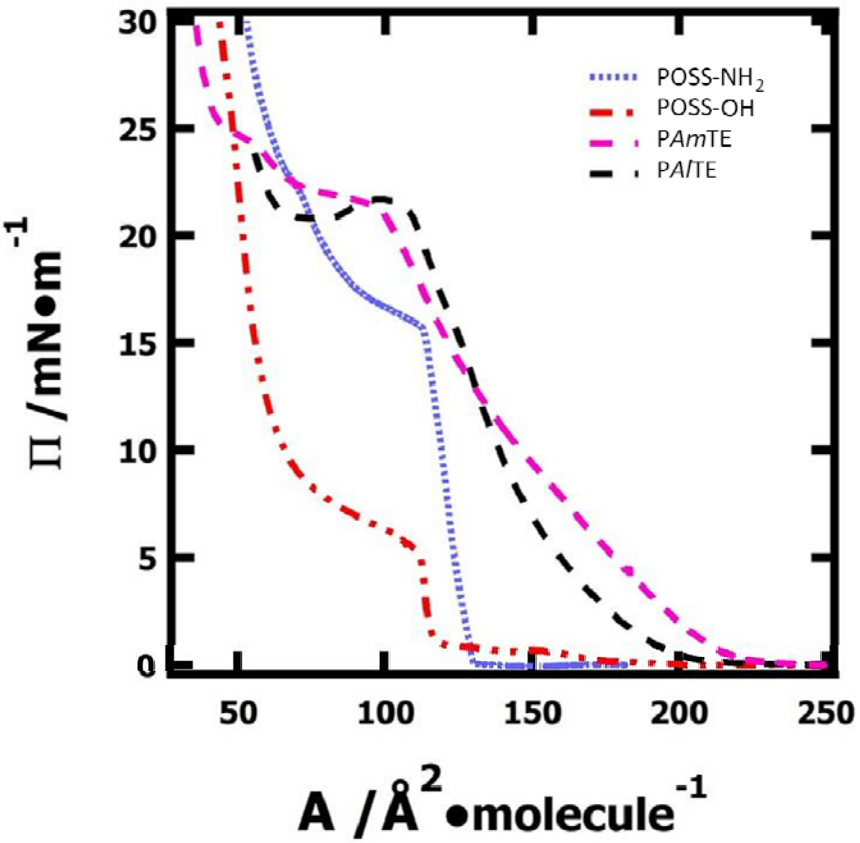

Figure 4.11 Π-*A* isotherms for POSS-NH_2, POSS-OH, P*Am*TE and P*Al*TE at the A/W interface at 22.5 °C.

4.5 Conclusions

A new closed-cage POSS derivative, P*Am*TE was synthesized and characterized. Π-*A* isotherm studies of P*Am*TE at the A/W interface revealed a similar behavior to that of P*Al*TE. This behavior was interpreted as P*Am*TE initially lying on the water surface with the POSS cage and *tert*-butyl groups in the same plane. In the monolayer region, the POSS cage may exhibit a vertex-on conformation as the film is compressed and ultimately a face-on conformation upon

collapse. Compared to P*Al*TE, P*Am*TE has a larger lift-off area and smaller collapse area leading to a softer LE monolayer. Even though POSS-OH and POSS-NH_2 exhibit similar collapse areas and very different collapse pressures, the fact that P*Am*TE and P*Al*TE collapse at the same area and surface pressure suggests the triester portion of the molecule dominates the interaction with water while POSS cages control the packing with a face-on conformation near the collapse point of the film.

Chapter 5

Synthesis and Characterization of POSS-OH Based Diester at the Air/Water Interface

5.1Abstract

A diester, polyhedral oligomeric silsesquioxane (POSS) derivative was synthesized from (3-hydroxypropyl)-heptaisobutyl-POSS (POSS-OH) and an isocyanate diester. Surface pressure-area per molecule (Π-*A*) isotherm studies and Brewster angle microscopy (BAM) confirmed POSS-OH and POSS-OH based diester (P*Al*DE) were amphiphilic at the air/water (A/W) interface. Analysis of the Π-*A* isotherms revealed packing of POSS-OH at the A/W interface was significantly different from previously reported POSS amphiphiles. Whereas trisilanol-POSS derivatives pack with a vertex-on conformation, POSS-OH packs with a face-on conformation. Π-*A* isotherms show that P*Al*DE Langmuir monolayers exhibit a liquid expanded-to-condensed (LE/LC) phase transition with an apparent critical temperature (T_c) near room temperature. The two-dimensional (2D) Clausius-Clapeyron equation yields an apparent T_c = 37.5 ± 2.3 °C for non-equilibrium compression at a fixed rate experiments. Stepwise compression experiments show the observed non-equilibrium phase transition is strongly influenced by film collapse. For P*Al*DE, the LE/LC phase transition may correspond to a transition from a vertex-on to face-on conformation during compression of the molecules at the A/W interface.

5.2 Introduction

Polyhedral oligomeric silsesquioxane (POSS) molecules have attracted considerable attention in the past decades as shape memory materials,[123] coatings,[7d, e, 30b, 41h, 124] low-*k* dielectric materials,[125] and catalysts for the preparation of nanostructured materials,[7c, 126] and dendrimers.[7g, 88a, 127] Due to the core-shell structure and intermediate properties between ceramics and polymers, POSS cages have been increasingly incorporated into polymers for the enhancement of the glass transition temperature[123h, 128] and thermal stability and the development of superoleophobic surfaces.[127c, 128a, b, 128d, 128l, 129-130] However, less research focused on the surface behavior of POSS as amphiphilic materials until Deng, *et. al.* provided a series of reports on the ability of trisilanol-POSS derivatives to form stable Langmuir monolayers at the air/water (A/W) interface.[30b, 83b] Multilayer POSS films,[30c, 83c] POSS/polymer blends,[131, 133] and phase behavior of POSS on solid substrates were subsequently studied.[30o, 113, 118d, 134]

Trisilanol-POSS derivatives have been more thoroughly studied at the A/W interface since they are amphiphilic and exhibit more interesting phase behavior than most commercially available closed-cage POSS derivatives which are hydrophobic and aggregate at the A/W interface. Furthermore, the Esker group achieved progress on the modification and characterization of octafunctional-POSS.[47d] A triester (P*AI*TE) was created from a purified closed-cage POSS (POSS-OH) and characterized by surface pressure-area per molecule (Π-*A*) isotherms and Brewster angle microscopy (BAM) to probe the quasi-two-dimensional thermodynamic and morphological properties of these materials, respectively, at the A/W interface. The results indicate that P*AI*TE is surface active and forms a liquid expanded (LE) monolayer at the A/W interface.

Traditional Langmuir monolayers are composed of amphiphiles with polar head groups, which anchor them at the interface and hydrophobic tail parts that prevent their dissolution into the subphase.[1b] The progress in the study of Langmuir monolayers have been reported in fields of chemistry, physics, and life sciences.[1c, d, 47a, 135] Long-chain fatty acids[136] and lipids[137] are classical amphiphiles which have been thoroughly studied at the A/W interface. As a two-dimensional (2D) analog of three dimensional (3D) pressure-volume (*P*-*V*) isotherms, Π-*A* isotherms also had different phases: gas (G) where molecules are far apart and interactions are negligible, liquid-expanded (LE) where molecules are loosely packed, liquid-condensed (LC) where molecules are closely packed with defined tilt angles, and solid (S) where the monolayer collapses into multilayers. Phase transitions, such as G/LC, G/LE, LE/LC, and LC/S could be observed. Among these phase transitions, the LE/LC phase transition is the most interesting since the key difference between liquid phases are their densities and long-range order.[47a] Brewster angle microscopy (BAM),[41] X-ray diffraction techniques (XRD),[42] fluorescence microscopy (FM),[43] have all been used to study these differences.

Although the LE/LC phase transition mostly appears as a non-zero slope "plateau" in the isotherms, its first-order nature was revealed by fluorescence imaging,[67] electron microscopy,[138] and BAM.[40c, 139] Normally, the non-zero slope correlates to artifacts from impurities, the formation of small molecular aggregates or surface micelles, or non-equilibrium effects such as finite compression rates.[40a, 47a] Therefore, it was necessary to develop a very careful experimental protocol to observe a zero slope for a LE/LC phase transition. This protocol required an ultra-clean system, pure materials, extremely slow compression rates, and a stable film.[140]

The traditional model for amphiphilic molecules, such as fatty acids, can be simplified as rod-like objects due to their large length/diameter ratio (Figure 5.1). As the length/diameter ratio decreases,

the traditional amphiphiles become water-soluble leading to Gibbs monolayers.[67] Additionally, the complicated regions of the monolayer phase diagram shifts to temperatures that are experimentally inaccessible for these short chain amphiphiles. As a result, short chain fatty acids only form a liquid-expanded monolayer phase. Trisilanol-POSS derivatives were also expected to have simple phase diagrams at experimentally accessible temperatures because of their small length/diameter ratios and barrel-like shapes. This chapter will challenge this prediction.

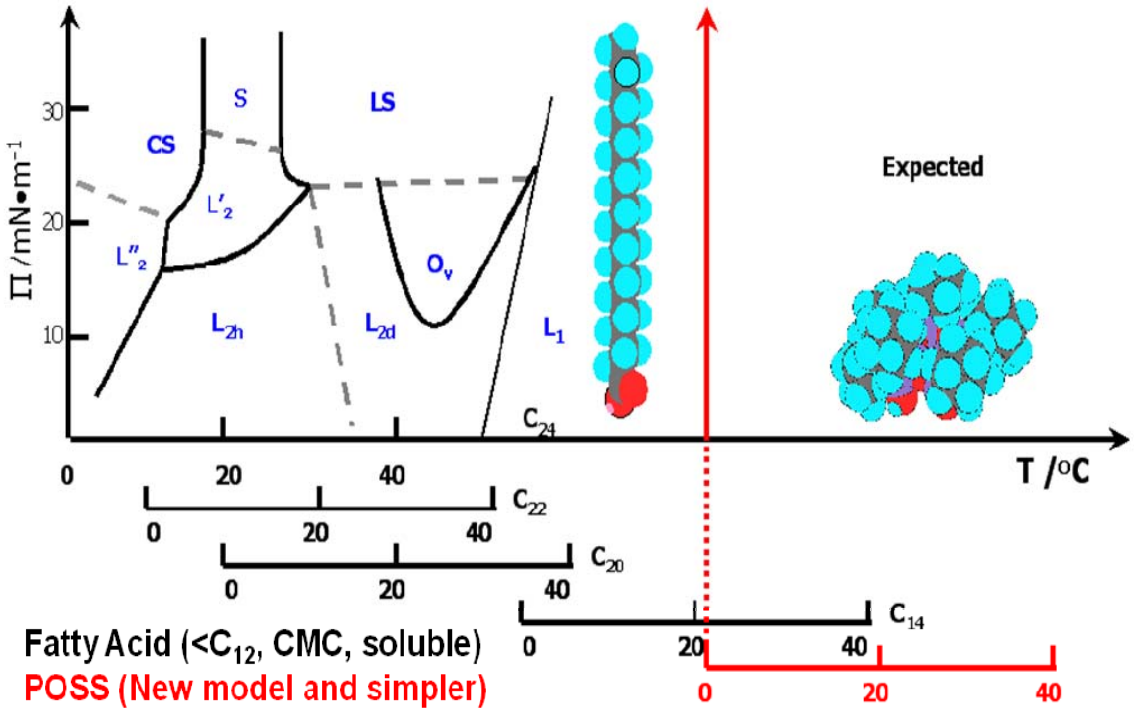

Figure 5.1 Experimentally accessible windows of Π-*A* isotherms for fatty acids and barrel-like POSS model.[85]

In this study, a POSS-OH based diester (P*Al*DE) was synthesized and characterized from (3-hydroxypropyl)-heptaisobutyl-POSS (POSS-OH) and an isocyanate diester by ^{1}H NMR, ^{13}C NMR, high resolution mass spectrometry (HRMS), and melting point measurement. P*Al*DE Langmuir monolayers were examined at the A/W interface and a LE/LC phase transition was observed. This is the first known POSS material which has a LE/LC phase transition. The critical temperature (T_c) obtained through the 2D Clausius-Clapeyron equation agrees well with the experimental results. The conformation of the P*Al*DE is explained based on the study on P*Al*TE.

5.3 Experimental

Experimental details regarding the synthesis of P*Al*DE (**3** in Scheme 3.2) were provided in Chapter 3.1.2.2. Experimental methods for Π-*A* isotherm (Chapter 3.3.1) and BAM (Chapter 3.3.3) studies were covered in Chapter 3.3.

5.4 Results and Discussion

5.4.1 Synthesis and Characterization of POSS-OH Based Diester (P*Al*DE)

POSS-OH (**1 i**n Scheme 3.1) was insufficiently pure to begin the synthesis of P*Al*DE (**3** in Scheme 3.1). Flash column separation was ultimately chosen for purification over recrystallization because it afforded better yields. In Scheme 3.1, a slight molar excess of isocyanate diester (**2** in Scheme 3.1) reacted with POSS-OH (**1** in Scheme 3.1) with a molar ratio of **1**:**2** = 1:1.05.

Chemical composition and purity were confirmed via ^{1}H NMR, ^{13}C NMR, melting point, and HRMS. Figures 5.2 and 5.4 contain the ^{1}H NMR spectra with melting point ranges for POSS-OH and P*Al*DE in $CDCl_3$, respectively. Figures 5.3 and 5.5 contain the ^{13}C NMR spectra for POSS-OH, and P*Al*DE in $CDCl_3$, respectively. In order to clarify different peaks, an expanded ^{13}C NMR spectrum is provided in Figure 5.6 for P*Al*DE. The spectra reveal sharp, well-resolved peaks. The characteristic differences in the splitting pattern of the protons of the linker and essentially quantitative integrations were consistent with the labeled structures on each spectrum.

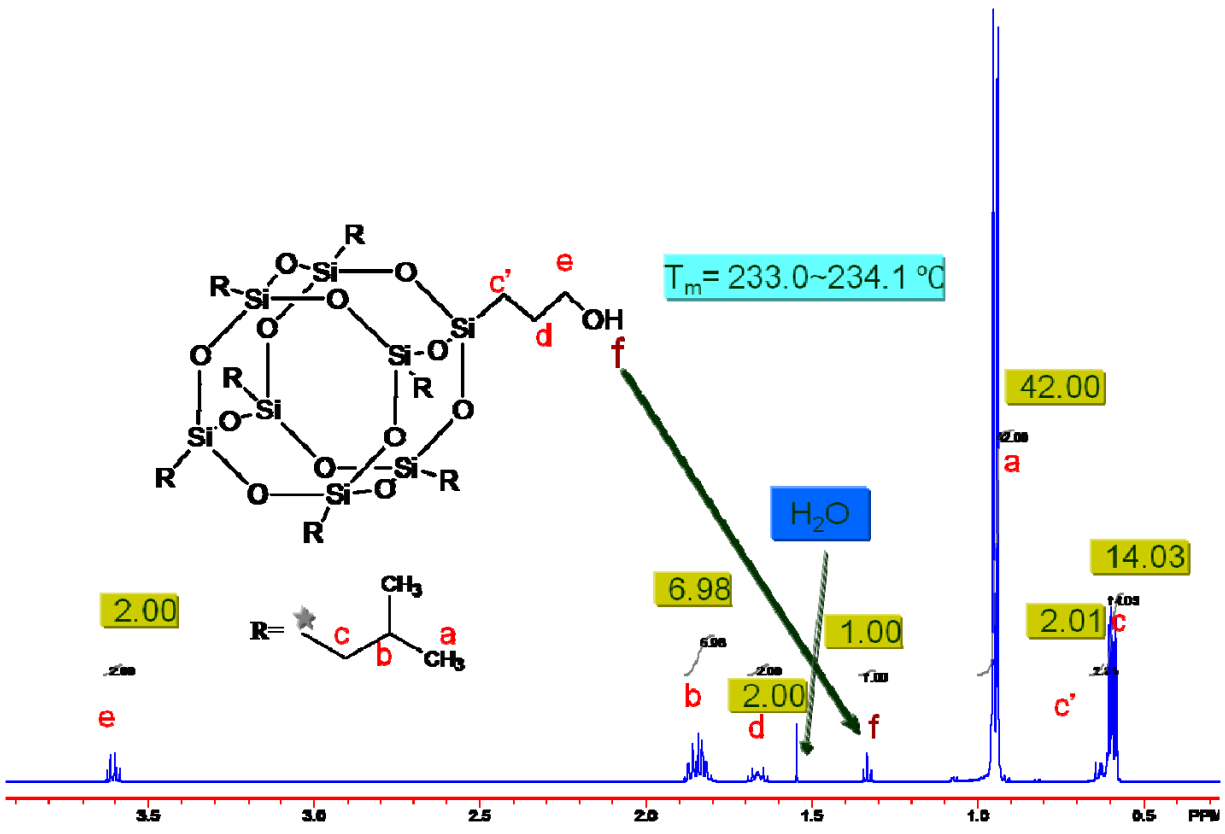

Figure 5.2 ^{1}H NMR and T_m of purified POSS-OH.

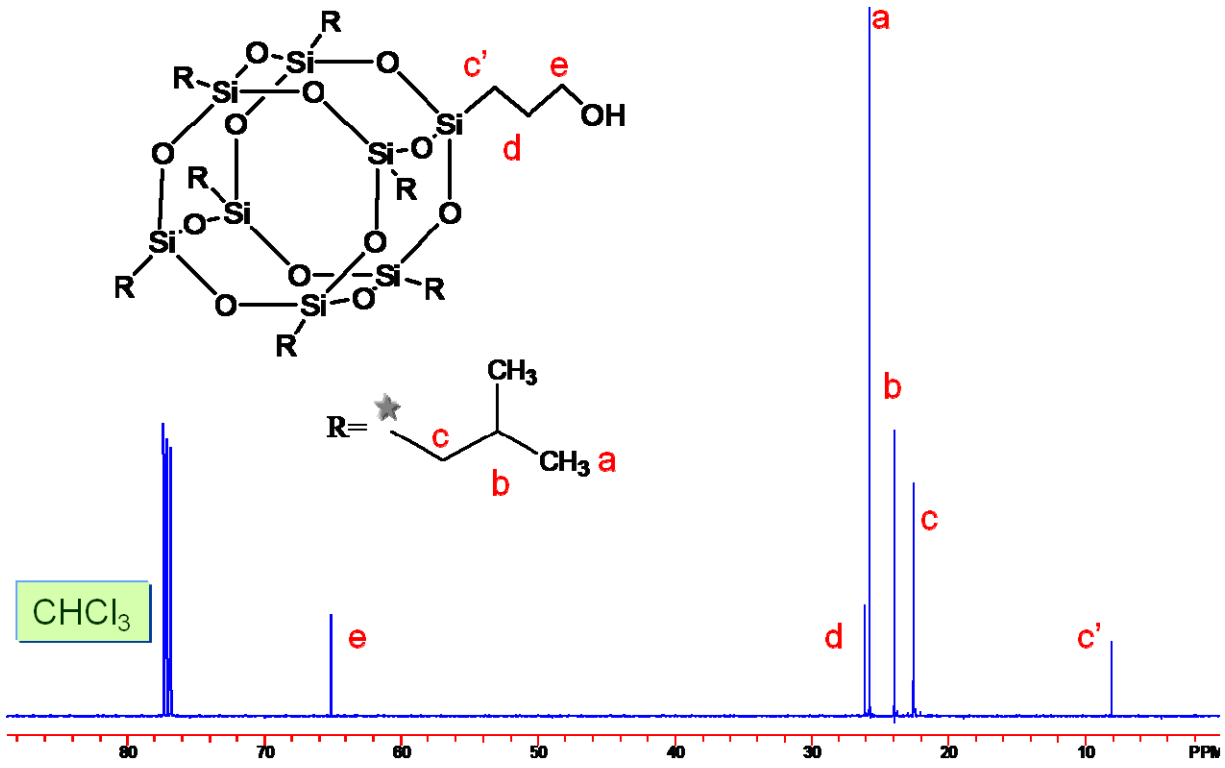

Figure 5.3 ^{13}C NMR of purified POSS-OH.

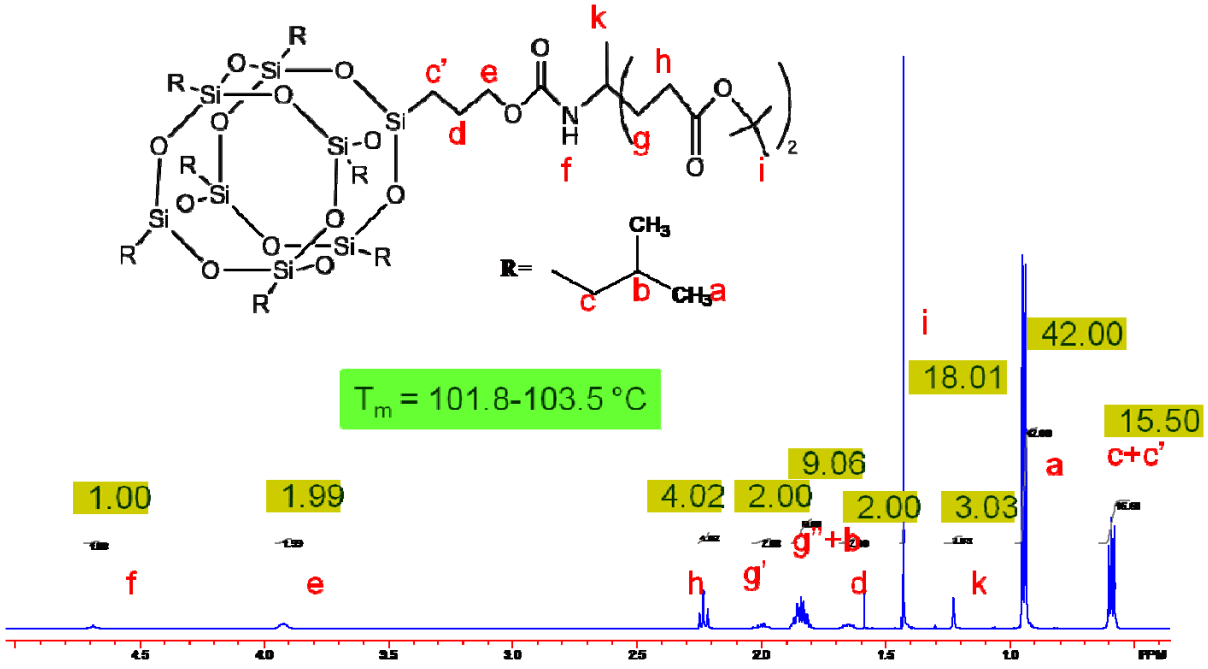

Figure 5.4 ^{1}H NMR and T_m of P*Al*DE.

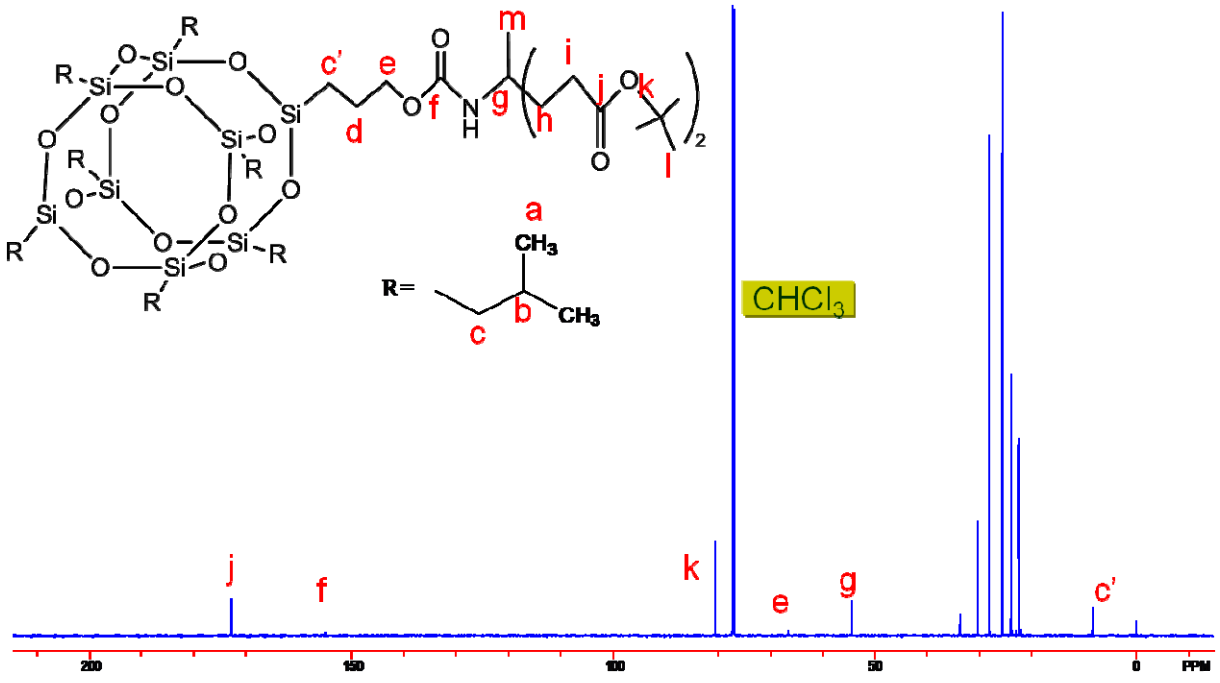

Figure 5.5 ^{13}C NMR of P*Al*DE.

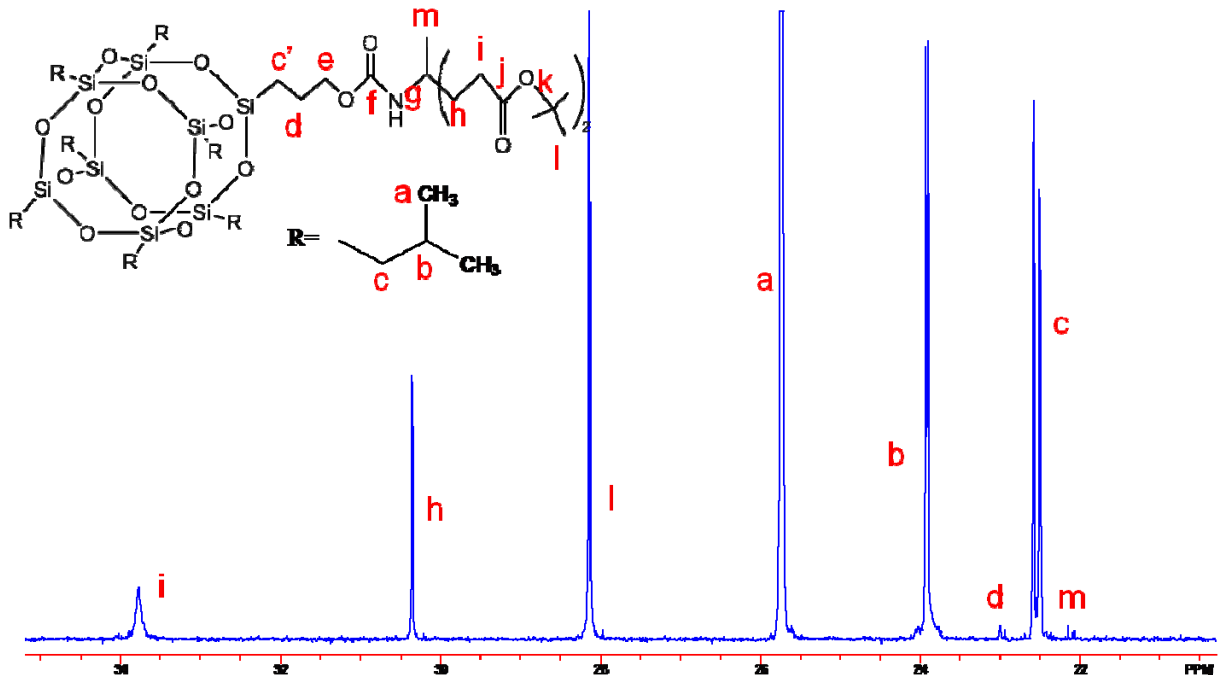

Figure 5.6 Expanded ^{13}C NMR of P*AI*DE.

5.4.2 Observation of a LE/LC Phase Transition

Figure 5.7 shows Π-*A* isotherms for P*AI*DE at the A/W interface at 5 °C. Four different regions are depicted: (a) $A > 182$ Å^2•molecule^{-1} where Π ~ 0 and the film is either a G or G/LE film; (b) $140.5 < A < 182.0$ Å^2•molecule^{-1}, a highly compressible LE monolayer with Π between 0 and 9.4 mN•m^{-1}; (c) $134.1 < A < 140.5$ Å^2•molecule^{-1}, LE-LC phase coexistence with a non-zero slope around Π ~ 9.4 mN•m^{-1}; and (d) $116.3 < A < 134.1$ Å^2•molecule^{-1}, a less compressible LC monolayer with Π between 9.4 and 21.9 mN•m^{-1}.

The biphasic nature of the LE/LC phase transition has been observed by BAM.[121, 139, 141] In Region *b* (Figure 5.7), a uniform film is formed without obvious features indicating a homogeneous monolayer (BAM image *i* in Figure 5.7). In Region *c*, coexistence of LE and LC phases is observed. Circular domains are dispersed in another phase (BAM image *ii* in Figure 5.7). Similar results have been reported for diethylene glycol mono-*N*-octadecyl ether,[142] di-*n*-tetradecyl hydrogen phosphate (DTP),[143] dimyristoyl phosphatidyl serine (DMPS)[3a], dipalmitoyl phosphatidyl choline (DPPC)[144], and even poly(*L*-lactic acid).[121] This feature can be understood from the change of density during the first-order transition. Upon compression, the LC phase forms through nucleation and growth inside the LE phase. Therefore, at the end of Region *c* with a transition pressure (Π_{tr}) of 9.4 $mN \bullet m^{-1}$, the circular domains disappear (BAM image *iii* in Figure 5.7) and give way to a uniform monolayer in region *d* (BAM image *iv* in Figure 5.7).

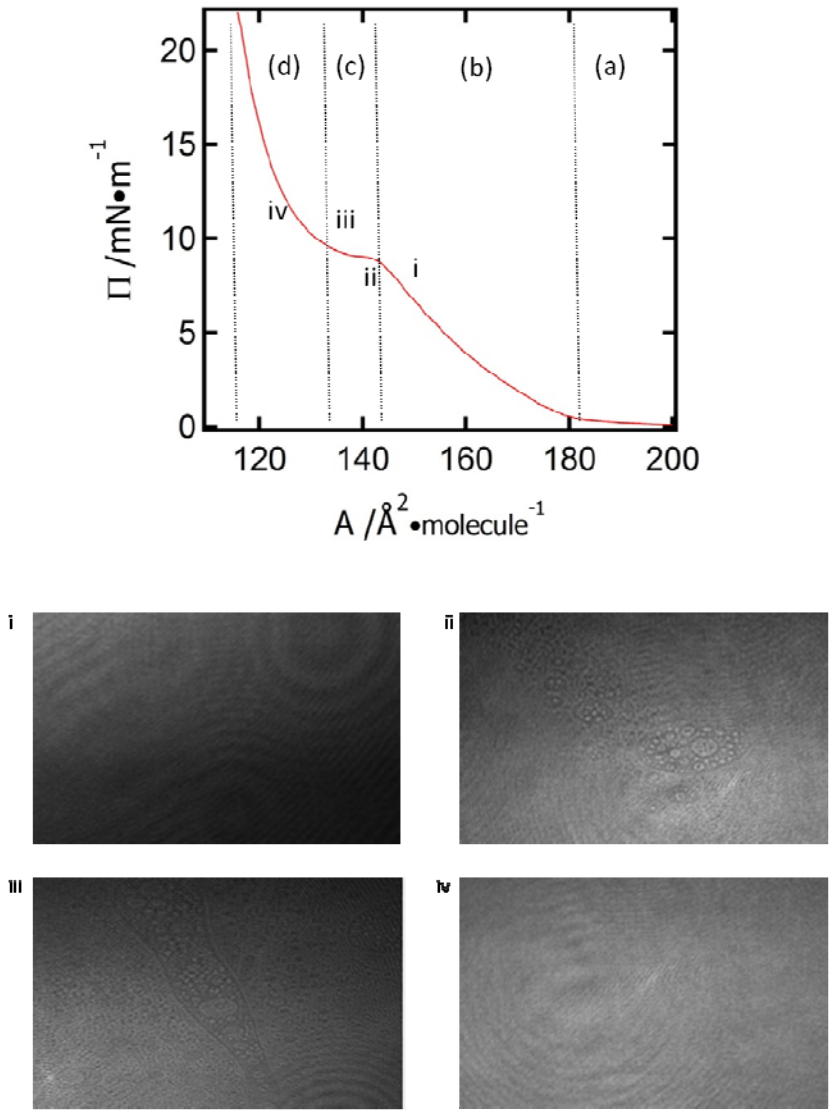

Figure 5.7 Π-*A* isotherms of P*Al*DE at the A/W interface at 5 °C. Four regions are depicted: (a) G or G/LE; (b) a LE phase; (c) LE/LC coexistence; and (d) a LC phase. BAM images at different *A* are provided: (i) 141.0 Å^2•molecule^{-1}, LE monolayer prior to phase transition; (ii) 136.8 Å^2•molecule^{-1}, circular domains of coexistent LE and LC domains; (iii) 133.8 Å^2•molecule^{-1}, approaching the end of the plateau; and (iv) 133.8 Å^2•molecule^{-1}, a LC monolayer. All BAM images are 2.0 × 2.4 mm^2, cut from the original BAM images. Each BAM image has an independent gray scale.

5.4.3 Different Compressibility between the LE and LC Phases

As a 2D analog of a 3D *P*-*V* isotherm, Π-*A* isotherms also have compressibilities (κ_s) and static elastic moduli (ε_s): $\varepsilon_s = \kappa_s{}^{-1} = -A\left(\frac{\partial \pi}{\partial A}\right)_T$. Hence 2D Π-*A* isotherms can be used to estimate the stiffness of the Langmuir film through ε_s.

A plot of ε_s -*A* is compared with the Π-*A* isotherm at 5.0 °C in Figure 5.8. In the first plateau (*A* > 182.0 Å^2•molecule^{-1}) of the Π-*A* isotherm, ε_s is essentially zero and increases slowly as the monolayer forms. As the film is compressed in the LE region (140.5 < *A* < 182.0 Å^2•molecule^{-1}), ε_s increases faster until it reaches the first maximum, shortly before the kink in the ∏-*A* isotherm that signifies the starting point of LE/LC phase transition. The value of the static elasticity maximum, $\varepsilon_{s,\,max}$ ~ 50 mN•m^{-1}, is consistent with a LE monolayer. However, an ideal plateau value of ε_s = 0 mN•m^{-1} is not observed due to the non-zero slope in the LE/LC phase transition region. This result may be due to the artifacts of impurities, small molecular aggregates or surface micelles, or nonequilibrium effects such as finite compression rates.[67] After the second plateau (134.1 < *A* < 140.5 Å^2•molecule^{-1}), ε_s increases obviously corresponding to the formation of rigid LC Langmuir monolayer. The second maximum of ε_s is observed at *A* ~ 117.1 Å^2•molecule^{-1} and Π = 20.2 mN•m^{-1}. The value, $\varepsilon_{s,\,max}$ ~ 218 mN•m^{-1}, is consistent with a LC monolayer. Collapse of the LC monolayer into multilayers occurs in region *e*.

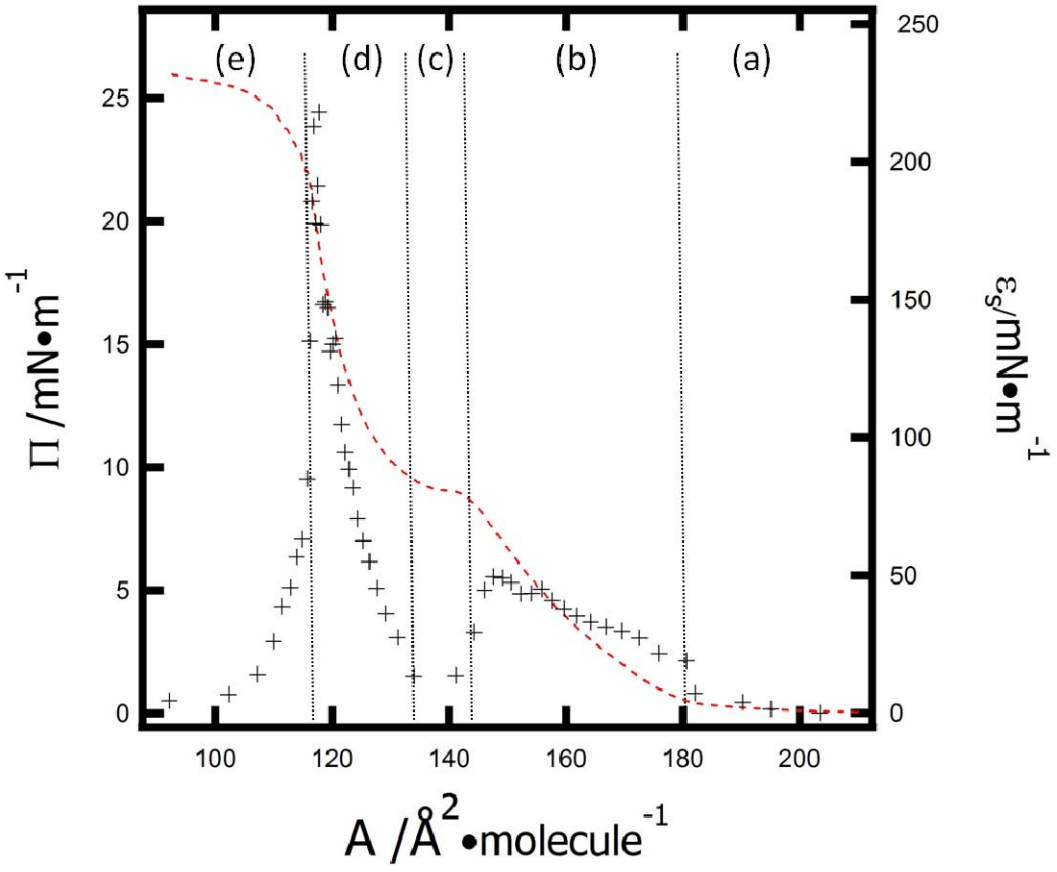

Figure 5.8 Comparison of the ∏-*A* isotherm (red dotted lines ----) and ε_s-*A* plot (black crosses +) for P*Al*DE at 5.0 °C. The dashed vertical lines break the isotherms into the same regions defined in Figure 5.7.

5.4.4 Temperature Dependence of the LE/LC Phase Transition

The temperature dependence of the non-equilibrium LE/LC phase transition of P*Al*DE at the A/W interface for experiments performed at a constant compression rate is shown in Figure 5.9. As temperature increases, several changes occur in the ∏-*A* isotherms of these Langmuir monolayers. First, the onset of the LE monolayer shifts to a larger lift-off area ($A_{lift\text{-}off}$), where Π

increases from zero. This result is expected because molecules possess greater thermal energy at higher temperature and have larger effective cross-sectional areas. Second, Π at the onset of the LE/LC phase transition (Π_{tr}) increases while the corresponding area (A_{tr}) decreases. Meanwhile, the area at the end of the LE/LC phase transition increases leading to a shorter plateau as temperature increases. These changes in Π_{tr} and A_{tr} are also related to the enhanced molecular mobility. Third, an apparent critical temperature (T_c) is approached from below as temperature increases. At 37.5 °C, an obvious phase transition is still observed while a smoother curve is observed at 40 °C suggesting the apparent T_c lies between 37.5 °C and 40 °C.

It is also interesting to note that the collapse pressure ($\prod_{collapse}$) of P*Al*DE decreases and the collapse area ($A_{collapse}$) increases as temperature increases. The temperature dependence of $\prod_{collapse}$ and $A_{collapse}$ for P*Al*DE is shown in Figure 5.10. This tendency is opposite to that of $\prod_{tr}$ and A_{tr} and is expected because it is easier for Langmuir monolayers to overcome the energy barrier associated with the nucleation and growth of the 3D structures at higher temperatures. At each temperature, three experiments were performed and the average values with one standard deviation error bars are used in Figure 5.10.

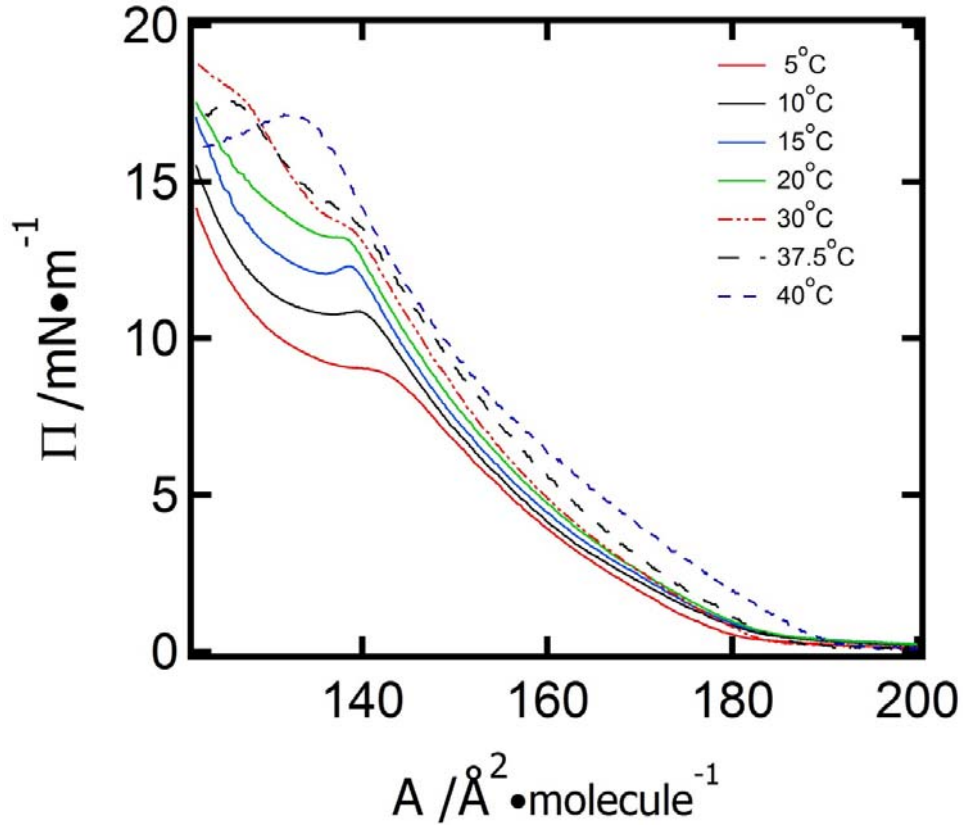

Figure 5.9 Temperature dependence of the LE/LC phase transition of P*Al*DE at the A/W interface. Isotherms at different temperatures are labeled by different colors and different line styles. LE/LC phase coexistence is observed for isotherms below 37.5 °C, and is not observed at 40 °C, indicating the critical temperature (T_c) lies between 37.5 °C and 40 °C.

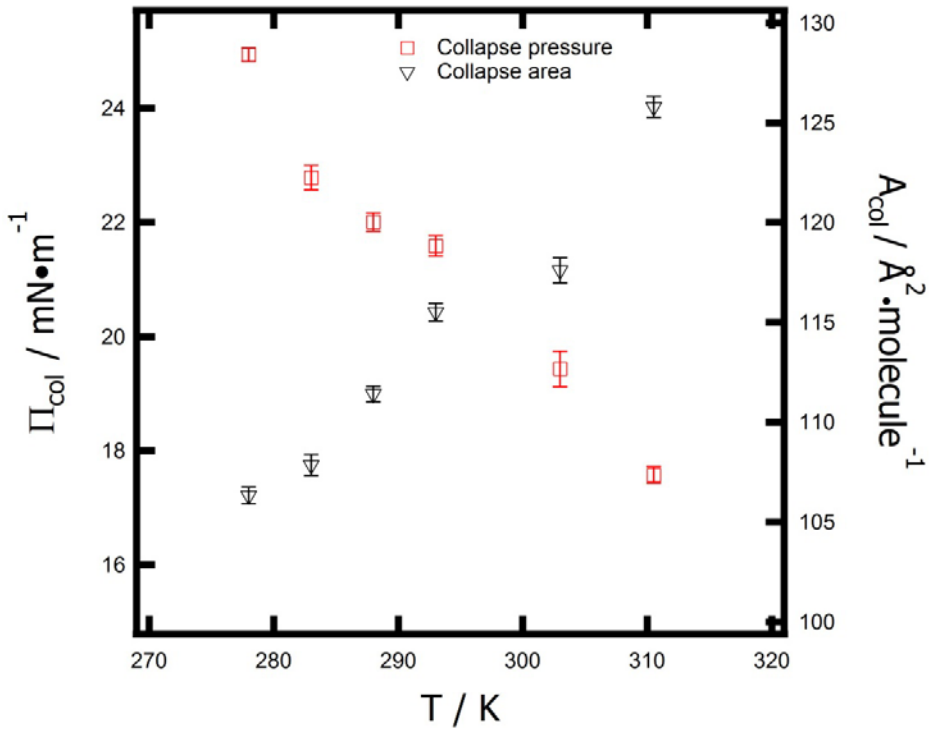

Figure 5.10 Temperature dependence of $\prod_{collapse}$ (red squares) and A_{collapse} (black triangles) for P*Al*DE Langmuir films at the A/W interface. Each point is the average value from three experiments. The standard deviation error bars are provided to indicate uncertainties.

In order to estimate the value of T_c predicted from the $\prod$-A isotherms, a 2D Maxwell relationship for the entropy of the transition (S_{tr}):

$$\left(\frac{\partial S_{tr}}{\partial \pi}\right)_T = -\left(\frac{\partial A}{\partial T}\right)_\pi \tag{5.1}$$

leads to two different forms of the 2D Clausius-Clapeyron equation:[47a, 145]

$$\Delta S_{tr} = \left(\frac{d\pi_{tr}}{dT}\right)(A_{LC} - A_{LE}) \tag{5.2}$$

$$\Delta H_{tr} = T(\frac{d\pi_{tr}}{dT})(A_{LC} - A_{LE}) \quad (5.3)$$

ΔS_{tr} represents the entropy change during the LE/LC transition and ΔH_{tr} represents the enthalpy change during the LE/LC transition. $\prod_1$, the same as $\prod_{tr}$, is the surface pressure of the onset of LE/LC phase transition while $\prod_2$ is the surface pressure at the end of the LE/LC phase transition at a given temperature *T*. A_{LE} corresponds to the surface area at $\prod_{tr}$ while A_{LC} is the *A* value at the end of LE/LC phase transition.

A_{LE} is determined by the area where a kink is observed and $\prod_{tr}$ is the corresponding surface pressure. However, in view of experimental limits, it is difficult to determine A_{LC} by simply reading a value off the $\prod$-*A* isotherms.[146] Grazing incidence X-ray scattering (GIXS)[147] and BAM[148] have been applied to localize A_{LC}. However, the results are accurate only when the size and density of the LE/LC phase are homogeneous over the entire plateau region.[146] In another approach, the Butler equation was used for both coexisting 2D phases in equilibrium.[149] Nevertheless, this method seems intricate and is not suitable for subphases containing ions.[150] For example, dipalmitoyl phosphatidyl glycerol (DPPG) was spread on a physiological subphase containing Na^+ and Ca^{2+} ions. The strong influence of the ions on the properties of the monolayer led to invalid results from the Butler equation.[145] The limiting area (A_0), which was obtained by extrapolating the steepest portion of the Π-*A* isotherm back to Π = 0, is used to estimate the cross-sectional area of a molecule. When a LE/LC phase transition exhibits a non-zero slope, an approximation of A_{LC} is achieved from the intersection of the line used to estimate the limiting area of a LC monolayer and a horizontal line representing a constant $\prod_{tr}$ as depicted in Figure 5.11.

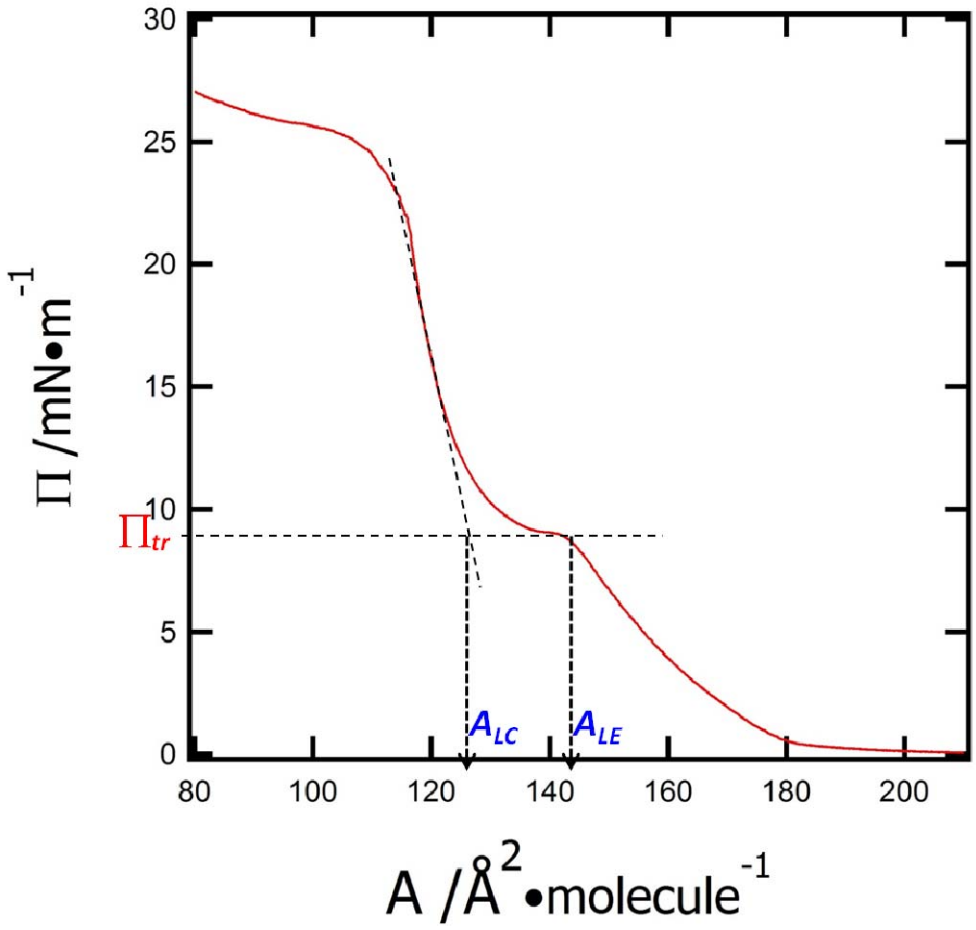

Figure 5.11 Schematic depiction of the procedure to determine A_{LC} at the end of LE/LC phase transition for an isotherm of P*Al*DE at 5 °C. A_{LE} is obtained from the kink in the $\prod$-*A* isotherm and a horizontal line represents $\prod_{tr}$ = 9.1 mN•m^{-1} at the onset of the LE/LC phase transition. A_{LC} is obtained from the intersection of the line used for obtaining the limiting area of the LC monolayer and the horizontal line.

In order to determine ΔS_{tr} and ΔH_{tr} in Equation 5.2 and 5.3, a plot of the temperature dependence of $\prod_{tr}$ is provided in Figure 5.12. A linear relationship is approximated with a slope of 0.15 ± 0.01 $mN \bullet m^{-1} \bullet K^{-1}$. An extrapolation of the best linear fit back to the x-axis yields a temperature of -60.6 ± 1.6 °C, the temperature below which no LE phase should be observed.[151] Noting the rather long extrapolation to obtain this value, it should be noted that the exact value is unimportant. Rather, it shows that the absence of an LE phase occurs at temperatures much lower than are experimentally accessible.

With the slope obtained from Figure 5.12, the temperature dependence of ΔH_{tr} and ΔS_{tr} for P*Al*DE Langmuir films at the A/W interface were calculated and are provided in Figure 5.13. ΔS_{tr} values are negative since ordered structures are formed from less ordered structures during the LE/LC phase transition.[1b] The 2D analog of heat capacity change between the LE and LC phases is defined as the slope of ΔH_{tr} versus T :

$$\Delta C_{\pi}^{tr} = \left(\frac{\partial \Delta H_{tr}}{\partial T}\right)_{\pi} \tag{5.4}$$

At the critical temperature (T_c), the LE/LC phase transition reduces to a single point when ΔH_{tr} = 0. Therefore, the critical temperature can be predicted by extrapolating the linear fit line to the x axis. The result, an apparent T_c = 37.5 ± 2.3 °C, agrees with the experimental prediction between 37.5 and 40 °C.

Data for temperature (T), the area at the LC end of the LE/LC phase transition (A_{LC}), the area at the onset of the LE/LC phase transition (A_{LE}), the difference of A_{LE} and A_{LC} (ΔA), and entropy changes (ΔS_{tr}) and enthalpy changes (ΔH_{tr}) during the LE/LC phase transition are shown in Table 5.1.

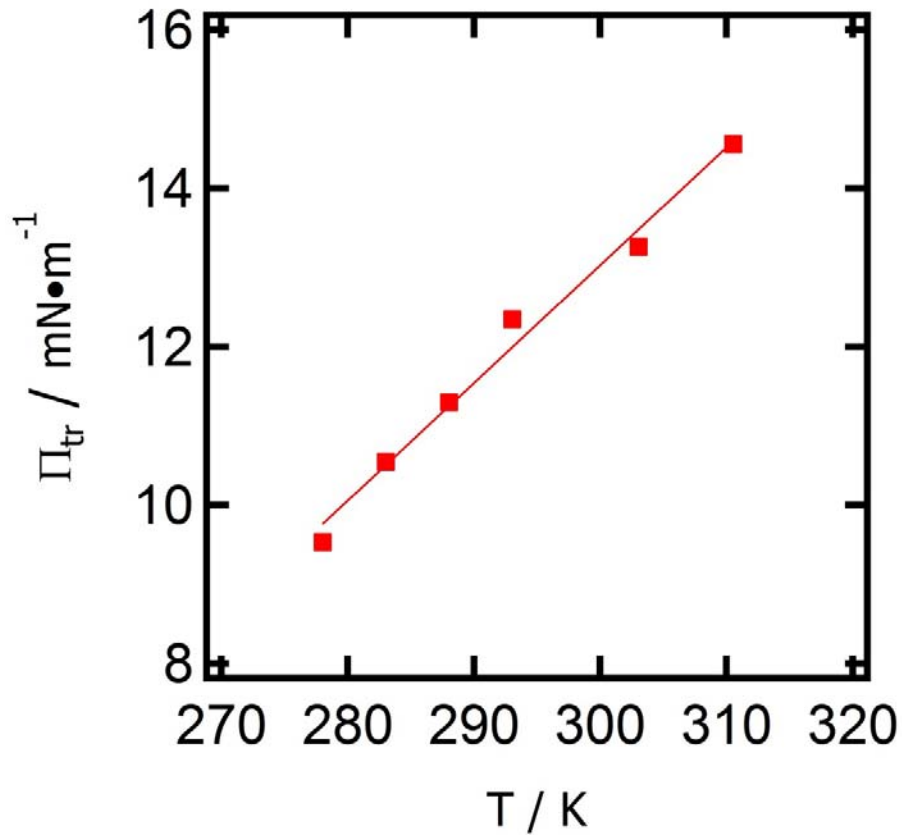

Figure 5.12 Temperature dependence $\prod_{tr}$ for P*Al*DE Langmuir films at the A/W interface. The linear fit provides a slope of 0.15 ± 0.01 mN•m^{-1}•K^{-1}.

The close proximity of the apparent Tc to the collapse transition and the dynamic nature of the constant compression rate experiments make it likely that there is a strong interplay between the LE/LC phase transition and film collapse. In order to examine the interplay between the LE/LC phase transition and collapse, stepwise compression experiments for 5 ^{o}C and 22.5 ^{o}C were performed (Figure 5.14). At 5 ^{o}C , the constant compression rate and stepwise compression experiments show agreement up to a surface pressure of Π ~ 7.8 mN•m^{-1} or *A* ~ 154 Å^{2}•molecule^{-1}. The decrease in transition pressure for the stepwise compression experiment is

caused by relaxation in surface pressure during stepwise compression, since compression at a constant rate does not allow molecules to reach equilibrium conformations. Similarly, the collapse pressure for stepwise compression is reduced. A LC region (albeit smaller for stepwise compression) is observed for both experiments even if the Π-*A* isotherms are obviously different overall. At 22.5 ^{o}C (Figure 5.14B), it is clear that $\prod_c$ is strongly influenced by compression rate and must impact the LE/LC phase transition even in constant compression rate experiments. For this reason, the T_c estimate from the 2D Clausius-Clapyeron analysis is regarded as an apparent T_c.

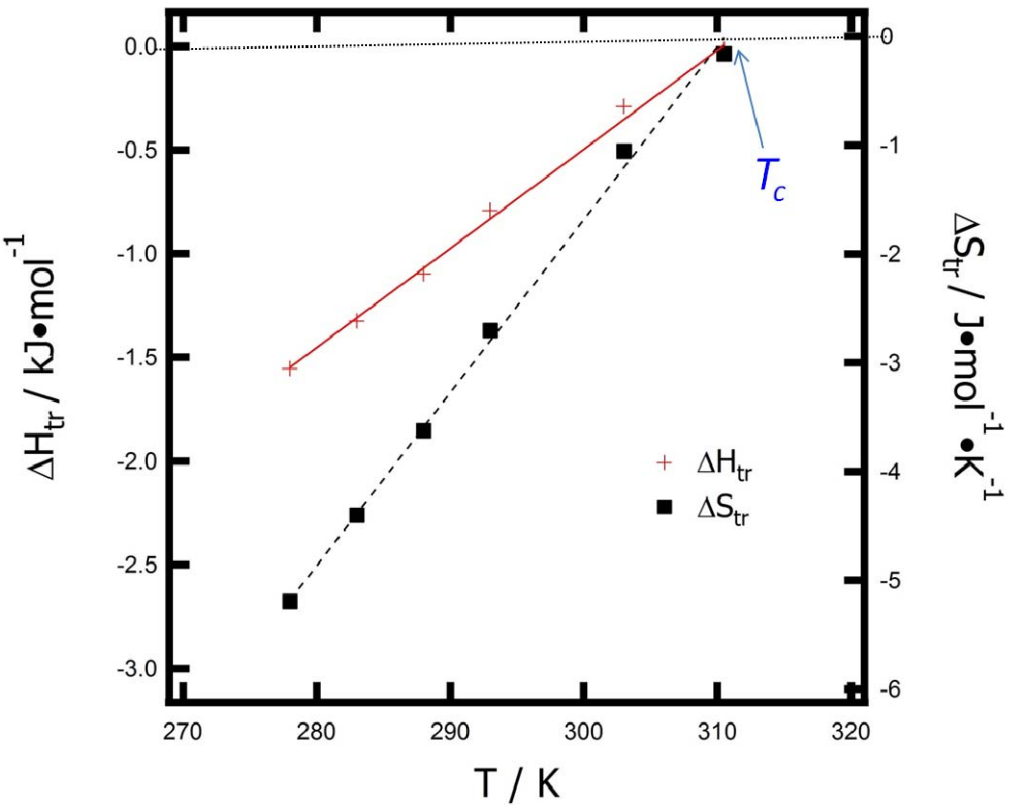

Figure 5.13 Temperature dependence of ΔH_{tr} (red crosses) and ΔS_{tr} (black filled squares) for P*Al*DE Langmuir films at the A/W interface. Both ΔS_{tr} and ΔH_{tr} were calculated using the linear fit from Figure 5.12.

Table 5.1 A_{LC}, A_{LE}, ΔA, ΔS_{tr}, and ΔH_{tr}, at different temperatures for the LE/LC phase transition of P*Al*DE.

T (K)	278.3	283.2	288.0	293.1	302.9	310.3
A_{LC} (Å^2•molecule^{-1})	134.0	134.3	134.7	135.6	137.5	138.1
A_{LE} (Å^2•molecule^{-1})	140.5	139.8	139.2	138.8	138.6	138.3
ΔA (Å^2•molecule^{-1})	-6.5	-5.5	-4.5	-3.2	-1.1	-0.2
ΔS_{tr} (J•mol^{-1}•K^{-1})	-5.6 ± 0.4	-4.7 ± 0.3	-3.8 ± 0.3	-2.7 ± 0.2	-0.95 ± 0.06	-0.17 ± 0.01
ΔH_{tr} (kJ•mol^{-1})	-1.6 ± 0.1	-1.3 ± 0.1	-1.1 ± 0.1	-0.79 ± 0.05	-0.29 ± 0.02	-0.053 ± 0.004

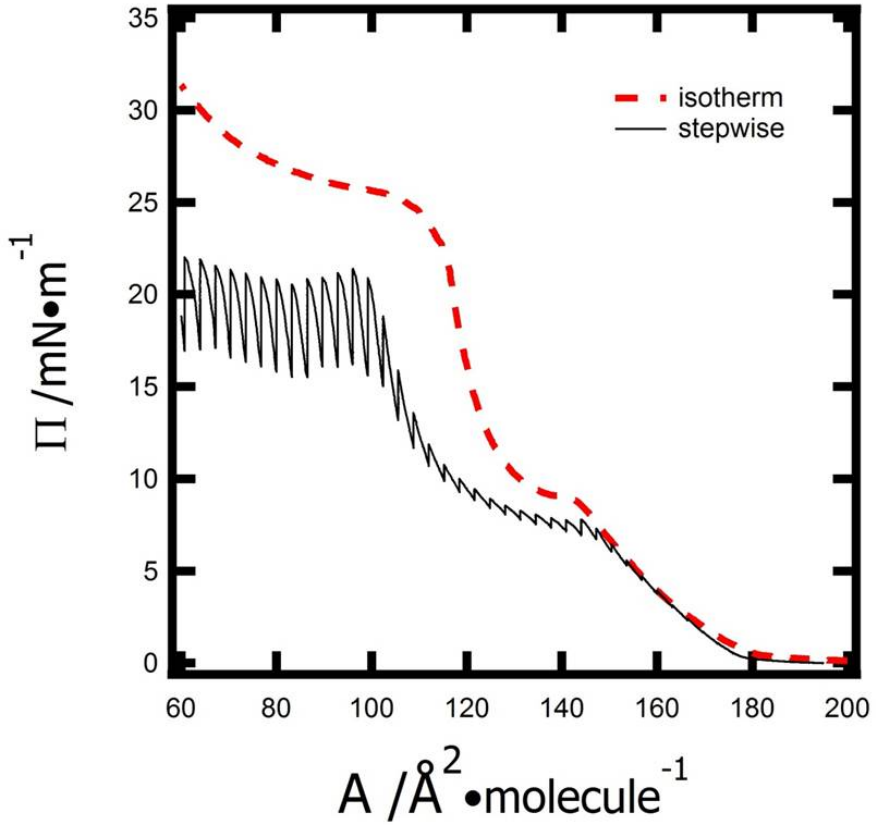

Figure 5.14 Π-*A* isotherms comparison for P*Al*DE at the A/W interface at (A) 5 ^{o}C and (B) 22.5 ^{o}C. The stepwise experiment is set up with a constant rate of 10 cm^{2}•min^{-1}, a trough area decrement of 20 cm^{2}, and a time interval between compressions of 300 seconds.

5.4.5 Possible Conformations for POSS-OH Based Diester at the A/W Interface

The POSS cage was treated as an ideal cube with the substituents evenly distributed at the vertices of the cage. In this model, *Si* atoms are located at the eight corners of the cube while omitted *O* atoms are in the middle of the 12 edges (Figure 2.18A).[47d] Therefore, the sizes

(limiting areas) of the POSS derivatives are effectively spherical areas determined by the largest cross-sectional areas. If the molecule is tilted on one corner, as proposed for TiBP,[30b] a vertex-on conformation would be observed that would look like the labeled "Atomium" built for the World's Fair in Brussels (Figure 2.18B).[119] On the other hand, a face-on conformation would be observed if the POSS cage is packed on one of its faces.

In order to understand the conformation of P*Al*DE, it is useful to consider the Π-*A* isotherm for poly(*tert*-butyl acrylate) (PtBA) (Figure 5.15B). Since POSS-OH based triester (P*Al*TE) is considered as POSS-OH plus three PtBA repeating units, P*Al*DE is essentially one PtBA less than P*Al*TE if one can neglect the short linker. Therefore, at 22.5 °C, $A_{lift\text{-}off,\ PAlDE} = A_{lift\text{-}off,\ PAlTE} - A_{0,PtBA} \approx 215 - 30$ Å^2·molecule^{-1} = 185 Å^2·molecule^{-1}. The result agrees with the experimental observation suggesting P*Al*DE starts with the POSS-cage and two *tert*-butyl esters adsorbed to the plane of the interface (Figure 5.16A). Throughout the LE monolayer regime, the POSS cage tends to rise on the top of the *tert*-butyl esters, perhaps with a vertex-on conformation (Figure 5.16B). Upon further compression, the POSS cage decreases its cross-sectional area by changing from a vertex-on to face-on conformation. Unlike the tripodal structure of three esters in P*Al*TE, P*Al*DE exhibit a somehow unstable dipodal structure. Therefore, this distinction may give rise to the observed LE/LC phase transition. A top view of P*Al*DE at the end of LC region is depicted in Figure 5.16C with an A_c = 125 Å^2·molecule^{-1} and an $A_{0,\ LC} \sim$ 135 Å^2·molecule^{-1}. This value is consistent with a face-on conformation for P*Al*DE at collapse.

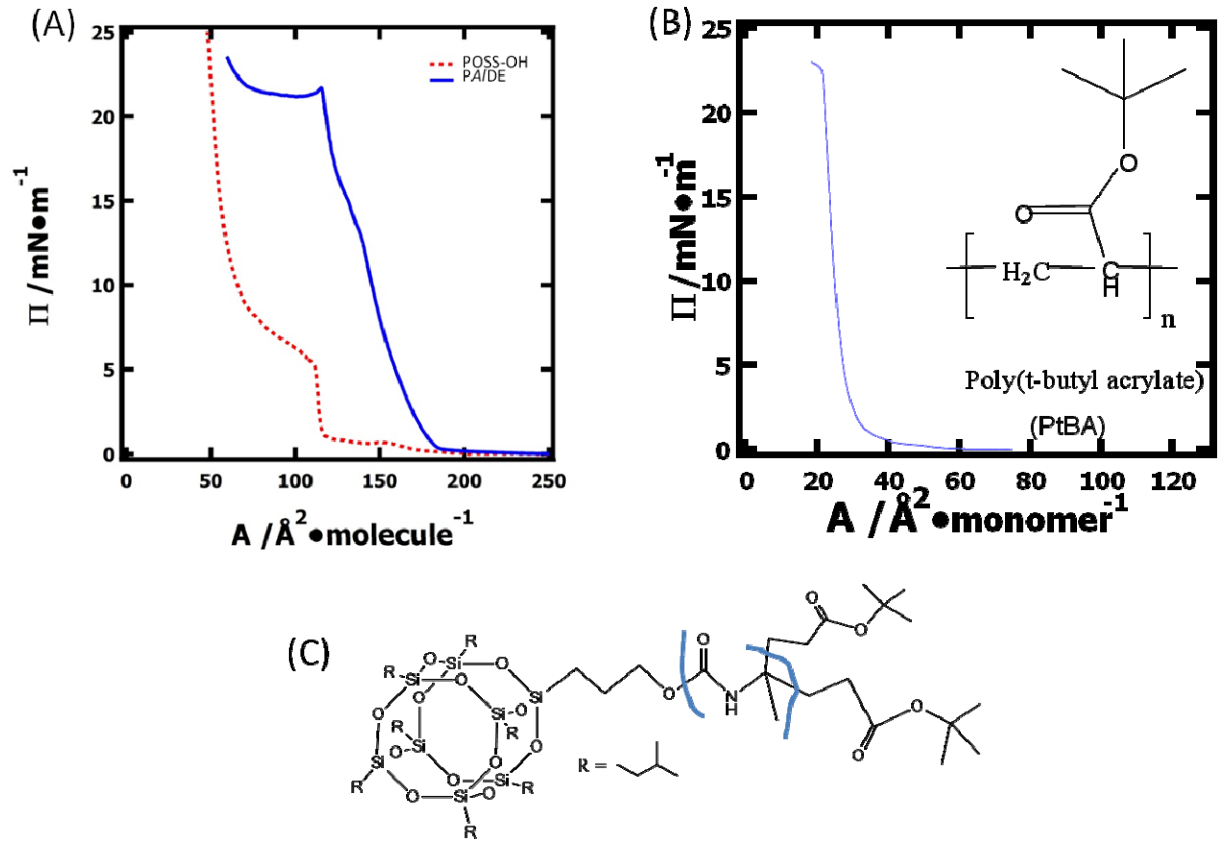

Figure 5.15 Π-*A* isotherms at the A/W interface (T= 22.5 °C) for (**A**) POSS-OH (red dotted line) and P*Al*DE (blue solid line) and (**B**) PtBA along with the chemical structure of PtBA. (**C**) The structure of P*Al*DE highlighting the POSS-OH piece and the two PtBA "repeating units" connected by a short linker.

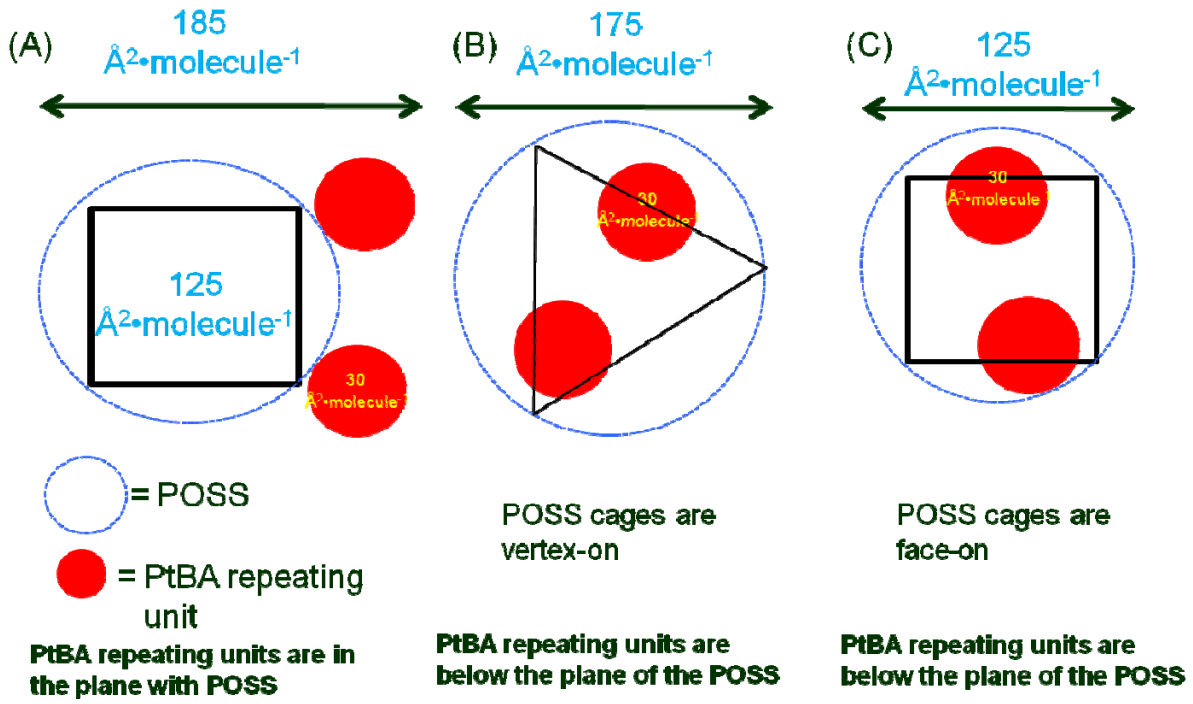

Figure 5.16 Schematic depictions of P*Al*DE (top view) in Langmuir films at various A: (**A**) $A = A_{lift\text{-}off}$, the size of P*Al*DE is determined by $A_{0,POSS\text{-}OH}$ (~125 Å^2·molecule^{-1}) with a face-on conformation plus 2 PtBA repeating units (~30 Å^2·molecule^{-1} each); (**B**) $A = A_{0,LE}$, the size of POSS cage is determined by the circumcircle of the equilateral triangle of a vertex-on conformation; and (**C**) $A = A_c$, the size of POSS cage is determined by the circumcircle of the square in a face-on conformation.

5.4.6 Comparison of POSS-OH Based Esters

Figure 5.17 contains surface pressure-area per molecule (Π-A) isotherms for POSS-OH, P*Al*TE and P*Al*DE. As one may notice, there is a "window" with respect to packing at the A/W

interface between the POSS-OH and P*Al*TE due to the large difference in collapse pressure. However, P*Al*DE exhibits a similar isotherm to P*Al*TE instead of filling this "window". The lift-off area of P*Al*DE is ~30 $Å^2 \cdot molecule^{-1}$ less than that of P*Al*TE, which is consistent with the difference in limiting area associated with one fewer PtBA repeating unit. It is also interesting to note that their collapse pressures are identical (~ 23 $mN \cdot m^{-1}$) although the collapse pressure of POSS-OH is ~ 6 $mN \cdot m^{-1}$, and their collapse areas agree with a face-on conformation. On the other hand, P*Al*TE has a smaller collapse area (~ 105 $Å^2 \cdot molecule^{-1}$) than P*Al*DE indicating that P*Al*TE forms a softer LE film in the monolayer regime even if P*Al*DE also exhibits a limiting area of ~ 175 $Å^2 \cdot molecule^{-1}$ in the LE region. This result is consistent with a vertex-on conformation in the LE monolayer region suggesting that P*Al*DE forms a more ordered vertex-on conformation. In addition, the additional ester group of P*Al*TE relative to P*Al*DE may hinder the packing of the vertex-on state. Furthermore, the conformational change from vertex-on to face-on for P*Al*TE is possibly easier than that of P*Al*DE since the tripodal structure could stabilize the POSS cage better. Therefore, the Π-*A* isotherm for P*Al*TE leads to a smoother transition.

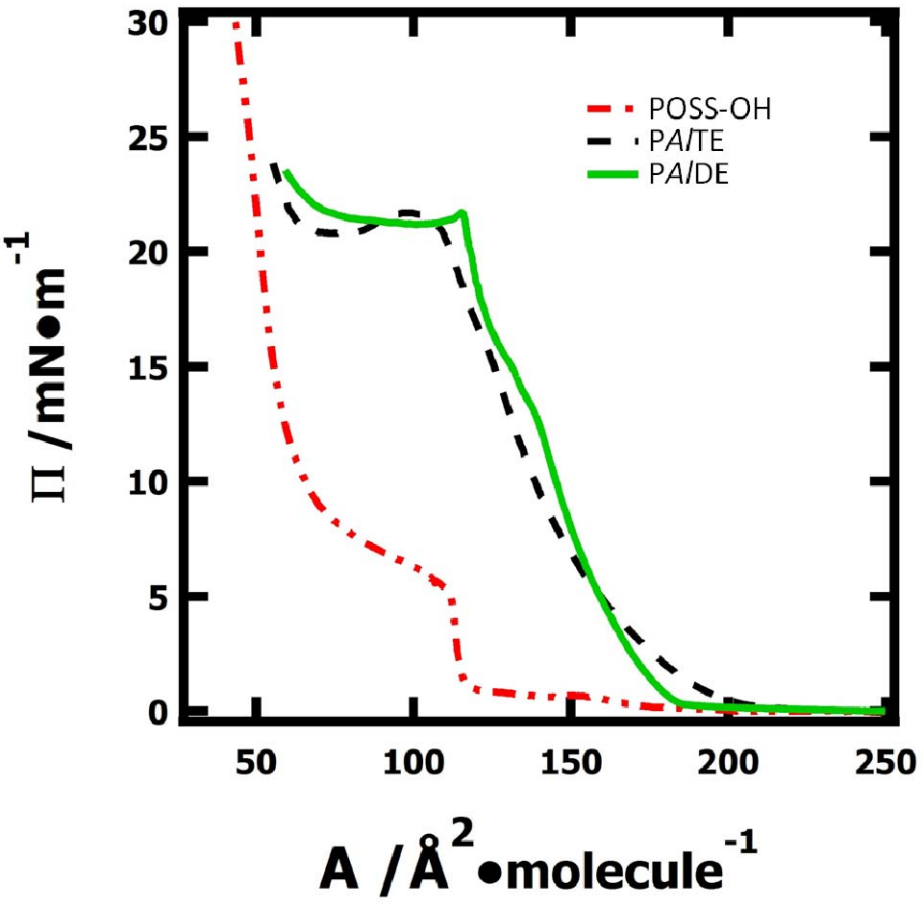

Figure 5.17 Π-*A* isotherms for POSS-OH, P*AI*TE, and P*AI*DE at the A/W interface at T = 22.5 °C.

5.5 Conclusions

A new closed-cage POSS derivative, P*AI*DE was synthesized and characterized. Π-*A* isotherm studies of P*AI*DE at the A/W interface reveal a non-equilibrium, first-order, LE/LC phase transition. This is the first POSS material exhibiting a LE/LC phase transition at the A/W

interface. The 2D Clausius-Clapeyron equation was used to obtain the critical temperature, and the result was consistent with estimates from the Π-*A* isotherms. However, stepwise compression experiments clearly show the observed LE/LC phase transition must be strongly influenced by its close proximity to the collapse transition. The conformational analysis for Π-*A* isotherms of P*Al*DE suggests that P*Al*DE initially lies on the water surface with POSS cage and two bulky *tert*-butyl groups in the same plane. In the LE monolayer region, the POSS cage may have a vertex-on conformation prior to LE/LC phase transition and a face-on conformation in the LC film until monolayer collapse. These studies provide new insights into design and interfacial properties of silicon based surfactants and surface modifying agents.

Chapter 6

Synthesis and Characterization of POSS-NH_2 Based Diester at the Air/Water Interface

6.1Abstract

A diester, polyhedral oligomeric silsesquioxane (POSS) derivative was synthesized from aminopropylisobutyl-POSS (POSS-NH_2) and an isocyanate diester. Surface pressure-area per molecule (Π-*A*) isotherm studies and Brewster angle microscopy (BAM) confirmed POSS-NH_2 and POSS-NH_2 based diester (P*Am*DE) were amphiphilic at the air/water (A/W) interface. Π-*A* isotherms show that P*Am*DE Langmuir monolayers exhibit a non-equilibrium liquid expanded-to-condensed (LE/LC) phase transition. BAM images show large islands of the LC phase are dispersed in the LE phase during phase coexistence. An apparent critical temperature (T_c) of the phase transition was obtained from the two-dimensional Clausius-Clapeyron equation. The result agrees well with the experimental window for T_c in non-equilibrium constant compression rate experiments. Analysis of the Π-*A* isotherms revealed packing of these amphiphiles at the A/W interface was similar to that of P*Al*DE discussed in Chapter 5. Unlike the vertex-on conformation for trisilanol-POSS derivatives, POSS-NH_2 exhibits a face-on conformation at the A/W interface. For P*Am*DE, there may also be a transition from vertex-on to face-on packing during compression of the molecules.

6.2 Introduction

Polyhedral oligomeric silsesquioxane (POSS) derivatives have received considerable attention for applications in shape memory materials,[123] coatings,[7d, e, 30b, 41h, 113a, 124] low-*k* dielectric materials,[125] and as catalysts for the preparation of nanostructured materials,[7c, 126] and dendrimers.[7g, 88a, 127] Based on the study of tradition trisilanol-POSS derivatives as Langmuir films at the air/water (A/W) interface,[30b, c, 30o, 83b, c, 113, 118d, 131, 133-134] the Esker group has also studied closed-cage POSS derivatives.[47d] From previous work, purified (3-hydroxypropyl)-heptaisobutyl-POSS (POSS-OH) was modified to a POSS-OH based triester (P*Al*TE)[47d] and diester (P*Al*DE, discussed in Chapter 5) with Weisocyanate and an isocyanate diester, respectively. Then, an aminopropylisobutyl-POSS (POSS-NH_2) based triester (P*Am*TE, discussed in Chapter 4) was synthesized. Further characterization by surface pressure-area per molecule (Π-*A*) isotherms and Brewster angle microscopy (BAM) were used to probe the quasi-two-dimensional (2D) thermodynamic and morphological properties of these materials at the A/W interface, respectively. Most amphiphiles exhibit 2D or 3D structures at the A/W interface, therefore face-on conformations and edge-on conformations are observed for polymers,[152] dendrimers,[153] organometallic supermolecules,[154] photoelectronic molecules,[155] and derivatives of natural products.[156] However, the vertex-on conformations are rarely discussed at the A/W interface. Results indicated that P*Al*TE was surface active and formed liquid expanded (LE) monolayers with different orientations at the A/W interface. Its conformation changed from vertex-on conformation to face-on conformation as discussed in Chapter 4 and 5. Similar behavior was reported for P*Am*TE (Chapter 4).

In addition, a liquid expanded-to-condensed (LE/LC) phase transition was observed during the analysis of P*Al*DE. This was the first known POSS material with a LE/LC phase transition.

Compared to traditional models for amphiphilic molecules, such as fatty acids, previously studied POSS molecules exhibited simpler phase diagrams within experimentally accessible temperature windows. Although the LE/LC phase transition normally appears as a non-zero slope plateau in Π-*A* isotherms, fluorescence imaging,[67] electron microscopy,[138] and BAM[40c, 139] showed it was first order. Normally, the non-zero slope correlates to artifacts from impurities, the formation of small molecular aggregates or surface micelles, or non-equilibrium effects such as finite compression rates.[40a, 47a] However, a zero slope LE/LC phase transition plateau could be obtained by using a very careful experimental protocol: an ultra-clean system, pure materials, extremely slow compression rates, and a stable film.[140]

In this study, P*Am*DE was synthesized and characterized by ^{1}H NMR, ^{13}C NMR, high resolution mass spectrometry (HRMS), and melting point measurements. P*Am*DE Langmuir monolayers were examined at the A/W interface and a LE/LC phase transition was observed. This is the second known POSS material which has a LE/LC phase transition. The critical temperature (T_c) obtained from the 2D Clausius-Clapeyron equation is within the range expected from the experimental Π-*A* isotherms. Possible conformations of the P*Am*DE in Langmuir films are discussed with respect to P*Al*DE.

6.3 Experimental

Experimental details regarding the synthesis of P*Al*DE (**7** in Scheme 3.4) were provided in Chapter 3.1.2.4. Experimental methods for Π-*A* isotherm (Chapter 3.3.1) and BAM (Chapter 3.3.3) were covered in Chapter 3.3.

6.4 Results and Discussion

6.4.1 Synthesis and Characterization of POSS-NH_2 Based Diester (P*Am*DE)

Chemical compositions and purity were confirmed via ^{1}H NMR, ^{13}C NMR, melting point, and HRMS. Figure 6.1 contains the ^{1}H NMR spectrum for P*Am*DE in $CDCl_3$. Figures 6.2 and 6.3 contain the ^{13}C NMR and expanded ^{13}C NMR spectra for P*Am*DE in $CDCl_3$, respectively. The spectra reveal sharp, well-resolved peaks. The characteristic differences in the splitting patterns of the protons of the linker and essentially quantitative integrations were consistent with the labeled structures on each spectrum.

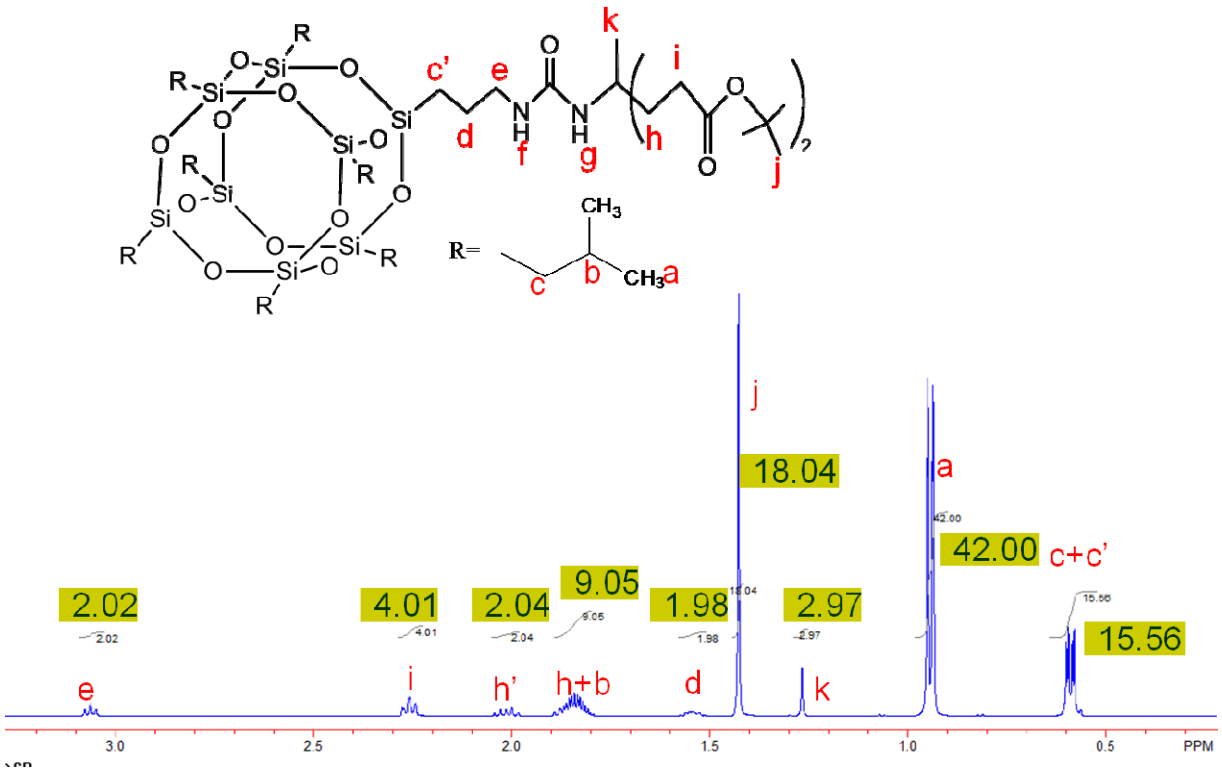

Figure 6.1 ^{1}H NMR of P*Am*DE.

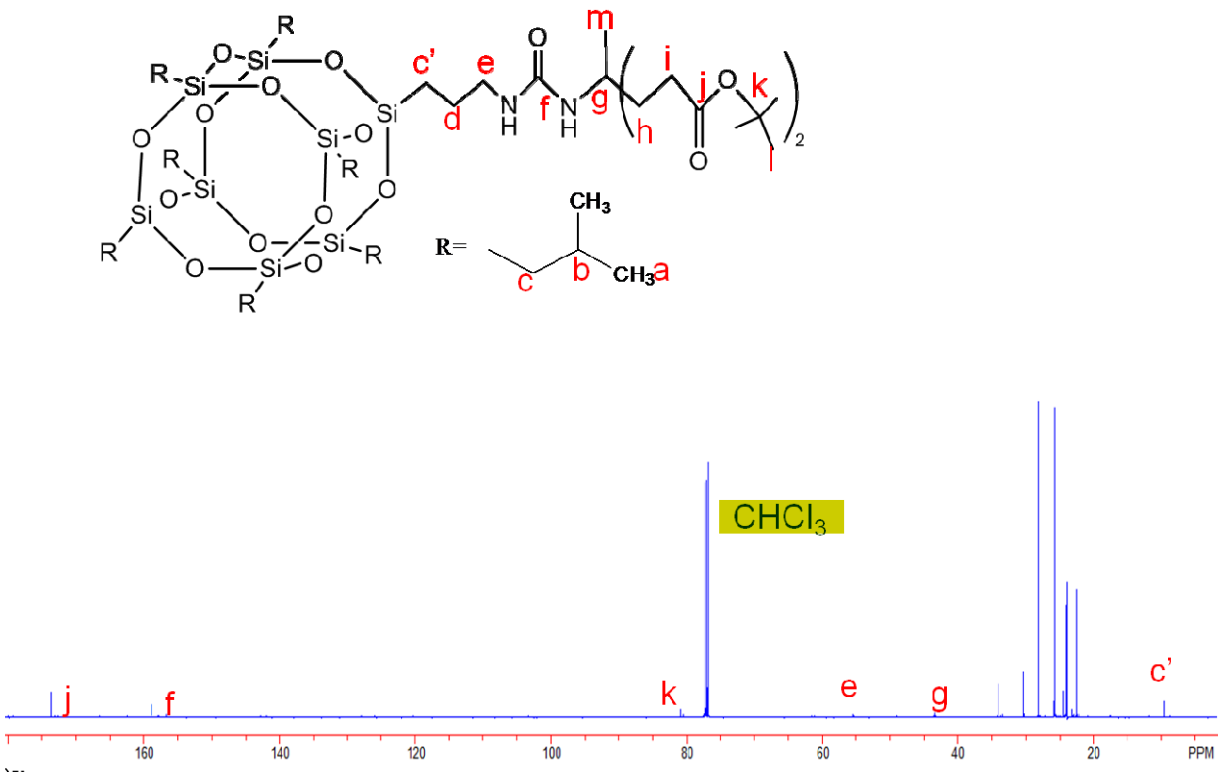

Figure 6.2 ^{13}C NMR of P*Am*DE.

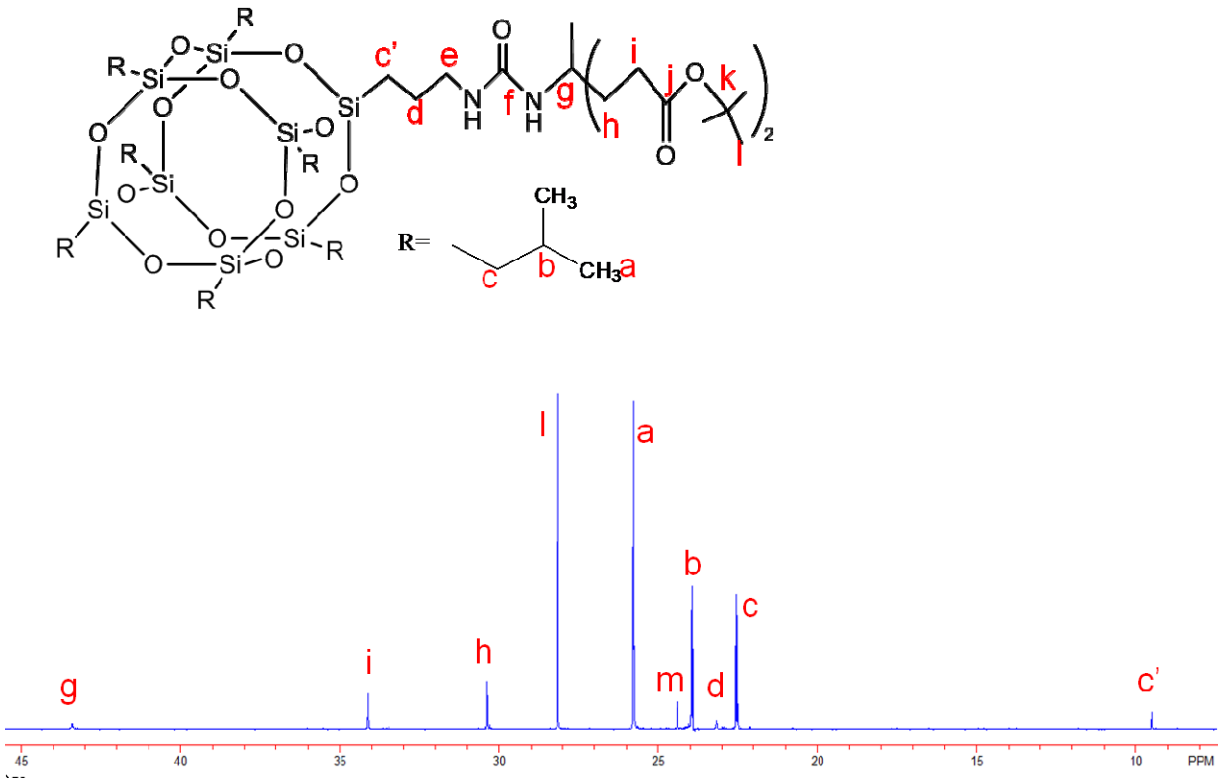

Figure 6.3 Expanded ^{13}C NMR of P*Am*DE.

6.4.2 Observation of a LE/LC Phase Transition

Figure 6.4 shows a Π-*A* isotherm for P*Am*DE at the A/W interface at 5 °C. Four different regions are depicted: (a) $A > 185.2$ Å^2•molecule^{-1}, G or G/LE films; (b) $123.3 < A < 185.2$ Å^2•molecule^{-1}, a highly compressible LE monolayer with a surface pressure between 0 and 10.6 mN•m^{-1}; (c) $111.0 < A < 123.3$ Å^2•molecule^{-1}, a LE/LC phase transition with a non-zero slope starting at Π = 10.6 mN•m^{-1}; and (d) $80.2 < A < 111.0$ Å^2•molecule^{-1}, a LC monolayer with Π between 10.6 and 19.8 mN•m^{-1}.

The biphasic nature of the LE/LC phase transition has been revealed through BAM observations.[121, 139, 141] In Region *b* (Figure 6.4), a uniform film is formed without obvious features indicating a uniform film (BAM image *i* in Figure 6.4). In Region *c*, a LE monolayer is slowly converted into a LC film starting at a transition pressure of at Π_{tr} = 10.6 mN•m^{-1}. Circular domains dispersed in another phase (BAM image *ii* in Figure 6.4) confirm the region is biphasic. Similar results were shown in Chapter 5 for P*Al*DE, and have also been reported for diethylene glycol mono-*N*-octadecyl ether,[142] di-*N*-tetradecyl hydrogen phosphate (DTP),[143] dimyristoyl phosphatidyl serine (DMPS),[3a] dipalmitoyl phosphatidyl choline (DPPC),[144] and even poly(*L*-lactic acid).[121] This feature can be understood from the change of density during the first-order phase transition. Upon compression, the LC phase forms through nucleation growth inside the LE phase. Therefore, at the end of Region *c*, the circular domains disappear (BAM image *iii* in Figure 6.4) to form another uniform monolayer in Region *d* (BAM image *iv* in Figure 6.4).

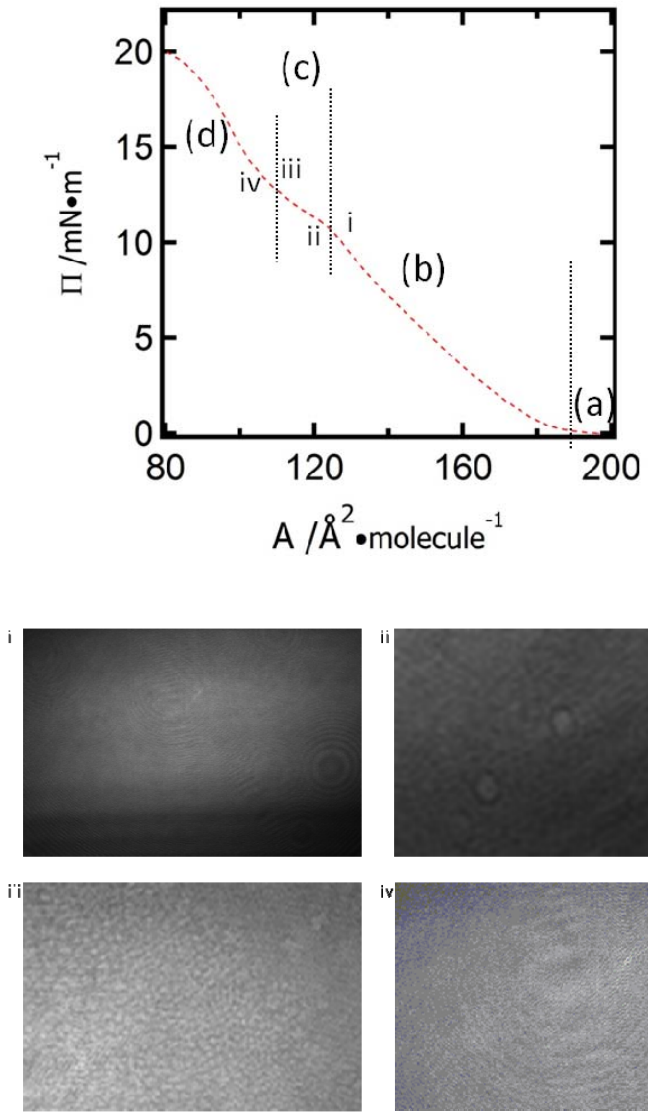

Figure 6.4 Π-*A* isotherm of P*Am*DE at the A/W interface at 5 °C. Four regions are depicted: (a) a G or G/LE phase; (b) a LE phase; (c) LE/LC coexistence; and (d) a LC phase. BAM images at different *A* are provided: (i) 125.2 $Å^2$•$molecule^{-1}$, monolayer prior to the LE/LC phase transition; (ii) 120.5 $Å^2$•$molecule^{-1}$, circular LC domains growing in the LE film; (iii) 117.6 $Å^2$•$molecule^{-1}$, approaching the end of the plateau; and (iv) 110.3 $Å^2$•$molecule^{-1}$, formation of a LC monolayer. BAM image i is 4.8 × 6.4 mm^2 while images ii-iv are 2.0 × 2.4 mm^2, cut from the original BAM images. Each BAM image has an independent gray scale.

6.4.3 Different Compressibility between the LE and LC Phases

As a Π-*A* isotherm is an analog of a three-dimensional (3D) pressure-volume (*P-V)* isotherm, parameters such as the surface compressibility (κ_s) and static elastic modulus (ε_s) can be calculated from Π-*A* isotherms of Langmuir monolayers:

$$\varepsilon_s = \kappa_s{}^{-1} = -A\left(\frac{\partial \pi}{\partial A}\right)_T \tag{6.1}$$

ε_s is an elastic response of the film to an applied lateral pressure. A plot of ε_s -*A* is compared with the Π-*A* isotherm of P*Am*DE at 5.0 °C in Figure 6.5. In Regime *a*, the first plateau (*A* > 185.2 Å^2•molecule^{-1}) of Π-*A* isotherm, ε_s increases slowly at the end of the gaseous phase as the monolayer forms. As the film is compressed in the LE region (Regime *b*, 123.3 < *A* < 185.2 Å^2•molecule^{-1}), ε_s increases faster until it reaches a maximum at A ~ 127.4 Å^2•molecule^{-1} with a value of $\varepsilon_{s,\,max}$ ~ 32 mN•m^{-1}. Shortly after $\varepsilon_{s,\,max}$, the LE/LC phase transition starts. However, an ideal plateau of ε_s = 0 mN•m^{-1} is not observed due to the non-zero slope in the LE/LC phase transition region. This result may be due to artifacts like impurities, small molecular aggregation or surface micelles, or nonequilibrium effects such as finite compression rates.[67] After the LE/LC phase transition (111.0 < *A* < 123.3 Å^2•molecule^{-1}), ε_s increases as a rigid LC Langmuir monolayer forms. The second maximum for ε_s with a value of $\varepsilon_{s,\,max}$ ~ 38 mN•m^{-1} is observed at *A* = 97.5 Å^2•molecule^{-1} and Π = 15.2 mN•m^{-1}. With further compression, ε_s again falls as the LC monolayer starts to collapse into multilayers. The value of $\varepsilon_{s,\,max}$ in the LC phase is smaller for P*Am*DE than P*Al*DE. This difference is likely due to the lower collapse for PAmDE, which limits the Π range over which the LC phase exists.

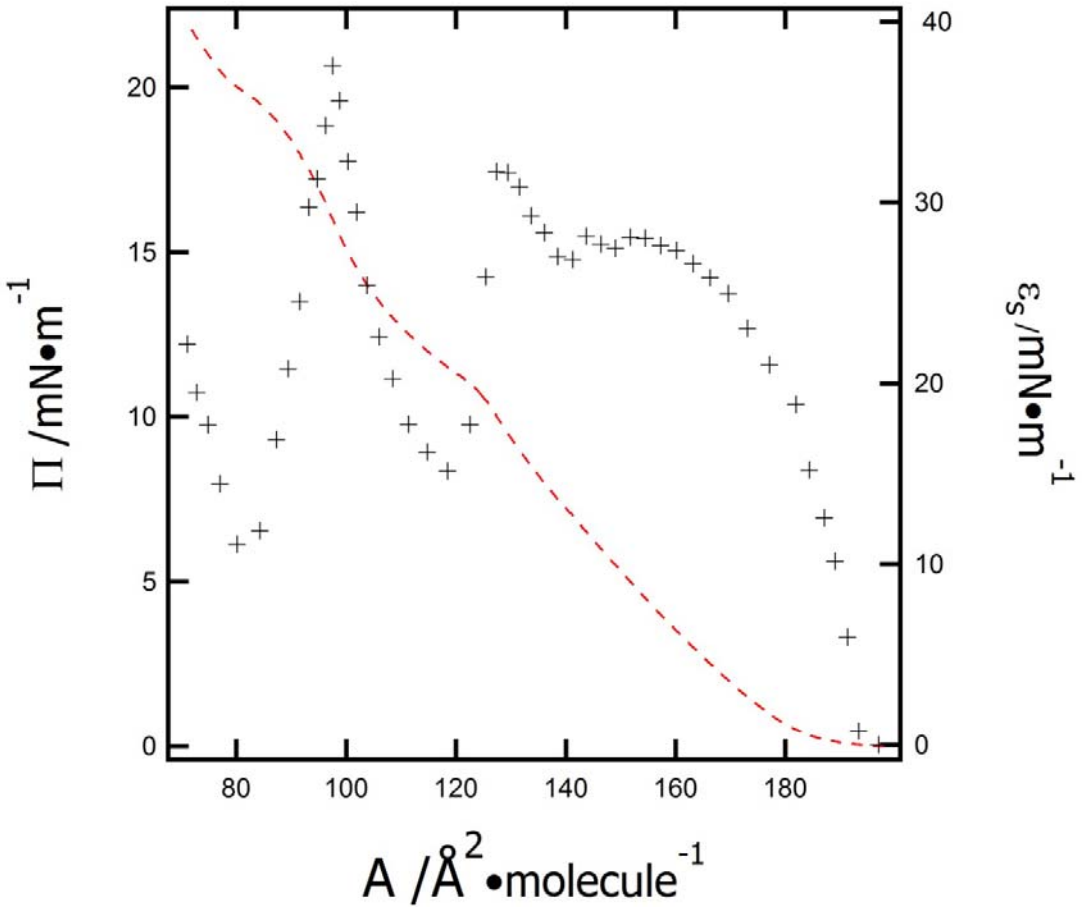

Figure 6.5 Comparison of the ∏-*A* isotherm (red dotted lines ----) and ε_s-*A* plot (black crosses +) for P*Am*DE at 5.0 °C.

6.4.4 Temperature Dependence of the LE/LC Phase Transition

The temperature dependence of the LE/LC phase transition of P*Am*DE at the A/W interface is shown in Figure 6.6. As temperature increases, several changes occur in the Langmuir monolayers. First of all, the onset of the liquid expanded monolayer shifts to a larger lift-off area

($A_{lift\text{-}off}$), where Π increases from zero. This result is expected because molecules possess more thermal energy at higher temperature. Molecules at higher temperature have a larger effective cross-sectional area. Second, Π for the onset of the LE/LC phase transition (Π_{tr}) increases while the corresponding area (A_{LE} or A_{tr}) decreases. Meanwhile, the area at the LC end of the LE/LC phase transition (A_{LC}) increases leading to a shorter plateau as temperature increases. These changes in Π_{tr} and A_{tr} are also related to the enhanced molecular mobility. Third, a critical temperature (T_c) is approached from below as temperature increases. At 27.5 °C, an obvious phase transition is still observed while a smoothened curve is seen at 30 °C suggesting T_c lies between 27.5 °C and 30 °C.

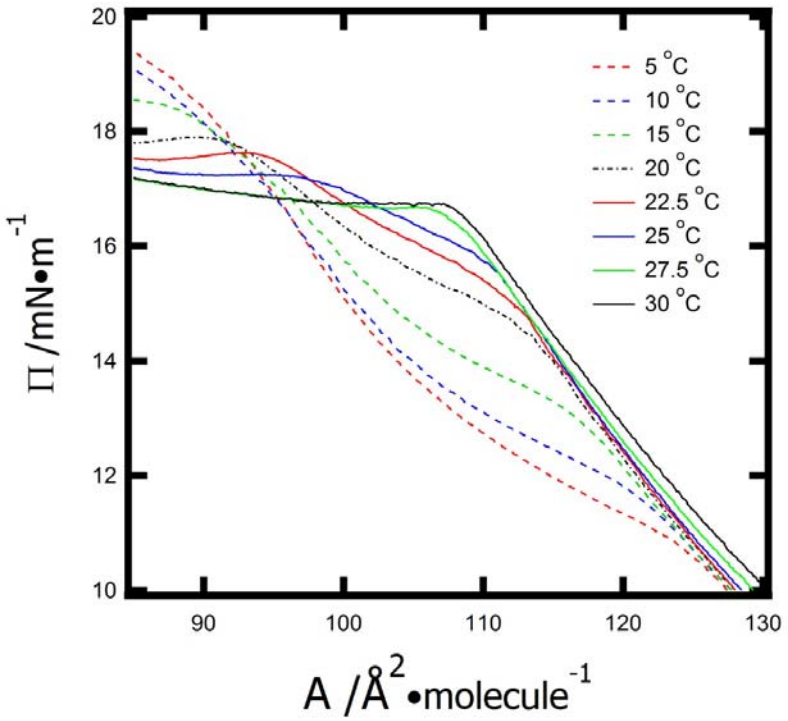

Figure 6.6 Temperature dependence of the LE/LC phase transition of P*Am*DE at the A/W interface. LE/LC phase coexistence is observed for isotherms below 27.5 °C, and is not observed at 30 °C, indicating the critical temperature (T_c) lies between 27.5 °C and 30 °C.

Similar to the observations for P*Al*DE in Chapter 5, the collapse pressure ($\prod_{collapse}$) of P*Am*DE decreases and collapse area ($A_{collapse}$) increases as temperature increases. The temperature dependence of $\prod_{collapse}$ and $A_{collapse}$ for P*Am*DE is shown in Figure 6.7 where individual data points are averages of three experiments with one standard deviation error bars. This tendency is opposite to that of $\prod_{tr}$ and A_{tr}, but is expected because it is easier for Langmuir monolayers to overcome the energy barrier associated with the nucleation and growth of the 3D structures at higher temperatures.

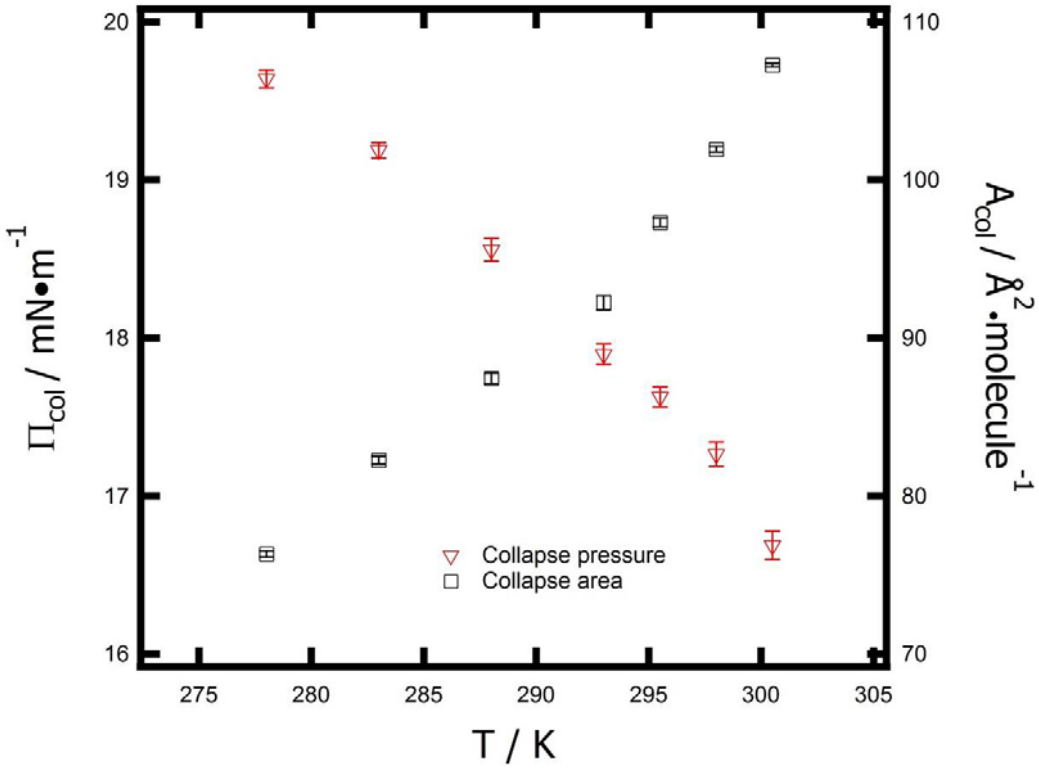

Figure 6.7 Temperature dependence of $\prod_{collapse}$ (red triangles) and $A_{collapse}$ (black squares) for P*Am*DE Langmuir films at the A/W interface. Each point is the average of three measurements with one standard deviation error bars.

In order to estimate the value of T_c from the $\prod$-A isotherms, a 2D Maxwell relation (Equation 5.1) that leads to 2D Clausius-Clapeyron equations (Equations 5.2 and 5.3)[47a, 145] is used. Figure 6.8 shows a plot of temperature dependence of $\prod_{tr}$. A linear relationship is observed with a slope of 0.15 ± 0.01 mN•m^{-1}•K^{-1}. An extrapolation of the best linear fit line back to the x-axis yields a temperature of -31.8 ± 1.3 °C, the temperature below which no LE phase should be observed.[151] As with P*Al*DE in Chapter 5, this estimate simply shows the LE phase exists over the experimentally accessible temperature window.

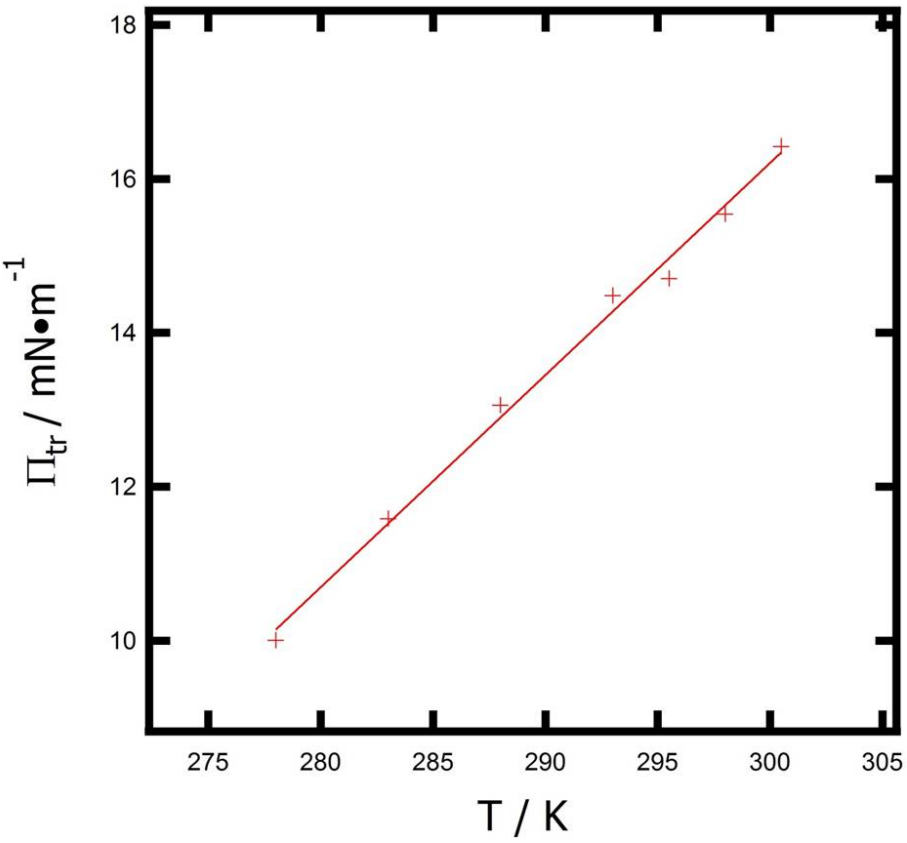

Figure 6.8 Temperature dependence of $\prod_{tr}$ for the LE/LC phase transition of P*Am*DE Langmuir films at the A/W interface. The best fit yields a slope of 0.15 ± 0.01 mN•m^{-1}•K^{-1}.

With the slope obtained from Figure 6.8, the temperature dependence of the molar enthalpy (ΔH_{tr}) and molar entropy (ΔS_{tr}) of the transition for P*Am*DE Langmuir films at the A/W interface are calculated from Equations 5.2 and 5.3 and displayed in Figure 6.9. Both ΔH_{tr} and ΔS_{tr} are negative because ordered structures are formed from less ordered structures during the LE/LC phase transition.[1b] At the critical temperature (T_c), the LE/LC phase transition should be reduced from a plateau to a single point, and $\Delta H_{tr} = 0$. Therefore, the apparent critical temperature can be predicted by extrapolating the linear fit line for ΔH_{tr} in Figure 6.9 to the x axis. The result, 28.6 ± 1.8 °C, agrees with the window between 27.5 and 30 °C inferred from the Π-*A* isotherms.

Data for temperature (*T*), the area at the LC end of the LE/LC phase transition (A_{LC}), the area at the onset of the LE/LC phase transition (A_{LE}), the difference of A_{LE} and A_{LC} (ΔA), and entropy changes (ΔS_{tr}) and enthalpy changes (ΔH_{tr}) during the LE/LC phase transition are shown in Table 6.1.

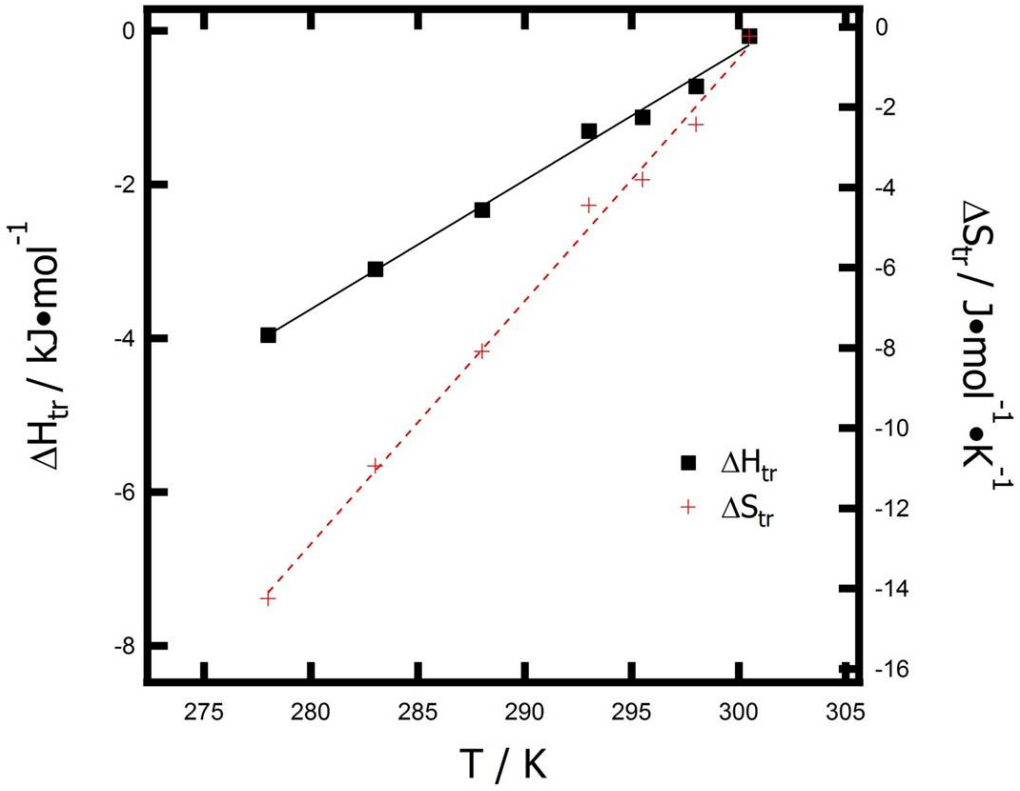

Figure 6.9 Temperature dependence of ΔH_{tr} (red crosses) and ΔS_{tr} (black filled squares) for P*Am*DE Langmuir films at the A/W interface. Both ΔS_{tr} and ΔH_{tr} are calculated using the linear fit from Equations 5.2, 5.3, and Figure 6.8.

Table 6.1 A_{LC}, A_{LE}, ΔA, ΔS_{tr}, and ΔH_{tr}, at different temperatures for the LE/LC phase transition of P*Am*DE.

T (K)	278.4	283.2	288.1	293.0	295.3	297.8	300.1
A_{LC} (Å²•molecule⁻¹)	113.8	112.6	111.5	111.0	110.5	109.6	108.9
A_{LE} (Å²•molecule⁻¹)	122.4	119.2	116.4	113.7	112.8	111.0	109.0
ΔA (Å²•molecule⁻¹)	-8.6	-6.6	-4.9	-2.7	-2.3	-1.4	-0.1
ΔS_{tr} (J•mol⁻¹•K⁻¹)	-14.2 ± 0.9	-10.9 ± 0.7	-8.1 ± 0.5	-4.5 ± 0.3	-3.8 ± 0.3	-2.4 ± 0.2	-0.24 ± 0.01
ΔH_{tr} (kJ•mol⁻¹)	-3.9 ± 0.3	-3.1 ± 0.2	-2.3 ± 0.1	-1.3 ± 0.1	-1.1 ± 0.1	-0.73 ± 0.05	-0.071 ± 0.005

It is interesting to note that the LC region for P*Am*DE (in Figure 6.6) tends to be ambiguous suggesting possible overlap of LE/LC phase transition and collapse. Stepwise compression experiments demonstrate the stability of the film and quasi-static behavior while compression experiments indicate dynamic behavior of the film in response to compression (Figure 6.10). For the stepwise compression experiment at 5 °C, the transition pressure is slightly lower than the collapse pressure after 300 s at a constant area. In contrast, the transition pressure is almost the same as the relaxed collapse pressure for stepwise compression experiment at 22.5 °C although a sharp increase in surface pressure between LE/LC phase transition and collapse is still observed in the region of $81 < A < 93$ Å^2·molecule^{-1}. These features indicate that the LE/LC phase transition is strongly influenced by the collapse transition for P*Am*DE.

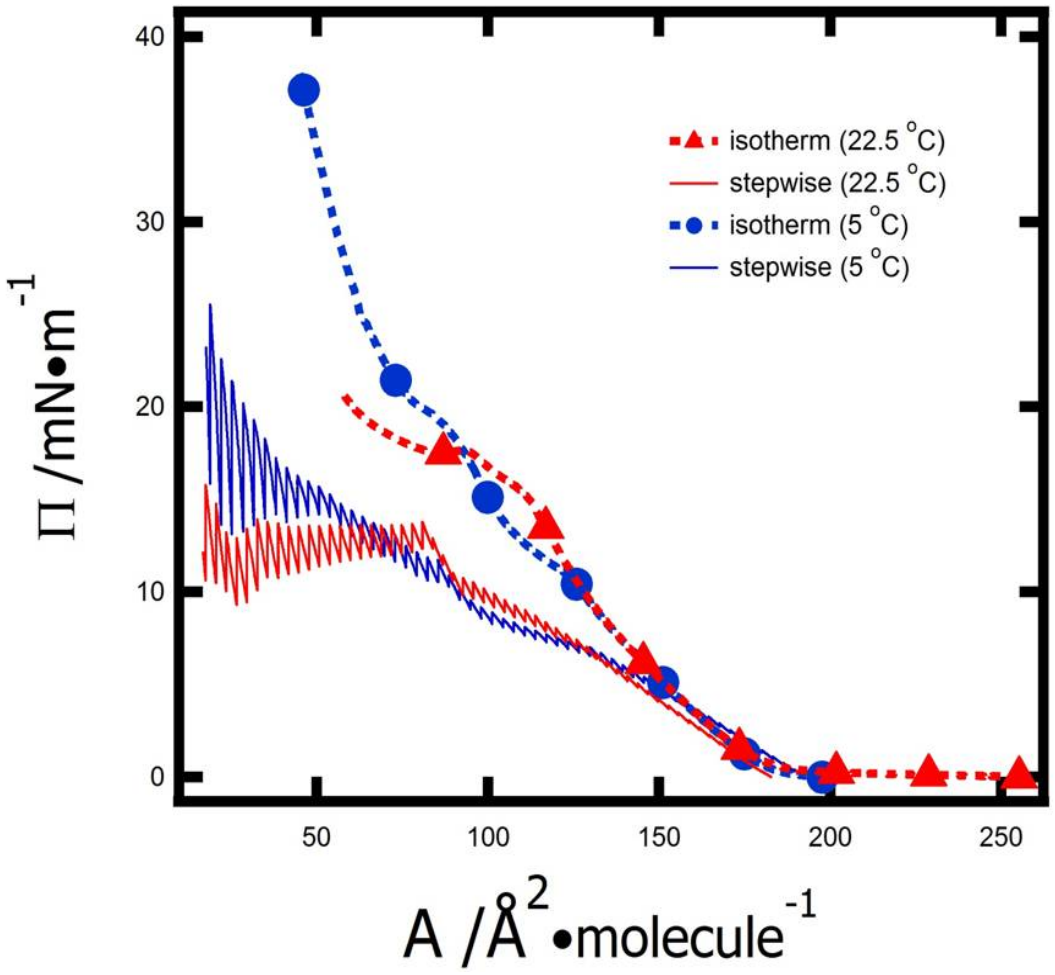

Figure 6.10 Π-*A* isotherms comparison for P*Am*DE at the A/W interface. Red and blue curves represent experiments at 22.5 °C and 5 °C, respectively. The stepwise experiments are set up with a constant compression rate of 10 $cm^2 \bullet min^{-1}$, a trough area decrement of 20 cm^2, and a time interval of 300 seconds between compressions.

6.4.5 Possible Conformations for POSS-NH_2 Based Diester at the A/W Interface

Following from the discussion of the conformations for P*Al*DE in Chapter 5, the conformation of P*Am*DE prior to monolayer formation is considered as the addition of POSS-NH_2 and two poly(*tert*-butyl acrylate) (PtBA) repeating units if one can neglect the short linker. Therefore, there is a relationship between their lift-off areas ($A_{lift\text{-}off,}$ where Π increases from zero) and limiting areas (A_0, obtained by extrapolating the steepest portion of the Π-*A* isotherm back to Π = 0). At 22.5 °C, $A_{lift\text{-}off,\ PAmDE} = A_{o\ POSS\text{-}NH2} + 2A_{0,PtBA} \approx 130 + 2 \times 30$ Å^2·molecule^{-1} = 190 Å^2·molecule^{-1} (Figure 6.11A). The result agrees with the experimental observation suggesting P*Am*DE starts with the POSS-cage and two *tert*-butyl esters adsorbed to the plane of the interface (Figure 6.11A). Throughout the regime of the LE monolayer, the POSS cage could rest on top of the *tert*-butyl esters with a vertex-on conformation (Figure 6.11B). Upon further compression, the POSS cage could decrease its cross-sectional area by changing from a vertex-on to face-on conformation. A top view of P*Am*DE at the end of LC region is depicted in Figure 6.11C with an $A_{0,LC} \sim 140$ Å^2·molecule^{-1}. Similar to the structure of P*Al*DE, P*Am*DE may also exhibit a dipodal structure. Therefore, these conformational changes provide a plausible explanation for the LE/LC phase transition.

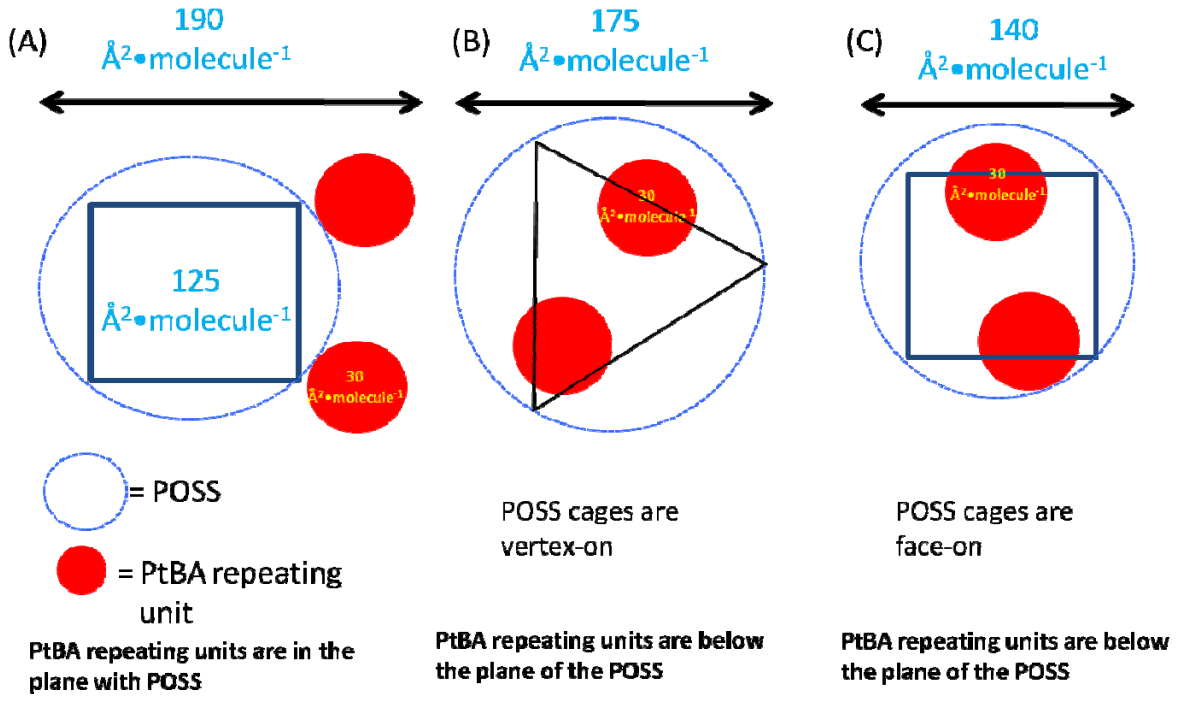

Figure 6.11 Schematic depictions of P*Am*DE (top view) in Langmuir films at various *A*: (**A**) $A = A_{lift\text{-}off}$, the size of P*Am*DE is determined by $A_{0,POSS\text{-}NH2}$ (~130 Å^2·molecule^{-1}) with a face-on conformation plus 2 PtBA repeating units (~30 Å^2·molecule^{-1} each). (**B**) $A = A_{0,LE}$, the size of POSS cage is determined by the circumcircle of the equilateral triangle in a vertex-on conformation. (**C**) $A = A_{0,\,LC}$, the size of POSS cage is determined by the circumcircle of the square in a face-on conformation.

6.4.6 Comparison of POSS-Based Diesters

Figure 6.12 contains Π-*A* isotherms for P*Al*DE, and P*Am*DE at the A/W interface at T= 5.0 °C. The small difference (~5 Å^2·molecule^{-1}) in $A_{lift\text{-}off}$ between the diesters agrees with an initial face-on conformation for the POSS cage plus 2 PtBA repeating units. In addition, $A_{0,\,LE}$ for P*Al*DE (green dashed line) leads to almost identical value as P*Am*DE (blue dashed line). This result is

consistent with a vertex-on conformation in the LE monolayer. As one may notice, the Π_{tr} for P*Am*DE is ~ 1 mN·m^{-1} larger than P*Al*DE and A_{tr} is ~ 17 Å^2·molecule^{-1} smaller for P*Am*DE than P*Al*DE. This may mean that nucleation of the LC phase for P*Am*DE is more difficult. In Figure 6.12, P*Am*DE shows a similar $A_{0,\,LE}$ with P*Al*DE indicating face-on conformation in the LE monolayer regime. It is also worth noting that the extrapolated areas for the LC phases ($A_{0,\,LC}$) corresponding to the solid lines in Figure 6.12 are also nearly identical.

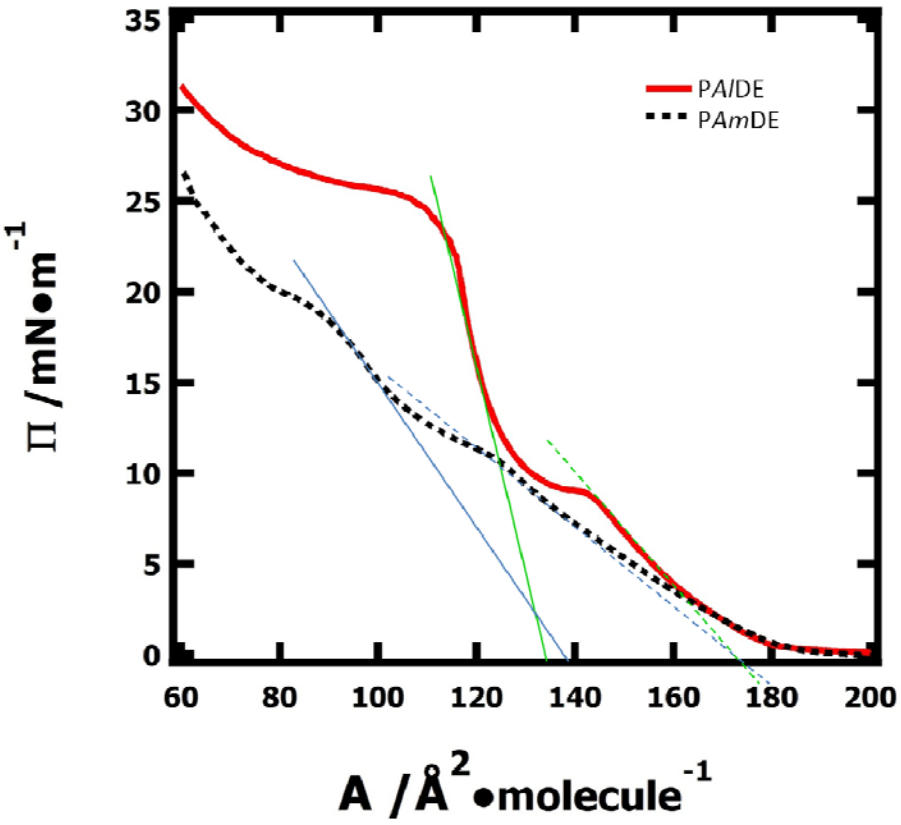

Figure 6.12 Π-*A* isotherms for P*Al*DE, and P*Am*DE at the A/W interface at T= 5.0 °C. Green dotted line and solid line are $A_{0,LE}$ and $A_{0,LC}$ for P*Al*DE, respectively. Blue dotted line and solid line are $A_{0,LE}$ and $A_{0,LC}$ for P*Am*DE, respectively.

It is surprising but interesting to note that A_c for both diesters is smaller than 120 $Å^2 \cdot molecule^{-1}$, which is the value of face-on conformation. In addition, values of A_c and Π_c for P*Am*DE are ~20 $Å^2 \cdot molecule^{-1}$ and ~ 6 $mN \cdot m^{-1}$ smaller, respectively than the values for P*Al*DE. These differences are larger for the diesters than the triesters where the differences were nearly zero. A schematic depiction in Figure 6.13 may explain these results. For triesters, LE monolayers have a uniform thickness since carbamate and ureido groups are evenly distributed by three *tert*-butyl esters (Figure 6.13A). However, for diesters, a methyl group replaces one of the *tert*-butyl esters destabilizing the films leading to decrement in molecular thickness upon compression (Figure 6.13B). The greater Π_c of P*Al*DE relative to P*Am*DE suggests stronger interaction between carbamate group and water surface.

From another standpoint, some key parameters, such as maximal static elastic modulus ($\varepsilon_{s,\,max}$) in LE and LC regime, critical temperature (T_c), and the minimal temperature to observe LE phase (T_0), of the diesters are compared in Table 6.2. P*Am*DE exhitibs smaller $\varepsilon_{s,\,max}$ in the LE regime and much smaller $\varepsilon_{s,\,max}$ in the LC regime corresponding to weaker interaction between ureido group and H_2O. In addition, PAmDE has a smaller T_c but a greater T_0 suggesting a less ordered LC phase forms.

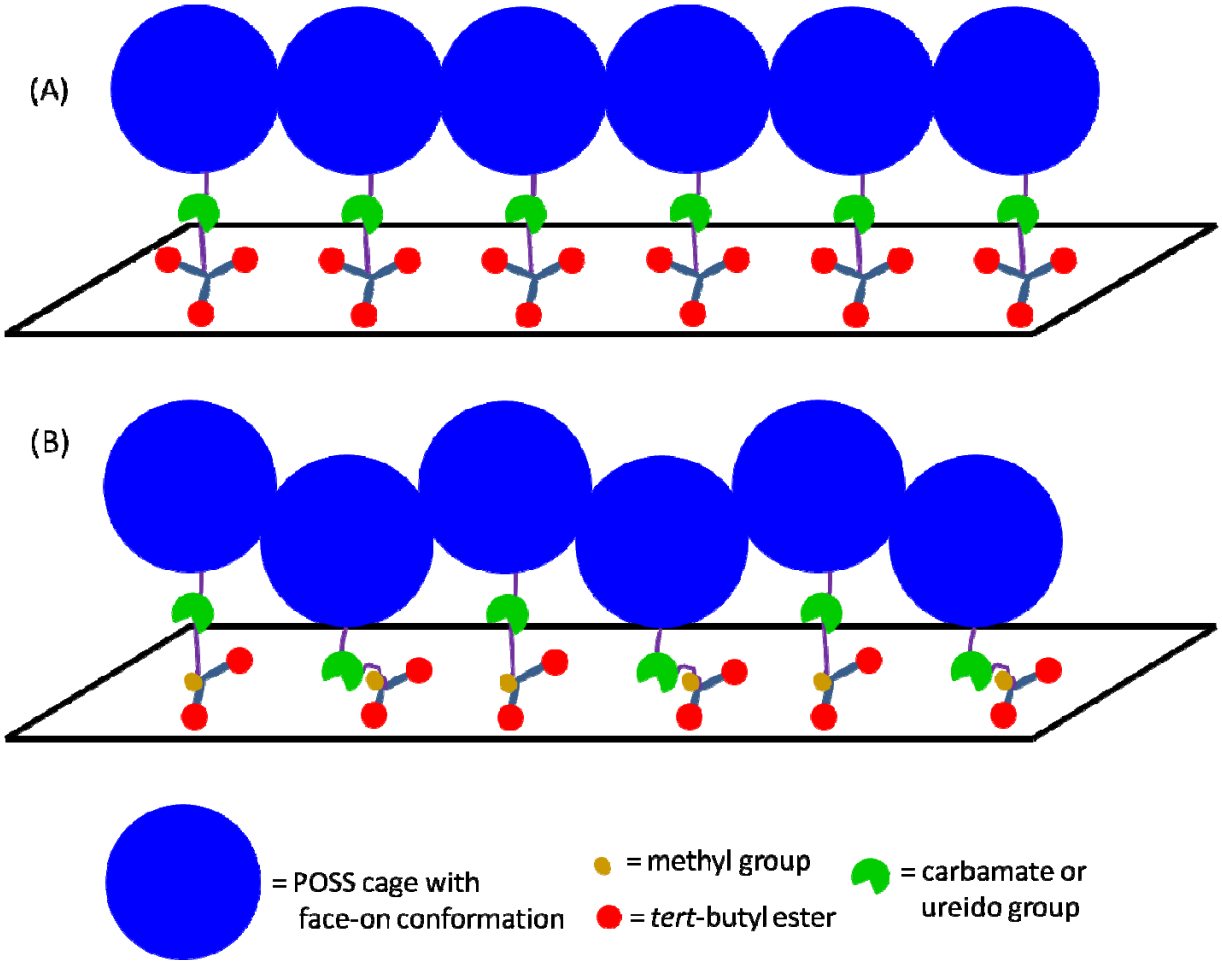

Figure 6.13 Schematic depictions for packing of (**A**) triesters and (**B**) diesters at the A/W interface.

Table 6.2 Comparison of $\varepsilon_{s,\,max}$, T_c, and T_0, for P*Al*DE and P*Am*DE.

	$\varepsilon_{s,\,max}$ in LE	$\varepsilon_{s,\,max}$ in LC	T_c	T_0
P*Al*DE	50 mN•m^{-1}	218 mN•m^{-1}	37.5 ± 2.3 °C	-60.6 ± 1.6 °C
P*Am*DE	32 mN•m^{-1}	38 mN•m^{-1}	28.6 ± 1.8 °C	-31.8 ± 1.3 °C

6.5 Conclusions

A new close-cage POSS derivative, P*Am*DE was synthesized and characterized. Π-*A* isotherm studies of P*Am*DE at the A/W interface reveal a first-order LE/LC phase transition. The 2D Clausius-Clapeyron equations were used to deduce the apparent critical temperature. The result agrees with the estimation from Π-*A* isotherms. The LE/LC phase transition is strongly interfered by the collapse. Conformational analysis for Π-*A* isotherms of P*Am*DE indicates that P*Am*DE initially lies on the water surface with the POSS cage and two *tert*-butyl groups in the same plane. In the LE monolayer region, POSS cage may have a vertex-on conformation in the LE phase and a face-on conformation in the LC phase.

Chapter 7

Overall Conclusions and Future Work

7.1 Overall Conclusions

Polyhedral oligomeric silsesquioxane (POSS) devivatives, from aminopropylisobutyl-POSS (POSS-NH_2) with two (P*Am*DE) or three (P*Am*TE) *tert*-butyl esters, or purified (3-hydroxypropyl)-heptaisobutyl-POSS (POSS-OH) with two (P*Al*DE) or three (P*Al*TE) *tert*-butyl esters have been synthesized and characterized by ^{1}H NMR, ^{13}C NMR, high resolution mass spectrometry (HRMS), melting point testing, and surface pressure-area per molecule (Π-*A*) isotherms and Brewster angle microscopy (BAM) at the air/water (A/W) interface. All the POSS derivatives are amphiphilic. Unlike trisilanol-POSS derivatives, these esters have greater lift-off areas ($A_{lift\text{-}off}$) as well as limiting areas (A_0) with smaller collapse areas (A_c). Therefore, POSS-based esters initially form softer monolayer films than the trisilanol-POSS derivatives.

The monolayer phase of P*Am*TE can be described as a liquid-expanded (LE) phase before the two-dimensional (2D) film collapses into three-dimensional (3D) multilayers. This result is comparable with the observation for previously studied POSS-OH based triester P*Al*TE. However, the analysis of P*Al*DE reveals a liquid expanded-to-condensed (LE/LC) phase transition, the first observed for POSS materials. A LE/LC phase transition was also observed in the study of P*Am*DE. BAM images show large islands of the LC phase are dispersed in the LE phase in the two-phase coexistence region. The apparent critical temperatures (T_c) of the non-

equilibrium phase transitions were obtained from the 2D Clausius-Clapeyron equations. The results of this analysis are consistent with the Π-*A* isotherms.

Deng, *et al*.[30b] proposed a vertex-on conformation for trisilanol-POSS derivatives. This concept was used to explain features in the Π-*A* isotherm of P*Al*TE.[47d] In this thesis face-on and vertex-on conformations were used to provide a speculative molecular basis for the LE/LC phase transitions seen in P*Al*DE and P*Am*DE during non-equilibrium experiments where Π-*A* isotherms were obtained at a constant compression rate. In general, POSS-based esters initially lie on the water surface with the POSS cage and *tert*-butyl groups in the same plane. In the monolayer region, the POSS cage may exhibit a vertex-on conformation as the film is compressed in the LE phase with a face-on conformation prior to collapse for LC films

.

7.2 Suggestions for Future Work

7.2.1 Synthesis and Characterization of POSS-Based Monoesters

This dissertation shows rational changes in POSS structure lead to new phase behavior for POSS derivatives. After the synthesis and characterization of POSS-based triesters and diesters, POSS-based monoesters would be a natural extension. Compared to the tripodal structure of triesters and dipodal structure of diesters, monoesters would have an even more difficult time supporting the Si-O cage. As discussed in Chapters 5 and 6, the LE/LC phase transition for diesters is possibly due to a change in packing of the POSS cages as one ester group is removed. The ∏-*A* isotherms of monoesters may exhibit even more complicated phase diagrams in the monolayer region.

Possible POSS-based monoesters are proposed in Figure 7.1. The structures are simplest when the substituent R′ = R″ = CH_3. Such monoesters can be obtained from POSS-OH, POSS-NH_2, and an appropriate isocyanatemonoester.

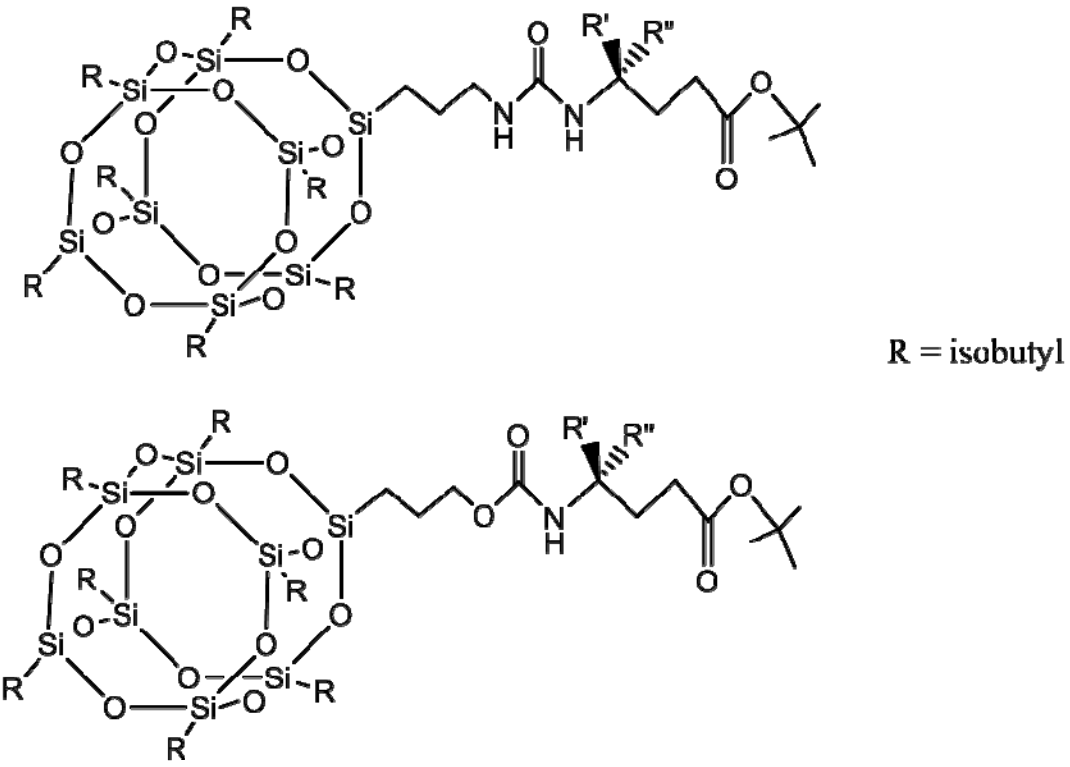

Figure 7.1 Structures of POSS-NH_2 and POSS-OH based monoester.

A possible synthetic scheme for the synthesis of an isocyanatemonoester is motivated by the synthesis of isocyanatediester (**2** in Figure 3.1).[157] The synthetic route for a nitromonoester, *tert*-butyl 4-methyl-4-nitropentanoate (**3**), is proposed in Scheme 7.1. Newkome *et al*. have published several methods for preparing dendritic headgroups with two *tert*-butyl ester groups.[158] Through

their efforts, the yield increases to 95% although low temperature is required for work with liquid NH_3. In order to avoid the inconvenience of working at low temperature, Actis accomplished the synthesis of nitrodiester by a reaction of nitroethane and two equivalents of *tert*-butyl acrylate (**2**) with Triton B (benzyltrimethylammonium hydroxide, 40 wt % solution in methanol) as a catalyst in yields as high as 44%.[159] The purified yield was modest because of the difficulty in removing excess acrylate. Other work by the Gandour group[160] reported using 1,8-diazabicyclo[5.4.0]undec-7-ene (DBU) as a catalyst for the Michael addition reaction at 40 ^{o}C. After comparison, the best result was achieved with 5 mol % DBU.[157] Therefore, the same reaction condition is proposed in Scheme 7.1. Slow addition of one equivalent of **2** is suggested. 2-nitropropane (**1**), *tert*-butyl acrylate (**2**), and DBU are commercially available from Sigma-Aldrich Corporation.

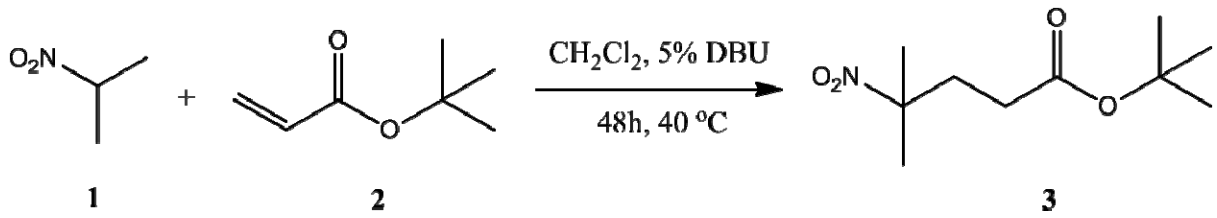

Scheme 7.1 Synthetic scheme for *tert*-butyl 4-methyl-4-nitropentanoate (**3**).

After **3** is obtained, Raney Ni and H_2 can be used to reduce the nitro group to an amine (Scheme 7.2). This hydrogenation reaction usually requires elevated pressure (50 – 60 psi).[158a] The bulky *tert*-butyl ester may even prevent possible intramolecular cyclization observed for less bulky esters (such as methyl).[158c] Heptanes have been used instead of methanol with a higher

purity and yield (98%) in a mechanically stirred sealed reactor.[161] However, this method is inconvenient for the desired scale of the reaction. As a result, I would suggest optimizing the reaction yield by altering the pressure of the reaction.

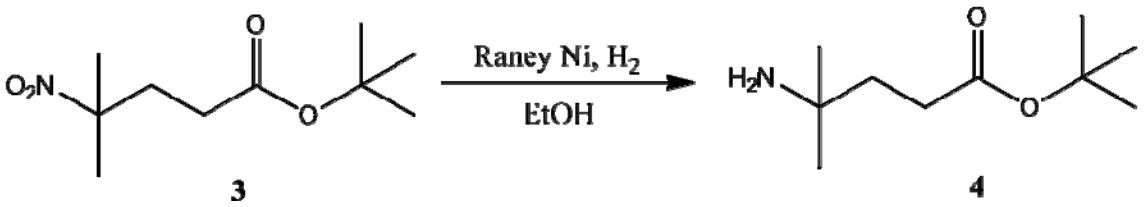

Scheme 7.2 Synthetic scheme for *tert*-butyl 4-amino-4-methylpentanoate (**4**).

Isocyanate esters were prepared from compounds similar to **4** in the presence of triphosgene with an inorganic or organic base in an ice-bath.[162] Scheme 7.3 is suggested as a modification of these reaction conditions to obtain 4-isocyanato-4-methylpentanoate, isocyanatemonoester (**7**). The recation can be completed within 15 minutes with dimethyl amino pyridine (DMAP, **5)** and di-*tert*-butyl dicarbonate ($(Boc)_2O$, **13)** in methylene dichloride at room temperature.[120a, 163] DMAP and $(Boc)_2O$ can be purchased from Sigma-Aldrich Corporation.

According to the synthesis of diesters and triesters,[47d] POSS-OH based monoester (P*Al*ME, **10**) and POSS-NH_2 based monoester (P*Am*ME, **11**) can be obtained in the presence of triethylamine (TEA)[117] when X = O and X= NH, respectively (Scheme 7.4).

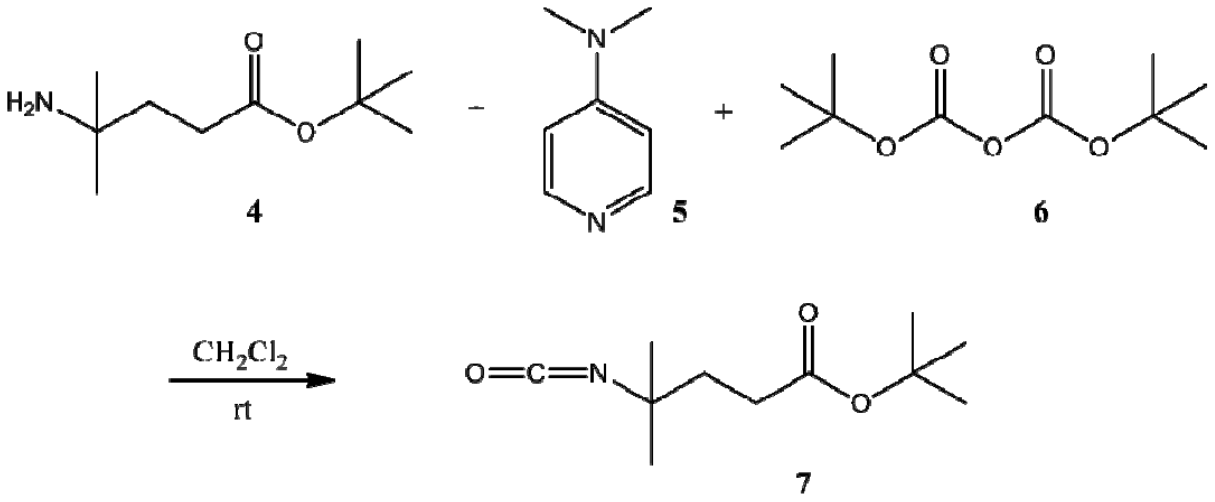

Scheme 7.3 Synthetic scheme for *tert*-butyl 4-isocyanato-4-methylpentanoate, isocyanatemonoester (**7**).

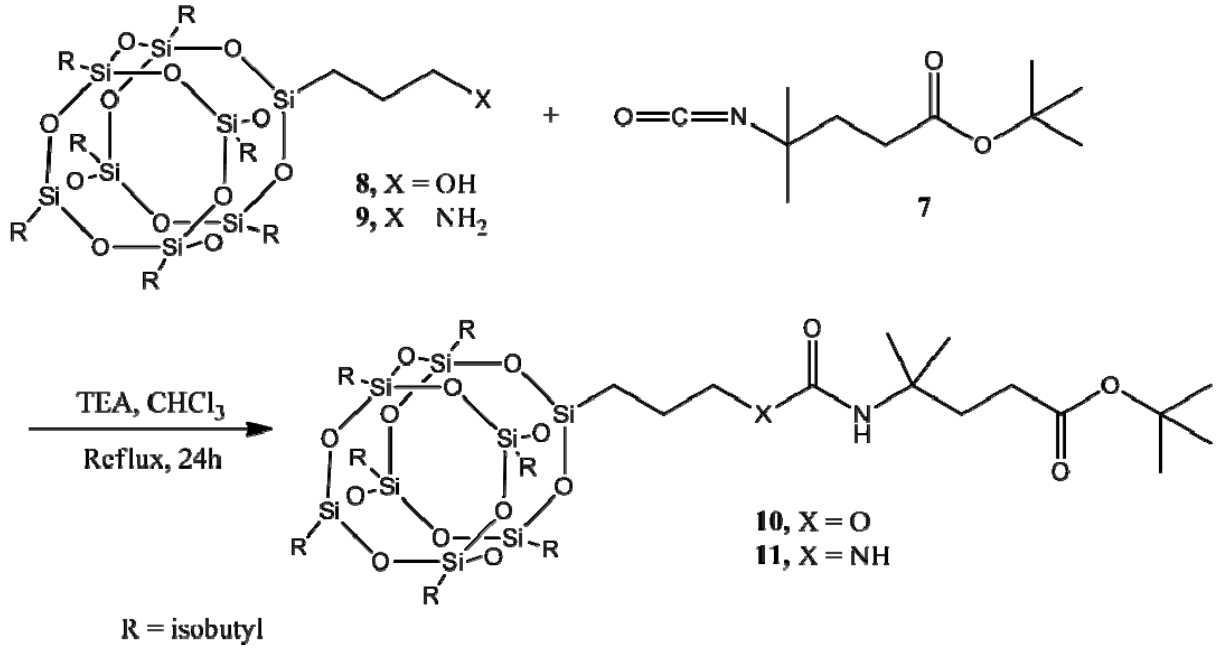

Scheme 7.4 Synthetic scheme for obtaining POSS-OH based monoester (P*Al*ME, **10**) and POSS-NH_2 based monoester (P*Am*ME, **11**).

7.2.2 Synthesis and Characterization of POSS-Based Monoesters with Different Linkers

In Section 7.2.1, R′ = R″ = CH_3 was chosen as the simplest possible linker to afford **10** and **11**. As the length of R′ and R″ increases (Figure 7.2), closed-cage POSS-based esters would become more hydrophobic. Their synthesis would follow from appropriate modification of **1** in Scheme 7.1. An alternative approach would be used to modify the length of the methylene spacer between the POSS cage and the carbamate group in **10**. Due to the availability of samples, I would suggest that POSS-based carbamate esters be pursued first. Examples are provided in Figure 7.2. R′ and R″ can be different or the same as the case for -CH_2-CH_2-COO-$C(CH_3)_3$ in P*Al*TE and P*Am*TE. Less bulky R′ and R″ groups, such as –CH_3, are initially preferred as an analog of fatty acids.

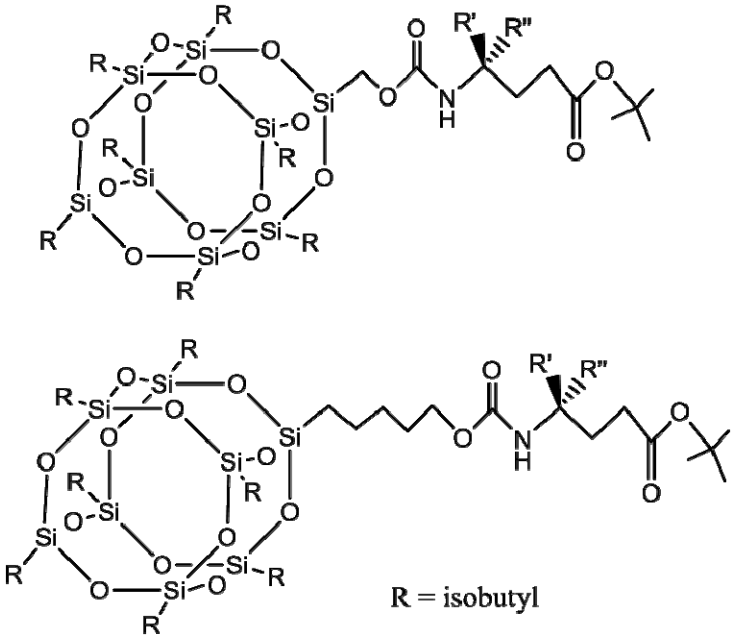

Figure 7.2 Examples of POSS-based carbamate esters with different linker lengths.

Fatty acids dissolve in water forming Gibbs monolayers with shorter alkyl chains (number of carbons < 13) and form Langmuir monolayers at the A/W interface with longer alkyl chains (number of carbons > 13).[84, 86-87] Therefore, as the methylene spacer of the POSS-based carbamate esters increases, closed-cage POSS derivatives may exhibit phase diagrams as complicated as long chain fatty acids. Meanwhile, the possible phase transitions may shift to an experimentally accessible temperature window.

The aim would be to synthesize a shorter chain methoxylisobutyl-POSS (**13** in Scheme 7.5). **13** can be achieved from the hydrolysis of methacrylate isobutyl-POSS (**12** in Scheme 7.5), which is available from Hybrid Plastics Incorporated. After the synthesis of esters, corresponding acids could be obtained by removing the *tert*-butyl esters with trifluoroacetic acid (TFA). It would also be interesting to directly compare closed cage POSS-based carbamate acids with traditional fatty acids.

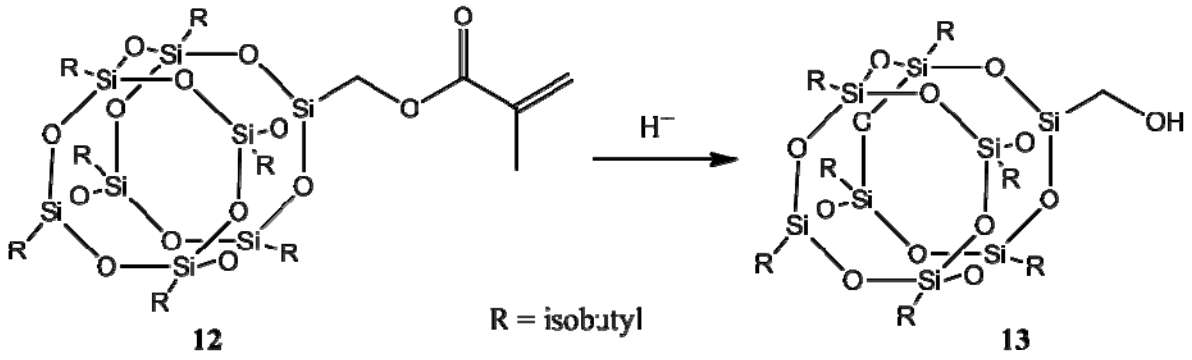

Scheme 7.5 Synthetic scheme for methoxylisobutyl-POSS (**13**) from methacrylate isobutyl-POSS (**12**).

Starting from **13**, the synthesis of monoester and monoacid carbamates with a single methylene unit as a linker are shown in Scheme 7.6 as an example of what is possible.

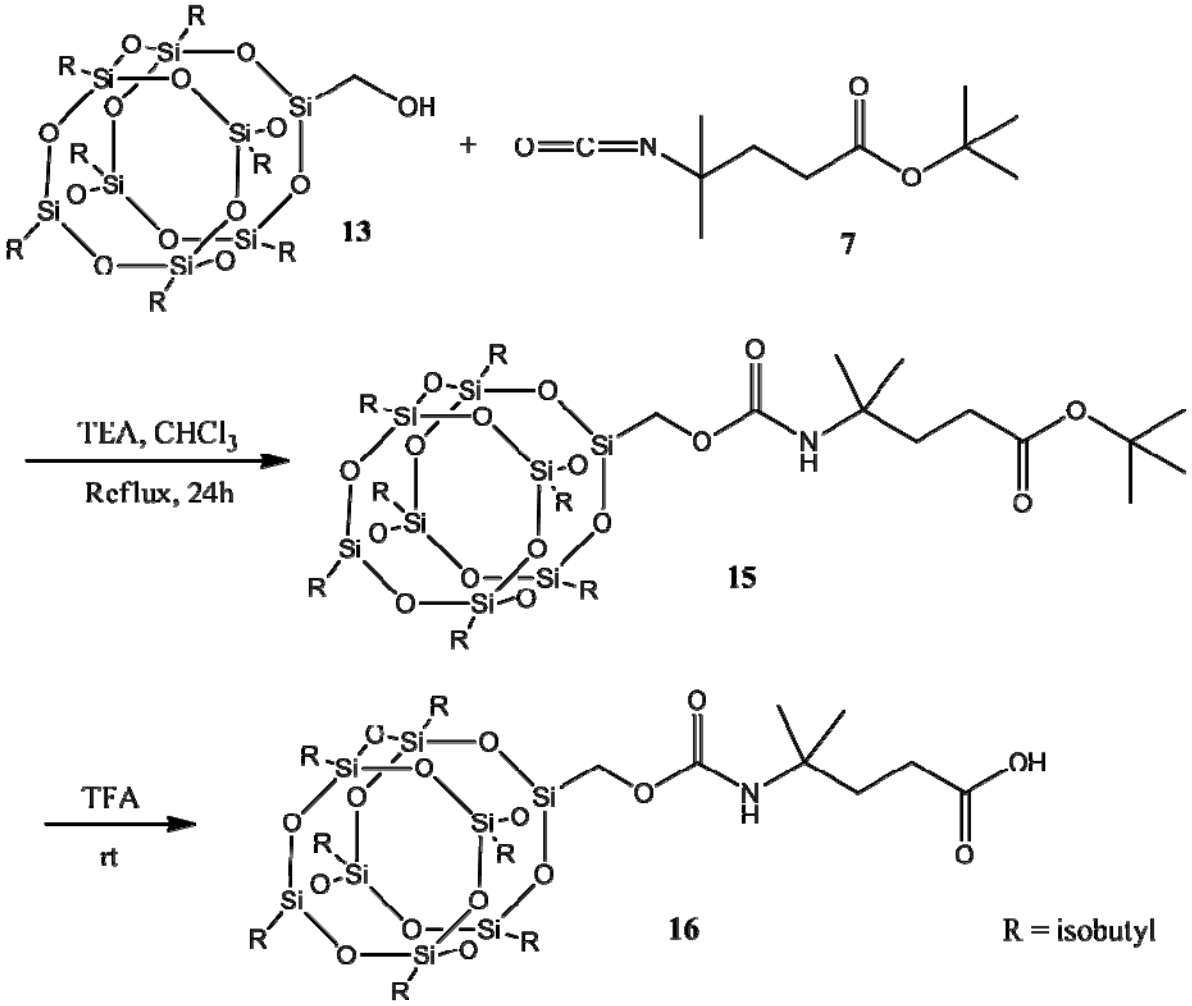

Scheme 7.6 Synthetic scheme for POSS-based carbamate monoester (**15**) and monoacid (**16**) with a single linking methylene unit between the POSS cage and the carbamate.

13 can be modified by 1,n-diols (**17**, in Scheme 7.7) to design longer chain carbamate esters. The length of side chain can be controlled by the number of methylene groups. For **17**, diols with n varying from 2 to 10 are available from Sigma-Aldrich Corporation. Then, closed cage POSS-based carbamate esters and acids can be synthesized using reaction conditions similar to Scheme 7.6.

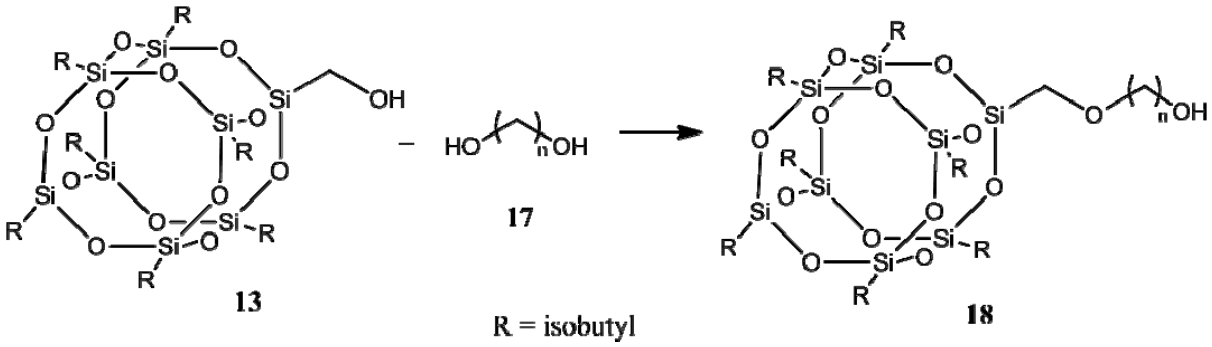

Scheme 7.7 Synthetic scheme for POSS-OH derivatives (**15**) with different length, methylene spacers.

7.2.3 Synthesis and Characterization of POSS-Based Non-*tert*-butyl Esters

Figure 7.3 contains surface pressure-area per molecule (Π-*A*) isotherms for POSS-OH and P*AI*TE from Chapter 4 (Figure 4.11). As one may notice in Figure 7.3, there is a "window" with respect to packing at the A/W interface between the POSS-OH and P*AI*TE. It should be possible to design, synthesize, and characterize POSS molecules to fill this "window". This thesis reveals that the number of ester groups has a small effect on the collapse area and collapse pressure of the POSS derivatives in dynamic, constant compression experiments. Instead, the surface

properties of the t-butylester play an important role. Therefore, I would like to change the sizes of the tripodal esters by substituting bulky *tert*-butyl groups with other alkyl groups. After different esters based upon POSS-OH are synthesized and characterized, similar work can be done on the corresponding POSS-NH_2 derivatives. Some suggestions are provided in Figure 7.4. R′ can be methyl, ethyl, isopropyl, etc.

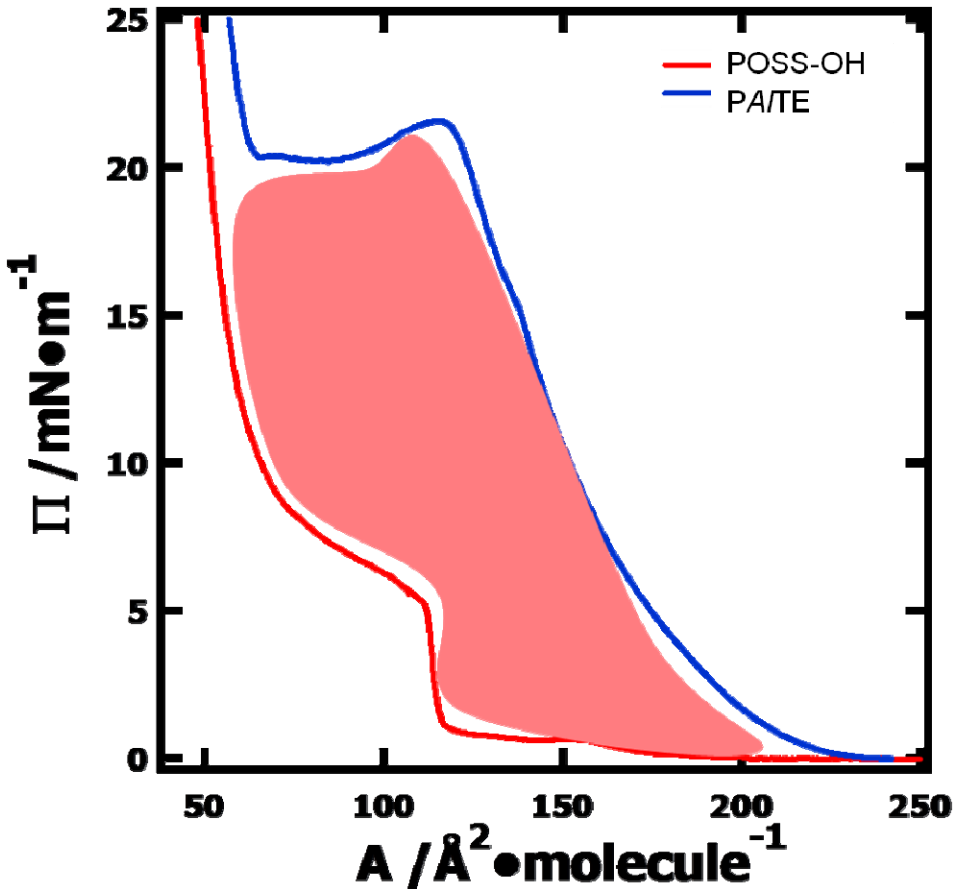

Figure 7.3 Π-*A* isotherms of POSS-OH and P*AI*TE at the A/W interface at 22.5 °C. The shaded peach region represents a region of interest for controlling POSS packing through the synthesis of new POSS amphiphiles.

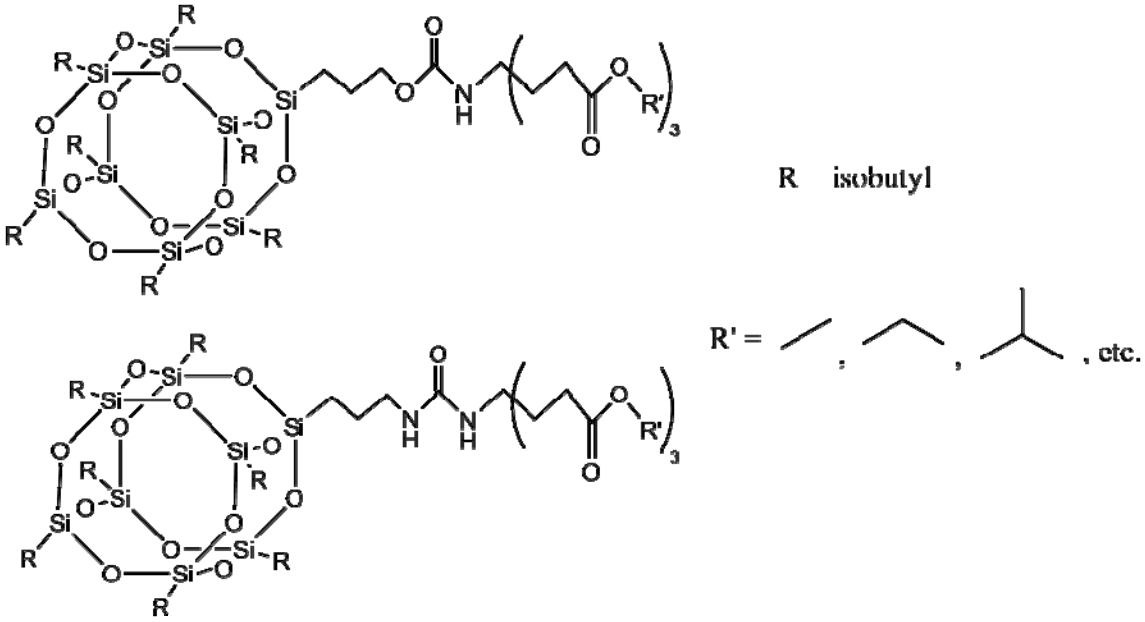

Figure 7.4 Examples of POSS-OH and POSS-NH_2 based non-^{t}butyl esters.

POSS-OH based triacid (**20**, P*AI*TA) has been synthesized from the hydrolysis of P*AI*TE (**19**, Scheme 7.8) in the presence of TFA at room temperature for 30 hours.[47d] In the past few decades, multiple synthetic strategies have been developed to obtain functional dendrimers.[164] **20** will be treated with alcohol in the presence of CH_2Cl_2 using pyridinium *p*-toluenesulfonate (PPTS) as a catalyst.[165] As an example, POSS-OH based trimethylester could be obtained from Scheme 7.9.

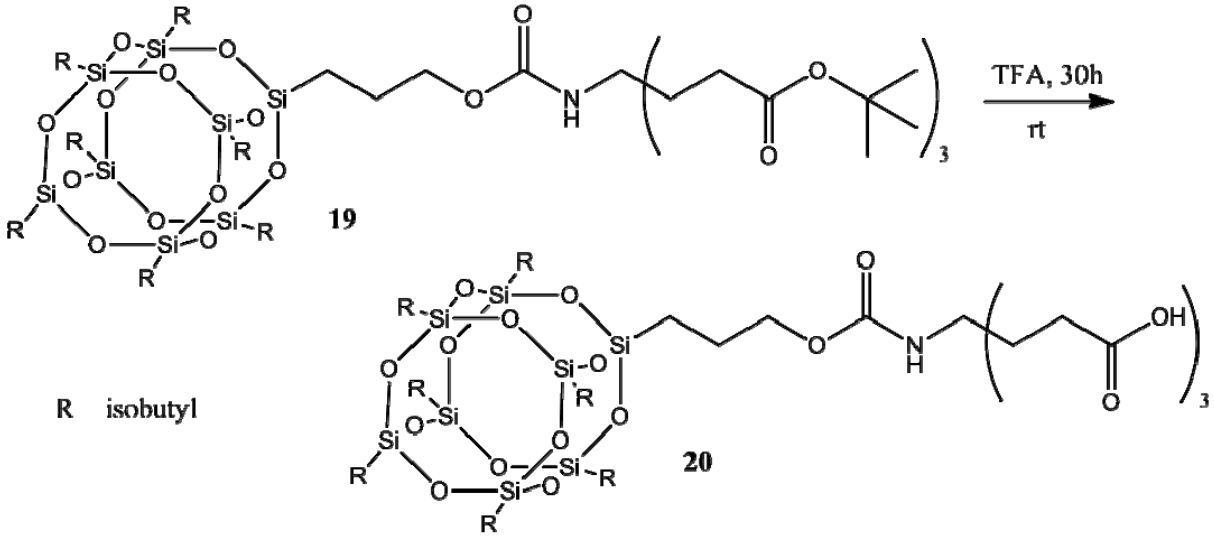

Scheme 7.8 Synthetic scheme for POSS-OH based triacid (**20**).

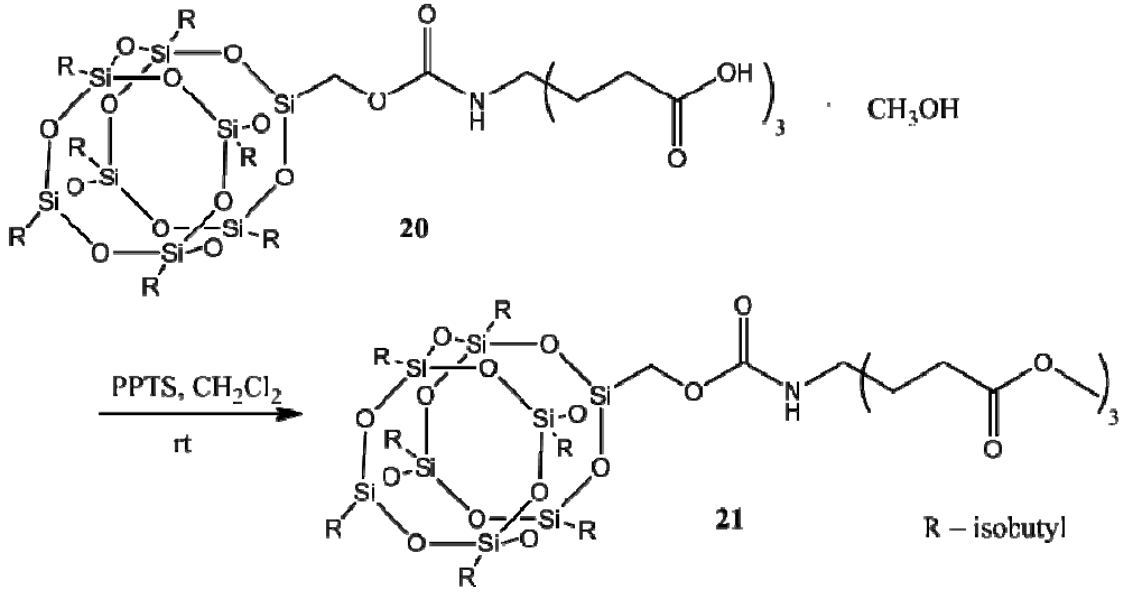

Scheme 7.9 Synthetic scheme for POSS-OH based trimethylester (**21**).

Similarly, acids can be obtained through the hydrolysis of P*Al*DE, P*Am*TE, and P*Am*DE. Chemical composition and purity were confirmed via ^{1}H NMR, ^{13}C NMR, and HRMS. Figures 7.5, 7.6, and 7.9 contain the ^{1}H NMR spectra for POSS-NH_2 based triacid (P*Am*TA), POSS-OH based diacid (P*Al*DA), and POSS-NH_2 based diacid (P*Am*DA) in $CDCl_3$, respectively. Figures 7.7 and 7.8 contain the ^{13}C NMR and expanded ^{13}C NMR spectrum for P*Al*DA in $CDCl_3$, respectively. Other esters could be made from P*Am*TA, P*Al*DA, and P*Am*DA via Scheme 7.9.

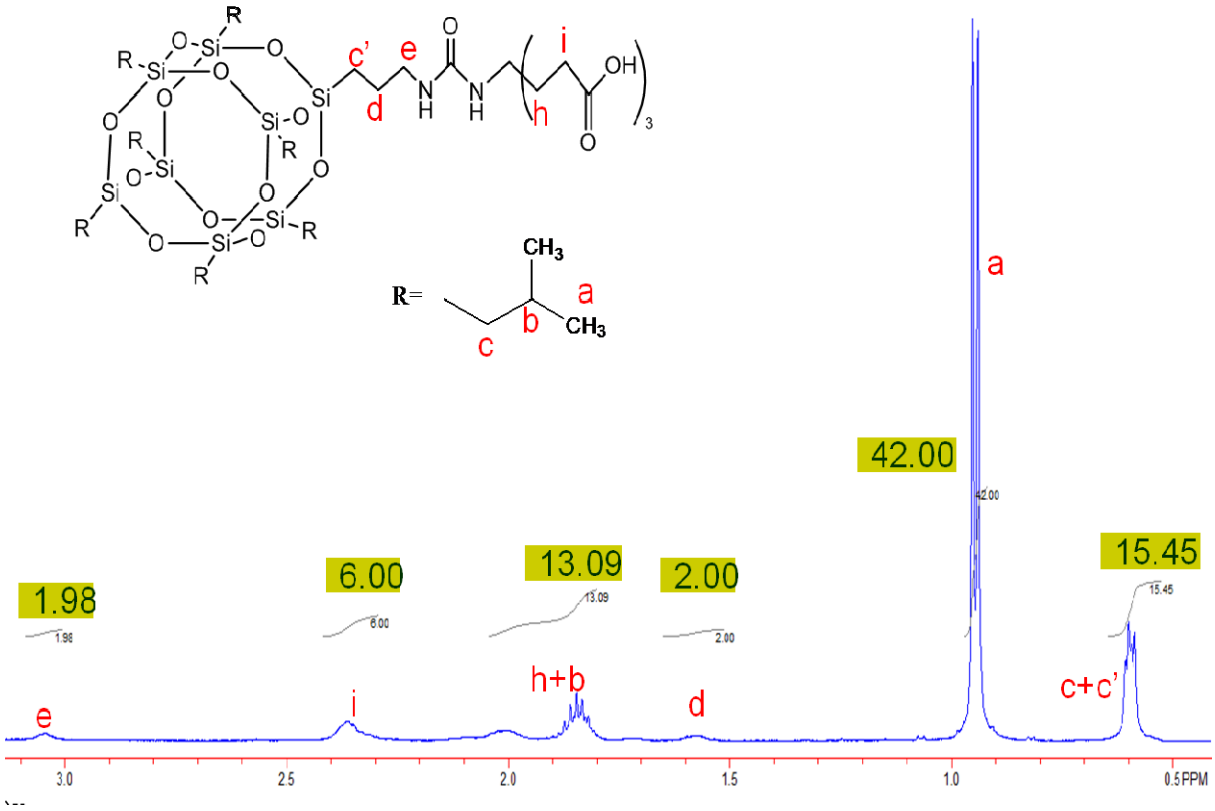

Figure 7.5 ^{1}H NMR of POSS-NH_2 based triacid (P*Am*TA).

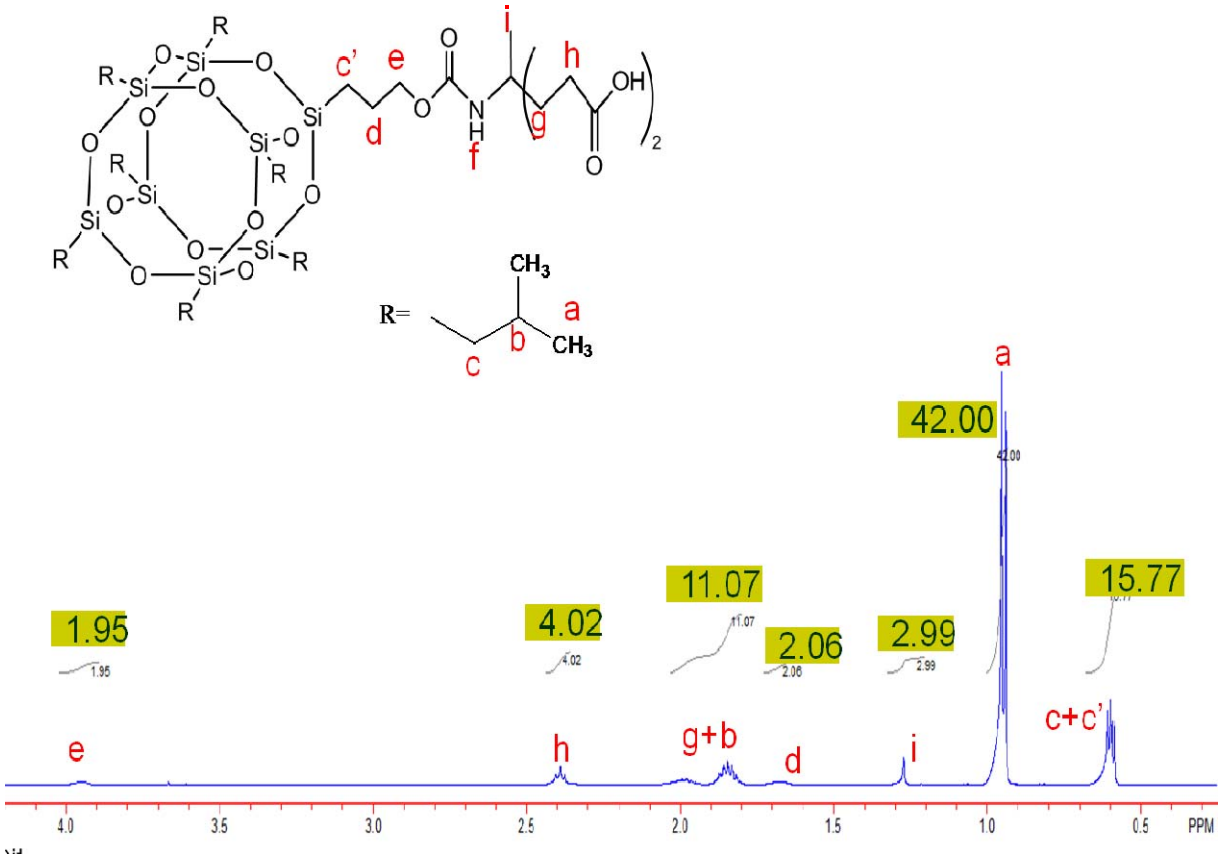

Figure 7.6 ^{1}H NMR of POSS-OH based diacid (P*Al*DA).

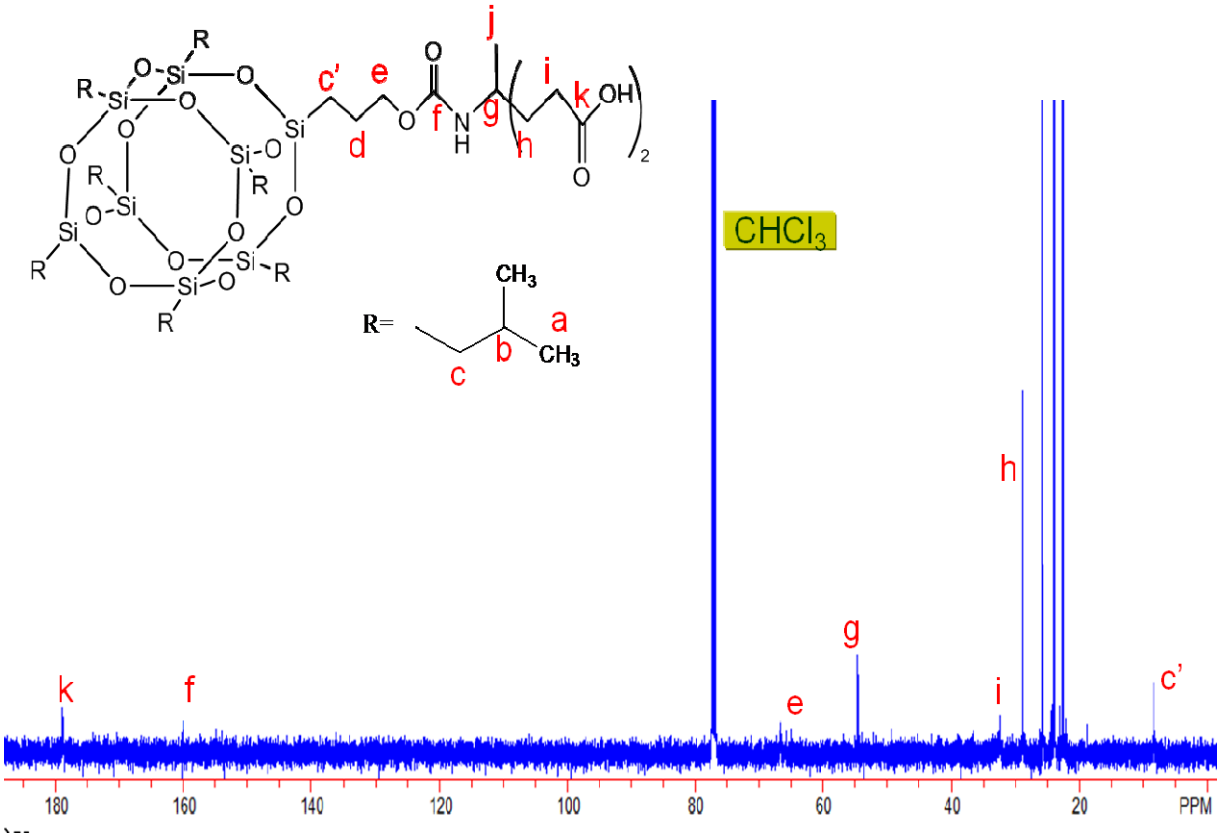

Figure 7.7 ^{13}C NMR of POSS-OH based diacid (P*Al*DA).

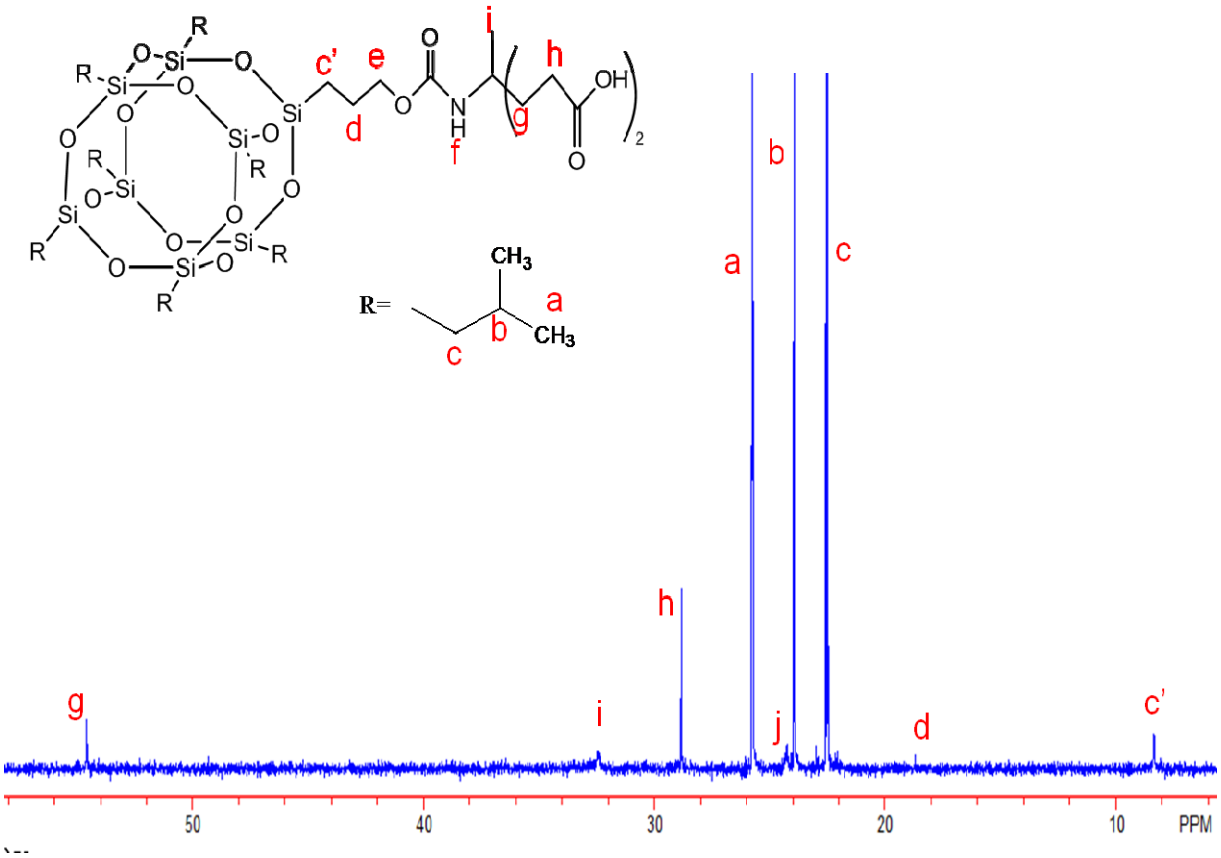

Figure 7.8 Expanded ^{13}C NMR of POSS-OH based diacid (P*Al*DA).

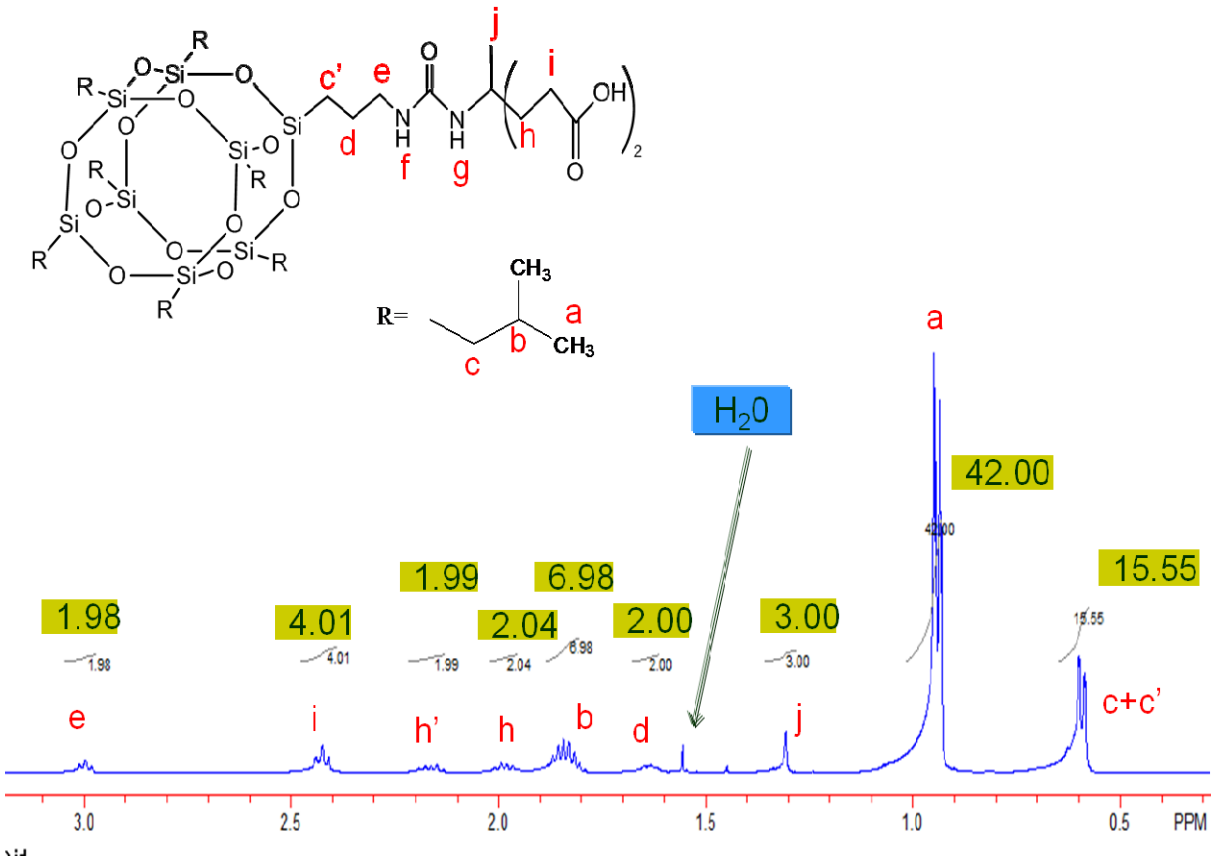

Figure 7.9 ^{1}H NMR of POSS-NH_2 based diacid (P*Am*DA).

7.2.4 Synthesis and Characterization of POSS-Based Esters with Different Substituents on the POSS Cage

To this point, the POSS cages have had the same R substituent (isobutyl). It is also possible to vary R through the amine-based linking chemistry. For the long term, I propose to expand the library of POSS-based esters and acids by creating amino functionalized branches from trisilanol-POSS derivatives with different substituents on the cage (Scheme 7.10).[107, 123c, 166] With

POSS-NH_2 possessing different R, it would be straight forward to create other POSS-NH_2 based esters and acids. With these materials, the relationship between the interfacial properties of POSS-based surfactants and chemical structure would be better understood. Trisilanolethyl-POSS, trisilanolcyclohexyl-POSS, trisilanolcyclopentyl-POSS, and trisilanolphenyl-POSS can be purchased from Hybrid Plastics Incorporated. (3-Aminopropyl) trimethoxysilane (**23**) is commercially available from Sigma-Aldrich Corporation.

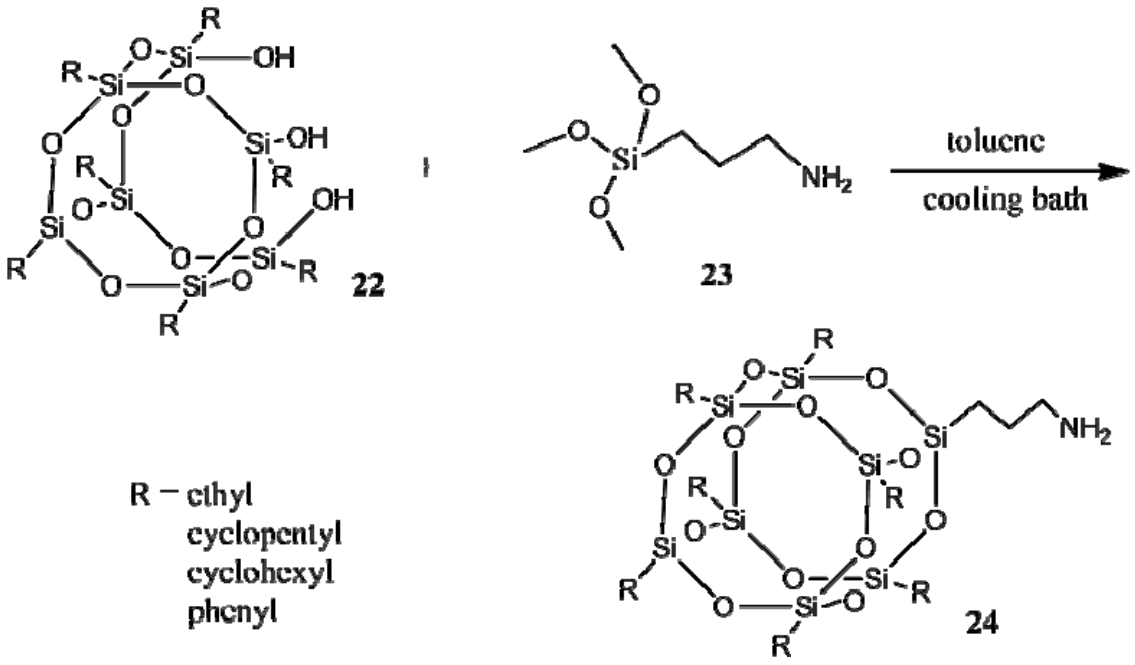

Scheme 7.10 Synthetic scheme for obtaining closed-cage POSS derivatives with a single primary amine from trisilanol-POSS with different R.

7.2.5 Blends of Amphiphilic POSS Derivatives at the A/W Interface

With a core-shell structure exhibiting organic/inorganic hybrid properties, POSS molecules have been treated as the smallest particles of silica.[7b, 167] Over recent decades, the well defined and easily modified chemical structure served as a building block for composite materials. The mechanical, optical, and thermal properties of POSS copolymers and POSS/polymer blends have been extensively studied.[168] The Esker group has studied interactions between polymer and POSS as nanofillers in 2D Langmuir monolayers.[118a, 131, 133] Therefore, I suggest these new POSS derivatives be examined as nanofillers in Langmuir films. Polydimethylsiloxane **(**PDMS) is a material known to form stable flexible monolayers and multilayers at the A/W interface.[169] Blends of PDMS and trisilanol-POSS derivatives at the A/W interface have been examined with respect to aggregate formation[170] and rheological properties.[112, 171] Since closed-cage POSS are normally non-amphiphilic and tend to form rigid multilayer aggregates at the A/W interface, octaalkyl-POSS/PDMS blends show filler reinforcement when dispersed in PDMS.[131] The POSS-based triester and triacid derivatives I have made are also closed-cage; however, the hydrophilic arm makes them amphiphilic. As such, I hypothesize these materials can significantly enhance the dilational modulus of PDMS films at the A/W interface.

In addition, a blend of trisilanolisooctyl-POSS (TiOP) and trisilanolphenyl-POSS (TPP) has been examine by $\prod$-*A* isotherms and BAM. The preliminary work is represented in Figure 7.10. TiOP is considered as a true liquid trisilanol-POSS since it behaves as a liquid in the monolayer region and exists as liquid in bulk. The Π-*A* isotherm for TiOP has a lift-off surface concentration ($A_{lift\text{-}off,}$ where Π increases from zero) around $A_{lift\text{-}off}$ ~ 220 $Å^2$•molecule^{-1}. Its limiting area (A_0), which is obtained by extrapolating the steepest portion of the Π-*A* isotherm back to $\Pi = 0$, is coincident with $A_{lift\text{-}off}$. At a collapse pressure (Π_c) of ~ 13.5 mN•m^{-1}, the TiOP

film collapses into multilayer domains. The second plateau (60 Å^2•molecule^{-1} < A < 180 Å^2•molecule^{-1}) corresponds to multilayer formation. The factor of three changes in area may be consistent with trilayer formation. The shape of the isotherm for TPP is similar to that of TiOP with $A_{lift\text{-}off}$ ~ 155 Å^2•molecule^{-1} and A_0 ~ 150 Å^2•molecule^{-1}. In the monolayer region, the steeper isotherm of TPP suggests a more rigid film. At a lower Π_c (~ 12.5 mN•m^{-1}), TPP exhibits a plateau (50 Å^2•molecule^{-1} < A < 140 Å^2•molecule^{-1}). The small limiting area for TPP was explained by the "interlocking" space-filling model of rigid phenyl groups (Figure 7.11).[85]

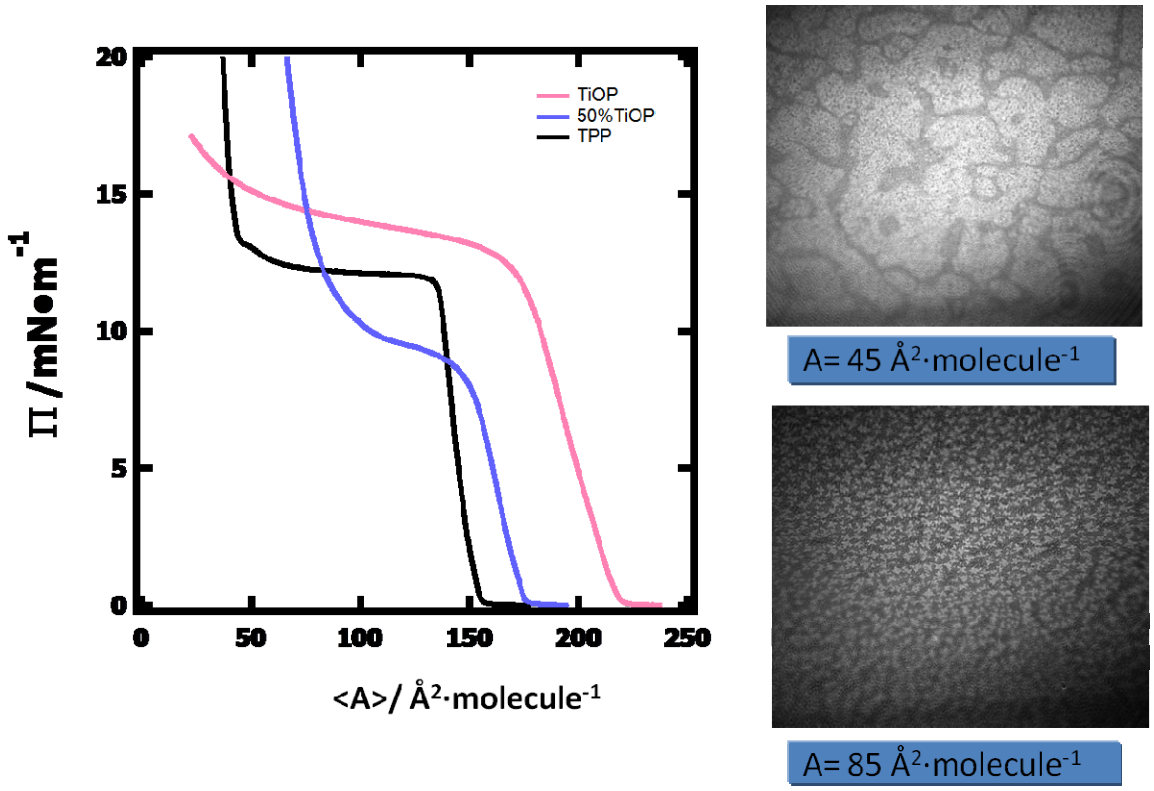

Figure 7.10 Π-A isotherms of TiOP, TPP, and a 50 : 50 blend by mass at the A/W interface at T = 22.5 °C. The 4.8 mm × 6.4 mm BAM images for 50% TiOP were captured at A = 85 and 45 Å^2·molecule^{-1}.

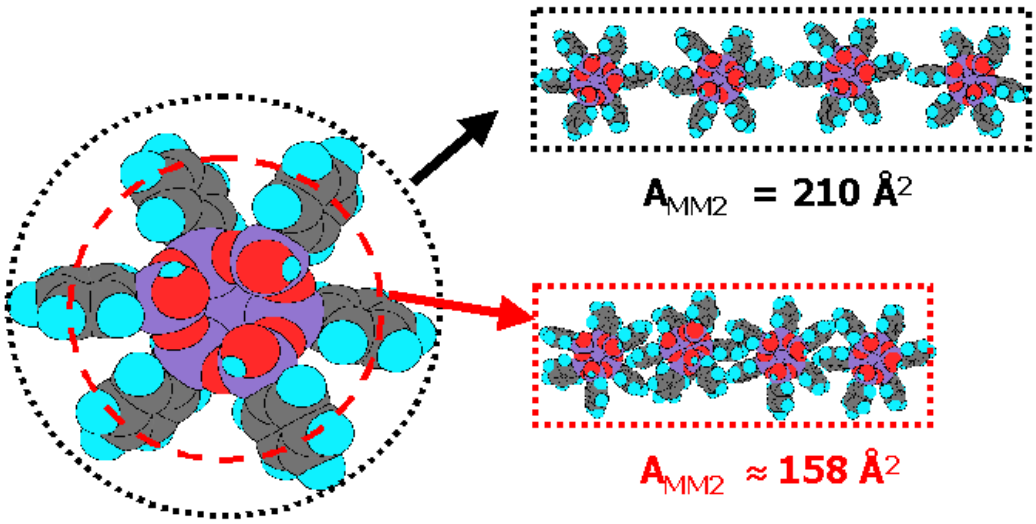

Figure 7.11 A demonstration of "interdigitating" or "interlocking" phenyl groups for TPP at the A/W interface. Gray atoms are carbon, red atoms are oxygen, purple atoms are silicon, and green atoms are hydrogen. The model represents the configuration where the three silanol groups of POSS are exposed to water (out of the page). With the "interdigitating" phenyl groups, the recalculated cross-sectional area (*AMM2* = 158 Å^2•molecule^{-1}) of TPP is smaller than the one without interdigitation (*AMM2* ≈ 210 Å^2•molecule^{-1}) and close to the experimental limiting area (A_o = 152 ± 8 Å^2•molecule^{-1}) obtained from Π-*A* isotherms.[85]

Moving onto the blend of 50 : 50 by mass blend of TiOP, the isotherm exhibits a smaller collapse pressure (~ 8 mN•m^{-1}) and negative excess areas of mixing that suggest greater cohesive interactions due to intermolecular hydrogen bonding. Aggregate formation is not observed for neat TPP even at the end of the compression suggesting uniform gels or liquid crystals rather than the rigid and crystal-like films.[85] However, at the end of collapse (~85 Å^2•molecule^{-1}) of

---

TPP/TiOP blend, BAM images reveal regular star-shaped heterogeneous films, which are not observed for the blends of TiOP/TiBP, TiOP/TCyP, and TiOP/TCpP. These results may be related to more ordered structure. It is possible that the isooctyl groups of TiOP fill gaps between rigid phenyl groups of TPP. Therefore, I suggest altering the composition of the TPP and comparing their isotherms as future work. BAM should be able to provide more details about the collapse process. Then, the molar Gibbs excess free energy of mixing (ΔG_{excess}) obtained from Π-*A* isotherms as a function of mole fraction of TiOP (X_{TiOP}) can be interpreted and related to the BAM studies.

References

1. (a) Dutta, P., Order in Langmuir monolayers and in the aqueous subphase. *Studies in Interface Science* **2002,** *16* (Organized Monolayers and Assemblies: Structure, Processes and Function), 1-12; (b) Gaines, G. L., Jr., *Insoluble Monolayers at Liquid-Gas Interfaces*. 1966; p 386 pp; (c) Knobler, C. M.; Desai, R. C., Phase transitions in monolayers. *Annual Review of Physical Chemistry* **1992,** *43*, 207-236; (d) McConnell, H. M., Structures and transitions in lipid monolayers at the air-water interface. *Annual Review of Physical Chemistry* **1991,** *42*, 171-195; (e) Petty, M. C., Langmuir-Blodgett Films; Cambridge University Press: London. **1996**; (f) Ulman, A., *An Introduction to Ultrathin Organic Films: From Langmuir-Blodgett to Self-Assembly*; Academic Press: Boston. **1991**.

2. (a) Andelman, D.; Brochard, F.; Knobler, C.; Rondelez, F., Structures and phase transitions in Langmuir monolayers. *Micelles, Membr., Microemulsions, Monolayers* **1994**, 559-602; (b) Fendler, J. H.; Meldrum, F. C., The colloid chemical approach to nanostructured materials. *Advanced Materials (Weinheim, Germany)* **1995,** *7* (7), 607-632; (c) Moewald, H., Surfactant layers at water surfaces. *Reports on Progress in Physics* **1993,** *56* (5), 653-685.

3. (a) Schief, W. R.; Dennis, S. R.; Frey, W.; Vogel, V., Light scattering microscopy from monolayers and nanoparticles at the air/water interface. *Colloids and Surfaces, A: Physicochemical and Engineering Aspects* **2000,** *171* (1-3), 75-86; (b) Lu, W.; Knobler, C. M.; Bruinsma, R. F.; Twardos, M.; Dennin, M., Folding Langmuir Monolayers. *Physical Review Letters* **2002,** *89* (14), 146107/1-146107/4.

4. Lipp, M. M.; Lee, K. Y. C.; Zasadzinski, J. A.; Waring, A. J., Design and performance of an integrated fluorescence, polarized fluorescence, and Brewster angle microscope/Langmuir trough assembly for the study of lung surfactant monolayers. *Review of Scientific Instruments* **1997,** *68* (6), 2574-2582.

5. (a) Angelova, A.; Vollhardt, D.; Ionov, R., 2D-3D Transformations of Amphiphilic Monolayers Influenced by Intermolecular Interactions: A Brewster Angle Microscopy Study. *Journal of Physical Chemistry* **1996,** *100* (25), 10710-10720; (b) Lu, Z.; Nakahara, H., Collapsing processes in stearic acid monolayer studied by Brewster angle microscope. *Chemistry Letters* **1994,** (11), 2005-2008; (c) Lheveder, C.; Henon, S.; Mercier, R.; Tissot, G.; Fournet, P.; Meunier, J., A new Brewster angle microscope. *Review of Scientific Instruments* **1998,** *69* (3), 1446-1450.

6. (a) Gopal, A.; Lee, K. Y. C., Morphology and Collapse Transitions in Binary Phospholipid Monolayers. *Journal of Physical Chemistry B* **2001,** *105* (42), 10348-10354; (b) Hatta, E.; Fischer, T. M., Modulation crack growth and crack coalescence upon Langmuir monolayer collapse. *Journal of Physical Chemistry B* **2002,** *106* (3), 589-592; (c) Schief, W. R.; Antia, M.; Discher, B. M.; Hall, S. B.; Vogel, V., Liquid-crystalline collapse of pulmonary surfactant monolayers. *Biophysical Journal* **2003,** *84* (6), 3792-3806; (d) Schief, W. R.; Hall, S. B.; Vogel, V., Spatially patterned static roughness superimposed on thermal roughness in a condensed phospholipid monolayer. *Physical Review E: Statistical Physics, Plasmas, Fluids, and Related Interdisciplinary Topics* **2000,** *62* (5-B), 6831-6837; (e) Schief, W. R.; Touryan, L.; Hall, S. B.; Vogel, V., Nanoscale topographic instabilities of a phospholipid monolayer. *Journal of Physical Chemistry B* **2000,** *104* (31), 7388-7393; (f) Ybert, C.; Lu, W.; Moeller, G.; Knobler, C.

M., Collapse of a monolayer by three mechanisms. *Journal of Physical Chemistry B* **2002,** *106* (8), 2004-2008.

7. (a) Bornhauser, P.; Calzaferri, G., Ring-Opening Vibrations of Spherosiloxanes. *Journal of Physical Chemistry* **1996,** *100* (6), 2035-2044; (b) Baney, R. H.; Itoh, M.; Sakakibara, A.; Suzuki, T., Silsesquioxanes. *Chemical Reviews (Washington, D. C.)* **1995,** *95* (5), 1409-1430; (c) Duchateau, R.; Abbenhuis, H. C. L.; van Santen, R. A.; Meetsma, A.; Thiele, S. K. H.; van Tol, M. F. H., Ethylene Polymerization with Dimeric Zirconium and Hafnium Silsesquioxane Complexes. *Organometallics* **1998,** *17* (26), 5663-5673; (d) Gonzalez, R. I.; Phillips, S. H.; Hoflund, G. B., In situ oxygen-atom erosion study of polyhedral oligomeric silsesquioxane-siloxane copolymer. *Journal of Spacecraft and Rockets* **2000,** *37* (4), 463-467; (e) Hoflund, G. B.; Gonzalez, R. I.; Phillips, S. H., In situ oxygen atom erosion study of a polyhedral oligomeric silsesquioxane-polyurethane copolymer. *Journal of Adhesion Science and Technology* **2001,** *15* (10), 1199-1211; (f) Mengel, C.; Meyer, W. H.; Wegner, G., Photocrosslinkable star polymers: precursors for model polyelectrolyte networks. *Macromolecular Chemistry and Physics* **2001,** *202* (7), 1138-1149; (g) Ropartz, L.; Foster, D. F.; Morris, R. E.; Slawin, A. M. Z.; Cole-Hamilton, D. J., Hydrocarbonylation reactions using alkylphosphine-containing dendrimers based on a polyhedral oligosilsesquioxane core. *Journal of the Chemical Society, Dalton Transactions* **2002,** (9), 1997-2008.

8. Hans-Jurgen Butt, K. G., Michael Kappl, Physics and chemistry of Interfaces. **2003**.

9. (a) Smirnova, Y. G.; Marrink, S.-J.; Lipowsky, R.; Knecht, V., Solvent-Exposed Tails as Prestalk Transition States for Membrane Fusion at Low Hydration. *Journal of the American Chemical Society* **2010,** *132* (19), 6710-6718; (b) Schneggenburger, P. E.; Muellar, S.; Worbs, B.; Steinem, C.; Diederichsen, U., Molecular Recognition at the Membrane-Water Interface:

Controlling Integral Peptide Helices by Off-Membrane Nucleobase Pairing. *Journal of the American Chemical Society* **2010,** *132* (23), 8020-8028; (c) Nagata, Y.; Mukamel, S., Vibrational Sum-Frequency Generation Spectroscopy at the Water/Lipid Interface: Molecular Dynamics Simulation Study. *Journal of the American Chemical Society* **2010,** *132* (18), 6434-6442; (d) Jurak, M.; Chibowski, E., Influence of (phospho)lipases on properties of mica supported phospholipid layers. *Applied Surface Science* **2010,** *256* (21), 6304-6312.

10. (a) Prakash, B. S. J., Surface thermodynamics of clays. *Interface Sci. Technol.* **2004,** *1* (Clay Surfaces), 90-117; (b) Kaneko, M. L. Q. A.; Yoshida, I. V. P., Effect of natural and organically modified montmorillonite clays on the properties of polydimethylsiloxane rubber. *Journal of Applied Polymer Science* **2008,** *108* (4), 2587-2596; (c) Deka, M.; Kumar, A., Enhanced electrical and electrochemical properties of PMMA-clay nanocomposite gel polymer electrolytes. *Electrochim. Acta* **2010,** *55* (5), 1836-1842.

11. (a) Stine, C. M.; Patton, S., Preparation of milk fat. II. A new method of manufacturing butter oil. *J. Dairy Sci.* **1952,** *35*, 655-60; (b) Segall, K. I.; Goff, H. D., Secondary adsorption of milk proteins from the continuous phase to the oil-water interface in dairy emulsions. *Int. Dairy J.* **2002,** *12* (11), 889-897; (c) Pelan, B. M. C.; Watts, K. M.; Campbell, I. J.; Lips, A., The stability of aerated milk protein emulsions in the presence of small molecule surfactants. *J. Dairy Sci.* **1997,** *80* (10), 2631-2638; (d) Jebson, R. S., Butter and allied products. *Fats Food Prod.* **1994**, 69-109.

12. (a) Molina, R.; Esquena, J.; Erra, P., Interfacial processes in textile materials: relevance to adhesion. *Journal of Adhesion Science and Technology* **2010,** *24* (1), 7-33; (b) Foose, L. L. Proteolysis of immobilized proteins at the solid/aqueous interface: Implications for detergency. 2008.

13. (a) Wasyluk, J.; Perova, T. S.; Kukushkin, S. A.; Osipov, A. V.; Feoktistov, N. A.; Grudinkin, S. A., Raman investigation of different polytypes in SiC thin films grown by solid-gas phase epitaxy on Si (111) and 6H-SiC substrates. *Mater. Sci. Forum* **2010,** *645-648* (Pt. 1, Silicon Carbide and Related Materials 2009), 359-362; (b) Sumigawa, T.; Shishido, T.; Murakami, T.; Kitamura, T., Interface crack initiation due to nano-scale stress concentration. *Mater. Sci. Eng., A* **2010,** *527* (18-19), 4796-4803; (c) Jahromi, S. S.; Masoudi, S. F., Detection of nano scale thin films with polarized neutron reflectometry at the presence of smooth and rough interfaces. *Appl. Phys. A Mater. Sci. Process.* **2010,** *99* (1), 255-263.

14. (a) Wang, P.; Schaefer, D. W., Hygrothermal aging of silane-laced epoxy coatings. *Journal of Adhesion Science and Technology* **2010,** *24* (4), 699-708; (b) Singh, A.; Bakshi, S. R.; Agarwal, A.; Harimkar, S. P., Microstructure and tribological behavior of spark plasma sintered iron-based amorphous coatings. *Mater. Sci. Eng., A* **2010,** *527* (18-19), 5000-5007; (c) Huang, Y.; Zeng, X., Investigation on cracking behavior of Ni-based coating by laser-induction hybrid cladding. *Applied Surface Science* **2010,** *256* (20), 5985-5992; (d) Corwin, A. D.; de Boer, M. P., Frictional aging, de-aging, and re-aging in a monolayer-coated micromachined interface. *Phys. Rev. B Condens. Matter Mater. Phys.* **2010,** *81* (17), 174109/1-174109/11.

15. (a) Zhang, J.; Li, R.; Yu, Q., Effect of plasma interface treatment and cathodic electrophoretic coating on Mg alloys. *Mater. Sci. Forum* **2009,** *610-613* (Pt. 2, Materials Research: Eco/Environmental Materials, Energy Materials, Magnesium, Aerospace Materials and Biomaterials for Medical Application), 984-990; (b) Liu, J.; Chaudhury, M. K.; Berry, D. H.; Seebergh, J. E.; Osborne, J. H.; Blohowiak, K. Y., Effect of processing conditions on adhesion performance of a sol-gel reinforced epoxy/aluminum interface. *Journal of Adhesion Science and Technology* **2008,** *22* (10-11), 1159-1180; (c) Gruchow, F.; Machill, S.; Thiele, S.; Herm, C.;

Salzer, R., Imaging FTIR spectroscopic investigations of wood: paint interface of aged polychrome art objects. *e-Preserv. Sci.* **2009,** *6*, 145-150.

16. Panayiotou, C., Interfacial tension and interfacial profiles of fluids and their mixtures. *Langmuir* **2002,** *18* (23), 8841-8853.

17. Locklin, J.; Bao, Z., Effect of morphology on organic thin film transistor sensors. *Analytical and Bioanalytical Chemistry* **2006,** *384* (2), 336-342.

18. Muccini, M., A bright future for organic field-effect transistors. *Nature Materials* **2006,** *5* (8), 605-613.

19. (a) Sariciftci, N. S.; Smilowitz, L.; Heeger, A. J.; Wudl, F., Photoinduced electron transfer from a conducting polymer to buckminsterfullerene. *Science (Washington, DC, United States)* **1992,** *258* (5087), 1474-1476; (b) Yu, G.; Gao, J.; Hummelen, J. C.; Wudl, F.; Heeger, A. J., Polymer photovoltaic cells: enhanced efficiencies via a network of internal donor-acceptor heterojunctions. *Science (Washington, D. C.)* **1995,** *270* (5243), 1789-1791.

20. (a) Burroughes, J. H.; Bradley, D. D. C.; Brown, A. R.; Marks, R. N.; Mackay, K.; Friend, R. H.; Burns, P. L.; Holmes, A. B., Light-emitting diodes based on conjugated polymers. *Nature (London, United Kingdom)* **1990,** *347* (6293), 539-541; (b) Sirringhaus, H.; Tessler, N.; Friend, R. H., Integrated optoelectronic devices based on conjugated polymers. *Science (Washington, D. C.)* **1998,** *280* (5370), 1741-1744.

21. Brown, A. R.; Pomp, A.; Hart, C. M.; de Leeuw, D. M., Logic gates made from polymer transistors and their use in ring oscillators. *Science (Washington, D. C.)* **1995,** *270* (5238), 972-974.

22. (a) Balazs, A. C.; Singh, C.; Zhulina, E.; Chern, S.-S.; Lyatskaya, Y.; Pickett, G., Theory of polymer chains tethered at interfaces. *Progress in Surface Science* **1997,** *55* (3), 181-269; (b)

Holy, C. E.; Fialkov, J. A.; Davies, J. E.; Shoichet, M. S., Use of a biomimetic strategy to engineer bone. *Journal of Biomedical Materials Research, Part A* **2003,** *65A* (4), 447-453; (c) Sigal, G. B.; Mammen, M.; Dahmann, G.; Whitesides, G. M., Polyacrylamides Bearing Pendant alpha -Sialoside Groups Strongly Inhibit Agglutination of Erythrocytes by Influenza Virus: The Strong Inhibition Reflects Enhanced Binding through Cooperative Polyvalent Interactions. *Journal of the American Chemical Society* **1996,** *118* (16), 3789-800.

23. (a) Boland, S. W.; Haile, S. M., Barium metaplumbate (BaPbO3) electrodes for ferroelectric thin films. *Proceedings - Electrochemical Society* **2005,** *2004-18* (Electrode Processes VII), 288-293; (b) Johnson, M.; Li, Z.; Yan, Y.; Wang, J., Determination of the modulus and hardness of spin-on zeolite low-K thin films. *Materials Research Society Symposium Proceedings* **2005,** *880E* (Mechanical Properties of Nanostructured Materials), No pp given, Paper #: BB7 4; (c) Koeppe, R.; Sariciftci, N. S.; Troshin, P. A.; Lyubovskaya, R. N., Complexation of pyrrolidinofullerenes and zinc-phthalocyanine in a bilayer organic solar cell structure. *Applied Physics Letters* **2005,** *87* (24), 244102/1-244102/3; (d) Kumar, M.; Roy, S.; Bhatnagar, M.; Agarwal, S.; Sharma, G., Study of Dielectric and Pyroelectric Properties of Sol-Gel Derived BST Thin Films. *Ferroelectrics* **2005,** *329*, 33-37; (e) Li, Y.; Yang, Y.; Yu, F.; Dong, L., Surface and interface morphology of polystyrene/poly(methyl methacrylate) thin-film blends and bilayers. *Journal of Polymer Science, Part B: Polymer Physics* **2005,** *44* (1), 9-21; (f) Mata, A.; Fleischman, A. J.; Roy, S., Characterization of polydimethylsiloxane (PDMS) properties for biomedical micro/nanosystems. *Biomedical Microdevices* **2005,** *7* (4), 281-293; (g) Mitzi, D. B.; Copel, M.; Murray, C. E.; Kosbar, L. L.; Afzali, A., Thin-film transistors based on spin-coated chalcogenide semiconductor channels. *Proceedings - Electrochemical Society* **2005,** *2004-15* (Thin Film Transistor Technologies (TFTT VII)), 189-199; (h) Ploetner, M.; Richter, S.;

Nguyen, P.-T.; Heuer, H.; Heinzig, A.; Wegener, T.; Plieth, W.; Fischer, W.-J., Study of organic field-effect transistors from poly-3-octylthiophene solutions on different gate dielectrics. *Proceedings - Electrochemical Society* **2005,** *2004-15* (Thin Film Transistor Technologies (TFTT VII)), 263-269; (i) Rast, L.; Stanishevsky, A., Aggregated nanoparticle structures prepared by thermal decomposition of poly(vinyl)-N-pyrrolidone/Ag nanoparticle composite films. *Applied Physics Letters* **2005,** *87* (22), 223118/1-223118/3; (j) Singh, R.; Sharma, S.; Chandra, S.; Goel, T., Dielectric, Ferroelectric and Electrical Properties of Sol-Gel Prepared La Modified PZT Thin Films. *Ferroelectrics* **2005,** *328*, 27-32; (k) Wu, K. H.; Li, M. C.; Chang, T. C.; Yang, C. C., Characterization and corrosion resistance of organically modified silicate/MO2 (M = Zr, Ti, or Ce) hybrid coatings on a 6061-T6 aluminum alloy. *Journal of Polymer Science, Part A: Polymer Chemistry* **2005,** *44* (1), 335-342; (l) Xia, D.; Brueck, S. R. J., Fabrication of enclosed nanochannels using silica nanoparticles. *Journal of Vacuum Science & Technology, B: Microelectronics and Nanometer Structures--Processing, Measurement, and Phenomena* **2005,** *23* (6), 2694-2699; (m) Kaya, A.; Du, X.; Liu, Z.; Lu Jessica, W.; Morris John, R.; Glasser Wolfgang, G.; Heinze, T.; Esker Alan, R., Surface plasmon resonance studies of pullulan and pullulan cinnamate adsorption onto cellulose. *Biomacromolecules* **2009,** *10* (9), 2451-2459.

24. Vozzi, G.; Flaim, C.; Ahluwalia, A.; Bhatia, S., Fabrication of PLGA scaffolds using soft lithography and microsyringe deposition. *Biomaterials* **2003,** *24* (14), 2533-2540.

25. Moriguchi, I.; Maeda, H.; Teraoka, Y.; Kagawa, S., Preparation of TiO2 Ultrathin Film by Newly Developed Two-Dimensional Sol-Gel Process. *Journal of the American Chemical Society* **1995,** *117* (3), 1139-1140.

26. White, M., Coating Technology Handbook; CRC Press: Boca Raton. **2006**.

27. Miller, C.; Shanks, H.; Witt, A.; Rutkowski, G.; Mallapragada, S., Oriented Schwann cell growth on micropatterned biodegradable polymer substrates. *Biomaterials* **2001,** *22* (11), 1263-1269.

28. Halperin, A.; Tirrell, M.; Lodge, T. P., Tethered chains in polymer microstructures. *Advances in Polymer Science* **1992,** *100* (Macromol.: Synth., Order Adv. Prop.), 31-71.

29. (a) Trankhtenberg, S., Organized organic thin films: structure, phase transitions and chemical reactions. *Thin Films and Nanostructures* **2007,** *34* (Physico-Chemical Phenomena in Thin Films and at Solid Surfaces), 639-664; (b) Coffee, S. S.; Winkenwarder, W. A.; Stanley, S. K.; Davood, S.; Banerjee, S. K.; Ekerdt, J. G., Using Self-assembly and Selective Chemical Vapor Deposition for Precise Positioning of Individual Germanium Nanoparticles on Hafnia. *Materials Research Society Symposium Proceedings* **2006,** *921E* (Nanomanufacturing).

30. (a) Deng, J.; Farmer-Creely, C. E.; Viers, B. D.; Esker, A. R., Unique Rodlike Surface Morphologies in Trisilanolcyclohexyl Polyhedral Oligomeric Silsesquioxane Films. *Langmuir* **2004,** *20* (7), 2527-2530; (b) Deng, J.; Hottle, J. R.; Polidan, J. T.; Kim, H.-J.; Farmer-Creely, C. E.; Viers, B. D.; Esker, A. R., Polyhedral Oligomeric Silsesquioxane Amphiphiles: Isotherm and Brewster Angle Microscopy Studies of Trisilanolisobutyl-POSS at the Air/Water Interface. *Langmuir* **2004,** *20* (1), 109-115; (c) Deng, J.; Viers, B. D.; Esker, A. R.; Anseth, J. W.; Fuller, G. G., Phase Behavior and Viscoelastic Properties of Trisilanolcyclohexyl-POSS at the Air/Water Interface. *Langmuir* **2005,** *21* (6), 2375-2385; (d) Esker, A. R.; Gruell, H.; Wegner, G.; Satija, S. K.; Han, C. C., Isotopic selectivity in ultrathin Langmuir-Blodgett membranes of a crosslinked cellulose derivative. *Langmuir* **2001,** *17* (16), 4688-4692; (e) Esker, A. R.; Mengel, C.; Wegner, G., Ultrathin films of a polyelectrolyte with layered architecture. *Science (Washington, D. C.)* **1998,** *280* (5365), 892-895; (f) Ferguson-McPherson, M. K.; Low, E. R.; Esker, A. R.; Morris, J.

R., Sorption of Dimethyl Methylphosphonate within Langmuir-Blodgett Films of Trisilanolphenyl Polyhedral Oligomeric Silsesquioxane. *Journal of Physical Chemistry B* **2005,** *109* (40), 18914-18920; (g) Lee, W.; Ni, S.; Deng, J.; Kim, B.-S.; Satija, S. K.; Mather, P. T.; Esker, A. R., Telechelic Poly(ethylene glycol)-POSS Amphiphiles at the Air/Water Interface. *Macromolecules* **2007,** *40* (3), 682-688; (h) Li, B.; Esker, A. R., Molar Mass Dependent Growth of Poly(e-caprolactone) Crystals in Langmuir Films. *Langmuir* **2007,** *23* (5), 2546-2554; (i) Li, B.; Esker, A. R., Blends of Poly(e-caprolactone) and Intermediate Molar Mass Polystyrene as Langmuir Films at the Air/Water Interface. *Langmuir* **2007,** *23* (2), 574-581; (j) Li, B.; Marand, H.; Esker, A. R., Dendritic growth of poly(e-caprolactone) crystals from compatible blends with poly(t-butyl acrylate) at the air/water interface. *Journal of Polymer Science, Part B: Polymer Physics* **2007,** *45* (24), 3300-3318; (k) Li, B.; Wu, Y.; Liu, M.; Esker, A. R., Brewster Angle Microscopy Study of Poly(e-caprolactone) Crystal Growth in Langmuir Films at the Air/Water Interface. *Langmuir* **2006,** *22* (11), 4902-4905; (l) Mengel, C.; Esker, A. R.; Meyer, W. H.; Wegner, G., Preparation and Modification of Poly(methacrylic acid) and Poly(acrylic acid) Multilayers. *Langmuir* **2002,** *18* (16), 6365-6372; (m) Ni, S.; Lee, W.; Li, B.; Esker, A. R., Thermodynamics of the Liquid Expanded to Condensed Phase Transition of Poly(L-lactic acid) in Langmuir Monolayers. *Langmuir* **2006,** *22* (8), 3672-3677; (n) Ni, S.; Yin, W.; Ferguson-McPherson, M. K.; Satija, S. K.; Morris, J. R.; Esker, A. R., Nanoscale Surface Patterns from 103 Single Molecule Helices of Biodegradable Poly(L-lactic acid). *Langmuir* **2006,** *22* (14), 5969-5973; (o) Paul, R.; Karabiyik, U.; Swift, M. C.; Esker, A. R., Phase Separation in Poly(tert-butyl acrylate)/Polyhedral Oligomeric Silsesquioxane (POSS) Thin Film Blends. *Langmuir* **2008,** *24* (9), 5079-5090.

31. Swalen, J. D., Molecular films. *Annual Review of Materials Science* **1991,** *21*, 373-408.

32. Braslau, A.; Deutsch, M.; Pershan, P. S.; Weiss, A. H.; Als-Nielsen, J.; Bohr, J., Surface roughness of water measured by x-ray reflectivity. *Physical Review Letters* **1985,** *54* (2), 114-117.

33. Lopez-Montero, I.; Arriaga, L. R.; Monroy, F.; Rivas, G.; Tarazona, P.; Velez, M., High Fluidity and Soft Elasticity of the Inner Membrane of Escherichia coli Revealed by the Surface Rheology of Model Langmuir Monolayers. *Langmuir* **2008,** *24* (8), 4065-4076.

34. Hann, R. A., *Langmuir-Blodgett Films* (Gareth, R.), Plenum Press: New York. **1990**.

35. Tabor, D., Role of molecular forces in contact deformations. Reply to comments. *Journal of Colloid and Interface Science* **1980,** *73* (1), 294.

36. Franklin, B., *Phil. Trans. Res. Soc. (London)* **1774,** (64), 445.

37. Langmuir, I., Constitution and fundamental properties of solids and liquids. II. Liquids. *Journal of the American Chemical Society* **1917,** *39*, 1848-1906.

38. Langmuir, I., The mechanism of the surface phenomena of flotation. *Transactions of the Faraday Society* **1920,** *15* (Pt. 3), 62-74.

39. Blodgett, K. B.; Langmuir, I., Built-up films of barium stearate and their optical properties. *Physical Review* **1937,** *51*, 964-982.

40. (a) Pallas, N. R.; Pethica, B. A., Liquid-expanded to liquid-condensed transition in lipid monolayers at the air/water interface. *Langmuir* **1985,** *1* (4), 509-513; (b) Harkins, W. D.; Boyd, E., The states of monolayers. *Journal of Physical Chemistry* **1941,** *45*, 20-43; (c) Overbeck, G. A.; Hoenig, D.; Moebius, D., Visualization of first- and second-order phase transitions in eicosanol monolayers using Brewster angle microscopy. *Langmuir* **1993,** *9* (2), 555-560.

41. (a) Badis, M.; Van der Heyden, A.; Heck, R.; Marsura, A.; Gauthier-Manuel, B.; Zywocinski, A.; Rogalska, E., Formation of Langmuir Layers and Surface Modification Using

---

New Upper-Rim Fully Tethered Bipyridinyl or Bithiazolyl Cyclodextrins and Their Fluorescent Metal Complexes. *Langmuir* **2004,** *20* (13), 5338-5346; (b) Byrd, H.; Pike, J. K.; Talham, D. R., Single layers of inorganic extended lattices formed at Langmuir-Blodgett templates. *Thin Solid Films* **1994,** *242* (1-2), 100-5; (c) Chi, L. F.; Rakers, S.; Hartig, M.; Fuchs, H.; Schmid, G., Preparation and characterization of Langmuir monolayers and Langmuir-Blodgett films of nanosized Au55-clusters. *Thin Solid Films* **1998,** *327-329*, 520-523; (d) Clemente-Leon, M.; Coronado, E.; Lopez-Munoz, A.; Repetto, D.; Ito, T.; Konya, T.; Yamase, T.; Constable, E. C.; Housecroft, C. E.; Doyle, K.; Graber, S., Dual-Emissive Photoluminescent Langmuir-Blodgett Films of Decatungstoeuropate and an Amphiphilic Iridium Complex. *Langmuir* **2010,** *26* (2), 1316-1324; (e) Dhathathreyan, A., Dissociation constants of long-chain hydroxy fatty acids in Langmuir-Blodgett films. *Colloids and Surfaces, A: Physicochemical and Engineering Aspects* **2008,** *318* (1-3), 307-314; (f) Hirano, K.; Fukuda, H.; Kakimoto, M.-a., Monolayer Behavior of Poly(amic Acid) Alkylamine Salts Containing the Dimethylsiloxane Structure and Their Langmuir-Blodgett Films. *Langmuir* **1998,** *14* (8), 2134-2138; (g) Hsiao, F.-W.; Lee, Y.-L.; Chang, C.-H., On the characteristics of mixed Langmuir monolayer templates containing dipalmitoyl phosphatidylcholine for gold nanoparticle formation. *Colloids and Surfaces, B: Biointerfaces* **2009,** *73* (1), 110-115; (h) Kucuk, A. C.; Matsui, J.; Miyashita, T., Langmuir-Blodgett films composed of amphiphilic double-decker shaped polyhedral oligomeric silsesquioxanes. *Journal of Colloid and Interface Science* **2011,** *355* (1), 106-114; (i) Kumar, B.; Prajapati, A. K.; Varia, M. C.; Suresh, K. A., Novel Mesogenic Azobenzene Dimer at Air-Water and Air-Solid Interfaces. *Langmuir* **2009,** *25* (2), 839-844; (j) Liu, H.-G.; Feng, X.-S.; Xue, Q.-B.; Wang, L.; Yang, K.-Z., Central metal effect on the organization of porphyrin LB films. *Thin Solid Films* **1999,** *340* (1,2), 265-270; (k) Martin, S.; Cea, P.; Pera, G.; Haro, M.; Lopez, M. C.,

---

Pure and mixed films of a nitrostilbene derivative at the air-water interface, Langmuir-Blodgett multilayer fabrication, and optical characterization. *Journal of Colloid and Interface Science* **2007,** *308* (1), 239-248; (l) Reuter, S.; Hofmann, A. M.; Busse, K.; Frey, H.; Kressler, J., Langmuir and Langmuir-Blodgett Films of Multifunctional, Amphiphilic Polyethers with Cholesterol Moieties. *Langmuir* **2011,** *27* (5), 1978-1989; (m) Roldan-Carmona, C.; Gonzalez-Delgado, A. M.; Guerrero-Martinez, A.; De Cola, L.; Giner-Casares, J. J.; Perez-Morales, M.; Martin-Romero, M. T.; Camacho, L., Molecular organization and effective energy transfer in iridium metallosurfactant-porphyrin assemblies embedded in Langmuir-Schaefer films. *Physical Chemistry Chemical Physics* **2011,** *13* (7), 2834-2841; (n) Sankaranarayanan, K.; Dhathathreyan, A.; Miller, R., Assembling Fibrinogen at Air/Water and Solid/Liquid Interfaces Using Langmuir and Langmuir-Blodgett Films. *Journal of Physical Chemistry B* **2010,** *114* (24), 8067-8075; (o) Shen, Y.-J.; Lee, Y.-L.; Yang, Y.-M., Monolayer Behavior and Langmuir-Blodgett Manipulation of CdS Quantum Dots. *Journal of Physical Chemistry B* **2006,** *110* (19), 9556-9564; (p) Valkova, L. A.; Valli, L.; Casilli, S.; Giancane, G.; Borovkov, N. Y.; Sibrina, G. V.; Glibin, A. S.; Koifman, O. I.; Pisani, M.; Rustichelli, F., Nanoaggregates of Copper Porphyrazine in Floating Layers and Langmuir-Schaefer Films. *Langmuir* **2008,** *24* (9), 4857-4864; (q) Xu, M.; Sun, L.; Yin, S.; Liu, C.; Wu, L., Monolayer behavior of a pyridyl head-group-containing amphiphile and its miscibility with poly(D,L-lactide-co-glycolide) on different pH subphase. *Journal of Colloid and Interface Science* **2007,** *316* (2), 912-920; (r) Zhang, L.; Jiang, S.; Liu, M., Configuration and photochemical reaction of a bola-amphiphilic diacid with a diazo resin in monolayers and Langmuir-Blodgett films. *Journal of Colloid and Interface Science* **2003,** *261* (2), 417-422.

42. (a) Liu, L.; Hu, L.; Fu, H.; Fu, Q.-M.; Liu, S.-Z.; Du, Z.-L.; Wong, W.-Y.; Harvey, P. D., Preparation, luminescence and photoelectric properties of Langmuir-Blodgett films of

alkynylplatinum(II)-zinc(II) porphyrinate/heteropolyoxometalate hybrid composites. *Journal of Organometallic Chemistry* **2011,** *696* (6), 1319-1324; (b) Pan, X.; Jiang, H.; Wang, Y.; Lei, Z.; Zou, G.; Zhang, Q.; Wang, K., Supramolecular chirality formation of bisazobenzene-substituted polydiacetylene LB films. *Journal of Colloid and Interface Science* **2011,** *354* (2), 880-886; (c) Martin, M. G.; Rodriguez-Mendez, M. L.; de Saja, J. A., Films of lutetium bisphthalocyanine nanowires as electrochemical sensors. *Langmuir* **2010,** *26* (24), 19217-19224; (d) Sawant, S. N.; Kulshreshtha, S. K.; Yakhmi, J. V.; Doble, M.; Miyazaki, A.; Enoki, T., Langmuir-Blodgett films of ethylenedithiotetrathiafulvalene derivative containing hydroxyl groups. *Thin Solid Films* **2010,** *518* (20), 5820-5826; (e) Mattu, J. S.; Leach, G. W., Large Scale Crystallinity in Kinetically Stable Polythiophene-Based Langmuir-Blodgett Films. *Journal of the American Chemical Society* **2010,** *132* (9), 3204-3210; (f) Tatewaki, Y.; Okada, S.; Itagaki, R.; Nakamura, T.; Fujimori, A., Study of molecular arrangement of organized molecular films of charge-transfer complexes containing 1,3-dithiole-2-thione-4,5-dithiolate by in-plane and out-of-plane X-ray diffractions. *Journal of Colloid and Interface Science* **2010,** *343* (1), 281-290; (g) Liu, P. F.; Gemeiner, P.; Meng, X. J.; Chu, J. H.; Geiger, S.; Dkhil, B., The Debye-like relaxation mechanism in poly(vinylidene fluoride-trifluoroethylene) ferroelectric polymers. *Journal of Applied Physics* **2009,** *106* (10), 104113/1-104113/4; (h) Umemura, Y.; Shinohara, E.; Schoonheydt, R. A., Preparation of Langmuir-Blodgett films of aligned sepiolite fibers and orientation of methylene blue molecules adsorbed on the film. *Physical Chemistry Chemical Physics* **2009,** *11* (42), 9804-9810; (i) Liu, P. F.; Gemeiner, P.; Shen, H.; Meng, X. J.; Chu, J. H.; Geiger, S.; Guiblin, N.; Dkhil, B., Structural and dielectric properties of ferroelectric poly(vinylidene fluoride-trifluoroethylene) thin films with different bottom electrodes. *Journal of Applied Physics* **2009,** *106* (5), 054111/1-054111/4; (j) Ito, Y.; Virkar, A. A.; Mannsfeld, S.; Oh,

J. H.; Toney, M.; Locklin, J.; Bao, Z., Crystalline Ultrasmooth Self-Assembled Monolayers of Alkylsilanes for Organic Field-Effect Transistors. *Journal of the American Chemical Society* **2009,** *131* (26), 9396-9404; (k) Mai, L.; Gu, Y.; Han, C.; Hu, B.; Chen, W.; Zhang, P.; Xu, L.; Guo, W.; Dai, Y., Orientated Langmuir-Blodgett Assembly of VO2 Nanowires. *Nano Letters* **2009,** *9* (2), 826-830; (l) Choudhury, S.; Betty, C. A.; Girija, K. G., On the preparation of ultrathin tin dioxide by Langmuir-Blodgett films deposition. *Thin Solid Films* **2008,** *517* (2), 923-928; (m) Yan, B.; Xu, B., Molecular assembly and photophysical properties of Langmuir-Blodgett films with novel lanthanide complexes of long chain para-dodecanoyl and para-myristoyl oxybenzoate. *Applied Surface Science* **2008,** *254* (22), 7237-7242; (n) Lu, F.; Zhao, X.; Zhou, G.; Wang, H.-S.; Ozaki, Y., Control for oriented growth of large size KCl crystals by the competition between spontaneous and induced nucleation/growth on a Langmuir-Blodgett film. *Chemical Physics Letters* **2008,** *458* (1-3), 67-70; (o) Xu, M.; Li, Y.; Li, W.; Sun, C.; Wu, L., Structure, photochromic, and electrochemical properties of dioctadecylamine/H3PMo12O40 Langmuir-Blodgett film. *Journal of Colloid and Interface Science* **2007,** *315* (2), 753-760; (p) Yamamoto, T.; Einaga, Y., Photomagnetic hybrid ultrathin films. *Journal of Solid State Electrochemistry* **2006,** *11* (6), 781-790; (q) Liu, L.; Liu, Z.; Xu, W.; Xu, H.; Zhang, D.; Zhu, D., Special fluorescence enhancement and aggregation in Langmuir-Blodgett films of 4,4'-dicyano-(3,4-dibutyl-2-thienylethynyl)biphenyl. *Thin Solid Films* **2006,** *515* (4), 2596-2601; (r) Xu, Y.; Guo, J.; Long, C.; Li, Y.; Liu, Y.; Yao, Y.; Zhu, D., Formation and structural characteristics of Langmuir-Blodgett films of C60 and C70. *Thin Solid Films* **1994,** *242* (1-2), 45-9; (s) Durfee, W. S.; Storck, W.; Willig, F.; Von Frieling, M., Davydov splitting in 7-(2-anthryl)-1-heptanoic acid Langmuir-Blodgett films. *Journal of the American Chemical Society* **1987,** *109* (5), 1297-301; (t) Vincett, P. S.; Barlow, W. A., Highly organized aromatic molecular systems using Langmuir-

Blodgett films: structure, optical properties and probable epitaxy of anthracene-derivative multilayers. *Thin Solid Films* **1980,** *71* (2), 305-26; (u) Adler, G., Inhomogeneities in the structure of built-up monolayers of two porphyrin compounds. *Journal of Colloid and Interface Science* **1979,** *72* (1), 164-9; (v) Clint, J. H.; Walker, T., Interaction energies between layers of alkyl and partially fluorinated alkyl chains in Langmuir-Blodgett multilayers. *Journal of Colloid and Interface Science* **1974,** *47* (1), 172-85.

43. (a) Hassanzadeh, A.; Mittler, S., Waveguide evanescent field fluorescence microscopy: high contrast imaging of a domain forming mixed lipid Langmuir-Blodgett monolayer mimicking lung surfactant. *Journal of Biomedical Optics* **2011,** *16* (4), 046022/1-046022/4; (b) Rajesh, K.; Rajendra, K.; Radhakrishnan, T. P., Fluorescence Enhancement in Langmuir-Blodgett Films: Role of Amphiphile Structure, Orientation, and Assembly. *Journal of Physical Chemistry B* **2010,** *114* (2), 849-856; (c) Santos, T. C. F.; Peres, L. O.; Wang, S. H.; Oliveira, O. N., Jr.; Caseli, L., Mixing Alternating Copolymers Containing Fluorenyl Groups with Phospholipids to Obtain Langmuir and Langmuir-Blodgett Films. *Langmuir* **2010,** *26* (8), 5869-5875; (d) Qaqish, S. E.; Urquhart, S. G.; Lanke, U.; Brunet, S. M. K.; Paige, M. F., Phase Separation of Palmitic Acid and Perfluorooctadecanoic Acid in Mixed Langmuir-Blodgett Monolayer Films. *Langmuir* **2009,** *25* (13), 7401-7409; (e) Livanec, P. W.; Dunn, R. C., Single-Molecule Probes of Lipid Membrane Structure. *Langmuir* **2008,** *24* (24), 14066-14073; (f) Meli, M.-V.; Lin, I. H.; Abbott, N. L., Preparation of Microscopic and Planar Oil-Water Interfaces That Are Decorated with Prescribed Densities of Insoluble Amphiphiles. *Journal of the American Chemical Society* **2008,** *130* (13), 4326-4333; (g) Nag, K.; Fritzen-Garcia, M.; Devraj, R.; Panda, A. K., Interfacial Organizations of Gel Phospholipid and Cholesterol in Bovine Lung Surfactant Films. *Langmuir* **2007,** *23* (8), 4421-4431; (h) Sun, X.-L.; Biswas, N.; Kai, T.; Dai, Z.;

Dluhy, R. A.; Chaikof, E. L., Membrane-Mimetic Films of Asymmetric Phosphatidylcholine Lipid Bolaamphiphiles. *Langmuir* **2006,** *22* (3), 1201-1208; (i) Togashi, D. M.; Romao, R. I. S.; Goncalves da Silva, A. M.; Sobral, A. J. F. N.; Costa, S. M. B., Self-organization of a sulfonamido-porphyrin in Langmuir monolayers and Langmuir-Blodgett films. *Physical Chemistry Chemical Physics* **2005,** *7* (22), 3874-3883; (j) Bhaumik, A.; Ramakanth, M.; Brar, L. K.; Raychaudhuri, A. K.; Rondelez, F.; Chatterji, D., Formation of a DNA layer on Langmuir-Blodgett films and its enzymatic digestion. *Langmuir* **2004,** *20* (14), 5891-5896; (k) Baumgart, T.; Offenhaeusser, A., Polysaccharide-Supported Planar Bilayer Lipid Model Membranes. *Langmuir* **2003,** *19* (5), 1730-1737; (l) Chen, X.; Li, L.; Liu, M., Assembly and Characterization of Ternary SV-DNA-TMPyP Complex Langmuir-Blodgett Films. *Langmuir* **2002,** *18* (11), 4449-4454; (m) Messerschmidt, C.; Schulz, A.; Rabe, J. P.; Simon, A.; Marti, O.; Fuhrhop, J.-H., Formation of Stable Singularities in Mixed Monolayers of Porphyrins and Tetracosanoic Acid upon SFM Tapping. *Langmuir* **2000,** *16* (3), 1299-1305; (n) Laguitton-Pasquier, H.; Van der Auweraer, M.; De Schryver, F. C., Bidimensional distribution of a cyanine dye in Langmuir-Blodgett (LB) monolayers studied by time-resolved and spatially resolved fluorescence. *Langmuir* **1998,** *14* (18), 5172-5183; (o) Ram, M. K.; Mascetti, G.; Paddeu, S.; Maccioni, E.; Nicolini, C., Optical, structural and fluorescence microscopic studies on reduced form of polyaniline: the leucoemeraldine base. *Synthetic Metals* **1997,** *89* (1), 63-69; (p) Ariga, K.; Shin, J. S.; Kunitake, T., Interaction of lipid monolayers with aqueous neutral polymers and the consequent monolayer stabilization and improved Langmuir-Blodgett transfer. *Journal of Colloid and Interface Science* **1995,** *170* (2), 440-8; (q) Spratte, K.; Riegler, H., Steady State Morphology and Composition of Mixed Monomolecular Films (Langmuir Monolayers) at the Air/Water Interface in the Vicinity of the Three-Phase Line: Model Calculations and

Experiments. *Langmuir* **1994,** *10* (9), 3161-73; (r) Riegler, J. E.; LeGrange, J. D., Observation of a monolayer phase transition on the meniscus in a Langmuir-Blodgett transfer configuration. *Physical Review Letters* **1988,** *61* (21), 2492-5; (s) Loesche, M.; Rabe, J.; Fischer, A.; Rucha, B. U.; Knoll, W.; Moehwald, H., Microscopically observed preparation of Langmuir-Blodgett films. *Thin Solid Films* **1984,** *117* (4), 269-80.

44. (a) Abraham, N.; Dekany, I., Size-dependent photoluminescence properties of bare ZnO and polyethylene imine stabilized ZnO nanoparticles and their Langmuir-Blodgett films. *Colloids and Surfaces, A: Physicochemical and Engineering Aspects* **2010,** *364* (1-3), 26-33; (b) Aoki, Y.; Kato, K.; Shinbo, K.; Kaneko, F.; Wakamatsu, T., Evaluation of surface roughness of metal thin films and Langmuir-Blodgett ultrathin films from scattered light due to surface plasmon polariton. *Molecular Crystals and Liquid Crystals Science and Technology, Section A: Molecular Crystals and Liquid Crystals* **1999,** *327*, 127-130; (c) Aoki, Y.; Kato, K.; Shinbo, K.; Kanekob, F.; Wakamatsu, T., Scattered light due to excited surface plasmon in arachidic acid LB ultrathin films on silver thin films. *Thin Solid Films* **1998,** *327-329*, 360-363; (d) Cao, B. H.; Kim, M. W.; Peiffer, D. G., Interfacial Properties of Model Graft Copolymers. *Langmuir* **1995,** *11* (5), 1645-52; (e) Kato, K.; Terakado, M.; Shinbo, K.; Kaneko, F.; Wakamatsu, T., Emission from merocyanine Langmuir-Blodgett films utilizing surface plasmon excitation. *Thin Solid Films* **2001,** *393* (1,2), 97-102; (f) Kurihara, K.; Murase, Y., Polyelectrolyte brushes. *Handbook of Polyelectrolytes and Their Applications* **2002,** *1*, 207-221; (g) Leverette, C. L.; Dluhy, R. A., A Novel Fiber-Optic Interface for Unenhanced External Reflection Raman Spectroscopy of Supported Monolayers. *Langmuir* **2000,** *16* (8), 3977-3983; (h) Place, J. F.; Sutherland, R. M.; Daehne, C., Optoelectronic immunosensors: a review of optical immunoassay at continuous surfaces. *Biosensors* **1985,** *1* (4), 321-53; (i) Shinbo, K.; Honma, K.; Terakado, M.; Nakano, T.;

Kato, K.; Kaneko, F.; Wakamatsu, T., Scattered light and emission from Ag thin film and merocyanine Langmuir-Blodgett film on Ag thin film due to surface plasmon polariton excitation. *Studies in Interface Science* **2001,** *11* (Novel Methods to Study Interfacial Layers), 71-83; (j) Swalen, J. D., Optical properties of Langmuir-Blodgett films. *Journal of Molecular Electronics* **1986,** *2* (4), 155-81; (k) Yazdanian, M.; Yu, H.; Zografi, G.; Kim, M. W., Divalent cation-stearic acid monolayer interactions at the air/water interface. *Langmuir* **1992,** *8* (2), 630-6; (l) Zanoni, R.; Naselli, C.; Bell, J.; Stegeman, G.; Sprague, R.; Seaton, C.; Lindsay, S., Brillouin spectroscopy of Langmuir-Blodgett films. *Thin Solid Films* **1985,** *134* (1-3), 179-86.

45. (a) Luedtke, K.; Jordan, R.; Hommes, P.; Nuyken, O.; Naumann, C. A., Lipopolymers from new 2-substituted-2-oxazolines for artificial cell membrane constructs. *Macromolecular Bioscience* **2005,** *5* (5), 384-393; (b) Brooks, C. F.; Fuller, G. G.; Frank, C. W.; Robertson, C. R., An Interfacial Stress Rheometer To Study Rheological Transitions in Monolayers at the Air-Water Interface. *Langmuir* **1999,** *15* (7), 2450-2459; (c) Naumann, C. A.; Brooks, C. F.; Fuller, G. G.; Knoll, W.; Frank, C. W., Viscoelastic Properties of Lipopolymers at the Air-Water Interface: A Combined Interfacial Stress Rheometer and Film Balance Study. *Langmuir* **1999,** *15* (22), 7752-7761.

46. (a) Alliprandini-Filho, P.; da Silva, G. B.; Barbosa Neto, N. M.; Silva, R. A.; Marletta, A., Induced secondary structure in nanostructured films of poly(p-phenylene vinylene). *Journal of Nanoscience and Nanotechnology* **2009,** *9* (10), 5981-5989; (b) Chiarelli, P. A.; Liu, D.-G.; Watkins, E. B.; Trouw, F. R.; Majewski, J.; Casson, J. L.; Tang, Z.; Johal, M. S.; Robinson, J. M.; Wang, H.-L., Molecular order in Langmuir-Blodgett assembled films of an azobenzene amphiphile. *Thin Solid Films* **2009,** *517* (16), 4638-4643; (c) Habibi, Y.; Foulon, L.; Aguie-Beghin, V.; Molinari, M.; Douillard, R., Langmuir-Blodgett films of cellulose nanocrystals:

Preparation and characterization. *Journal of Colloid and Interface Science* **2007,** *316* (2), 388-397; (d) Ifuku, S.; Kamitakahara, H.; Takano, T.; Tsujii, Y.; Nakatsubo, F., Preparation and Characterization of 6-O-(4-stearyloxytrityl)Cellulose acetate Langmuir-Blodgett Films. *Cellulose (Dordrecht, Netherlands)* **2005,** *12* (4), 361-369; (e) Kang, S. T.; Ahn, H., Dicyanopyrazine-linked porphyrin Langmuir-Blodgett films. *Journal of Colloid and Interface Science* **2008,** *320* (2), 548-554; (f) Korlacki, R.; Johnson, J. T.; Kim, J.; Ducharme, S.; Thompson, D. W.; Fridkin, V. M.; Ge, Z.; Takacs, J. M., Oligo(vinylidene fluoride) Langmuir-Blodgett films studied by spectroscopic ellipsometry and the density functional theory. *Journal of Chemical Physics* **2008,** *129* (6), 064704/1-064704/4; (g) Kozma, P.; Fodor, B.; Deak, A.; Petrik, P., Optical Models for the Characterization of Silica Nanosphere Monolayers Prepared by the Langmuir-Blodgett Method Using Ellipsometry in the Quasistatic Regime. *Langmuir* **2010,** *26* (20), 16122-16128; (h) Martin, B.; Vizdrik, G.; Kliem, H., Influence of the relative humidity on the properties of ferroelectric poly(vinylidene fluoride-trifluoroethylene). *Journal of Applied Physics* **2009,** *105* (8), 084114/1-084114/7; (i) Mattu, J.; Johansson, T.; Holdcroft, S.; Leach, G. W., Highly Ordered Polymer Films of Amphiphilic, Regioregular Polythiophene Derivatives. *Journal of Physical Chemistry B* **2006,** *110* (31), 15328-15337; (j) Nagy, N.; Deak, A.; Horvoelgyi, Z.; Fried, M.; Agod, A.; Barsony, I., Ellipsometry of Silica Nanoparticulate Langmuir-Blodgett Films for the Verification of the Validity of Effective Medium Approximations. *Langmuir* **2006,** *22* (20), 8416-8423; (k) Seitz, P. C.; Reif, M.; Yoshikawa, K.; Jordan, R.; Tanaka, M., Dissipative Structure Formation in Lipid/Lipopolymer Monolayers. *Journal of Physical Chemistry B* **2011,** *115* (10), 2256-2263; (l) Vidawati, S.; Sitterberg, J.; Bakowsky, U.; Rothe, U., AFM and ellipsometric studies on LB films of natural asymmetric and symmetric bolaamphiphilic archaebacterial tetraether lipids on silicon wafers. *Colloids and*

Surfaces, B: Biointerfaces **2010,** *78* (2), 303-309; (m) Wang, C.; Ma, S.; Zeng, H.; Li, J.; Chen, L.; Wang, W.; Tian, H., Spectroscopic ellipsometry on a novel cyanine dyes in Langmuir-Blodgett multilayers. *Colloids and Surfaces, A: Physicochemical and Engineering Aspects* **2006,** *284+285*, 414-418; (n) Zeng, H.; Gao, F.; Ma, S., Spectroscopic ellipsometer studies on new cyanine dye in Langmuir-Blodgett films. *Colloids and Surfaces, A: Physicochemical and Engineering Aspects* **2008,** *321* (1-3), 2-6.

47. (a) Kaganer, V. M.; Mohwald, H.; Dutta, P., Structure and phase transitions in Langmuir monolayers. *Reviews of Modern Physics* **1999,** *71* (3), 779-819; (b) Broniatowski, M.; Sandez Macho, I.; Dynarowicz-Latka, P., Study of perfluorooctyl-n-alkanes monolayers at the air-water interface. *Thin Solid Films* **2005,** *493* (1-2), 249-257; (c) Takiue, T.; Vollhardt, D., Miscibility of alkanol and fluoroalkanol in Langmuir film at the air/water interface. *Colloids and Surfaces, A: Physicochemical and Engineering Aspects* **2002,** *198-200*, 797-804; (d) Liu, Y., Synthesis and Characterization of Polyhedral Oligomeric Silsesquioxane (POSS) Based Amphiphiles, M.S. thesis, Virginia Polytechnic Institute and State Univeristy, Blacksburg, VA. **2010**.

48. (a) Sauer, B. B.; Yu, H., Adsorption kinetics of poly(ethylene oxide) at the air/water interface. *Macromolecules* **1989,** *22* (2), 786-791; (b) Shuler, R. L.; Zisman, W. A., Study of the behavior of polyoxyethylene at the air-water interface by wave damping and other methods. *Journal of Physical Chemistry* **1970,** *74* (7), 1523-1534; (c) Watanabe, M.; Kosaka, Y.; Oguchi, K.; Sanui, K.; Ogata, N., Regulation of supermolecular structure of amphiphilic polymers by means of the Langmuir-Blodgett technique. *Macromolecules* **1988,** *21* (10), 2997-3003; (d) Watanabe, M.; Kosaka, Y.; Sanui, K.; Ogata, N.; Oguchi, K.; Yoden, T., Stepwise deposition of oriented monolayer-polymer films by the Langmuir-Blodgett technique. *Macromolecules* **1987,** *20* (2), 452-454.

49. (a) Lee, W.-K.; Nowak, R. W.; Gardella, J. A., Jr., Hydrolytic Degradation of Polyester Blend Monolayers at the Air/Water Interface: Effects of a Slowly Degrading Component. *Langmuir* **2002,** *18* (6), 2309-2312; (b) Lee, W.-K.; Gardella, J. A., Jr., Hydrolytic Kinetics of Biodegradable Polyester Monolayers. *Langmuir* **2000,** *16* (7), 3401-3406; (c) Sugandhi, E. W.; Macri, R. V.; Williams, A. A.; Kite, B. L.; Slebodnick, C.; Falkinham, J. O., III; Esker, A. R.; Gandour, R. D., Synthesis, Critical Micelle Concentrations, and Antimycobacterial Properties of Homologous, Dendritic Amphiphiles. Probing Intrinsic Activity and the "Cutoff" Effect. *Journal of Medicinal Chemistry* **2007,** *50* (7), 1645-1650.

50. (a) Mann, E. K.; Henon, S.; Langevin, D.; Meunier, J., Molecular layers of a polymer at the free water surface: microscopy at the Brewster angle. *Journal de Physique II* **1992,** *2* (9), 1683-704; (b) Noll, W.; Steinbach, H.; Sucker, C., Monolayers of poly(organosiloxanes) on water. *Journal of Polymer Science, Polymer Symposia* **1971,** *No. 34*, 123-139; (c) Fox, H. W.; Taylor, P. W.; Zisman, W. A., Polyorganosiloxanes-surface-active properties. *Journal of Industrial and Engineering Chemistry (Washington, D. C.)* **1947,** *39*, 1401-1409; (d) Buzin, A. I.; Godovsky, Y. K.; Makarova, N. N.; Fang, J.; Wang, X.; Knobler, C. M., Stepwise Collapse of Monolayers of Cyclolinear Poly(organosiloxane)s at the Air/Water Interface: A Brewster-Angle Microscopy and Scanning Force Microscopy Study. *Journal of Physical Chemistry B* **1999,** *103* (51), 11372-11381; (e) Fang, J.; Dennin, M.; Knobler, C. M.; Godovsky, Y. K.; Makarova, N. N.; Yokoyama, H., Structures of Collapsed Polysiloxane Monolayers Investigated by Scanning Force Microscopy. *Journal of Physical Chemistry B* **1997,** *101* (16), 3147-3154.

51. (a) Williams, A. A.; Day, B. S.; Kite, B. L.; McPherson, M. K.; Slebodnick, C.; Morris, J. R.; Gandour, R. D., Homologous, long-chain alkyl dendrons form homologous thin films on silver oxide surfaces. *Chemical Communications (Cambridge, United Kingdom)* **2005,** (40),

5053-5055; (b) Gabrielli, G.; Maddii, A., Mixtures of poly(methyl methacrylate) and carboxylic acids in monolayers. *Journal of Colloid and Interface Science* **1978,** *64* (1), 19-27.

52. (a) Grimalt, J. O.; Yruela, I.; Saiz-Jimenez, C.; Toja, J.; De Leeuw, J. W.; Albaiges, J., Sedimentary lipid biogeochemistry of an hypereutrophic alkaline lagoon. *Geochimica et Cosmochimica Acta* **1991,** *55* (9), 2555-2577; (b) Ligon, W. V., Jr.; Valenty, S. J., Analysis of monolayer films at the air-water interface by field desorption mass spectrometry. *Journal of the American Chemical Society* **1979,** *101* (6), 1612-1614; (c) Rogge, W. F.; Hildemann, L. M.; Mazurek, M. A.; Cass, G. R.; Simoneit, B. R. T., Sources of fine organic aerosol. 1. Charbroilers and meat cooking operations. *Environmental Science and Technology* **1991,** *25* (6), 1112-1125.

53. (a) Agarwal, M. K.; Neter, E., Effect of selected lipids and surfactants on immunogenicity of several bacterial antigens. *Journal of Immunology* **1971,** *107* (5), 1448-1456; (b) Joos, P., Clausius-Clapeyron equation in monolayers. II. Experimental evidence. *Bulletin des Societes Chimiques Belges* **1970,** *79* (11-12), 655-63; (c) Muramatsu, M.; Ohno, T., Radiotracer study on hydrolysis of methyl-14C palmitate in insoluble monolayers. *Journal of Colloid and Interface Science* **1971,** *35* (3), 469-474; (d) Pollack, J. D.; Tourtellotte, M. E., Synthesis of saturated long chain fatty acids from sodium acetate-1-C14 by Mycoplasma. *Journal of bacteriology* **1967,** *93* (2), 636-641; (e) Spector, A. A.; John, K.; Fletcher, J. E., Binding of long-chain fatty acids to bovine serum albumin. *Journal of lipid research* **1969,** *10* (1), 56-67.

54. (a) Chowdhry, B. Z.; Lipka, G.; Dalziel, A. W.; Sturtevant, J. M., Multicomponent phase transitions of diacylphosphatidylethanolamine dispersions. *Biophysical Journal* **1984,** *45* (5), 901-904; (b) Gagne, J.; Stamatatos, L.; Diacovo, T.; Hui, S. W.; Yeagle, P. L.; Silvius, J. R., Physical properties and surface interactions of bilayer membranes containing N-methylated phosphatidylethanolamines. *Biochemistry* **1985,** *24* (16), 4400-4408; (c) Kamlekar, R. K.;

Satyanarayana, S.; Marsh, D.; Swamy, M. J., Miscibility and phase behavior of N-acylethanolamine/diacylphosphatidylethanolamine binary mixtures of matched acyl chainlengths (n = 14, 16). *Biophysical Journal* **2007,** *92* (11), 3968-3977; (d) Kleinschmidt, J. H.; Tamm, L. K., Structural transitions in short-chain lipid assemblies studied by 31P-NMR spectroscopy. *Biophysical Journal* **2002,** *83* (2), 994-1003; (e) Lohner, K.; Balgavy, P.; Hermetter, A.; Paltauf, F.; Laggner, P., Stabilization of non-bilayer structures by the etherlipid ethanolamine plasmalogen. *Biochimica et Biophysica Acta, Biomembranes* **1991,** *1061* (2), 132-140; (f) Pascher, I.; Sundell, S.; Hauser, H., Polar group interaction and molecular packing of membrane lipids. The crystal structure of lysophosphatidylethanolamine. *Journal of Molecular Biology* **1981,** *153* (3), 807-824.

55. (a) Hauser, H.; Guyer, W.; Pascher, I.; Skrabal, P.; Sundell, S., Polar group conformation of phosphatidylcholine. Effect of solvent and aggregation. *Biochemistry* **1980,** *19* (2), 366-373; (b) Hauser, H.; Pascher, I.; Sundell, S., Conformation of phospholipids. Crystal structure of a lysophosphatidylcholine analog. *Journal of Molecular Biology* **1980,** *137* (3), 249-264; (c) Smaby, J. M.; Hermetter, A.; Schmid, P. C.; Paltauf, F.; Brockman, H. L., Packing of ether and ester phospholipids in monolayers. Evidence for hydrogen-bonded water at the sn-1 acyl group of phosphatidylcholines. *Biochemistry* **1983,** *22* (25), 5808-5813; (d) Yokoyama, Y.; Negishi, L.; Kitoh, T.; Sonoyama, M.; Asami, Y.; Mitaku, S., Effect of Lipid Phase Transition on Molecular Assembly and Structural Stability of Bacteriorhodopsin Reconstituted into Phosphatidylcholine Liposomes with Different Acyl-Chain Lengths. *Journal of Physical Chemistry B* **2010,** *114* (47), 15706-15711.

56. (a) Bruening, M. L.; Zhou, Y.; Aguilar, G.; Agee, R.; Bergbreiter, D. E.; Crooks, R. M., Synthesis and Characterization of Surface-Grafted, Hyperbranched Polymer Films Containing

Fluorescent, Hydrophobic, Ion-Binding, Biocompatible, and Electroactive Groups. *Langmuir* **1997,** *13* (4), 770-778; (b) Joncheray, T. J.; Bernard, S. A.; Matmour, R.; Lepoittevin, B.; El-Khouri, R. J.; Taton, D.; Gnanou, Y.; Duran, R. S., Polystyrene-b-Poly(tert-butyl acrylate) and Polystyrene-b-Poly(acrylic acid) Dendrimer-Like Copolymers: Two-Dimensional Self-Assembly at the Air-Water Interface. *Langmuir* **2007,** *23* (5), 2531-2538; (c) Li, B.; Marand, H.; Esker, A. R., Dendritic growth of poly(ε-caprolactone) crystals from compatible blends with poly(t-butyl acrylate) at the air/water interface. *Journal of Polymer Science, Part B: Polymer Physics* **2007,** *45* (24), 3300-3318; (d) Mudgil, P.; Dennis, G. R.; Millar, T. J., Interactions of Poly(tert-butyl acrylate)-Poly(styrene) Diblock Copolymers with Lipids at the Air-Water Interface. *Langmuir* **2006,** *22* (18), 7672-7677.

57. (a) Chaudhury, M. K.; Owen, M. J., Adhesion hysteresis and friction. *Langmuir* **1993,** *9* (1), 29-31; (b) Chaudhury, M. K.; Whitesides, G. M., Correlation between surface free energy and surface constitution. *Science (New York, N.Y.)* **1992,** *255* (5049), 1230-1232; (c) Ferguson, G. S.; Chaudhury, M. K.; Biebuyck, H. A.; Whitesides, G. M., Monolayers on disordered substrates: self-assembly of alkyltrichlorosilanes on surface-modified polyethylene and poly(dimethylsiloxane). *Macromolecules* **1993,** *26* (22), 5870-5875; (d) Mann, E. K.; Langevin, D., Poly(dimethylsiloxane) molecular layers at the surface of water and of aqueous surfactant solutions. *Langmuir* **1991,** *7* (6), 1112-1117; (e) Runge, F. E.; Yu, H., Thin films of a binary polymer system: poly(vinyl acetate)/poly(dimethylsiloxane) layers at the air/water interface. *Langmuir* **1993,** *9* (11), 3191-3199.

58. (a) Esker, A. R.; Zhang, L. H.; Sauer, B. B.; Lee, W.; Yu, H., Dilational viscoelastic behaviors of homopolymer monolayers: surface light scattering analysis. *Colloids and Surfaces, A: Physicochemical and Engineering Aspects* **2000,** *171* (1-3), 131-148; (b) Kawaguchi, M.;

Tohyama, M.; Mutoh, Y.; Takahashi, A., Ellipsometric study of polymer monolayers spread at the air-water interface. 1. Thickness of monolayers. *Langmuir* **1988,** *4* (2), 407-410; (c) Kawaguchi, M.; Tohyama, M.; Takahashi, A., Ellipsometric study of polymer monolayers spread at the air-water interface. 2. Adsorbed amount of polymers. *Langmuir* **1988,** *4* (2), 411-413.

59. (a) Kawaguchi, M.; Yamamoto, M.; Kato, T., Mixed monolayers of lipid and polymer spread at the air-water interface. *Langmuir* **1997,** *13* (8), 2414-2416; (b) Monroy, F.; Esquinas, M. J.; Ortega, F.; Rubio, R. G., Monolayers of hydrogen-bonded polymer blends at the air-water interface. Poly(vinyl acetate) and poly(4-hydroxystyrene). *Colloid and Polymer Science* **1998,** *276* (11), 960-967; (c) Monroy, F.; Rivillon, S.; Ortega, F.; Rubio, R. G., Dilational rheology of Langmuir polymer monolayers: Poor-solvent conditions. *Journal of Chemical Physics* **2001,** *115* (1), 530-539.

60. www.chem1.com/acad/webtext/states/liquids.html.

61. Petty, M. C., *Langmuir-Blodgett Films; Cambridge University Press* **1996**.

62. Peterson, I. R., Langmuir-Blodgett films. *Journal of Physics D: Applied Physics* **1990,** *23* (4), 379-395.

63. (a) Galletti, G. S.; Guiseppi-Elie, A., Vinyl stearate monolayers for Langmuir-Blodgett film applications. *Thin Solid Films* **1985,** *132*, 163-172; (b) Lloyd, J. P.; Petty, M. C.; Roberts, G. G.; Lecomber, P. G.; Spear, W. E., Amorphous silicon/Langmuir-Blodgett film field effect transistor. *Thin Solid Films* **1983,** *99* (1-3), 297-304.

64. Dynarowicz-Latka, P.; Dhanabalan, A.; Oliveira, O. N., Modern physicochemical research on Langmuir monolayers. *Advances in Colloid and Interface Science* **2001,** *91* (2), 221-293.

65. (a) Young, T., *Phil. Trans. Roy. Soc. London* **1805,** *95*, 65; (b) de Laplace, P. S., *Mecanique Celeste, suppl. au X. Livre, Crouier, Paris* **1805**.

66. www.people.eku.edu/ritchisong/554notes1.html.

67. Knobler, C. M., Seeing phenomena in flatland: studies of monolayers by fluorescence microscopy. *Science (Washington, DC, United States)* **1990,** *249* (4971), 870-874.

68. Kaganer, V. M.; Peterson, I. R.; Kenn, R. M.; Shih, M. C.; Durbin, M.; Dutta, P., Tilted phases of fatty acid monolayers. *Journal of Chemical Physics* **1995,** *102* (23), 9412-9422.

69. Stine, K. J.; Stratmann, D. T., Fluorescence microscopy study of Langmuir monolayers of stearylamine. *Langmuir* **1992,** *8* (10), 2509-14.

70. Werkman, P. J.; Wilms, H.; Wieringa, R. H.; Schouten, A. J., Formation of mono- and multilayers of metal complexes of 4-(((10,12-pentacosadiynoyl)oxy)methyl)pyridine. *Thin Solid Films* **1998,** *325* (1,2), 238-245.

71. Fu, J. A.; Cheng, Q.; Stevens, R., Epi-fluorescence microscopic and monolayer studies of four amino acid functionalized diacetylene lipids. *Berkeley Sci.* **1998,** *2* (2), 99-103.

72. Wang, R.; Parikh, A. N.; Beers, J. D.; Shreve, A. P.; Swanson, B., Nonequilibrium Pattern Formation in Langmuir-Phase Assisted Assembly of Alkylsiloxane Monolayers. *Journal of Physical Chemistry B* **1999,** *103* (46), 10149-10157.

73. Zhai, X.; Brezesinski, G.; Moehwald, H.; Li, J., Thermodynamics and Structures of Amide Phospholipid Monolayers. *Journal of Physical Chemistry B* **2004,** *108* (35), 13475-13480.

74. Ni, S.; Satija, S. K.; Esker, A. R., Surface patterns of poly(L-lactic acid) 103 helices at the air/water interface and on solid substrates. *PMSE Preprints* **2005,** *93*, 436-437.

75. Yue, X.; Dobner, B.; Iimura, K.; Kato, T.; Moehwald, H.; Brezesinski, G., Weak First-Order Tilting Transition in Monolayers of Mono- and Bipolar Docosanol Derivatives. *Journal of Physical Chemistry B* **2006,** *110* (44), 22237-22244.

76. Kaganer, V. M.; Loginov, E. B., Symmetry and phase transitions in Langmuir monolayers: The Landau theory. *Physical Review E: Statistical Physics, Plasmas, Fluids, and Related Interdisciplinary Topics* **1995,** *51* (3-A), 2237-49.

77. (a) Miller, A.; Moehwald, H., Diffusion limited growth of crystalline domains in phospholipid monolayers. *Journal of Chemical Physics* **1987,** *86* (7), 4258-65; (b) Suresh, K. A.; Nittmann, J.; Rondelez, F., Pattern formation during phase transition in Langmuir monolayers near critical temperature. *Europhys. Lett.* **1988,** *6* (5), 437-43; (c) Hossain, M. M.; Kato, T., Line tension induced instability of condensed domains formed in adsorbed monolayers at the air-water interface. *Langmuir* **2000,** *16* (26), 10175-10183.

78. Fox, H. W.; Zisman, W. A., Some advances in techniques for the study of adsorbed monolayers at the liquid-air interface. *Review of Scientific Instruments* **1948,** *19*, 274-283.

79. Honig, E. P., Molecular constitution of X- and Y-type Langmuir-Blodgett films. *Journal of Colloid and Interface Science* **1973,** *43* (1), 66-72.

80. Holley, C.; Bernstein, S., Grating space of barium copper stearate films. *Physical Review* **1937,** *52*, 525-530.

81. (a) Hoenig, D.; Moebius, D., Direct visualization of monolayers at the air-water interface by Brewster angle microscopy. *Journal of Physical Chemistry* **1991,** *95* (12), 4590-4592; (b) Henon, S.; Meunier, J., Microscope at the Brewster angle: direct observation of first-order phase transitions in monolayers. *Review of Scientific Instruments* **1991,** *62* (4), 936-939; (c) Siegel, S.;

Hoenig, D.; Vollhardt, D.; Moebius, D., Direct observation of three-dimensional transformation of insoluble monolayers. *Journal of Physical Chemistry* **1992,** *96* (20), 8157-8160.

82. Derude, *Annual Review of Physical Chemistry* **1891,** *43*, 126.

83. (a) Li, B.; Wu, Y.; Liu, M.; Esker Alan, R., Brewster angle microscopy study of poly(epsilon-caprolactone) crystal growth in Langmuir films at the air/water interface. *Langmuir : the ACS journal of surfaces and colloids* **2006,** *22* (11), 4902-4905; (b) Deng, J.; Polidan, J. T.; Hottle, J. R.; Farmer-Creely, C. E.; Viers, B. D.; Esker, A. R., Polyhedral Oligomeric Silsesquioxanes: A New Class of Amphiphiles at the Air/Water Interface. *Journal of the American Chemical Society* **2002,** *124* (51), 15194-15195; (c) Deng, J.; Farmer-Creely Catherine, E.; Viers Brent, D.; Esker Alan, R., Unique rodlike surface morphologies in trisilanolcyclohexyl polyhedral oligomeric silsesquioxane films. *Langmuir* **2004,** *20* (7), 2527-2530.

84. (a) Stallberg-Stenhagen, S. S., E., *Nature (London, United Kingdom)* **1945,** *156*, 239; (b) Stenhagen, E., Surface films. *Determination of Organic Structures by Physical Methods* **1955**, 325-371.

85. Deng, J., Interfacial characterization of polyhedral oligomeric silsesquioxane (POSS) amphiphiles and polymer blends: thermodynamics, morphology, and rheology, Ph. D. thesis, Virginia Polytechnic Institute and State Univeristy, Blacksburg, VA. **2005**.

86. (a) Riviere, S.; Henon, S.; Meunier, J.; Schwartz, D. K.; Tsao, M. W.; Knobler, C. M., Textures and phase transitions in Langmuir monolayers of fatty acids. A comparative Brewster angle microscope and polarized fluorescence microscope study. *Journal of Chemical Physics* **1994,** *101* (11), 10045-10051; (b) Bibo, A. M.; Knobler, C. M.; Peterson, I. R., A monolayer phase miscibility comparison of long-chain fatty acids and their ethyl esters. *Journal of Physical Chemistry* **1991,** *95* (14), 5591-5599; (c) Overbeck, G. A.; Moebius, D., A new phase in the

generalized phase diagram of monolayer films of long-chain fatty acids. *Journal of Physical Chemistry* **1993,** *97* (30), 7999-8004; (d) Swalen, J. D.; Allara, D. L.; Andrade, J. D.; Chandross, E. A.; Garoff, S.; Israelachvili, J.; McCarthy, T. J.; Murray, R.; Pease, R. F.; et al., Molecular monolayers and films. A panel report for the Materials Sciences Division of the Department of Energy. *Langmuir* **1987,** *3* (6), 932-950.

87. (a) Peterson, I. R.; Brzezinski, V.; Kenn, R. M.; Steitz, R., Equivalent states of amphiphilic lamellae. *Langmuir* **1992,** *8* (12), 2995-3002; (b) Kaganer, V. M.; Indenbom, V. L., Symmetry, structural phase transitions and phase diagram of Langmuir monolayers. *Journal de Physique II* **1993,** *3* (6), 813-827; (c) Overbeck, G. A.; Hoenig, D.; Moebius, D., Long-range order and textures in lipid monolayers. *Biosensors & Bioelectronics* **1995,** *10* (1/2), 99-103.

88. (a) Pielichowski, K.; Njuguna, J.; Janowski, B.; Pielichowski, J., Polyhedral oligomeric silsesquioxanes (POSS)-containing nanohybrid polymers. *Advances in Polymer Science* **2006,** *201* (Supramolecular Polymers, Polymeric Betains, Oligomers), 225-296; (b) Hacker, N. P., *MRS Bulletin* **1997,** *22*, 33; (c) Laine, R. M.; Zhang, C.; Sellinger, A.; Viculis, L., Polyfunctional cubic silsesquioxanes as building blocks for organic/inorganic hybrids. *Applied Organometallic Chemistry* **1998,** *12* (10/11), 715-723; (d) Laine, R. M., Nanobuilding blocks based on the [OSiO1.5]x (x = 6, 8, 10) octasilsesquioxanes. *Journal of Materials Chemistry* **2005,** *15* (35-36), 3725-3744; (e) Provatas, A.; Matisons, J. G., Silsesquioxanes: synthesis and applications. *Trends in Polymer Science (Cambridge, United Kingdom)* **1997,** *5* (10), 327-332; (f) Voronkov, M. G.; Lavrent'yev, V. I., Polyhedral oligosilsesquioxanes and their homo derivatives. *Topics in Current Chemistry* **1982,** *102*, 199-236; (g) Iacono, S. T.; Budy, S. M.; Mabry, J. M.; Smith, D. W., Jr., Synthesis, Characterization, and Surface Morphology of Pendant Polyhedral Oligomeric

Silsesquioxane Perfluorocyclobutyl Aryl Ether Copolymers. *Macromolecules (Washington, DC, United States)* **2007,** *40* (26), 9517-9522.

89. Harrison, P. G., Silicate cages: precursors to new materials. *Journal of Organometallic Chemistry* **1997,** *542* (2), 141-183.

90. (a) Feher, F. J.; Budzichowski, T. A., Silasesquioxanes as ligands in inorganic and organometallic chemistry. *Polyhedron* **1995,** *14* (22), 3239-3253; (b) Carniato, F.; Boccaleri, E.; Marchese, L., A versatile route to bifunctionalized silsesquioxane (POSS): synthesis and characterisation of Ti-containing aminopropylisobutyl-POSS. *Dalton transactions (Cambridge, England : 2003)* **2008,** (1), 36-39; (c) Mantz, R. A.; Jones, P. F.; Chaffee, K. P.; Lichtenhan, J. D.; Gilman, J. W.; Ismail, I. M. K.; Burmeister, M. J., Thermolysis of Polyhedral Oligomeric Silsesquioxane (POSS) Macromers and POSS-Siloxane Copolymers. *Chemistry of Materials* **1996,** *8* (6), 1250-1259.

91. (a) Sprung, M. M.; Guenther, F. O., The partial hydrolysis of methyltriethoxysilane. *Journal of the American Chemical Society* **1955,** *77*, 3990-3996; (b) Barry, A. J.; Daudt, W. H.; Domicone, J. J.; Gilkey, J. W., Crystalline organosilsesquioxanes. *Journal of the American Chemical Society* **1955,** *77*, 4248-4252; (c) Vogt, L. H., Jr.; Brown, J. F., Jr., Crystalline methylsilsesquioxanes. *Inorganic Chemistry (Washington, DC, United States)* **1963,** *2*, 189-192.

92. Feher, F. J.; Budzichowski, T. A.; Blanski, R. L.; Weller, K. J.; Ziller, J. W., Facile syntheses of new incompletely condensed polyhedral oligosilsesquioxanes: [(c-C5H9)7Si7O9(OH)3], [(c-C7H13)7Si7O9(OH)3], and [(c-C7H13)6Si6O7(OH)4]. *Organometallics* **1991,** *10* (7), 2526-2528.

93. (a) Feher, F. J.; Soulivong, D.; Lewis, G. T., Facile Framework Cleavage Reactions of a Completely Condensed Silsesquioxane Framework. *Journal of the American Chemical Society*

1997, *119* (46), 11323-11324; (b) Feher, F. J.; Nguyen, F.; Soulivong, D.; Ziller, J. W., A new route to incompletely condensed silsesquioxanes: acid-mediated cleavage and rearrangement of (c-C6H11)6Si6O9 to C2-[(c-C6H11)6Si6O8X2]. *Chemical Communications (Cambridge)* **1999,** (17), 1705-1706; (c) Feher, F. J.; Soulivong, D.; Nguyen, F., Practical methods for synthesizing four incompletely condensed silsesquioxanes from a single R8Si8O12 framework. *Chemical Communications (Cambridge)* **1998,** (12), 1279-1280.

94. Schwab, J. J.; Lichtenhan, J. D., Polyhedral oligomeric silsesquioxane (POSS)-based polymers. *Applied Organometallic Chemistry* **1998,** *12* (10/11), 707-713.

95. Lee, Y.-J.; Huang, J.-M.; Kuo, S.-W.; Chang, F.-C., Low-dielectric, nanoporous polyimide films prepared from PEO-POSS nanoparticles. *Polymer* **2005,** *46* (23), 10056-10065.

96. Yen, Y.-C.; Kuo, S.-W.; Huang, C.-F.; Chen, J.-K.; Chang, F.-C., Miscibility and Hydrogen-Bonding Behavior in Organic/Inorganic Polymer Hybrids Containing Octaphenol Polyhedral Oligomeric Silsesquioxane. *Journal of Physical Chemistry B* **2008,** *112* (35), 10821-10829.

97. (a) Iacona, S. T.; Budy, S. M.; Smith, R. C.; Neilson, A. R.; Ballato, J.; Smith, D. W., Step-Growth Polyaddition and Polycondensation Reactions of Aromatic Trifluorovinyl Ethers. *Abstracts, 42nd Western Regional Meeting of the American Chemical Society, Las Vegas, NV, United States, September 23-27* **2008**, WRM-176; (b) Pyun, J.; Miller, P. J.; Matyjaszewski, K.; Kickelbick, G.; Schwab, J.; Lichtenhan, J. D., Synthesis of organic/inorganic hybrid materials from polysiloxane precursors using atom-transfer radical polymerization. *Book of Abstracts, 218th ACS National Meeting, New Orleans, Aug. 22-26* **1999**, POLY-513; (c) Kolel-Veetil, M. K.; Keller, T. M. Polymers made from polyhedral oligomeric silsesquioxanes and diacetylene-containing compounds, acetylene compounds and crosslinked product. 2009-427084

2010267913, 20090421., 2010.

98. Choi, J.; Kim, S. G.; Laine, R. M., Organic/Inorganic Hybrid Epoxy Nanocomposites from Aminophenylsilsesquioxanes. *Macromolecules* **2004,** *37* (1), 99-109.

99. (a) Choi, J.; Tamaki, R.; Kim, S. G.; Laine, R. M., Organic/Inorganic Imide Nanocomposites from Aminophenylsilsesquioxanes. *Chemistry of Materials* **2003,** *15* (17), 3365-3375; (b) Tamaki, R.; Choi, J.; Laine, R. M., A Polyimide Nanocomposite from Octa(aminophenyl)silsesquioxane. *Chemistry of Materials* **2003,** *15* (3), 793-797.

100. (a) Kim, K.-M.; Chujo, Y., Synthesis and characterization of liquid-crystalline silsesquioxanes. *Polymer Bulletin (Berlin, Germany)* **2001,** *46* (1), 15-21; (b) Unno, M.; Suto, A.; Takada, K.; Matsumoto, H., Synthesis of ladder and cage silsesquioxanes from 1,2,3,4-tetrahydroxycyclotetrasiloxane. *Bulletin of the Chemical Society of Japan* **2000,** *73* (1), 215-220; (c) Cordes, D. B.; Lickiss, P. D.; Rataboul, F., Recent Developments in the Chemistry of Cubic Polyhedral Oligosilsesquioxanes. *Chem. Rev. (Washington, DC, U. S.)* **2010,** *110* (4), 2081-2173; (d) Lickiss, P. D.; Rataboul, F., Fully condensed polyhedral oligosilsesquioxanes (POSS): from synthesis to application. *Adv. Organomet. Chem.* **2008,** *57*, 1-116.

101. Shawn, P. H., Hybrid POSS-polymer technology for rocket & space application. *AFRL/PRSM - polymer working group propulsion sciences division* **1999**.

102. (a) Feher, F. J.; Phillips, S. H.; Ziller, J. W., Synthesis and structural characterization of a remarkably stable, anionic, incompletely condensed silsesquioxane framework. *Chemical Communications (Cambridge)* **1997,** (9), 829-830; (b) Feher, F. J.; Budzichowski, T. A.; Rahimian, K.; Ziller, J. W., Reactions of incompletely-condensed silsesquioxanes with pentamethylantimony: a new synthesis of metallasilsesquioxanes with important implications for the chemistry of silica surfaces. *Journal of the American Chemical Society* **1992,** *114* (10), 3859-

3866; (c) Feher, F. J.; Newman, D. A.; Walzer, J. F., Silsesquioxanes as models for silica surfaces. *Journal of the American Chemical Society* **1989,** *111* (5), 1741-1748.

103. Abbenhuis, H. C. L.; Krijnen, S.; van Santen, R. A., Modeling the active sites of heterogeneous titanium epoxidation catalysts using titanium silasesquioxanes: insight into specific factors that determine leaching in liquid-phase processes. *Chemical Communications (Cambridge)* **1997,** (3), 331-332.

104. Murugavel, R.; Chandrasekhar, V.; Roesky, H. W., Discrete Silanetriols: Building Blocks for Three-Dimensional Metallasiloxanes. *Accounts of Chemical Research* **1996,** *29* (4), 183-189.

105. Haddad, T. S.; Mather, P. T.; Jeon, H. G.; Chun, S. B.; Phillips, S. H., Hybrid inorganic/organic diblock copolymers - Nanostructure in polyhedral oligomeric silsesquioxane polynorbornenes. *Materials Research Society Symposium Proceedings* **2001,** *628* (Organic/Inorganic Hybrid Materials), CC2 6 1-CC2 6 7.

106. Knight, P. T.; Lee, K. M.; Chung, T.; Mather, P. T., PLGA-POSS End-Linked Networks with Tailored Degradation and Shape Memory Behavior. *Macromolecules (Washington, DC, United States)* **2009,** *42* (17), 6596-6605.

107. Lichtenhan, J. D.; Otonari, Y. A.; Carr, M. J., Linear Hybrid Polymer Building Blocks: Methacrylate-Functionalized Polyhedral Oligomeric Silsesquioxane Monomers and Polymers. *Macromolecules* **1995,** *28* (24), 8435-8347.

108. Tant, M. R.; Wilkes, G. L., Physical aging studies of styrene-butadiene and carbonate-siloxane block copolymers. *Polymer Engineering and Science* **1981,** *21* (6), 325-330.

109. Pyun, J.; Matyjaszewski, K.; Wu, J.; Kim, G.-M.; Chun, S. B.; Mather, P. T., ABA triblock copolymers containing polyhedral oligomeric silsesquioxane pendant groups: synthesis and unique properties. *Polymer* **2003,** *44* (9), 2739-2750.

110. Fu, B. X.; Hsiao, B. S.; Pagola, S.; Stephens, P.; White, H.; Rafailovich, M.; Sokolov, J.; Mather, P. T.; Jeon, H. G.; Phillips, S.; Lichtenhan, J.; Schwab, J., Structural development during deformation of polyurethane containing polyhedral oligomeric silsesquioxanes (POSS) molecules. *Polymer* **2000,** *42* (2), 599-611.

111. Karabiyik, U.; Paul, R.; Swift, M. C.; Esker, A. R., Nanofiller effects on glass transition temperatures of ultrathin polymer films and bulk blends. *PMSE Preprints* **2008,** *98*, 863-864.

112. Yin, W.; Huffer, S. M.; Deng, J.; Hottle, J. R.; Kim, H.-J.; Esker, A. R., Dilational viscoelastic behavior in two-dimensional polymer systems with nanofillers. *Polymer Preprints (American Chemical Society, Division of Polymer Chemistry)* **2007,** *48* (1), 674-675.

113. (a) Paul, R.; Karabiyik, U.; Swift, M. C.; Hottle, J. R.; Esker, A. R., Morphological Evolution in Dewetting Polystyrene/Polyhedral Oligomeric Silsesquioxane Thin Film Bilayers. *Langmuir* **2008,** *24* (9), 4676-4684; (b) Hosaka, N.; Otsuka, H.; Hino, M.; Takahara, A., Control of Dispersion State of Silsesquioxane Nanofillers for Stabilization of Polystyrene Thin Films. *Langmuir* **2008,** *24* (11), 5766-5772; (c) Mitsuishi, M.; Zhao, F.; Kim, Y.; Watanabe, A.; Miyashita, T., Preparation of Ultrathin Silsesquioxane Nanofilms via Polymer Langmuir-Blodgett Films. *Chemistry of Materials* **2008,** *20* (13), 4310-4316.

114. (a) Lorenz-Haas, C.; Muller-Buschbaum, P.; Kraus, J.; Bucknall, D. G.; Stamm, M., Nucleated dewetting of thin polymer films. *Applied Physics A: Materials Science & Processing* **2002,** *74* (Suppl., Pt. 1), S383-S385; (b) Xie, R.; Karim, A.; Douglas, J. F.; Han, C. C.; Weiss, R. A., Spinodal Dewetting of Thin Polymer Films. *Physical Review Letters* **1998,** *81* (6), 1251-1254; (c) Kumar, S.; Matar, O. K., Dewetting of thin liquid films near soft elastomeric layers. *Journal of Colloid and Interface Science* **2004,** *273* (2), 581-588.

115. Lee, A.; Lichtenhan, J. D., Viscoelastic Responses of Polyhedral Oligosilsesquioxane Reinforced Epoxy Systems. *Macromolecules* **1998,** *31* (15), 4970-4974.

116. Fu, B. X.; Namani, M.; Lee, A., Influence of phenyltrisilanol polyhedral silsesquioxane on properties of epoxy network glasses. *Polymer* **2003,** *44* (25), 7739-7747.

117. Williams, A. A.; Sugandhi, E. W.; Macri, R. V.; Falkinham, J. O., III; Gandour, R. D., Antimicrobial activity of long-chain, water-soluble, dendritic tricarboxylato amphiphiles. *J. Antimicrob. Chemother.* **2007,** *59* (3), 451-458.

118. (a) Kim, H.-J.; Deng, J.; Lalli, J. H.; Riffle, J. S.; Viers, B. D.; Esker, A. R., Blends of Amphiphilic Trisilanolisobutyl-POSS and Phosphine Oxide Substituted Poly(dimethylsiloxane) at the Air/Water Interface. *Langmuir* **2005,** *21* (5), 1908-1916; (b) Ferguson-McPherson, M. K.; Low, E. R.; Esker, A. R.; Morris, J. R., Sorption of Dimethyl Methylphosphonate within Langmuir-Blodgett Films of Trisilanolphenyl Polyhedral Oligomeric Silsesquioxane. *J. Phys. Chem. B* **2005,** *109* (40), 18914-18920; (c) Paul, R.; Swift, M. C.; Hottle, J. R.; Esker, A. R., Instability and dewetting of polystyrene/polyhedral oligomeric silsesquioxane (POSS) bilayer films. *PMSE Preprints* **2006,** *94*, 778-779; (d) Paul, R.; Esker Alan, R., Pattern formation in dewetting poly(tert-butyl acrylate)/polyhedral oligomeric silsesquioxane (POSS) bilayer films. *Langmuir : the ACS journal of surfaces and colloids* **2006,** *22* (16), 6734-6738; (e) Yin, W.; Deng, J.; Esker, A. R., Surface Rheology of Trisilanolisobutyl-POSS at the Air/Water Interface. *Langmuir* **2009,** *25* (13), 7181-7184.

119. jmg.centerblog.net/3455607-L-Atomium-Belgique.

120. (a) Basel, Y.; Hassner, A., Di-tert-butyl Dicarbonate and 4-(Dimethylamino)pyridine Revisited. Their Reactions with Amines and Alcohols. *Journal of Organic Chemistry* **2000,** *65* (20), 6368-6380; (b) Maisuria, B. B.; Actis, M. L.; Hardrict, S. N.; Falkinham, J. O., III; Cole, M.

F.; Cihlar, R. L.; Peters, S. M.; Macri, R. V.; Sugandhi, E. W.; Williams, A. A.; Poppe, M. A.; Esker, A. R.; Gandour, R. D., Comparing micellar, hemolytic, and antibacterial properties of di- and tricarboxyl dendritic amphiphiles. *Bioorganic & Medicinal Chemistry* **2011,** *19* (9), 2918-2926; (c) Newkome, G. R.; Weis, C. D.; Childs, B. J., Syntheses of 1 -> 3 branched isocyanate monomers for dendritic construction. *Designed Monomers and Polymers* **1998,** *1* (1), 3-14.

121. Ni, S., POLY(L-LACTIC ACID) LANGMUIR MONOLAYERS AT THE AIR/WATER INTERFACE AND LANGMUIR-BLODGETT FILMS ON SOLID SUBSTRATES: PHASE BEHAVIOR, SURFACE MORPHOLOGY, AND CRYSTALLINITY. *Ph. D. thesis at Virginia Tech* **2006**.

122. Scott, D. W., Thermal rearrangement of branched-chain methylpolysiloxanes. *Journal of the American Chemical Society* **1946,** *68*, 356-8.

123. (a) Filion Tera, M.; Xu, J.; Prasad Manju, L.; Song, J., In vivo tissue responses to thermal-responsive shape memory polymer nanocomposites. *Biomaterials* **2011,** *32* (4), 985-91; (b) Filion, T. M.; Xu, J.; Prasad, M. L.; Song, J., In vivo tissue responses to thermal-responsive shape memory polymer nanocomposites. *Biomaterials* **2010,** *32* (4), 985-991; (c) Jeon, H. G.; Mather, P. T.; Haddad, T. S., Shape memory and nanostructure in poly(norbornyl-POSS) copolymers. *Polymer International* **2000,** *49* (5), 453-457; (d) Joshi, M.; Butola, B. S., Polymeric nanocomposites-polyhedral oligomeric silsesquioxanes (POSS) as hybrid nanofiller. *Journal of Macromolecular Science, Polymer Reviews* **2004,** *C44* (4), 389-410; (e) Jung, Y. C.; So, H. H.; Cho, J. W., Water-responsive shape memory polyurethane block copolymer modified with polyhedral oligomeric silsesquioxane. *Journal of Macromolecular Science, Part B: Physics* **2006,** *45* (4), 453-461; (f) Madbouly, S. A.; Lendlein, A., Shape-memory polymer composites. *Advances in Polymer Science* **2010,** *226* (Shape-Memory Polymers), 41-95; (g) Mather, P. T.;

Jeon, H. G.; Haddad, T. S., Strain recovery in POSS hybrid thermoplastics. *Polymer Preprints (American Chemical Society, Division of Polymer Chemistry)* **2000,** *41* (1), 528-529; (h) Mya, K. Y.; Gose, H. B.; Pretsch, T.; Bothe, M.; He, C., Star-shaped POSS-polycaprolactone polyurethanes and their shape memory performance. *Journal of Materials Chemistry* **2011,** *21* (13), 4827-4836; (i) Xie, K.; Liu, X.; Zhang, Y., Modification of cellulose fabrics with reactive polyhedral oligomeric silsesquioxanes to improve their shape-memory performance. *Journal of Applied Polymer Science* **2010,** *118* (4), 1872-1877; (j) Knight, P. T.; Lee, K. M.; Qin, H.; Mather, P. T., Biodegradable Thermoplastic Polyurethanes Incorporating Polyhedral Oligosilsesquioxane. *Biomacromolecules* **2008,** *9* (9), 2458-2467.

124. (a) Deng, J.; Hottle John, R.; Polidan Joseph, T.; Kim, H.-J.; Farmer-Creely Catherine, E.; Viers Brent, D.; Esker Alan, R., Polyhedral oligomeric silsesquioxane amphiphiles: isotherm and brewster angle microscopy studies of trisilanolisobutyl-POSS at the air/water interface. *Langmuir* **2004,** *20* (1), 109-15; (b) Gao, Y.; He, C.; Huang, Y.; Qing, F.-L., Novel water and oil repellent POSS-based organic/inorganic nanomaterial: Preparation, characterization and application to cotton fabrics. *Polymer* **2010,** *51* (25), 5997-6004; (c) Hao, W.; Hu, J.; Chen, L.; Zhang, J.; Xing, L.; Yang, W., Isoconversional analysis of non-isothermal curing process of epoxy resin/epoxide polyhedral oligomeric silsesquioxane composites. *Polymer Testing* **2011,** *30* (4), 349-355; (d) Jerman, I.; Orel, B.; Surca Vuk, A.; Kozelj, M.; Kovac, J., A structural and corrosion study of triethoxysilyl and perfluorooctyl functionalized polyhedral silsesquioxane nanocomposite films on AA 2024 alloy. *Thin Solid Films* **2010,** *518* (10), 2710-2721; (e) Jia, P.; Argun, A. A.; Xu, J.; Xiong, S.; Ma, J.; Hammond, P. T.; Lu, X., Enhanced Electrochromic Switching in Multilayer Thin Films of Polyaniline-Tethered Silsesquioxane Nanocage. *Chemistry of Materials* **2009,** *21* (19), 4434-4441; (f) Jia, P.; Argun, A. A.; Xu, J.; Xiong, S.; Ma,

---

J.; Hammond, P. T.; Lu, X., High-Contrast Electrochromic Thin Films via Layer-by-Layer Assembly of Starlike and Sulfonated Polyaniline. *Chemistry of Materials* **2010,** *22* (22), 6085-6091; (g) Kang, J.-M.; Cho, H.-J.; Lee, J.; Lee, J.-I.; Lee, S.-K.; Cho, N.-S.; Hwang, D.-H.; Shim, H.-K., Highly Bright and Efficient Electroluminescence of New PPV Derivatives Containing Polyhedral Oligomeric Silsesquioxanes (POSSs) and Their Blends. *Macromolecules* **2006,** *39* (15), 4999-5008; (h) Lai, Y. S.; Tsai, C. W.; Yang, H. W.; Wang, G. P.; Wu, K. H., Structural and electrochemical properties of polyurethanes/polyhedral oligomeric silsesquioxanes (PU/POSS) hybrid coatings on aluminum alloys. *Materials Chemistry and Physics* **2009,** *117* (1), 91-98; (i) Majumdar, P.; He, J.; Lee, E.; Kallam, A.; Gubbins, N.; Stafslien, S. J.; Daniels, J.; Chisholm, B. J., Antimicrobial activity of polysiloxane coatings containing quaternary ammonium-functionalized polyhedral oligomeric silsesquioxane. *Journal of Coatings Technology and Research* **2010,** *7* (4), 455-467; (j) Majumdar, P.; Lee, E.; Gubbins, N.; Stafslien, S. J.; Daniels, J.; Thorson, C. J.; Chisholm, B. J., Synthesis and antimicrobial activity of quaternary ammonium-functionalized POSS (Q-POSS) and polysiloxane coatings containing Q-POSS. *Polymer* **2009,** *50* (5), 1124-1133; (k) Misra, R.; Cook, R. D.; Morgan, S. E., Nonwetting, nonrolling, stain resistant polyhedral oligomeric silsesquioxane coated textiles. *Journal of Applied Polymer Science* **2010,** *115* (4), 2322-2331; (l) Wanke, C. H.; Feijo, J. L.; Barbosa, L. G.; Campo, L. F.; Bof de Oliveira, R. V.; Horowitz, F., Tuning of polypropylene wettability by plasma and polyhedral oligomeric silsesquioxane modifications. *Polymer* **2011,** *52* (8), 1797-1802.

125. (a) Hao, N.; Boehning, M.; Schoenhals, A., Dielectric Properties of Nanocomposites Based on Polystyrene and Polyhedral Oligomeric Phenethyl-Silsesquioxanes. *Macromolecules (Washington, DC, United States)* **2007,** *40* (26), 9672-9679; (b) Lee, Y.-J.; Huang, J.-M.; Kuo,

---

S.-W.; Lu, J.-S.; Chang, F.-C., Polyimide and polyhedral oligomeric silsesquioxane nanocomposites for low-dielectric applications. *Polymer* **2005,** *46* (1), 173-181; (c) Leu, C.-M.; Chang, Y.-T.; Wei, K.-H., Polyimide-Side-Chain Tethered Polyhedral Oligomeric Silsesquioxane Nanocomposites for Low-Dielectric Film Applications. *Chemistry of Materials* **2003,** *15* (19), 3721-3727; (d) Liu, Y.-L.; Fangchiang, M.-H., Polyhedral oligomeric silsesquioxane nanocomposites exhibiting ultra-low dielectric constants through POSS orientation into lamellar structures. *Journal of Materials Chemistry* **2009,** *19* (22), 3643-3647; (e) Liu, Y.-L.; Liu, C.-S.; Chen, W.-H.; Chen, S.-Y.; Wang, K.-S.; Hwu, M.-J., Ultra-low-k thin films of polyhedral oligomeric silsesquioxane/epoxy nanocomposites via covalent layer-by-layer assembly. *Journal of Nanoscience and Nanotechnology* **2009,** *9* (3), 1839-1843; (f) Liu, Y.-L.; Liu, C.-S.; Cho, C.-I.; Hwu, M.-J., Polyhedral oligomeric silsesquioxane monolayer as a nanoporous interlayer for preparation of low-k dielectric films. *Nanotechnology* **2007,** *18* (22), 225701/1-225701/5; (g) Tseng, M.-C.; Liu, Y.-L., Preparation, morphology, and ultra-low dielectric constants of benzoxazine-based polymers/polyhedral oligomeric silsesquioxane (POSS) nanocomposites. *Polymer* **2010,** *51* (23), 5567-5575; (h) Vasilopoulou, M.; Tsevas, S.; Douvas, A. M.; Argitis, P.; Davazoglou, D.; Kouvatsos, D., Characterization of various low-k dielectrics for possible use in applications at temperatures below 160 DegC. *Journal of Physics: Conference Series* **2005,** *10*, 218-221; (i) Xiao, Y.; He, C.; Lu, X.; Zhang, X., Organic-inorganic hybrid nanoparticles with quantum confinement effect. *International Journal of Nanoscience* **2009,** *8* (1 & 2), 185-190; (j) Zhang, C.; Guang, S.; Zhu, X.; Xu, H.; Liu, X.; Jiang, M., Mechanism of Dielectric Constant Variation of POSS-Based Organic-Inorganic Molecular Hybrids. *Journal of Physical Chemistry C* **2010,** *114* (51), 22455-22461.

126. (a) Fabritz, S.; Heyl, D.; Bagutski, V.; Empting, M.; Rikowski, E.; Frauendorf, H.; Balog, I.; Fessner, W.-D.; Schneider, J. J.; Avrutina, O.; Kolmar, H., Towards click bioconjugations on cube-octameric silsesquioxane scaffolds. *Organic & Biomolecular Chemistry* **2010,** *8* (9), 2212-2218; (b) Garcia, R. A.; Van Grieken, R.; Iglesias, J.; Sherrington, D. C.; Gibson, C. L., Modification of chiral dimethyl tartrate through transesterification: Immobilization on POSS and enantioselectivity reversal in sharpless asymmetric epoxidation. *Chirality* **2010,** *22* (7), 675-683; (c) Garcia-Orozco, I.; Velilla, T.; Galland, G. B.; dos Santos, J. H. Z.; Williams, R. J. J.; Quijada, R., Metallocene supported on a polyhedral oligomeric silsesquioxane-modified silica: structural characterization and catalytic activity for ethylene polymerization. *Journal of Polymer Science, Part A: Polymer Chemistry* **2010,** *48* (24), 5938-5944; (d) Lin, Y.; Jin, J.; Song, M.; Shaw, S. J.; Stone, C. A., Curing dynamics and network formation of cyanate ester resin/polyhedral oligomeric silsesquioxane nanocomposites. *Polymer* **2011,** *52* (8), 1716-1724; (e) Lu, C.-H.; Chang, F.-C., Polyhedral oligomeric silsesquioxane-encapsulating amorphous palladium nanoclusters as catalysts for Heck reactions. *ACS Catalysis* **2011,** *1* (5), 481-488; (f) Sakugawa, S.; Wada, K.; Inoue, M., Ti-bridged silsesquioxanes as precursors of silica-supported titanium oxide catalysts for the epoxidation of cyclooctene. *Journal of Catalysis* **2010,** *275* (2), 280-287; (g) Teo, J. K. H.; Toh, C. L.; Lu, X., Catalytic and reinforcing effects of polyhedral oligomeric silsesquioxane (POSS)-imidazolium modified clay in an anhydride-cured epoxy. *Polymer* **2011,** *52* (9), 1975-1982; (h) Feher, F. J.; Newman, D. A.; Walzer, J. F., Silsesquioxanes as models for silica surfaces. *Journal of the American Chemical Society* **1989,** *111* (5), 1741-1748.

127. (a) Wang, X.; Ervithayasuporn, V.; Zhang, Y.; Kawakami, Y., Reversible self-assembly of dendrimer based on polyhedral oligomeric silsesquioxanes (POSS). *Chemical Communications (Cambridge, United Kingdom)* **2011,** *47* (4), 1282-1284; (b) Yuan, H.; Luo, K.;

Lai, Y.; Pu, Y.; He, B.; Wang, G.; Wu, Y.; Gu, Z., A Novel Poly(L-glutamic acid) Dendrimer Based Drug Delivery System with Both pH-Sensitive and Targeting Functions. *Molecular Pharmaceutics* **2010,** *7* (4), 953-962; (c) Xiao, Y.; Lu, X.; Tan, L.-W.; Ong, K. S.; He, C., Thermally stable red electroluminescent hybrid polymers derived from functionalized silsesquioxane and 4,7-bis(3-ethylhexyl-2-thienyl)-2,1,3-benzothiadiazole. *Journal of Polymer Science, Part A: Polymer Chemistry* **2009,** *47* (21), 5661-5670; (d) Somboonsub, B.; Thongyai, S.; Praserthdam, P., Dielectric properties and solubility of multilayer hyperbranched polyimide/polyhedral oligomeric silsesquioxane nanocomposites. *Journal of Applied Polymer Science* **2009,** *114* (5), 3292-3302; (e) Andre, P.; Cheng, G.; Ruseckas, A.; van Mourik, T.; Fruchtl, H.; Crayston, J. A.; Morris, R. E.; Cole-Hamilton, D.; Samuel, I. D. W., Hybrid Dendritic Molecules with Confined Chromophore Architecture to Tune Fluorescence Efficiency. *Journal of Physical Chemistry B* **2008,** *112* (51), 16382-16392; (f) Tanaka, K.; Inafuku, K.; Naka, K.; Chujo, Y., Enhancement of entrapping ability of dendrimers by a cubic silsesquioxane core. *Organic & Biomolecular Chemistry* **2008,** *6* (21), 3899-3901; (g) Chen, K.-B.; Chang, Y.-P.; Yang, S.-H.; Hsu, C.-S., Novel dendritic light-emitting materials containing polyhedral oligomeric silsesquioxanes core. *Thin Solid Films* **2006,** *514* (1-2), 103-109; (h) Ropartz, L.; Haxton, K. J.; Foster, D. F.; Morris, R. E.; Slawin, A. M. Z.; Cole-Hamilton, D. J., Phosphine containing dendrimers for highly regioselective rhodium catalysed hydroformylation of alkenes: a positive dendritic effect. *Journal of the Chemical Society, Dalton Transactions* **2002,** (23), 4323-4334; (i) Ropartz, L.; Morris, R. E.; Cole-Hamilton, D. J.; Foster, D. F., Increased selectivity in hydroformylation reactions using dendrimer based catalysts; a positive dendrimer effect. *Chemical Communications (Cambridge, United Kingdom)* **2001,** (4), 361-362; (j) Ropartz, L.; Morris, R. E.; Schwarz, G. P.; Foster, D. F.; Cole-Hamilton, D. J., Dendrimer-bound

tertiary phosphines for alkene hydroformylation. *Inorganic Chemistry Communications* **2000,** *3* (12), 714-717.

128. (a) Devaraju, S.; Vengatesan, M. R.; Alagar, M., Studies on thermal and dielectric properties of ether linked cyclohexyl diamine (ELCD)-based polyimide POSS nanocomposites (POSS-PI). *High Performance Polymers* **2011,** *23* (2), 99-111; (b) Feng, Y.; Jia, Y.; Guang, S.; Xu, H., Thermal enhancement mechanism of POSS-containing hybrid nanocomposites and relationship between thermal properties and their molecular structure. *Journal of Applied Polymer Science* **2010,** *115* (4), 2212-2220; (c) Hussain, H.; Tan, B. H.; Mya, K. Y.; Liu, Y.; He, C. B.; Davis, T. P., Synthesis, micelle formation, and bulk properties of poly(ethylene glycol)-b-poly(pentafluorostyrene)-g-polyhedral oligomeric silsesquioxane amphiphilic hybrid copolymers. *Journal of Polymer Science, Part A: Polymer Chemistry* **2010,** *48* (1), 152-163; (d) Jahren, S.; Maennle, F.; Graff, J. M.; Olafsen, K., The effect of hybrid nanoparticle additives on epoxy-nanocomposite behavior and morphology. *Journal of Applied Polymer Science* **2011,** *120* (6), 3212-3216; (e) Normatov, J.; Silverstein, M. S., Highly porous elastomer-silsesquioxane nanocomposites synthesized within high internal phase emulsions. *Journal of Polymer Science, Part A: Polymer Chemistry* **2008,** *46* (7), 2357-2366; (f) Ragosta, G.; Musto, P.; Abbate, M.; Scarinzi, G., Reactivity, viscoelastic behavior and mechanical performances of hybrid systems based on epoxy resins and reactive polyhedral oligosilsesquioxanes. *Polymer* **2009,** *50* (23), 5518-5532; (g) Song, X. Y.; Geng, H. P.; Li, Q. F., The synthesis and characterization of polystyrene/magnetic polyhedral oligomeric silsesquioxane (POSS) nanocomposites. *Polymer* **2006,** *47* (9), 3049-3056; (h) Wu, F.; Xie, T.; Yang, G., Characterization of PBT/POSS nanocomposites prepared by in situ polymerization of cyclic poly(butylene terephthalate) initiated by functionalized POSS. *Journal of Polymer Science, Part B: Polymer Physics* **2010,** *48*

(16), 1853-1859; (i) Xu, H.; Yang, B.; Wang, J.; Guang, S.; Li, C., Preparation, Tg improvement, and thermal stability enhancement mechanism of soluble poly(methyl methacrylate) nanocomposites by incorporating octavinyl polyhedral oligomeric silsesquioxanes. *Journal of Polymer Science, Part A: Polymer Chemistry* **2007,** *45* (22), 5308-5317; (j) Yani, Y.; Lamm, M. H., Molecular dynamics simulation of mixed matrix nanocomposites containing polyimide and polyhedral oligomeric silsesquioxane (POSS). *Polymer* **2009,** *50* (5), 1324-1332; (k) Zeng, F.-l.; Sun, Y.; Zhou, Y.; Li, Q.-k., A molecular dynamics simulation study to investigate the elastic properties of PVDF and POSS nanocomposites. *Modelling and Simulation in Materials Science and Engineering* **2011,** *19* (2), 025005/1-025005/26; (l) Zhang, W.; Li, X.; Guo, X.; Yang, R., Mechanical and thermal properties and flame retardancy of phosphorus-containing polyhedral oligomeric silsesquioxane (DOPO-POSS)/polycarbonate composites. *Polymer Degradation and Stability* **2010,** *95* (12), 2541-2546.

129. (a) Fu, B. X.; DeArmitt, C.; Schwab, J., Nanostructured polyhedral oligomeric silsesquioxane (POSS) molecules enhanced thermosetting materials. *SAMPE Conference Proceedings* **2009,** *54*, fu1/1-fu1/10; (b) Constantin, F.; Garea, S. A.; Voicu, G.; Iovu, H., The influence of the organic substituents from the polyhedral oligomeric silsesquioxane (POSS) cage on the epoxy-POSS hybrid materials properties. *High Performance Polymers* **2010,** *22* (8), 905-915; (c) Butola, B. S.; Joshi, M.; Kumar, S., Hybrid organic-inorganic POSS (polyhedral oligomeric silsesquioxane)/polypropylene nanocomposite filaments. *Fibers and Polymers* **2010,** *11* (8), 1137-1145; (d) Zhang, P.; Song, L.; Dai, K.; Shan, X.; Lu, H.; Wang, J.; Hu, Y., Preparation and thermal properties of the UV-cured epoxy acrylate/microencapsulated phase-change material. *Industrial & Engineering Chemistry Research* **2011,** *50* (2), 785-790; (e) Tanaka, K.; Ishiguro, F.; Chujo, Y., POSS Ionic Liquid. *Journal of the American Chemical*

Society **2010,** *132* (50), 17649-17651; (f) Rahman, M. M.; Kim, E. Y.; Lee, W. K., Effect of DMPA-clay-POSS content on thermal and mechanical properties of nanostructured ionomeric polyurethanes. *Journal of Nanoscience and Nanotechnology* **2010,** *10* (10), 6981-6985; (g) Xu, Y.; Ma, Y.; Deng, Y.; Yang, C.; Chen, J.; Dai, L., Morphology and thermal properties of organic-inorganic hybrid material involving monofunctional-anhydride POSS and epoxy resin. *Materials Chemistry and Physics* **2011,** *125* (1-2), 174-183; (h) Gnanasekaran, D.; Reddy, B. S. R., Synthesis and characterization of nanocomposites based on copolymers of POSS-ONDI macromonomer and TFONDI: effect of POSS on thermal, microstructure and morphological properties. *Advanced Materials Research (Zuerich, Switzerland)* **2010,** *123-125* (Pt. 2, Multi-Functional Materials and Structures III), 775-778; (i) Chiu, Y.-C.; Chou, I. C.; Tsai, H.-C.; Riang, L.; Ma, C.-C. M., Morphology, thermal and mechanical properties of the polyhedral oligomeric silsesquioxane side-chain epoxy hybrid material. *Journal of Applied Polymer Science* **2010,** *118* (6), 3723-3732; (j) Wang, X.-T.; Yang, Y.-K.; Yang, Z.-F.; Zhou, X.-P.; Liao, Y.-G.; Lv, C.-C.; Chang, F.-C.; Xie, X.-L., Thermal properties and liquid crystallinity of side-chain azobenzene copolymer containing pendant polyhedral oligomeric silsequioxanes. *Journal of Thermal Analysis and Calorimetry* **2010,** *102* (2), 739-744; (k) Silva, R.; Salles, C.; Mauler, R.; Oliveira, R., Investigation of the thermal, mechanical and morphological properties of poly(vinyl chloride)/polyhedral oligomeric silsesquioxane nanocomposites. *Polymer International* **2010,** *59* (9), 1221-1225; (l) Su, C.-H.; Chiu, Y.-P.; Teng, C.-C.; Chiang, C.-L., Preparation, characterization and thermal properties of organic-inorganic composites involving epoxy and polyhedral oligomeric silsesquioxane (POSS). *Journal of Polymer Research* **2010,** *17* (5), 673-681; (m) Wu, Q.; Zhang, C.; Liang, R.; Wang, B., Combustion and thermal properties of epoxy/phenyltrisilanol polyhedral oligomeric silsesquioxane nanocomposites. *Journal of*

Thermal Analysis and Calorimetry **2010,** *100* (3), 1009-1015; (n) Chattopadhyay, D. K.; Webster, D. C., Thermal stability and flame retardancy of polyurethanes. *Progress in Polymer Science* **2009,** *34* (10), 1068-1133; (o) Guo, X.; Wang, W.; Liu, L., A novel strategy to synthesize POSS/PS composite and study on its thermal properties. *Polymer Bulletin (Heidelberg, Germany)* **2010,** *64* (1), 15-25.

130. (a) Iacono, S. T.; Vij, A.; Peloquin, A. J.; Yandek, G.; Smith, D. W., Jr.; Mabry, J. M., Fluorinated polyhedral oligomeric silsesquioxanes (F-POSS). *SAMPE Conference Proceedings* **2010,** *55* (SAMPE 2010), iacon1/1-iacon1/15; (b) Stone, R. L.; Haddad, T. S.; Mabry, J. M., Synthesis and characterization of long-chained fluorinated polyhedral oligomeric silsesquioxanes (F-POSS). *Abstracts of Papers, 241st ACS National Meeting & Exposition, Anaheim, CA, United States, March 27-31, 2011* **2011**, POLY-278; (c) Tuteja, A.; Choi, W.; Mabry, J. M.; McKinley, G. H.; Cohen, R. E., Designing superoleophobic surfaces with fluorinated polyhedral oligomeric silsesquioxanes. *Polymer Preprints (American Chemical Society, Division of Polymer Chemistry)* **2009,** *50* (2), 818-819.

131. Hottle, J. R.; Deng, J.; Kim, H.-J.; Farmer-Creely, C. E.; Viers, B. D.; Esker, A. R., Blends of Amphiphilic Poly(dimethylsiloxane) and Nonamphiphilic Octaisobutyl-POSS at the Air/Water Interface. *Langmuir* **2005,** *21* (6), 2250-2259.

132. Bennett, M. E.; Alexander, W. A.; Lu, J. W.; Troya, D.; Morris, J. R., Collisions of Polar and Nonpolar Gases with Hydrogen Bonding and Hydrocarbon Self-Assembled Monolayers. *Journal of Physical Chemistry C* **2008,** *112* (44), 17272-17280.

133. Hottle, J. R.; Kim, H.-J.; Deng, J.; Farmer-Creely, C. E.; Viers, B. D.; Esker, A. R., Blends of Amphiphilic PDMS and Trisilanolisobutyl-POSS at the Air/Water Interface. *Macromolecules* **2004,** *37* (13), 4900-4908.

134. (a) Tuteja, A.; Choi, W.; Ma, M.; Mabry, J. M.; Mazzella, S. A.; Rutledge, G. C.; McKinley, G. H.; Cohen, R. E., Designing Superoleophobic Surfaces. *Science (Washington, DC, U. S.)* **2007,** *318* (5856), 1618-1622; (b) Lee, C. W.; Josse, Y.; Hsu, C. H.; Nguyen, T. P., Green emitting polyhedral oligomeric silsesquioxanes/poly(phenylene vinylene) derivative materials for highly efficient organic light emitting diodes (OLEDs). *European Physical Journal: Applied Physics* **2008,** *42* (3), 213-218.

135. Mohwald, H., Phospholipid and phospholipid-protein monolayers at the air/water interface. *Annu Rev Phys Chem* **1990,** *41*, 441-476.

136. (a) Cantin, S.; Peralta, S.; Fontaine, P.; Goldmann, M.; Perrot, F., Evolution toward the X Phase of Fatty Acid Langmuir Monolayers on a Divalent Cation Solution. *Langmuir* **2010,** *26* (2), 830-837; (b) Dreger, K.; Zhang, L.; Galla, H.-J.; Fuchs, H.; Chi, L.; Wuerthwein, E.-U.; Schaefer, H. J., Influence of an Amide Group in Methyl Octadecanoates on the Monolayer Stability. *Langmuir* **2006,** *22* (4), 1586-1594; (c) Giner, I.; Gascon, I.; Vergara, J.; Lopez, M. C.; Ros, M. B.; Royo, F. M., Molecular Arrangement in Langmuir and Langmuir-Blodgett Films of a Mesogenic Bent-Core Carboxylic Acid. *Langmuir* **2009,** *25* (20), 12332-12339; (d) Goto, T. E.; Lopez, R. F.; Iost, R. M.; Crespilho, F. N.; Caseli, L., Monolayer Collapse Regulating Process of Adsorption-Desorption of Palladium Nanoparticles at Fatty Acid Monolayers at the Air-Water Interface. *Langmuir* **2011,** *27* (6), 2667-2675; (e) Kundu, S.; Langevin, D., Fatty acid monolayer dissociation and collapse. Effect of pH and cations. *Colloids and Surfaces, A: Physicochemical and Engineering Aspects* **2008,** *325* (1-2), 81-85; (f) Li, R.; Chen, Q.; Liu, H.; Hu, Y., Influence of Spacer of Gemini on the Interactions between Cationic Gemini Surfactant and Stearic Acid in Mixed Monolayers. *Langmuir* **2010,** *26* (12), 9342-9350; (g) Muro, M.; Itoh, Y.; Hasegawa, T., A Conformation and Orientation Model of the Carboxylic Group of Fatty Acids Dependent on

---

Chain Length in a Langmuir Monolayer Film Studied by Polarization-Modulation Infrared Reflection Absorption Spectroscopy. *Journal of Physical Chemistry B* **2010,** *114* (35), 11496-11501.

137. (a) Arriaga, L. R.; Lopez-Montero, I.; Ignes-Mullol, J.; Monroy, F., Domain-Growth Kinetic Origin of Nonhorizontal Phase Coexistence Plateaux in Langmuir Monolayers: Compression Rigidity of a Raft-Like Lipid Distribution. *Journal of Physical Chemistry B* **2010,** *114* (13), 4509-4520; (b) Backus, E. H. G.; Kuiper, J. M.; Engberts, J. B. F. N.; Poolman, B.; Bonn, M., Reversible Optical Control of Monolayers on Water through Photoswitchable Lipids. *Journal of Physical Chemistry B* **2011,** *115* (10), 2294-2302; (c) Broniatowski, M.; Flasinski, M.; Dynarowicz-Latka, P.; Majewski, J., Grazing Incidence Diffraction and X-ray Reflectivity Studies of the Interactions of Inorganic Mercury Salts with Membrane Lipids in Langmuir Monolayers at the Air/Water Interface. *Journal of Physical Chemistry B* **2010,** *114* (29), 9474-9484; (d) Flasinski, M.; Broniatowski, M.; Majewski, J.; Dynarowicz-Latka, P., X-ray grazing incidence diffraction and Langmuir monolayer studies of the interaction of beta -cyclodextrin with model lipid membranes. *Journal of Colloid and Interface Science* **2010,** *348* (2), 511-521; (e) Glomm, W. R.; Volden, S.; Halskau, O.; Ese, M.-H. G., Same System-Different Results: The Importance of Protein-Introduction Protocols in Langmuir-Monolayer Studies of Lipid-Protein Interactions. *Analytical Chemistry (Washington, DC, United States)* **2009,** *81* (8), 3042-3050; (f) Kurtz, R. E.; Toney, M. F.; Pople, J. A.; Lin, B.; Meron, M.; Majewski, J.; Lange, A.; Fuller, G. G., Langmuir Monolayers of Straight-Chain and Branched Hexadecanol and Eicosanol Mixtures. *Langmuir* **2008,** *24* (24), 14005-14014; (g) Landsberg, M. J.; Ruggles, J. L.; Hussein, W. M.; McGeary, R. P.; Gentle, I. R.; Hankamer, B., Molecular Packing of Functionalized Fluorinated Lipids in Langmuir Monolayers. *Langmuir* **2010,** *26* (24), 18868-18873; (h) Leontidis, E.; Aroti,

A.; Belloni, L., Liquid Expanded Monolayers of Lipids As Model Systems to Understand the Anionic Hofmeister Series: 1. A Tale of Models. *Journal of Physical Chemistry B* **2009,** *113* (5), 1447-1459; (i) Mogilevsky, A.; Jelinek, R., Gold Nanoparticle Self-Assembly in Two-Component Lipid Langmuir Monolayers. *Langmuir* **2011,** *27* (4), 1260-1268; (j) Perez-Lopez, S.; Vila-Romeu, N.; Esteller, M. A. A.; Espina, M.; Haro, I.; Mestres, C., Interaction of GB virus C/hepatitis G virus synthetic peptides with lipid Langmuir monolayers and large unilamellar vesicles. *Journal of Physical Chemistry B* **2009,** *113* (1), 319-327; (k) Petelska, A. D.; Figaszewski, Z. A., The equilibria of phosphatidylcholine-fatty acid and phosphatidylcholine-amine in monolayers at the air/water interface. *Colloids and Surfaces, B: Biointerfaces* **2011,** *82* (2), 340-344; (l) Sung, W.-M.; Seok, S.-J.; Kim, D.-S.; Tian, C. S.; Shen, Y. R., Sum-Frequency Spectroscopic Study of Langmuir Monolayers of Lipids Having Oppositely Charged Headgroups. *Langmuir* **2010,** *26* (23), 18266-18272; (m) Tzika, E. D.; Christoforou, M.; Pispas, S.; Zervou, M.; Papadimitriou, V.; Sotiroudis, T. G.; Leontidis, E.; Xenakis, A., Influence of Nanoreactor Environment and Substrate Location on the Activity of Horseradish Peroxidase in Olive Oil Based Water-in-Oil Microemulsions. *Langmuir* **2011,** *27* (6), 2692-2700.

138. Gaonkar, A. G.; Neuman, R. D., The effect of wettability of Wilhelmy plate and du Nouey ring on interfacial tension measurements in solvent extraction systems. *Journal of Colloid and Interface Science* **1984,** *98* (1), 112-119.

139. Islam, M. N.; Kato, T., Anomalous Phase Behavior in Langmuir Monolayers of Monomyristoyl-rac-Glycerol at the Air-Water Interface. *Langmuir* **2005,** *21* (24), 10920-10922.

140. Hifeda, Y. F.; Rayfield, G. W., Evidence for first-order phase transitions in lipid and fatty acid monolayers. *Langmuir* **1992,** *8* (1), 197-200.

141. Islam, M. N.; Kato, T., Influence of Temperature and Headgroup Size on Condensed-Phase Patterns in Langmuir Monolayers of Some Oxyethylenated Nonionic Surfactants. *Langmuir* **2005,** *21* (6), 2419-2424.

142. (a) Islam Md, N.; Kato, T., Faceted structures in Langmuir monolayers of diethylene glycol mono-n-octadecyl ether at the air--water interface. *Langmuir* **2004,** *20* (25), 10872-10877; (b) Islam, N.; Kato, T., Influence of temperature and alkyl chain length on phase behavior in Langmuir monolayers of some oxyethylenated nonionic surfactants. *J Colloid Interface Sci* **2006,** *294* (2), 288-294.

143. (a) Hossain Md, M.; Iimura, K.-I.; Kato, T., Surface phase behavior of di-n-tetradecyl hydrogen phosphate in Langmuir monolayers at the air-water interface. *J Colloid Interface Sci* **2006,** *302* (1), 272-7; (b) Hossain Md, M.; Iimura, K.-i.; Kato, T., Temperature and compression rate independent domain shape in Langmuir monolayers of di-n-dodecyl hydrogen phosphate at the air-water interface. *J Colloid Interface Sci* **2008,** *319* (1), 295-301; (c) Hossain, M. M.; Iimura, K.-i.; Kato, T., Temperature and compression rate independent domain shape in Langmuir monolayers of di-n-dodecyl hydrogen phosphate at the air-water interface. *Journal of Colloid and Interface Science* **2008,** *319* (1), 295-301.

144. Wang, Z.; Li, X.; Yang, S., Studies of Dipalmitoylphosphatidylcholine (DPPC) Monolayers Embedded with Endohedral Metallofullerene (Dy@C82). *Langmuir* **2009,** *25* (22), 12968-12973.

145. Grigoriev, D.; Miller, R.; Wuestneck, R.; Wuestneck, N.; Pison, U.; Moehwald, H., A Novel Method To Evaluate the Phase Transition Thermodynamics of Langmuir Monolayers. Application to DPPG Monolayers Affected by Subphase Composition. *Journal of Physical Chemistry B* **2003,** *107* (51), 14283-14288.

146. Mohwald, H., Handbook of Biological Physics; Elsevier: Amsterdam. **1995**.

147. Kjaer, K.; Als-Nielsen, J.; Helm, C. A.; Laxhuber, L. A.; Moehwald, H., Ordering in lipid monolayers studied by synchrotron x-ray diffraction and fluorescence microscopy. *Physical Review Letters* **1987,** *58* (21), 2224-2227.

148. Grigoriev, D.; Krustev, R.; Miller, R.; Pison, U., Effect of Monovalent Ions on the Monolayers Phase Behavior of the Charged Lipid DPPG. *Journal of Physical Chemistry B* **1999,** *103* (6), 1013-1018.

149. (a) Vollhardt, D.; Fainerman, V. B.; Siegel, S., Thermodynamic and Textural Characterization of DPPG Phospholipid Monolayers. *Journal of Physical Chemistry B* **2000,** *104* (17), 4115-4121; (b) Fainerman, V. B.; Lucassen-Reynders, E. H.; Miller, R., Adsorption of surfactants and proteins at fluid interfaces. *Colloids and Surfaces, A: Physicochemical and Engineering Aspects* **1998,** *143* (2-3), 141-165.

150. (a) Helm, C. A.; Laxhuber, L.; Loesche, M.; Moehwald, H., Electrostatic interactions in phospholipid membranes. I: Influence of monovalent ions. *Colloid and Polymer Science* **1986,** *264* (1), 46-55; (b) Losche, M. M., H., Electrostatic interactions in phospholipid membranes: II. Influence of divalent ions on monolayer structure. *Colloid Interface Sci.* **1989,** *131* (1), 56-57.

151. Yue, B. Y.; Jackson, C. M.; Taylor, J. A. G.; Mingins, J.; Pethica, B. A., Phospholipid monolayers at non-polar oil/water interfaces. Part 1. Phase transitions in distearoyl-lecithin films at the n-heptane aqueous sodium chloride interface. *Journal of the Chemical Society, Faraday Transactions 1: Physical Chemistry in Condensed Phases* **1976,** *72* (12), 2685-2693.

152. (a) Hao, X. T.; Hosokai, T.; Mitsuo, N.; Kera, S.; Okudaira, K. K.; Mase, K.; Ueno, N., Control of the interchain pi-pi interaction and electron density distribution at the surface of conjugated poly(3-hexylthiophene) thin films. *The journal of physical chemistry. B* **2007,** *111*

(35), 10365-10372; (b) Park, J. Y.; Ponnapati, R.; Taranekar, P.; Advincula, R. C., Carbazole Peripheral Poly(benzyl ether) Dendrimers at the Air-Water Interface: Electrochemical Cross-Linking and Electronanopatterning. *Langmuir* **2010,** *26* (9), 6167-6176; (c) Kim, J.; Levitsky, I. A.; McQuade, D. T.; Swager, T. M., Structural Control in Thin Layers of Poly(p-phenyleneethynylene)s: Photophysical Studies of Langmuir and Langmuir-Blodgett Films. *Journal of the American Chemical Society* **2002,** *124* (26), 7710-7718.

153. (a) Dighe, M. K.; Dover, F. J.; Stine, K. J.; Pigge, F. C., Monolayers of triaroylbenzene derivatives. *Thin Solid Films* **2008,** *516* (10), 3227-3238; (b) Youm, S.-G.; Paeng, K.; Choi, Y.-W.; Park, S.; Sohn, D.; Seo, Y.-S.; Satija, S. K.; Kim, B. G.; Kim, S.; Park, S. Y., Supramolecular Ordering of Tripod Dyes at the Air/Water Interface. *Langmuir* **2005,** *21* (13), 5647-5650.

154. (a) Karp, E.; Pecinovsky, C. S.; McNevin, M. J.; Gin, D. L.; Schwartz, D. K., Langmuir Monolayers of a Photoisomerizable Macrocycle Surfactant. *Langmuir* **2007,** *23* (15), 7923-7927; (b) Liu, H.-G.; Feng, X.-S.; Jiang, J.; Zhang, L.-J.; Lan, W.-Z.; Lee, Y.-I.; Jang, K.; Qian, D.-J.; Yang, K.-Z., Influence of molecular structures of europium bisphthalocyanines on organization of supramolecular assemblies formed at the air/water interface. *Materials Science & Engineering, C: Biomimetic and Supramolecular Systems* **2003,** *C23* (4), 501-507; (c) Del Cano, T.; Aroca, R.; De Saja, J. A.; Rodriguez-Mendez, M. L., Langmuir-Blodgett Mixed Films of Titanyl(IV) Phthalocyanine and Arachidic Acid. Molecular Orientation and Film Structure. *Langmuir* **2003,** *19* (9), 3747-3751; (d) Ariga, K.; Tanaka, K.; Katagiri, K.; Kikuchi, J.-i.; Shimakoshi, H.; Ohshima, E.; Hisaeda, Y., Langmuir monolayer of organoalkoxysilane for vitamin B12-modified electrode. *Physical Chemistry Chemical Physics* **2001,** *3* (16), 3442-3446.

155. (a) Sui, G.; Orbulescu, J.; Mabrouki, M.; Micic, M.; Leblanc, R. M.; Liu, S.; Cormier, R. A.; Gregg, B. A., Self-Assembly of Liquid Crystal Semiconductor Molecules at the Air/Water Interface. *Journal of Physical Chemistry B* **2002,** *106* (36), 9335-9340; (b) de Moura, A. F.; Trsic, M., Molecular Dynamics Simulation of a Perylene-Derivative Langmuir Film. *Journal of Physical Chemistry B* **2005,** *109* (9), 4032-4041.

156. Nayak, A.; Suresh, K. A.; Pal, S. K.; Kumar, S., Films of Novel Mesogenic Molecules at Air-Water and Air-Solid Interfaces. *Journal of Physical Chemistry B* **2007,** *111* (38), 11157-11161.

157. Maisuria, B., Synthesis, Characterization, Critical Micelle Concentration and Antimicrobial Activity of Two-headed Amphiphiles, M.S. thesis, Virginia Polytechnic Institute and State Univeristy, Blacksburg, VA. . **2009**.

158. (a) Newkome, G. R.; He, E.; Godinez, L. A.; Baker, G. R., Electroactive Metallomacromolecules via Tetrabis(2,2':6',2"-terpyridine)ruthenium(II) Complexes: Dendritic Nanonetworks toward Constitutional Isomers and Neutral Species without External Counterions. *Journal of the American Chemical Society* **2000,** *122* (41), 9993-10006; (b) Newkome, G. R.; Kim, H. J.; Moorefield, C. N.; Maddi, H.; Yoo, K.-S., Syntheses of New 1 → (2 + 1) C-Branched Monomers for the Construction of Multifunctional Dendrimers. *Macromolecules* **2003,** *36* (12), 4345-4354; (c) Newkome, G. R.; Behera, R. K.; Moorefield, C. N.; Baker, G. R., Chemistry of micelles. 18. Cascade polymers: syntheses and characterization of one-directional arborols based on adamantane. *Journal of Organic Chemistry* **1991,** *56* (25), 7162-7167.

159. Actis, M. L., Synthesis, Characterization, Critical Micelle Concentration and Biological Activity of Two-Headed Amphiphiles: Master of Science Thesis. Virginia Polytechnic Institute and State Univeristy, Blacksburg, VA. **2008**.

160. Tishkov, A. A.; Smirnov, V. O.; Nefed'eva, M. V.; Lyapkalo, I. M.; Semenov, S. E.; Ioffe, S. L.; Strelenko, Y. A.; Tartakovskii, V. A., General synthesis of γ-functionalized β-aryl-substituted primary nitro compounds. *Russian Journal of Organic Chemistry (Translation of Zhurnal Organicheskoi Khimii)* **2001,** *37* (3), 390-394.

161. (a) Akpo, C.; Weber, E.; Reiche, J., Synthesis, Langmuir and Langmuir-Blodgett film behaviour of new dendritic amphiphiles. *New Journal of Chemistry* **2006,** *30* (12), 1820-1833; (b) Grayson, S. M.; Frechet, J. M., Convergent dendrons and dendrimers: from synthesis to applications. *Chemical reviews* **2001,** *101* (12), 3819-3868; (c) Chow, H.-F.; Mong, T. K. K.; Nongrum, M. F.; Wan, C.-W., The synthesis and properties of novel functional dendritic molecules. *Tetrahedron* **1998,** *54* (30), 8543-8660.

162. Newkome, G. R.; Weis, C. D.; Moorefield, C. N.; Fronczek, F. R., Chemistry of micelles. 66. A useful dendritic building block: di-tert-butyl 4-[(2-tert-butoxycarbonyl)ethyl]-4-isocyanato-1,7-heptanedicarboxylate. *Tetrahedron Letters* **1997,** *38* (40), 7053-7056.

163. Newkome, G. R.; Weis, C. D.; Childs, B. J., Syntheses of 1 → 3 branched isocyanate monomers for dendritic construction. *Designed Monomers and Polymers* **1998,** *1* (1), 3-14.

164. (a) Newkome, G. R.; Shreiner, C. D., Poly(amidoamine), polypropylenimine, and related dendrimers and dendrons possessing different 1 → 2 branching motifs: An overview of the divergent procedures. *Polymer* **2008,** *49* (1), 1-173; (b) Newkome, G. R.; Yao, Z.; Baker, G. R.; Gupta, V. K., Micelles. Part 1. Cascade molecules: a new approach to micelles. A [27]-arborol. *Journal of Organic Chemistry* **1985,** *50* (11), 2003-2004; (c) Tomalia, D. A.; Baker, H.; Dewald, J.; Hall, M.; Kallos, G.; Martin, S.; Roeck, J.; Ryder, J.; Smith, P., A new class of polymers: starburst-dendritic macromolecules. *Polymer Journal (Tokyo, Japan)* **1985,** *17* (1), 117-132.

165. Lempens, E. H. M.; Helms, B. A.; Bayles, A. R.; Merkx, M.; Meijer, E. W., A Versatile, Modular Platform for Multivalent Peptide Ligands Based on a Dendritic Wedge. *European Journal of Organic Chemistry* **2010,** (1), 111-119, S111/1-S111/7.

166. (a) Haddad, T. S.; Lichtenhan, J. D., Hybrid Organic-Inorganic Thermoplastics: Styryl-Based Polyhedral Oligomeric Silsesquioxane Polymers. *Macromolecules* **1996,** *29* (22), 7302-7304; (b) Pescarmona, P. P.; Masters, A. F.; van der Waal, J. C.; Maschmeyer, T., Osmium silsesquioxane as model compound and homogeneous catalyst for the dihydroxylation of alkenes. *J. Mol. Catal. A Chem.* **2004,** *220* (1), 37-42; (c) Wheeler, P. A.; Fu, B. X.; Lichtenhan, J. D.; Weitao, J.; Mathias, L. J., Incorporation of metallic POSS, POSS copolymers, and new functionalized POSS compounds into commercial dental resins. *Journal of Applied Polymer Science* **2006,** *102* (3), 2856-2862.

167. Lichtenhan, J. D., Polyhedral oligomeric silsesquioxanes: building blocks for silsesquioxane-based polymers and hybrid materials. *Comments on Inorganic Chemistry* **1995,** *17* (2), 115-130.

168. (a) Choi, J.; Harcup, J.; Yee, A. F.; Zhu, Q.; Laine, R. M., Organic/Inorganic Hybrid Composites from Cubic Silsesquioxanes. *Journal of the American Chemical Society* **2001,** *123* (46), 11420-11430; (b) Haddad, T. S.; Viers, B. D.; Phillips, S. H., Polyhedral oligomeric silsesquioxane (POSS)-styrene macromers. *Journal of Inorganic and Organometallic Polymers* **2002,** *11* (3), 155-164; (c) Kopesky, E. T.; Haddad, T. S.; Cohen, R. E.; McKinley, G. H., Thermomechanical Properties of Poly(methyl methacrylate)s Containing Tethered and Untethered Polyhedral Oligomeric Silsesquioxanes. *Macromolecules* **2004,** *37* (24), 8992-9004; (d) Kopesky, E. T.; McKinley, G. H.; Cohen, R. E., Toughened poly(methyl methacrylate) nanocomposites by incorporating polyhedral oligomeric silsesquioxanes. *Polymer* **2006,** *47* (1),

299-309; (e) Wu, J.; Haddad, T. S.; Kim, G.-M.; Mather, P. T., Rheological Behavior of Entangled Polystyrene-Polyhedral Oligosilsesquioxane (POSS) Copolymers. *Macromolecules* **2007,** *40* (3), 544-554; (f) Zhang, H.; Kulkarni, S.; Wunder, S. L., Blends of POSS-PEO(n=4)8 and high molecular weight poly(ethylene oxide) as solid polymer electrolytes for lithium batteries. *Journal of Physical Chemistry B* **2007,** *111* (14), 3583-3590.

169. (a) Mark, J. E., Hybrid organic-inorganic composites containing mixed-oxide ceramics and high-temperature polymers. *Journal of Macromolecular Science, Pure and Applied Chemistry* **1996,** *A33* (12, First International Polymer Symposium on Polymers from Natural Sources, 1995), 2005-2012; (b) LeBaron, P. C.; Wang, Z.; Pinnavaia, T. J., Polymer-layered silicate nanocomposites: an overview. *Applied Clay Science* **1999,** *15* (1-2), 11-29; (c) Kickelbick, G.; Bauer, J.; Huesing, N., Structurally well-defined amphiphilic polysiloxane copolymers. *Silicon Chemistry* **2003**, 439-450.

170. Kim, H.-J.; Lalli, J. H.; Riffle, J. S.; Viers, B. D.; Esker, A. R., Brewster angle microscopy studies of aggregate formation in blends of amphiphilic trisilanolisobutyl-POSS and nitrile substituted poly(dimethylsiloxane) at the air-water interface. *ACS Symposium Series* **2007,** *964* (Science and Technology of Silicones and Silicone-Modified Materials), 268-289.

171. Huffer, S. M.; Yin, W.; Esker, A. R., Limiting rheological properties of octaisobutyl-POSS and poly(dimethylsiloxane) blends. *Polymer Preprints (American Chemical Society, Division of Polymer Chemistry)* **2007,** *48* (1), 717-718.